

UC San Diego

Research Theses and Dissertations

Title

The Role of Vanadium Bromoperoxidase in the Biosynthesis of Halogenated Marine Natural Products

Permalink

<https://escholarship.org/uc/item/8kr265qf>

Author

Franklin, Jayme N.

Publication Date

2003-12-01

Peer reviewed

NOTE TO USERS

This reproduction is the best copy available.

UMI[®]

UNIVERSITY OF CALIFORNIA

Santa Barbara

The Role of Vanadium Bromoperoxidase in the Biosynthesis of
Halogenated Marine Natural Products

A Dissertation submitted in partial satisfaction of the
requirements for the degree Doctor of Philosophy
in Chemistry

by

Jayne Nicole Franklin

Committee in charge:

Professor Alison Butler, Chair

Professor Norbert O. Reich

Professor J. Thomas Gerig

Professor Kevin W. Plaxco

December 2003

UMI Number: 3112889

INFORMATION TO USERS

The quality of this reproduction is dependent upon the quality of the copy submitted. Broken or indistinct print, colored or poor quality illustrations and photographs, print bleed-through, substandard margins, and improper alignment can adversely affect reproduction.

In the unlikely event that the author did not send a complete manuscript and there are missing pages, these will be noted. Also, if unauthorized copyright material had to be removed, a note will indicate the deletion.

UMI[®]

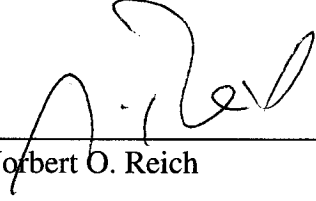
UMI Microform 3112889

Copyright 2004 by ProQuest Information and Learning Company.

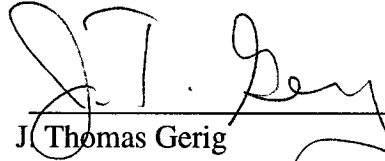
All rights reserved. This microform edition is protected against unauthorized copying under Title 17, United States Code.

ProQuest Information and Learning Company
300 North Zeeb Road
P.O. Box 1346
Ann Arbor, MI 48106-1346

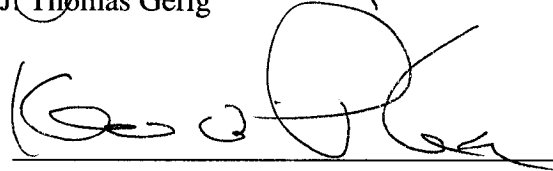
The dissertation of Jayme N. Carter Franklin is approved.



Norbert O. Reich



J. Thomas Gerig



Kevin W. Plaxco



Alison Butler, Committee Chair

October 2003

ACKNOWLEDGEMENTS

I would like to express my appreciation to Professor Alison Butler for her scientific guidance, encouragement and enthusiasm during my graduate experience. I would like to thank California Sea Grant for a Traineeship in support of the projects to Prof. Alison Butler (R/MP-69 and R/MP-76). I thank my committee members, Professors Norbert O. Reich, J. Thomas Gerig, and Kevin W. Plaxco for their time and commentary on my research. I also thank Professor R. Daniel Little for kindly answering many of my questions and serving as a second mentor.

Many thanks to Dr. James Pavlovich for considerable help on mass spectrometry and the many discussions on all aspects of mass spectrometry. I am grateful to all Butler lab members past and present for helpful scientific discussions.

Personally, I would like to thank Jennifer S. Martinez for her friendship and daily discussions about science and life. To my mom and brother, Janet Carter and Joshua Carter, words cannot express all that I am thankful for. Thank you to my vast extended family and friends for your many years of encouragement and support. Lastly, I would like to especially thank my husband Nathan R. Franklin, for everything!

Dedicated to the memory of James D. Wilson

VITA

EDUCATION

1995 B.S., Chemistry, Westmont College, Santa Barbara, CA
Advisor: Professor David Marten

PROFESSIONAL EMPLOYMENT:

1997 – 2003 Research Assistant, Department of Chemistry and Biochemistry,
University of California Santa Barbara.

1996 – 1997 Teaching Associate, Department of Chemistry, Westmont College.

1995 – 1996 Research Associate, Department of Clinical Neurology, University of
California Davis Medical School.

1994 – 1995 Undergraduate researcher, Department of Chemistry, Westmont
College.

PUBLICATIONS:

J.S. Martinez, J.N. Carter-Franklin, E.L. Mann, J.D. Martin, M.G. Haygood, A.
Butler. Structure and Dynamics of a New Suite of Amphiphilic Siderophores
Produced by a Marine Bacterium. *Proceedings of the National Academy of
Sciences*, 2002, 100:3754-3759.

J.N. Carter-Franklin, J.D. Parrish, R.A. Tschirret-Guth, R.D. Little, A. Butler.
Vanadium Haloperoxidase-Catalyzed Bromination and Cyclization of
Terpenes. *Journal of the American Chemical Society*, 2002, 125:3688-3689.

J.N. Carter, K.E. Beatty, M.T. Simpson A. Butler. Reactivity of Recombinant and
Mutant Vanadium Bromoperoxidase from the Red Alga *Corallina officinalis*.
Journal of Inorganic Biochemistry, 2002, 91:59-69.

A. Butler, J.N. Carter, M.T. Simpson., "Vanadium in Proteins and Enzymes" in
Handbook on Metalloproteins, I. Bertini, A. Sigel, and H. Sigel, eds., M.
Dekker, New York.

PRESENTATIONS:

2003 Center for Environmental Bioinorganic Chemistry (CEBIC) Conference,
Princeton University, Speaker- "Vanadium Bromoperoxidase: From the Global
Halogen Cycle to Molecular Transformations"

2003 Graduate Bioinorganic Gordon Research Conference, Ventura California; Invited Speaker- “Vanadium Bromoperoxidase: Enzyme Catalyzed Cyclization of Terpenes”

2002 Sea Grant Graduate Researcher Symposium, California and the World Ocean Conference, Santa Barbara, California: Poster presenter- “Vanadium Bromoperoxidase: Towards the Biosynthesis of Halogenated Marine Natural Products”

2002 Marine Natural Products Gordon Conference, Ventura California: Speaker- “Reactivity of Vanadium Bromoperoxidase from Marine Algae: Enzyme Induced Cyclization Reactions”

2002 Marine Natural Products Gordon Conference, Ventura California: Poster presenter- “Reactivity of Vanadium Bromoperoxidase from Marine Algae: Enzyme Induced Cyclization Reactions”

2001 Graduate Bioinorganic Gordon Research Conference, Ventura California: Poster presenter- “Reactivity of Recombinant Vanadium Bromoperoxidase and Mutant H480A”

1998 Marine Natural Products Gordon Conference, Ventura California, Poster presenter- “Polyunsaturated Fatty Acid Oxidase from the Marine Red Alga *Corallina officinalis*”

-
HONORS AND AWARDS:

2003 B.R. Baker Award, University of California, Santa Barbara CA

2002 Sea Grant Graduate Researcher Symposium, California and the World Ocean Conference, Santa Barbara, California: 2nd Place Best Poster Presentation- “Vanadium Bromoperoxidase: Towards the Biosynthesis of Halogenated Marine Natural Products”

1997 - 2003: California Sea Grant Traineeship, University of California, Santa Barbara.

Cum Laude Honors in Chemistry, Westmont College, 1995

Presidential Scholarship, Westmont College, 1993-1995

ABSTRACT

The Role of Vanadium Bromoperoxidase in the Biosynthesis of Halogenated Marine Natural Products

by

Jayne N. Franklin

The widespread occurrence of bromine- and chlorine-containing marine natural products has prompted investigations into the biosynthesis of halogenated marine metabolites. Halogenating enzymes, such as haloperoxidases, have long been thought to be involved in the biogenesis of halogenated marine natural products. Vanadium bromoperoxidases (V-BrPO) have been identified and isolated from all major classes of marine algae, and catalyze the two-electron oxidation of bromide by hydrogen peroxide.

To investigate V-BrPO in marine algae that produce halogenated natural products of interest, V-BrPO was cloned from four different red algae (*Corallina officinalis*, *Plocamium cartilagineum*, *Delisea pulchra* and *Laurencia pacifica*) using nucleotide probes based on a highly conserved sequence motif, P[S/A]YPSGHAT, for the class of vanadium haloperoxidases.. Design of a bacterial expression system and subsequent kinetic characterization of recombinant and mutant forms of V-BrPO

from *C. officinalis* were performed. In addition, steady state kinetics analysis of azide inhibition of V-BrPO from *C. officinalis* was completed.

V-BrPO was subsequently used to explore the biosynthesis of brominated terpene marine natural products. V-BrPO directed the bromination and cyclization of monoterpenes, including derivatives of geraniol to 5-, 6-, and 8-membered bromoether structures and brominated cyclized polyenes. In addition, V-BrPO reactions with the sesquiterpene (+)-nerolidol resulted in the production of previously reported marine natural products α - and β -snyderol, γ -snyderol, and (+)-3 β -bromo-8-epicaparrapi oxide. V-BrPO catalyzed the asymmetric bromination of (+)-nerolidol to produce single diastereomers of brominated marine natural products.

V-BrPO identified at the surface of the marine red alga *Delisea pulchra* was shown to brominate 3-oxo-acyl homoserine lactones, thereby interrupting quorum sensing in *Agrobacterium tumefaciens* bioassays. V-BrPO isolated from *D. pulchra* was also shown to mediate the bromolactonization of 4-pentynoic acid in the biosynthesis of synthetic halogenated furanones.

The structures of siderophores, produced by the coastal marine bacterial isolate *Vibrio* sp. Roatan-10, were completed and membrane partitioning into large unilamellar phosphatidylcholine vesicles evaluated. Membrane partitioning coefficients for the physiological mixture of amphibactins was compared to previously reported data for marinobactin siderophores.

TABLE OF CONTENTS

Acknowledgements		iii
Vita		iv
Abstract		vi
List of Figures		xii
List of Schemes		xx
List of Tables		xxiii
List of Abbreviations		xxiv
Chapter 1	Introduction	
	Bioinorganic role of vanadium	1
	Vanadium enzymes	3
	Vanadium nitrogenase	3
	Vanadium haloperoxidases	7
	Vanadium chloroperoxidase	8
	Vanadium bromoperoxidase	23
	The selectivity of vanadium bromoperoxidases	35
	Comparative aspects of vanadium haloperoxidases and phosphatidic acid phosphatases.	37
	Vanadium bromoperoxidase and the biosynthesis of halogenated marine natural products	39
	Biomimetic syntheses of halogenated marine natural products	39
	Haloperoxidases and the syntheses of halogenated marine natural products.	45
	References	47
Chapter 2	cDNA Cloning of V-BrPO from Marine Algae (Rhodophyta) and Kinetic Characterization	
	Introduction	55
	Methods and Materials	
	cDNA library construction and cloning of V-BrPO from <i>Corallina officinalis</i>	59
	RT-PCR cloning of marine red algae	61
	Expression and purification of recombinant CoV-BrPO	63
	Production of mutant H480A (V-BrPO, <i>C. officinalis</i>)	65
	Purification of native V-BrPO from marine red algae	65

Conditions for steady state kinetic analysis of native, recombinant and mutant V-BrPOs	66
Steady state kinetic analysis	67
Enzyme activity assays	69
Results	
DNA and amino acid sequence analysis of recombinant V-BrPO from marine red algae	70
Expression of recombinant CoV-BrPO and H480A in <i>E. coli</i>	79
Kinetic analysis of recombinant CoV-BrPO and mutant H480A	80
Vanadium bromoperoxidase from the marine red alga <i>Plocamium cartilagineum</i>	97
Isolation	97
Steady state kinetics	100
Inhibition of <i>P. cartilagineum</i> V-BrPO catalyzed bromination of MCD by hydrogen peroxide	100
Discussion	108
References	121
 Chapter 3	
The Role of Vanadium Bromoperoxidase in the Biosynthesis Of Halogenated Terpenes	
Introduction	125
Methods and materials	
General methods	131
V-BrPO catalyzed reactions with terpenes (product profile analysis)	133
Non-enzymatic reactions with terpene substrates	137
Large scale incubations with V-BrPO	137
Nerol	138
Geraniol	138
Geranyl acetate	139
Geranyl acetone	139
All <i>trans</i> (+)-nerolidol	140
Competitive substrate kinetics	141
Results	
Bromination of linalool by V-BrPO	142
Kinetic resolution of linalool using V-BrPO	145
Reaction of linalool with aqueous bromine	146
Bromination of nerol by V-BrPO	146
Reaction of nerol with aqueous bromine	150
Bromination of geraniol by V-BrPO	150
Reaction of geraniol with aqueous bromine and TBCO	156
Bromination of geranyl acetate by V-BrPO	158

Reaction of geranyl acetate with aqueous bromine and TBCO	161
Bromination of geranyl acetone by V-BrPO	162
Reaction of geranyl acetone with aqueous bromine and TBCO	164
Bromination of all- <i>trans</i> (+)-nerolidol by V-BrPO	165
Snyderol products	165
(+)-3 β -bromo-8-epicaparrapi oxide product	169
Reaction of all <i>trans</i> (+)-nerolidol by aqueous bromine and TBCO	176
Bromination of <i>cis</i> -5-octene-1-ol by V-BrPO	176
Bromination of <i>cis</i> -3-nonene-1-ol by V-BrPO	178
Competitive substrate kinetics	182
Discussion	185
References	202
Chapter 4	Chemical Defense of the Marine Red Alga <i>Delisea pulchra</i>
Introduction	207
Methods and Materials	
General methods	211
Reaction of acyl homoserine lactones with the marine macroalga <i>Delisea pulchra</i>	212
Quorum sensing of <i>Agrobacterium tumefaciens</i> NTL4 with products from reactions of 3-oxo-hexanoylhomoserine lactone with <i>Delisea pulchra</i> and purified V-BrPO	213
Biosynthesis of halogenated lactones by <i>Delisea pulchra</i> /V-BrPO	215
Results	
Detection of haloperoxidase activity in whole algal samples of <i>Delisea pulchra</i>	216
Reactivity of 3-oxo-hexanoylhomoserine lactone with whole algal pieces of <i>Delisea pulchra</i> and partially purified V-BrPO	219
Bromination of 3-oxo-hexanoylhomoserine lactone; effects on quorum sensing activity of <i>Agrobacterium tumefaciens</i> NTL4	227
Biomimetic synthesis of halogenated furanones by V-BrPO	231
Discussion	233
References	238
Chapter 5	Azide Inhibition of Vanadium Bromoperoxidase from the Red Alga <i>Corallina officinalis</i>
Introduction	242
Methods and Materials	

General methods	246
Bromoperoxidase activity measurements	246
Kinetics of inactivation of <i>CoV</i> -BrPO by sodium azide	246
Partition ratio titration	247
Protection against azide inactivation by bromide	248
Production of NO during azide inactivation of <i>CoV</i> -BrPO	248
Results	
Time-dependent inactivation of <i>CoV</i> -BrPO by sodium azide	250
Stoichiometry of azide binding to <i>CoV</i> -BrPO	255
Partition ratio for the inactivation of <i>CoV</i> -BrPO	258
Protection of <i>CoV</i> -BrPO against azide inactivation by bromide	261
Production of NO during azide inactivation of <i>CoV</i> -BrPO	268
Discussion	270
References	274
Chapter 6	Structure and Amphiphilic Properties of a Suite of Siderophores Isolated from a Marine Bacterium
Introduction	277
Methods and Materials	
General methods	283
Isolation of siderophores	284
Structure determination	285
Structural determination of fatty acid appendages	285
Membrane partition experiments with amphibactins	286
Results	
Amphibactin structure determination	288
Characterization of the fatty acid appendages in the amphibactins	289
Partition experiments with the physiological mixture of amphibactins	300
Discussion	307
References	312
Appendix	314

LIST OF FIGURES

Figure 1.1	Biologically important vanadium compounds.	4
Figure 1.2	Proposed structure of the M cluster of the V-Fe dinitrogenase.	6
Figure 1.3	Ribbon-type representation of V-CIPO structure.	12
Figure 1.4	Vanadium site of V-CIPO.	13
Figure 1.5	Monoperoxovanadium(V) site of V-CIPO.	15
Figure 1.6	Overlay of X-ray coordinates of the vanadium site of V-CIPO and mutant H496A.	19
Figure 1.7	Overlay of X-ray coordinates of the vanadium site of V-CIPO and mutant H404A.	20
Figure 1.8	Overlay of X-ray coordinates of the vanadium site of V-CIPO and mutant D292A.	21
Figure 1.9	Overlay of X-ray coordinates of the vanadium site of V-CIPO and mutant R360A.	22
Figure 1.10	Ribbon-type representation of V-BrPO homodimer of <i>Ascophyllum nodosum</i> .	28
Figure 1.11	Vanadium binding site of V-BrPO from <i>Ascophyllum nodosum</i> .	29
Figure 1.12	Diagram of the C _α backbone of V-BrPO from <i>Corallina officinalis</i> .	32
Figure 1.13	Vanadium binding site of V-BrPO from <i>Corallina officinalis</i> .	33
Figure 1.14	Halogenated C15 acetogenins from the marine red alga <i>Laurencia</i> .	44
Figure 2.1	Nucleotide and amino acid sequence for cloned V-BrPO from <i>Corallina officinalis</i> .	72
Figure 2.2	Nucleotide and amino acid sequence for cloned V-BrPO	73

from *Plocamium cartilagineum*.

Figure 2.3	Nucleotide and amino acid sequence for cloned V-BrPO from <i>Delisea pulchra</i> (clone E).	74
Figure 2.4	Nucleotide and amino acid sequence for cloned V-BrPO from <i>Delisea pulchra</i> (clone D).	75
Figure 2.5	Alignment of amino acid sequences for known vanadium bromoperoxidases.	76
Figure 2.6	Reducing SDS-PAGE gel for <i>E. coli</i> expression experiments for rCoV-BrPO.	80
Figure 2.7	Primary double reciprocal plot of the rate of MCD bromination as a function of hydrogen peroxide for rCoV-BrPO.	82
Figure 2.8	Primary double reciprocal plot of the rate of MCD bromination as a function of bromide for rCoV-BrPO.	83
Figure 2.9	Primary double reciprocal plot of the rate of MCD bromination as a function of hydrogen peroxide for native CoV-BrPO.	84
Figure 2.10	Primary double reciprocal plot of the rate of MCD bromination as a function of bromide for native CoV-BrPO.	85
Figure 2.11	In-gel activity analysis of V-BrPO isolated from <i>Corallina officinalis</i> , <i>E. coli</i> (rCoV-BrPO) or H480A.	88
Figure 2.12	Specific activity measurement of rCoV-BrPO and H480A as a function of pH.	89
Figure 2.13	Saturation kinetic plot of the rate of triiodide formation vs. hydrogen peroxide for H480A.	92
Figure 2.14	Saturation kinetic plot of the rate of triiodide formation vs. iodide for H480A.	93
Figure 2.15	Primary double reciprocal plot of the rate of triiodide formation as a function of hydrogen peroxide for H480A.	94
Figure 2.16	Primary double reciprocal plot of the rate triiodide formation as a function of iodide for H480A.	95

Figure 2.17	Improved specific activity measurements of H480A in the presence of hydrogen peroxide and vanadate.	96
Figure 2.18	Reducing SDS-PAGE gel for MonoQ fractions of V-BrPO isolated from <i>Plocamium cartilagineum</i> .	98
Figure 2.19	Vanadium dependence for the bromoperoxidase isolated from <i>Plocamium cartilagineum</i> .	99
Figure 2.20	Saturation kinetic plot of the rate of MCD bromination vs. hydrogen peroxide for V-BrPO from <i>Plocamium cartilagineum</i> .	102
Figure 2.21	Saturation kinetic plot of the rate of MCD bromination vs. bromide for V-BrPO from <i>Plocamium cartilagineum</i> .	103
Figure 2.22	Primary double reciprocal plot of the rate of MCD bromination as a function of hydrogen peroxide for V-BrPO from <i>Plocamium cartilagineum</i> .	104
Figure 2.23	Primary double reciprocal plot of the rate of MCD bromination as a function of bromide for V-BrPO from <i>Plocamium cartilagineum</i> .	105
Figure 2.24	Saturation kinetic plots of the rates of MCD bromination vs. hydrogen peroxide as a function of pH.	106
Figure 2.25	Saturation kinetic plots of the rates of MCD bromination vs. bromide as a function of pH.	107
Figure 2.26	Active site superposition of vanadium bromoperoxidase (<i>Corallina officinalis</i>) and vanadium chloroperoxidase (<i>Curvularia inaequalis</i>).	109
Figure 2.27	Consensus tree for orders of marine red algae.	111
Figure 2.28	Polyhalogenated monoterpenes from the red alga <i>Plocamium cartilagineum</i> .	118
Figure 3.1	GC-MS chromatogram of V-BrPO-catalyzed reaction with racemic linalool (1)	142
Figure 3.2	EIMS of 5-membered cyclic bromoether product 2 .	143

Figure 3.3	EIMS of 6-membered cyclic bromoether product 3 .	143
Figure 3.4	¹ H NMR of doublet of doublets for mixture of bromoethers 2 and 3 .	144
Figure 3.5	GC-MS chromatogram of aqueous bromine reaction with racemic linalool (1).	146
Figure 3.6	GC-MS chromatogram of V-BrPO catalyzed reaction with nerol (4).	147
Figure 3.7	EIMS of eight-membered cyclic bromoether product 5 .	149
Figure 3.8	GC-MS chromatograms of the bromination of nerol (4) by V-BrPO and aqueous bromine.	151
Figure 3.9	GC-MS chromatogram of V-BrPO catalyzed reaction with geraniol (6).	152
Figure 3.10	EIMS of monobrominated cyclized geraniol product 7 .	154
Figure 3.11	EIMS of monobrominated cyclized geraniol product 8 .	154
Figure 3.12	HPLC chromatograms of the bromination of geraniol (6) by V-BrPO and aqueous bromine.	157
Figure 3.13	GC-MS chromatogram of V-BrPO catalyzed reaction with geranyl acetate (9).	159
Figure 3.14	EIMS of monobrominated cyclized geranyl acetate product 10 .	160
Figure 3.15	EIMS of monobrominated cyclized geranyl acetate product 11 .	160
Figure 3.16	GC-MS chromatogram of V-BrPO catalyzed reaction with geranyl acetone (12).	163
Figure 3.17	EIMS of brominated bicyclic vinyl ether product 13 .	163
Figure 3.18	EIMS of α -snyderol (15).	166
Figure 3.19	EIMS of β -snyderol (16).	166
Figure 3.20	EIMS of γ -snyderol (17).	167

Figure 3.21	Chiral GC-MS analysis of β -snyderol (16).	170
Figure 3.22	Chiral GC-MS analysis of γ -snyderol (17).	171
Figure 3.23	One dimensional nOe of 3 β -bromo-8-epicaparrapi oxide (18), irradiation of 6.00 ppm signal.	174
Figure 3.24	Chiral GC-MS analysis of 3 β -bromo-8-epicaparrapi oxide (18).	175
Figure 3.25	HPLC chromatograms of the bromination of (+)-nerolidol (14) by V-BrPO and aqueous bromine.	177
Figure 3.26	GC-MS chromatogram of V-BrPO catalyzed reaction with <i>cis</i> -5-octene-1-ol (19).	179
Figure 3.27	EIMS of 6-membered cyclic bromoether product 20 .	179
Figure 3.28	GC-MS chromatogram of V-BrPO catalyzed reaction with <i>cis</i> -3-nonene-1-ol (21).	180
Figure 3.29	EIMS of 5-membered cyclic bromoether product 22 .	181
Figure 3.30	Competitive bromination of phenol red by V-BrPO as a function of geraniol (6) concentration.	182
Figure 3.31	Competitive bromination of phenol red by V-BrPO as a function of (+)-nerolidol (14) concentration.	183
Figure 3.32	Competitive bromination of phenol red by aqueous bromine as a function of (+)-nerolidol (14) concentration.	184
Figure 3.33	Halogenated C ₁₅ acetogenins, marine natural products from the red algal genus <i>Laurencia</i> .	186
Figure 3.34	Marine natural product thyransferyl acetate (26).	191
Figure 3.35	Halogenated marine natural products, monocyclofarnesanes (15), (16), and chamigranes (27).	193
Figure 4.1	Representative chemical structure of N-acyl homoserine lactones and halogenated furanones.	209
Figure 4.2	Bromination of phenol red by algal pieces of <i>Delisea pulcha</i>	217

Figure 4.3	Alignment of amino acid sequences for V-BrPO isoforms cloned from <i>Delisea pulchra</i> .	218
Figure 4.4	APCI mass spectrum of dibrominated-3-oxo-hexanoylhomoserine lactone 4 .	221
Figure 4.5	UV-visible spectrums of time-dependent bromination of 3-oxo-hexanoylhomoserine lactone (1) by partially purified V-BrPO.	222
Figure 4.6	APCI mass spectrum of α,α -dibromoethanoyl-2-(4-hydroxybutanoic acid (5)).	224
Figure 4.7	<i>Agrobacterium tumefaciens</i> bioassays: effects of V-BrPO bromination of 3-oxo-hexanoylhomoserine lactone (1) on the quorum sensing response.	229
Figure 4.8	^1H NMR of 5 <i>E</i> -bromomethylidenetetrahydro-2-furanone (3).	232
Figure 4.9	Structural comparison of 5 <i>E</i> -bromomethylidenetetrahydro-2-furanone (3) and synthetic halogenated furanone analogs.	233
Figure 5.1	Reaction scheme for the detection of nitric oxide (NO) by DAF-FM.	249
Figure 5.2	Plots of percent remaining activity vs. time at various azide concentrations.	251
Figure 5.3	Saturation kinetic plot of k_{obs} vs. azide concentration.	253
Figure 5.4	Plot of half-life of CoV-BrPO vs. reciprocal azide concentration.	254
Figure 5.5	Double reciprocal plot of k_{obs} vs. azide concentration.	256
Figure 5.6	Stoichiometry of azide binding to CoV-BrPO (Hill Plot).	257
Figure 5.7	Plot of percent remaining CoV-BrPO MCD activity vs. $[\text{azide}]/[\text{CoV-BrPO}]$.	259
Figure 5.8	Plot of percent remaining vulnerable CoV-BrPO MCD activity vs. $[\text{azide}]/[\text{CoV-BrPO}]$.	260
Figure 5.9	Plot of percent remaining CoV-BrPO activity vs. time in the presence of 0.25 mM bromide and various azide concentrations.	262

Figure 5.10	Plot of percent remaining <i>CoV</i> -BrPO activity vs. time in the presence of 0.5 mM bromide and various azide concentrations.	263
Figure 5.11	Plot of percent remaining <i>CoV</i> -BrPO activity vs. time in the presence of 2.5 mM bromide and various azide concentrations.	264
Figure 5.12(a)	Fluorescence emission spectra of DAF-FM in the presence of <i>CoV</i> -BrPO, azide, and HEPES buffer (pH 6.0).	266
Figure 5.12(b)	Fluorescence emission spectra of DAF-FM in the presence of <i>CoV</i> -BrPO, azide, bromide, hydrogen peroxide and HEPES buffer (pH 6.0).	266
Figure 5.13	Fluorescence emission spectrum of DAF-FM species in solution with <i>CoV</i> -BrPO, azide, hydrogen peroxide and HEPES buffer (pH 6.0).	267
Figure 6.1	Structures of amphiphilic marinobactins, aquachelins and mycobactins.	278
Figure 6.2	Structures of amphiphilic terrestrial siderophores.	280
Figure 6.3	Proposed structures of siderophores produced by the <i>Vibrio</i> sp. R-10.	282
Figure 6.4	HPLC chromatogram of ethanol extractable siderophores from the membrane of bacterial strain Roatan-10.	288
Figure 6.5 (a – d)	GC chromatograms of methyl esters extracted from the physiological mixture of amphibactins.	290
Figure 6.6 (a – h)	Mass spectrum of labeled GC peaks in Figure 6.5.	294
Figure 6.7	Proposed structure of amphibactin siderophores and their fatty acid appendages.	298
Figure 6.8	Mass spectrum of nonanal produced by ozonolysis of amphibactin-902.	299
Figure 6.9	Mass spectrum of methyl ester alkyl aldehyde species produced by ozonolysis of amphibactin-902.	299
Figure 6.10	HPLC chromatogram of amphibactin physiological mixture equilibrated with DMPC model membranes.	301

Figure 6.11	Partitioning curves for apo-amphibactins physiological mixture into large unilamellar DMPC vesicles.	303
Figure 6.12 (a – e)	Individual partitioning curves for apo-amphibactins-832, -848, -860, -886, -902.	304
Figure 6.13	Phylogenetic tree of siderophores producing bacteria based on maximum parsimony analysis of SSU rRNA DNA sequences.	308

LIST OF SCHEMES

Scheme 1.1	Overall reaction scheme for vanadium bromoperoxidase.	9
Scheme 1.2	Reaction scheme for the halogenation of monochlorodimedone.	9
Scheme 1.3	Proposed catalytic cycle for V-CIPO.	16
Scheme 1.4	Proposed catalytic cycle for V-BrPO.	34
Scheme 1.5	Reaction scheme for the bromination of 1,3- <i>di-tert</i> -butylindole by V-BrPO and aqueous bromine.	36
Scheme 1.6	Proposed biosynthetic scheme for the bromonium ion initiated cyclization of farnesyl pyrophosphate.	41
Scheme 1.7	Biomimetic syntheses of brominated marine natural products.	42
Scheme 1.8	Biomimetic bromination and cyclization of laurediol to laurencin and laureatin natural products.	44
Scheme 1.9	Proposed biosynthetic scheme for V-BrPO bromination and cyclization of monoterpenes geraniol and nerol.	46
Scheme 2.1	Schematic of V-BrPO reaction with bromide and hydrogen peroxide.	56
Scheme 2.2	Proposed catalytic cycle for vanadium-dependent haloperoxidases.	113
Scheme 2.3	Protonation of side-on bound peroxide moiety.	115
Scheme 3.1	Proposed pathway for bromonium-ion induced cyclization of sesquiterpenes.	126
Scheme 3.2	Proposed bromoetherification of laurediol by peroxidase enzymes.	127
Scheme 3.3	Bromination of 1,3- <i>di-tert</i> -butylindole by V-BrPO and aqueous bromine.	129
Scheme 3.4	V-BrPO catalyzed cyclization of linalool (1) to brominated	145

cyclic ethers **2** and **3**.

Scheme 3.5	Formation of nerol bromohydrin and epoxide species.	148
Scheme 3.6	V-BrPO catalyzed bromination and cyclization of nerol (4).	149
Scheme 3.7	V-BrPO catalyzed bromination and cyclization of geraniol (6).	155
Scheme 3.8	V-BrPO catalyzed bromination and cyclization of geranyl acetate (9).	161
Scheme 3.9	V-BrPO catalyzed bromination and cyclization of geranyl acetone (12).	164
Scheme 3.10	V-BrPO catalyzed bromination and cyclization of (+)-nerolidol (14) to α -snyderol (15), β -snyderol (16), and γ -snyderol (17).	172
Scheme 3.11	V-BrPO catalyzed bromination and cyclization of (+)-nerolidol (14) to 3 β -bromo-8-epicaparrapi oxide (18).	173
Scheme 3.12	V-BrPO catalyzed bromination and cyclization of <i>cis</i> -5-octen-1-ol (19).	180
Scheme 3.13	V-BrPO catalyzed bromination and cyclization of <i>cis</i> -3-nonen-1-ol (21).	181
Scheme 3.14	Mechanism of bromoetherification for production of laurencin (23) marine natural product.	187
Scheme 3.15	Kinetic resolution of racemic linalool (1) by V-BrPO.	189
Scheme 3.16	Biomimetic bromination and cyclization of geranyl acetate (9).	195
Scheme 3.17	Proposed stabilization of monocyclofarnesyl pyrophosphate cation by internal oxygen nucleophile.	195
Scheme 3.18	Proposed biosynthetic pathway to chamigrene skeleton (27) via tetrasubstituted monocyclofarnesane intermediate (30).	198
Scheme 3.19	Cyclization mechanism for (+)-nerolidol (14) leading to the observed stereochemistry of 3 β -bromo-8-epicaparrapi oxide (18).	198

Scheme 4.1 Proposed bromination pathway of 3-oxo-hexanoylhomoserine lactone (**1**) by V-BrPO. 226

LIST OF TABLES

Table 1.1	Kinetic parameters for V-BrPO catalyzed bromination of MCD or bromide assisted disproportionation of hydrogen peroxide.	25
Table 2.1	Primer sequences used in RT-PCR reactions.	62
Table 2.2	Kinetic parameters for V-BrPO obtained from the rates of MCD bromination and triiodide formation.	86
Table 4.1	List of <i>Delisea pulchra</i> /V-BrPO reactions used in <i>Agrobacterium tumefaciens</i> quorum sensing bioassays.	214
Table 4.2	Results from <i>Agrobacterium tumefaciens</i> bioassays.	228
Table 5.1	Table of calculated k_{obs} for azide inactivation of CoV-BrPO in the presence of bromide.	265
Table 6.1	Partition coefficients for the physiological mixtures of amphibactins and marinobactin siderophores in DMPC vesicles.	306

LIST OF ABBREVIATIONS

AHL	Acyl homoserine lactone
APCI	Atmospheric pressure chemical ionization
APT	Attached proton test
BCA	Bicinchoninic acid
BSA	Bovine serum albumin
CPO	Chloroperoxidase
DAF-FM	4-amino-5-methylamino-2',7'-difluorescein
ddH ₂ O	Doubly deionized water
DEAE	Diethylaminoethyl
DMPC	1,2-Dimyristoyl-sn-glycero-3-phosphocholine
EDTA	Ethylenediamine tetraacetic acid
EIMS	Electron ionization mass spectrometry
ESI	Electrospray mass spectrometry
ESR	Electron spin resonance
EXAFS	Extended X-ray absorption fine structure
FAB-MS	Fast atom bombardment mass spectrometry
FAME	Fatty acid methyl ester
GC-MS	Gas chromatography mass spectrometry
HDTMA	Hexadecyl-trimethylammonium bromide
HEPES	N-2-hydroxyethyl piperazine-N2-ethane sulfonic acid
HOCl	Hypochlorous acid
HPLC	High performance liquid chromatography
HRMS	High resolution mass spectrometry
HRP	Horseradish peroxidase
HSL	Homoserine lactone
IPO	Iodoperoxidase
IR	Infrared spectrometry
LPO	Lactoperoxidase
LUV	Large unilamellar vesicles
MCD	Monochlorodimedone
MHz	Mega hertz
MS-MS	Tandem mass spectrometry
nOe	Nuclear overhauser effect
NMR	Nuclear magnetic resonance
NSW	Natural seawater
ppm	parts per million
ROS	Reactive oxygen species
RPHPLC	Reversed-phase high performance liquid chromatography
SDS-PAGE	Sodium dodecylsulfate polyacrylamide gel electrophoresis
SOD	Superoxide dismutase
SUV	Small unilamellar vesicles

TBCO	2,4,4,6-tetrabromocyclohexa-2,5-dienone
TFA	Trifluoroacetic acid
TLC	Thin layer chromatography
Tris	Tris(hydroxymethyl)-aminomethane
TOF	Time-of-flight
V-BrPO	Vanadium bromoperoxidase
V-ClPO	Vanadium chloroperoxidase

Chapter One

Introduction

Bioinorganic role of vanadium:

Vanadium is widely present as a trace metal in the earth's soil, rivers, lakes, and oceans (Nriagu 1998). Vanadium exists in a wide range of oxidation states including -3, -1, and 0, +1, +2, +3, +4 and +5. Vanadium present in the earth's crust exists in the oxidation states III, IV, and V, and has a relative abundance of 135 ppm. In the world's oceans vanadium is the second most abundant transition metal ion at 30 – 50 nM after molybdenum (100 nM) (Collier 1984). In biological systems vanadium in the oxidation states III, IV and V have been identified, where the oxyanion vanadate(V) ($\text{HVO}_4^{2-} / \text{H}_2\text{VO}_4^-$; pKa 8.3) is the most common and stable species in aqueous solution at neutral pH. Vanadate is the most stable species in aqueous conditions at neutral pH, lower oxidation states do exist where the nature of coordinating ligands increase the stability of lower oxidation states. Vanadium can easily switch between oxidation states III, IV, and V at neutral pH, with reduction potentials of 0.99 V (vs. NHE) for vanadium(V) and 0.542 for vanadium(IV) (Butler 1990).

The ability of vanadium to interconvert between oxidation states allows this transition metal to function in an electron transfer capacity in biological systems. For example, Rush and Bielski showed that vanadium cycling between V(IV) (VO^{+2}) and V(V) (VO^{+3}) could catalyze the disproportionation of superoxide to dioxygen and hydrogen peroxide at pH 0 (Rush and Bielski 1985). The vanadium

system is not as efficient as the well known Cu,Zn-SOD system (i.e., $k \sim 10^4 \text{ M}^{-1} \text{ sec}^{-1}$ versus $10^9 \text{ M}^{-1} \text{ sec}^{-1}$ for Cu,Zn-SOD), but nevertheless exhibits a significant rate enhancement over the self-disproportionation of superoxide. In addition, the reactivity of vanadium peroxide complexes with halides is relevant to the mechanism of vanadium haloperoxidases (VHPOs). Biomimetic reactions with vanadium(V) complexes of $\text{HPS}^{2-}\text{VO}(\text{OH})$ coordinate hydrogen peroxide, forming a monoperoxospecies $(\text{HPS})\text{VO}(\text{O}_2)^-$. The monoperoxo species is able to oxidize bromide catalytically in the presence of acid (Clague et al. 1993).

An interesting feature of vanadium with respect to biological systems is the relationship between vanadate and phosphate (H_2VO_4^- and HPO_4^{2-}) at physiological pH. Vanadate is a known inhibitor of phosphate metabolizing enzymes (i.e., phosphatases, kinases, and ribonucleases), as well as acting to stimulate enzymes such as phosphomutases and isomerases (Mendz 1991; Rehder 1995; Littlechild et al. 2002). In addition, the active sites of vanadium-dependent haloperoxidases have sequence homology to acid phosphatases (Hemrika et al. 1997; Littlechild et al. 2002). Also, remetallation experiments of apo-haloperoxidases are inhibited by phosphate containing buffers (Soedjak et al. 1991b).

Living systems which accumulate vanadium include several genera of tunicates (order Ascidiacea), which acquire vanadate from seawater through phosphate and sulfate channels (Taylor et al. 1997). It is believed that vanadate is reduced to V(III) aided by organic compounds called tunicromes, which are modified peptide units consisting of hydroxyldopa residues [Figure 1.1] (Frank et al.

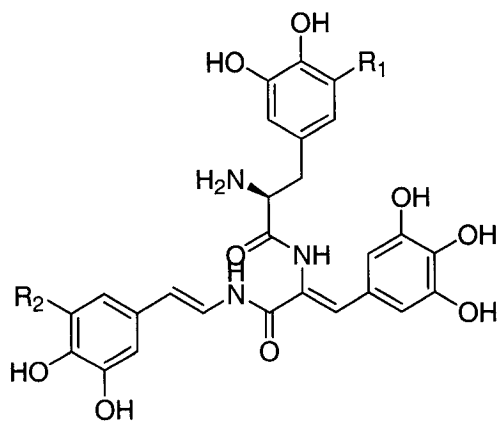
1995). Certain species of *Amanita* mushrooms are also known to accumulate vanadium. In this system, vanadium exists as a complex of non-oxo vanadium(IV) ligated to a carboxylate and side on bound hydroxylamido functionalities by compounds named amavadin [Figure 1.1] (Berry et al. 1999). The function of amavadin is still unclear.

Vanadium enzymes:

Biological systems have also evolved a wide variety of metalloenzymes.

Vanadium nitrogenase. Nitrogenases are microbial enzymes that reduce dinitrogen to ammonia coupled to the hydrolysis of MgATP. The nitrogenase enzyme is a two-component system consisting of a dinitrogenase made up of one of the Mo-Fe, Fe-only, or V-Fe cofactors and a dinitrogenase iron reductase that supplies electrons to the nitrogenase protein. The reductase donates electrons by docking with the nitrogenase and transfers electrons, one at a time, in a MgATP-dependent reaction. The vanadium nitrogenase has been purified from several species within the Azotobacteriaceae family, including *Azobacter vinelandii*, *A. chroococcum* and *A. paspali* (Robson et al. 1986; Hales et al. 1986a; Hales et al. 1986b; Fallik et al. 1993; Ruttimann-Johnson et al. 1998). Although all wild type nitrogen fixing organisms contain the Mo-nitrogenase, genetic and physiological studies revealed that the V-nitrogenase is made and active when molybdenum is a limiting nutrient or at temperatures below 30 °C (Miller and Eady 1988).

a



An-1 $R_1 = R_2 = \text{OH}$
An-2 $R_1 = \text{H}, R_2 = \text{OH}$
An-3 $R_1 = R_2 = \text{H}$

b

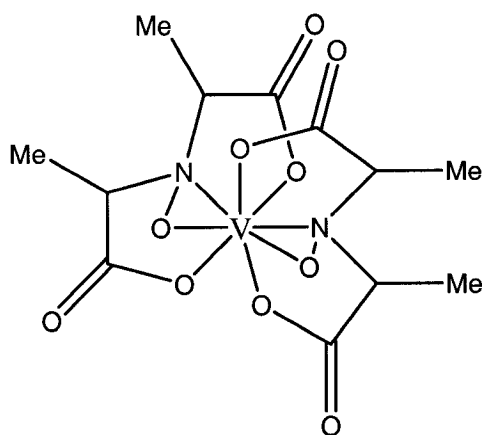
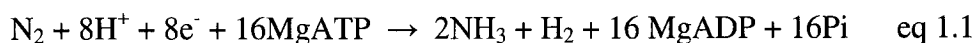


Figure 1.1: Biologically important vanadium compounds (a) tunichromes, “An” refers to species of *Ascidia* from which the tunichromes were isolated (b) Amavadin from *Amanita* mushrooms. Structure redrawn from (Rehder 2003).

The overall stoichiometry of dinitrogen reduction catalyzed by V-nitrogenase is the following:



In addition to the production of hydrogen in the above reaction, the V-nitrogenase also produces small amounts of hydrazine during catalytic turnover (Dilworth and Eady 1991). V-nitrogenase also reduces other substrates such as isonitriles and acetylene, similar to the Mo-nitrogenase enzymes (Gailus et al. 1994).

The structural genes for V-nitrogenase from *A. vinelandii* and *A. chroococcum* have been cloned and sequenced (Robson et al. 1989; Joerger et al. 1990). The dinitrogenase reductase for the vanadium system is similar to the molybdenum reductase. These enzymes share 95% amino acid sequence identity. The reductase is a homodimer of 64,000 Da and contains one iron ferredoxin cluster [4Fe-4S] and two binding sites for Mg^{2+}ATP (Joerger et al. 1990). The V-Fe metal site is located in the dinitrogenase protein of the two-component system. The quaternary structure of the dinitrogenase is an $\alpha_2\beta_2\gamma_2$ hexamer of 240,000 Da (Chatterjee et al. 1997), similar to the $\alpha_2\beta_2$ tetramer of Mo-nitrogenase (230,000 Da). The α and β subunits for the V-nitrogenase share 33% and 31% amino acid identity to the α and β subunits of the Mo-nitrogenase complex (Allen et al. 1993). The dinitrogenase component of the vanadium-dependent enzyme contains two P-clusters and two M-clusters. The P-clusters bridge the interfaces of the α and β subunits and are Fe_8S_8 sulfide-bridged

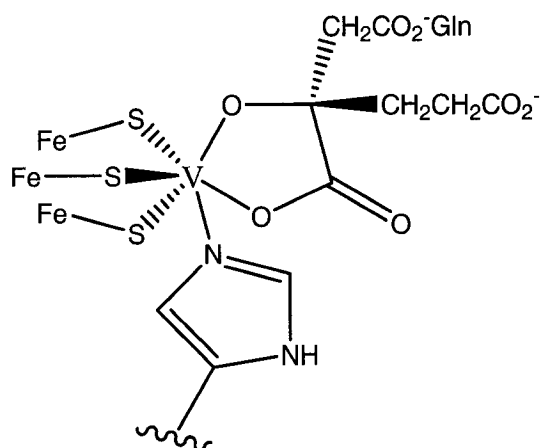
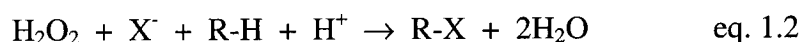


Figure 1.2: Proposed structure of the M cluster of the vanadium-containing dinitrogenase. Structure redrawn from (Rehder 2003).

double cubanes (Arber et al. 1989). The P-clusters of the V- and Mo-nitrogenases appear to be identical. The M clusters (MFe_7S_9 , with M being V or Mo) are located in the α -subunits and are believed to be the site of the Fe-V cofactor. The absolute structure of the vanadium metal site has not yet been determined, but data from magnetic circular dichroism (Morningstar et al. 1987), EXAFS (Arber et al. 1987; Chen et al. 1993) and Mossbauer (Ravi et al. 1994) suggest that it is similar to the $MoFe_7S_9$ cofactor. It is proposed that vanadium is part of an iron-sulfur system, linked to three iron centers by three bridging sulfides, and coordinated to a histidine, and the alkoxide and carboxylate moieties of homocitrate [Figure 1.2] (George et al. 1988; Arber et al. 1989; Harvey et al. 1990).

There are many questions surrounding the V-nitrogenase system, most of which are concerned with vanadium. Questions such as how vanadium enters the cell, the oxidation state of vanadium, and the mechanism by which the vanadium is incorporated (chaperones, vanadium storage proteins/insertases) during Fe-V cofactor synthesis are all being pursued.

Vanadium haloperoxidases. Vanadium haloperoxidases catalyze the oxidation of halides (iodide, bromide, chloride) by hydrogen peroxide. Vanadium haloperoxidases are classified according to the most electronegative halogen oxidized. Thus vanadium chloroperoxidases (V-ClPO) can oxidize chloride, bromide and iodide, and vanadium bromoperoxidases (V-BrPO) can oxidize bromide and iodide. Hydrogen peroxide does not have the driving force to oxidize fluoride, therefore there are no known fluoroperoxidase enzymes. The overall reaction that vanadium haloperoxidases catalyze is (equation 1.2):

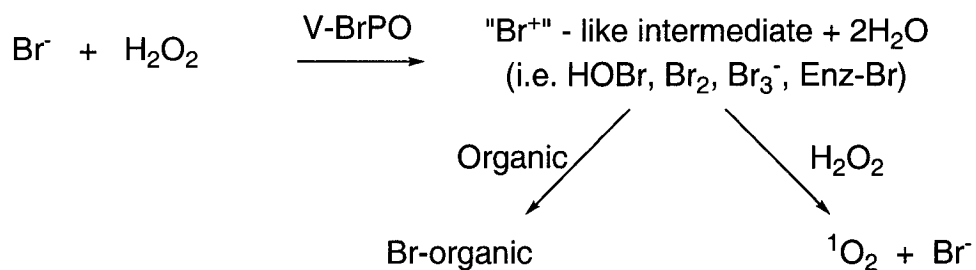


where X^- is chloride, bromide or iodide and R-H is an organic substrate. For optimal halogenation, 1 mol of halide is oxidized by 1 mol of hydrogen peroxide, producing 1 mol of halogenated organic substrate (Everett and Butler 1989; Butler 1998a). In the absence of R-H, more than 1 mol hydrogen peroxide is consumed. In the absence of RH the oxidized halogen intermediate reduces a second equivalent of

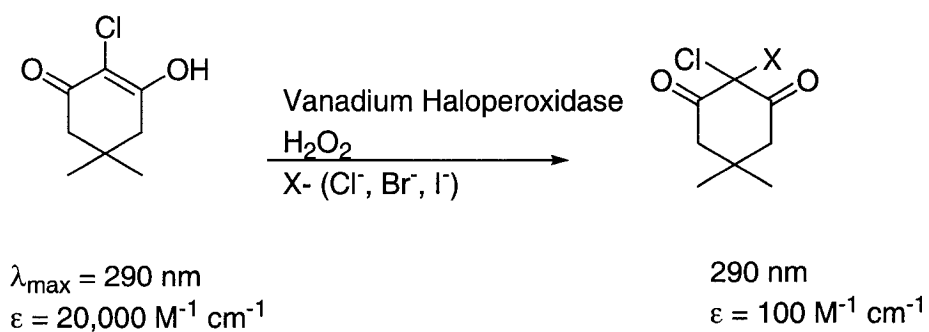
hydrogen peroxide, producing singlet oxygen and halide (Scheme 1.1) (Everett et al. 1990a).

The standard activity assay for vanadium haloperoxidase is the halogenation of monochlorodimedone (MCD; 2-chloro-5,5-dimethyl-1,3-dimedone) using hydrogen peroxide and halide (Hager et al. 1966). The halogenation of MCD is measured spectrophotometrically at 290 nm. The assay monitors the loss of MCD in the enol form ($\epsilon = 20,000 \text{ M}^{-1} \text{ cm}^{-1}$) (Scheme 1.2). Vanadium haloperoxidase activity is expressed as micromoles of MCD halogenated per minute per milligram of enzyme. Kinetic characterization of V-ClPOs and V-BrPOs has been performed using this assay. Also, MCD is not a natural substrate for vanadium-dependent haloperoxidase enzymes, and may not be useful for quantitating haloperoxidase activity for all enzymes.

Vanadium chloroperoxidase. The most studied vanadium chloroperoxidase (V-ClPO, E.C. 1.11.1.10) is from the fungi *Curvularia inaequalis*. *C. inaequalis* is a phytopathogen and during its life cycle must penetrate the cell wall of the host plant. There are no reports of halogenated natural products produced by *C. inaequalis*. It has therefore been proposed that the role of V-ClPO is to produce hypochlorous acid (HOCl) to aid in the degradation of the plant's cell wall.



Scheme 1.1: Overall reaction scheme for vanadium bromoperoxidase. The oxidized halide intermediate partitions between bromination of an appropriate organic acceptor or the bromide-assisted disproportionation of H_2O_2 to produce singlet O_2 .



Scheme 1.2: Reaction scheme for the halogenation of monochlorodimedone (MCD) by vanadium haloperoxidases.

V-CIPO Kinetics of chlorination. Under steady state catalytic conditions V-CIPO will oxidize chloride by hydrogen peroxide to produce HOCl, which can be separated from the reaction solution by ultrafiltration or detected spectrophotometrically (λ_{max} of 245 and 315 nm) (Van Schijndel et al. 1994). Optimal chloroperoxidase activity is detected in the pH range of 5.0 - 6.0. The MCD chlorination kinetics proceed by a bi bi ping pong mechanism, similar to V-BrPO catalyzed reactions with bromide (see below). The $K_m^{\text{H}_2\text{O}_2}$ and $K_m^{\text{Cl}^-}$ at optimal pH are 10 μM and 1 mM, respectively (Van Schijndel et al. 1993). The $K_m^{\text{H}_2\text{O}_2}$ is pH dependent, and the $\log K_m$ for H_2O_2 is linearly dependent on pH with a slope of -1 . The pH dependence on the K_m of H_2O_2 is proposed to reflect the need for protons to form the oxidized halogen intermediate HOCl (Hemrika et al. 1999). Chloride can act as was detected at lower pH values (below pH 4) with a $K_i^{\text{Cl}^-} = 6 \text{ mM}$. Above pH 4.0, mixed type inhibition of chloride is observed at higher concentrations ($K_i^{\text{Cl}^-} = 70 \text{ mM}$) (Van Schijndel et al. 1994).

V-CIPO structure determination and proposed mechanism. The structural gene for V-CIPO (*C. inaequalis*) has been cloned and sequenced. V-CIPO is a 67,488 Da protein containing 609 amino acid residues (Simons et al. 1995). The crystal structure for native V-CIPO (2.03 Å resolution) and in complex with azide (2.1 Å resolution) revealed the quaternary structure of the protein and the architecture and coordination of the vanadium-binding site (Messerschmidt and Wever 1996). V-CIPO has an overall cylindrical shape with a length of 80 Å and a diameter of 55 Å. The secondary structure is composed mainly of α -helices (20

helices) and with 6 short β -strands [Figure 1.3]. Two four-helix bundles are the main structural motifs (Messerschmidt and Wever 1996). The vanadium-binding site is located on the top of one of the four-helix bundles, where all of the residues building up the metal site are from the C-terminal half of the protein. The vanadium is positioned at the bottom of a broad channel lined on one half with polar residues and water molecules, and the other half with hydrophobic residues (Pro-47, Pro-211, Tyr-350, Phe-393, Pro-395, Pro-396, Phe-397). The broad active site channel supplies adequate access and release of substrates and products during V-CIPO turnover (Messerschmidt and Wever 1996).

Difference electron density maps of native V-CIPO show the vanadium bound to four oxygen atoms forming an orthovanadate group and to the N ^{ϵ 2} nitrogen atom of histidine-496. The vanadium coordination geometry is trigonal bipyramidal with vanadate oxygen atoms in the equatorial plane (bond lengths ~ 1.65 Å), one axial histidine ligand (His-496) (bond length ~ 1.96 Å), and an apical oxygen atom (bond length ~ 1.93 Å) of a proposed hydroxide ligand (Messerschmidt and Wever 1996). The oxygen atoms of the vanadate cofactor are all hydrogen-bonded to amino acid side chains or the peptide backbone of the protein, reducing negative charge around the metal center [Figure 1.4]. Amino acids involved in charge neutralization of the equatorial vanadate oxygens include Arg-360, Arg-490, Lys-353, Gly-403, and

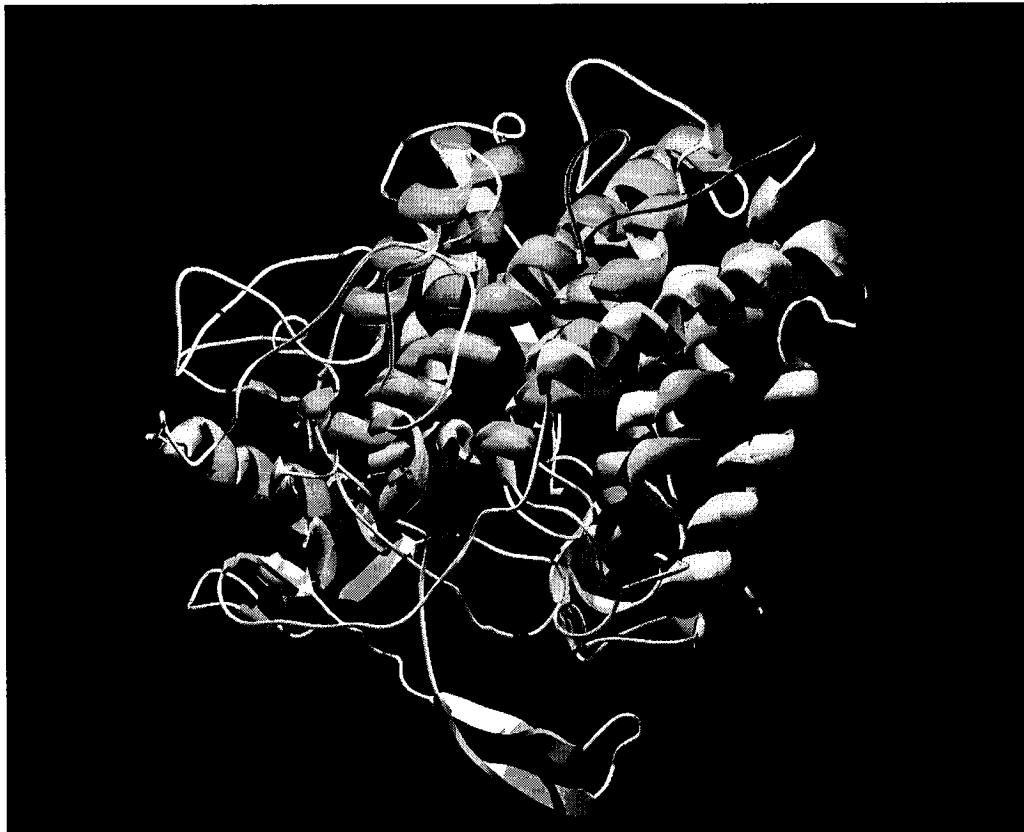


Figure 1.3: Ribbon-type representation of V-CIPO structure from *Curvularia inaequalis*. Structure drawn in Swiss-PDB viewer and rendered with gl_render and POV-ray software.

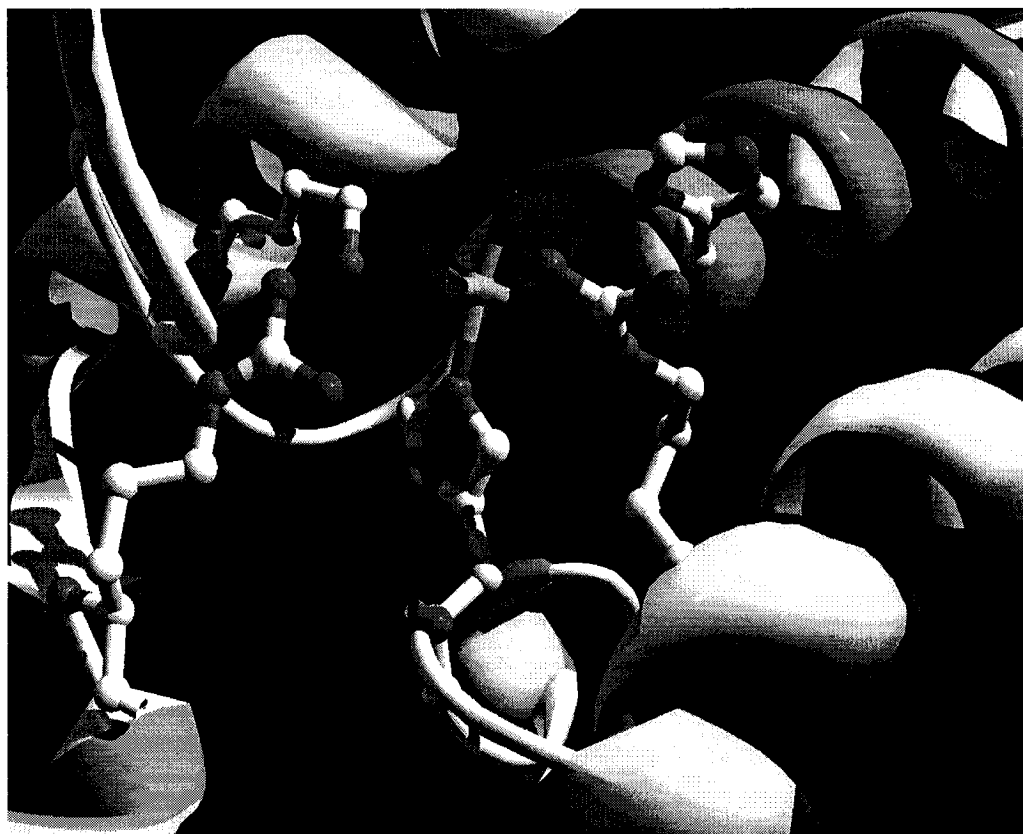


Figure 1.4: Vanadium site of V-ClPO (*Curvularia inaequalis*). Structure drawn in Swiss-PDB viewer and rendered with gl_render and POV-ray software.

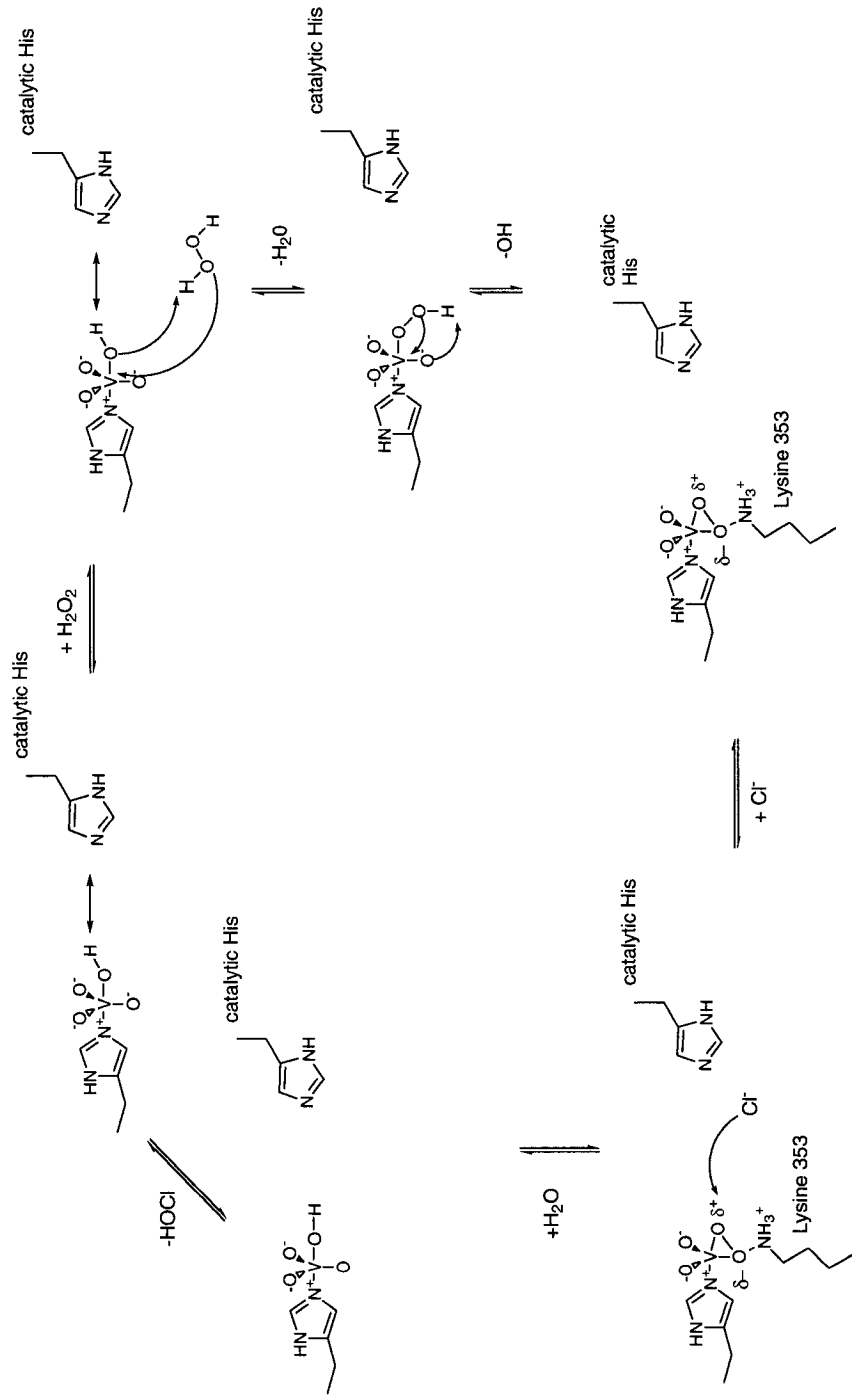
Ser-402. Histidine-404 is hydrogen-bonded to the apical hydroxide ligand.

The third structure of V-CIPO solved is the peroxide-bound intermediate (Messerschmidt et al. 1997). The difference electron density map demonstrates that the peroxide binds vanadium side-on in the equatorial plane with release of the apical vanadate oxygen. The vanadium monoperoxo intermediate has 5 direct ligands with coordination geometry of a distorted tetragonal pyramid. The apical ligand is identified as an oxygen with a bond length of 1.60 Å, identifying this as a vanadium-oxide. In addition, the structure shows that His-404 is no longer coordinated to the vanadate cofactor and Lys-353 is now hydrogen-bonded to one of the oxygens of the side-on bound peroxide [Figure 1.5] (Messerschmidt et al. 1997).

Based on kinetic characterization and X-ray crystal structures of the native and peroxide bound intermediate of V-CIPO a minimum catalytic mechanism has been proposed (Scheme 1.3, adapted from (Hemrika et al. 1999)). Vanadium is covalently linked to His-496 and acts as a Lewis acid to the first substrate in the catalytic cycle, hydrogen peroxide. Hydrogen peroxide is side-on bound as observed in the structure of the peroxide bound intermediate (Messerschmidt et al. 1997). The negative charge around the monoperoxo-vanadate intermediate is compensated by hydrogen bonds from positively charged residues in the active site. The hydrogen bond between Lys-353 and the bound peroxide is proposed to polarize the peroxide bond making it more susceptible to nucleophilic attack chloride (Hemrika et al. 1999).



Figure 1.5: Monoperoxovanadium (V) site of V-CIPO, *Curvularia inaequalis*. Structure drawn in Swiss-PDB viewer and rendered with gl_render and POV-ray software.



Scheme 1.3: Proposed catalytic cycle for V-CIPO, *Curvularia inaequalis* (adapted from (Henrika, et al. 1999)).

The oxidized chloride (OCl) species can then acquire a proton from an incoming water molecule to form hypochlorous acid, where the deprotonated water molecule occupies the empty coordination site on vanadium, regenerating the native structure (Scheme 1.3) (Simons et al. 1995; Messerschmidt et al. 1997; Hemrika et al. 1999)

V-CIPO active site mutants. Several structures of site-directed mutants of V-CIPO are known (Macedo-Ribeiro et al. 1999). The mutants were constructed to modify the axial histidine ligated to vanadium (H496A), the putative acid-base histidine (H404A), one of the arginines involved in charge neutralization of the vanadium cofactor (R360A), and an aspartic acid which makes a salt bridge with an active site arginine (R490) (D292A). The overall protein backbone of the mutants are the same as that of native V-CIPO, and are superimposable on one another except in certain regions of the vanadium binding site, as discussed below (Messerschmidt and Wever 1996; Hemrika et al. 1999; Macedo-Ribeiro et al. 1999)

Mutant H496A. The substitution of the histidine ligand H496 by alanine does not prevent vanadate coordination; however, H496A lacks haloperoxidase activity. Vanadate is coordinated as a tetrahedral anion with three non-protein oxygen ligands at 1.56 Å and one non-protein oxygen ligand at 1.67 Å. All of the side chain residues that hydrogen-bond to the vanadium center in the native structure also form hydrogen bonds in the H496A structure, including the hydrogen bond between His-404 and the apical oxygen of the vanadate ion. Superposition of the vanadium site of H496A on the structure of the wild-type V-CIPO vanadium site shows the differences in the coordination geometries of the

vanadium [Figure 1.6]. The superposition demonstrates the remarkable rigidity of the amino acids that frame the anion-binding site.

Mutant H404A. The most significant change in the structure of mutant H404A is the broken salt bridge between Arg-490 and Asp-292 [Figure 1.7]. Arg-490 moves into the place of His-404, and assumes hydrogen-bonding interactions between other side chain residues in place of the vanadate oxygen atoms in the native structure. Vanadium remains coordinated to His-496 (1.96 Å). The apical O atom sits 2.0 Å from the vanadium, corresponding to a mixture of water or hydroxide ligation, and the equatorial O atoms remain at 1.60 Å. The removal of His-404 abolishes chlorinating activity, which may be a result of the loss of the histidine residue or rearrangements in the active site.

Mutant 292A. Asp-292 forms a salt bridge with Arg-490 and helps to orient the side chain of Arg-490 so that it can hydrogen bond with two vanadate oxygen atoms at Nⁿ and N^e. In the mutant D292A there is little effect on the structure [Figure 1.8]. His-496 remains ligated to the vanadate ion, and vanadate remains in hydrogen-bonding contact with Lys-353, Ser-402, the amide backbone of Gly-403, Arg-360, and Arg-490. Despite the similarity to native V-CIPO, D292A has only 2% of the native enzyme activity.

Mutant R360A. In the native structure arginine-360 is directly involved in charge neutralization of the HVO_4^- center through a single hydrogen bond to one of the vanadate oxygen atoms. In mutant R360A, one might expect

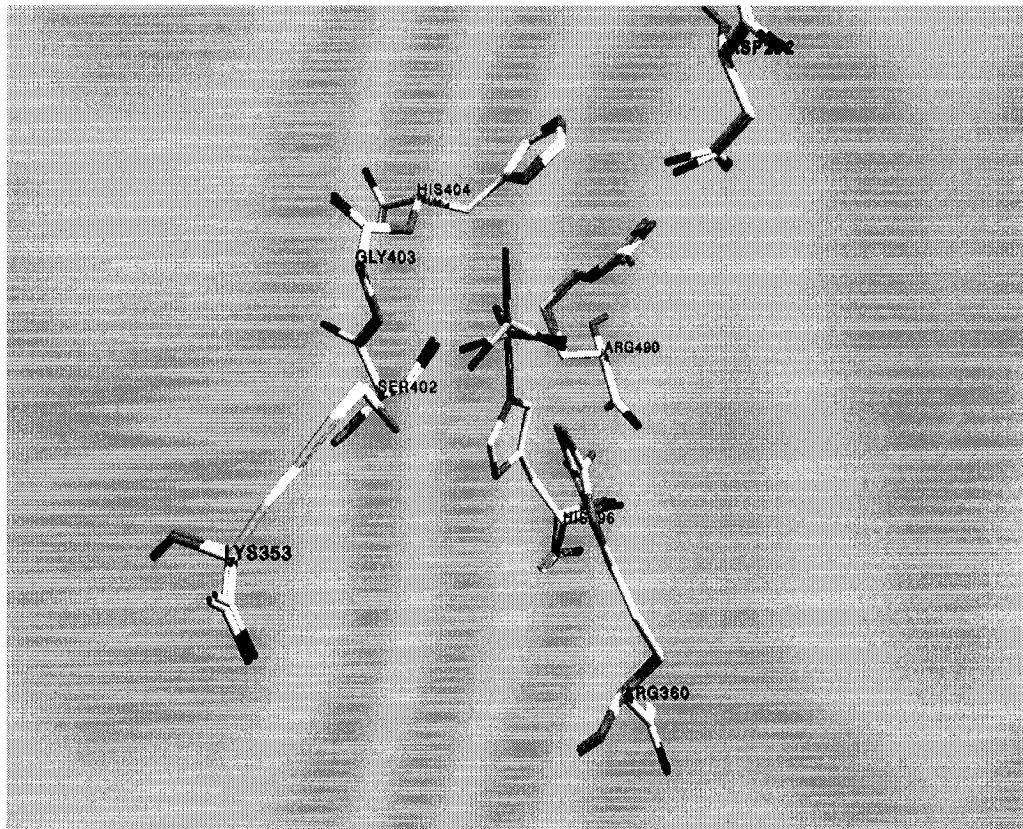


Figure 1.6: Overlay of X-ray coordinates of the vanadium site of wild-type V-CIPO (*C. inaequalis*) and mutant H496A. Structure drawn in Swiss-PDB viewer and rendered with gl_render and POV-ray software.

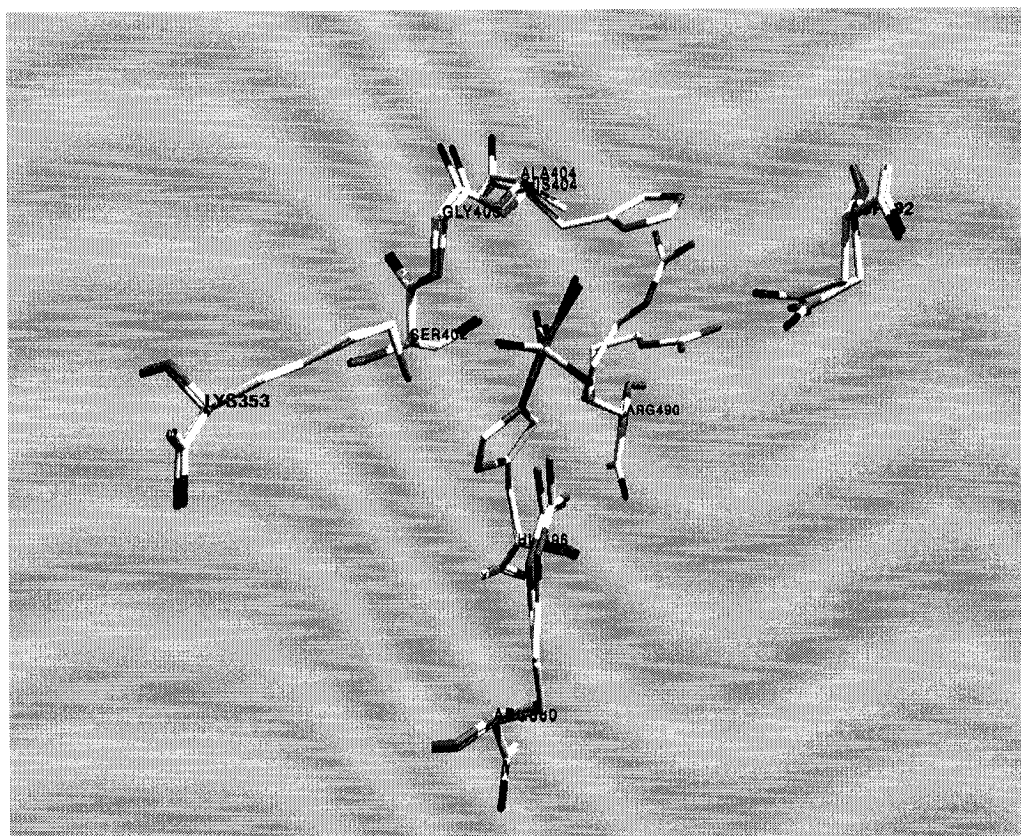


Figure 1.7: Overlay of X-ray coordinates of the vanadium site of wild type V-CIPO (*C. inaequalis*) and mutant H404A. Structure drawn in Swiss-PDB viewer and rendered with gl_render and POV-ray software.

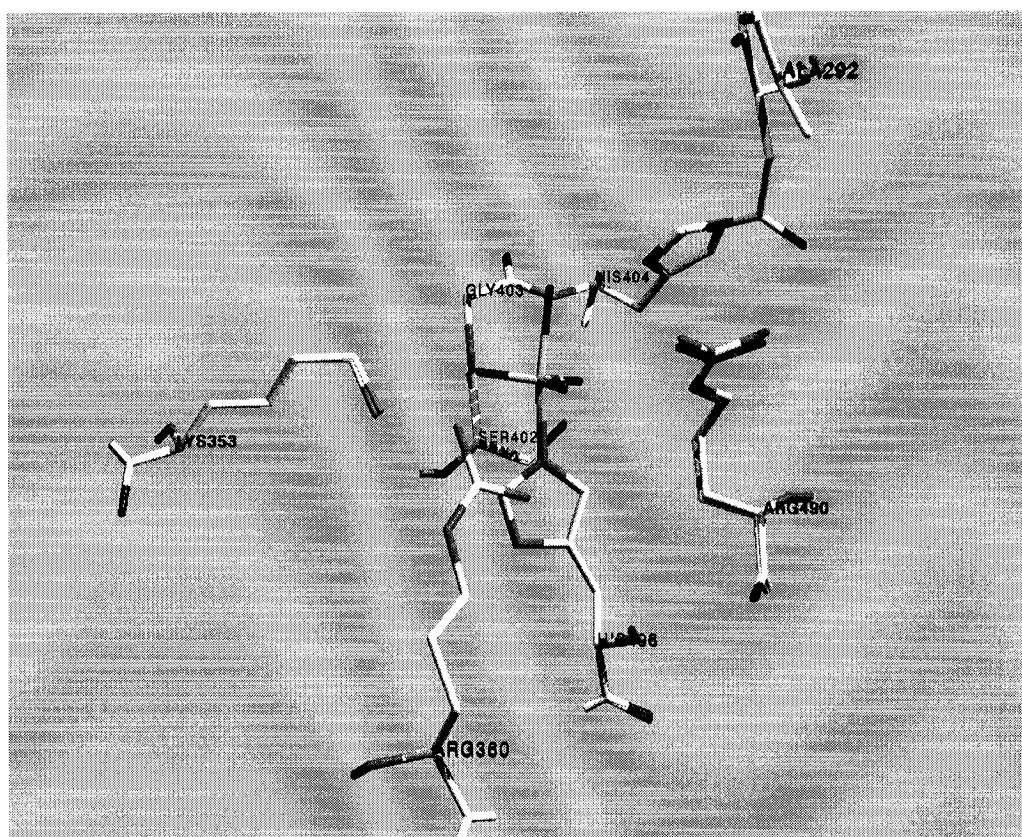


Figure 1.8: Overlay of X-ray coordinates of the vanadium site of wild type V-CIPO (*C. inaequalis*) and mutant D292A. Structure drawn in Swiss-PDB viewer and rendered with gl_render and POV-ray software.

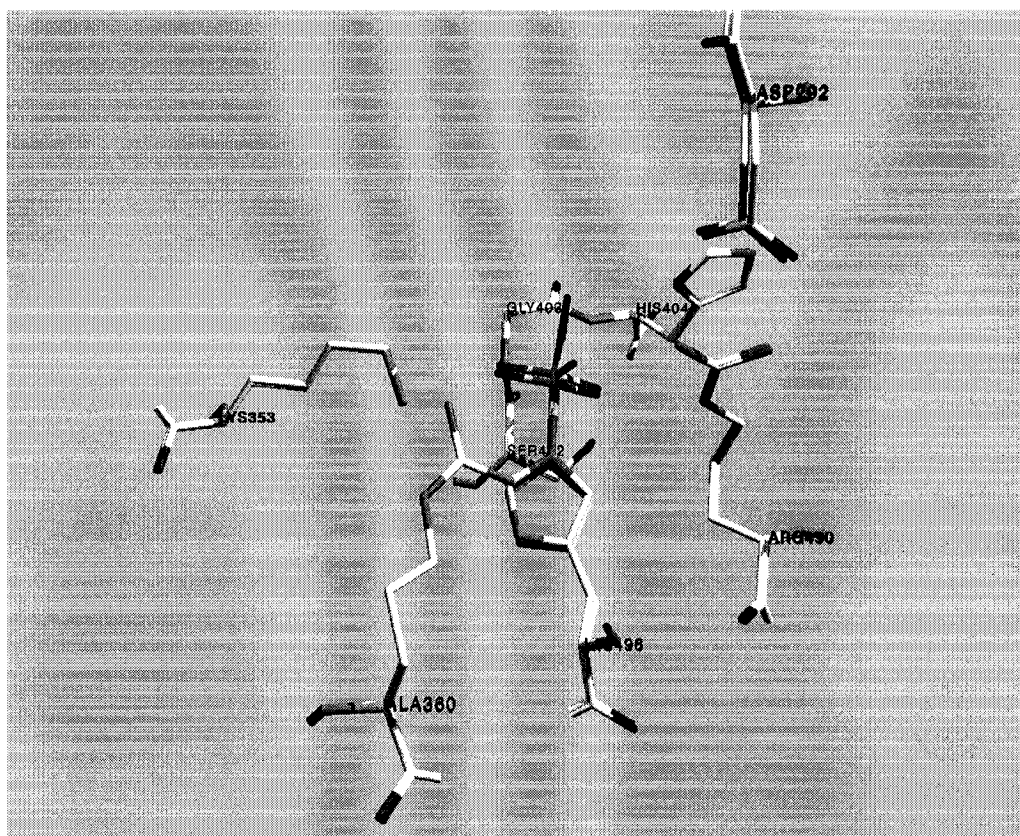


Figure 1.9: Overlay of X-ray coordinates of the vanadium site of wild type V-CIPO (*C. inaequalis*) and mutant R360A. Structure drawn in Swiss-PDB viewer and rendered with gl_render and POV-ray software.

a significant reorientation around vanadium in order to achieve charge neutralization as a result of the change in charge compensation. Somewhat surprisingly, however, the superposition of the vanadium site of R360A on the native V-CIPO shows little change in the position of the residues other than the lack of Arg-360 [Figure 1.9].

It is surprising how similar the overall structures of native V-CIPO and the active site mutants are; yet seemingly small changes affect significant consequences in reactivity (Hemrika et al. 1999).

Vanadium bromoperoxidase. Vanadium bromoperoxidase has been isolated from all major classes of marine algae, including chlorophyta (green algae), phaeophyta (brown algae) and rhodophyta (red algae). In some marine algae V-BrPO is thought to be involved in the biosynthesis of halogenated secondary metabolites. Halogenated compounds from marine organisms range from halogenated indoles, terpenes, acetogenins, and phenols, to volatile halogenated hydrocarbons (e.g., bromoform, chloroform, bromomethane, etc.), which are produced on a very large scale (Gshwend 1989; Faulkner 1998; Gribble 1998). Many halogenated compounds isolated from marine algae have important biological activities, such as antimicrobial properties, and feeding deterrent properties, suggesting that they play a defensive role in the marine organism. In many cases the halogenated compounds are also of pharmaceutical importance due to their antimicrobial, antifungal, antiviral, and anti-inflammatory activities.

V-BrPO kinetics of bromination. Steady state kinetics of MCD bromination and dioxygen formation has been well characterized for V-BrPO from many

different marine algae, most notably V-BrPO from the brown alga *Ascophyllum nodosum* (de Boer and Wever 1988; Everett and Butler 1989; Everett et al. 1990a; Everett et al. 1990b; Soedjak and Butler 1991a; Soedjak et al. 1995). V-BrPO catalyzes the oxidation of bromide by hydrogen peroxide by a substrate inhibited bi bi ping pong steady state mechanism, in which both bromide and hydrogen peroxide also act as inhibitors at certain pH's (de Boer and Wever 1988; Everett et al. 1990b). The kinetic parameters for different V-BrPOs is shown in Table 1.1 obtained from the rates of dioxygen formation or MCD bromination reactions (Itoh et al. 1987; Everett et al. 1990a; Soedjak and Butler 1991a; Carter et al. 2002). Kinetic constants for *A. nodosum* obtained from both MCD bromination rates and bromide-assisted disproportionation of H₂O₂ clearly indicated that the rate-determining step for both reactions is the same via a common intermediate (Scheme 1.1)(Everett et al. 1990a). The $K_m^{H_2O_2}$ is highly pH dependent, where V-BrPO has a higher affinity for H₂O₂ at higher pH values (pH 5 – pH 6) (Everett et al. 1990a). Bromide functions as both a substrate and a noncompetitive inhibitor of hydrogen peroxide binding at higher bromide concentrations (250 – 500 mM). Hydrogen peroxide also acts as a noncompetitive inhibitor of V-BrPO (Soedjak et al. 1995). Inhibition by hydrogen peroxide is pH dependent, and independent of bromide binding, with more inhibition observed at higher pHs. Hydrogen peroxide inhibition is fully reversible under steady state conditions.

V-BrPO	$K_m^{\text{Br}^{\text{a}}}$	$K_m^{\text{H}_2\text{O}_2^{\text{a}}}$	$K_m^{\text{Br}^{\text{b}}}$	$K_m^{\text{H}_2\text{O}_2^{\text{b}}}$
<i>A. nodosum</i> ^c	25.8 mM	113 μM	19.2 mM	94 μM
<i>M. pyrifer</i> ^c	--	--	21.2 mM	120 μM
<i>F. distichus</i> ^c	--	--	1.74 mM	18 μM
<i>C. officinalis</i> ^c	1.0 mM	60 μM	--	--
<i>rC. officinalis</i> ^c	1.2 mM	27 μM	--	--
<i>C. pilulifera</i> ^d	11 mM	90 μM	--	--
<i>P. cartilagineum</i> ^c	10 mM	90 μM	--	--

Table 1.1: Kinetic parameters for V-BrPO-catalyzed bromination of MCD or bromide-assisted disproportionation of hydrogen peroxide. (a) parameters determined using MCD, (b) parameters determined by measuring the disproportionation of H_2O_2 , (c) parameters determined at pH 6.5, (d) parameters determined at pH 6.0.

In addition, hydrogen peroxide inhibition as a function of pH indicates an amino acid with an ionizable group with a pK_a between 6.5 and 7 is involved in the inhibition (Soedjak et al. 1995).

Unlike the V-CIPO reactions with chloride, the halogenating intermediate produced in V-BrPO catalyzed reactions with bromide is not readily detected. Detection of the intermediate is hampered since its reaction with organic substrates or with excess hydrogen peroxide to produce singlet O_2 is faster than its formation, preventing its build up in solution (Scheme 1.1). V-BrPO produces an electrophilic oxidized bromide intermediate (i.e., Br^+) and not a radical species (Br^\bullet), indicating that V-BrPO catalyzes a single two-electron oxidation of bromide (Soedjak et al. 1995). The nature of the oxidized intermediate as either enzyme-bound, enzyme-

trapped, or a freely diffusible species is unclear and may actually depend on the nature of the organic substrate available to the enzyme (see section on Selectivity of V-BrPOs).

V-BrPO structure determination and proposed mechanism. The vanadium bromoperoxidases are all acidic proteins, with similar monomer molecular weights (~ 66 KDa), vanadium content, and electrostatic charges (pI 4 – 5). The X-ray crystal structures of native V-BrPO from the brown alga *A. nodosum* and the red alga *Corallina officinalis* have been reported at 2.0 Å and 2.3 Å resolution, respectively (Weyand et al. 1999; Isupov et al. 2000).

The structure of V-BrPO from *A. nodosum* is a homodimer with approximate dimensions of 90 Å x 77 Å x 75 Å (Weyand et al. 1999). The secondary structure is dominated by α -helices with a few short β -strands [Figure 1.10]. Each monomer contains three intramolecular disulfide bridges in addition to two intermolecular disulfide bridges linking the two monomers. In addition to the intermolecular disulfide bridges, four salt bridges, and numerous side-chain/side-chain, side-chain/main-chain interactions stabilize the dimer interface. In fact, each monomer contributes more than 46% of its surface to contacts in the dimer interface. The extensive monomer contacts are proposed to give rise to the observed thermal and chemical stability of this enzyme (Walker 1998; Weyand et al. 1999).

The main tertiary structural motif present is two four-helix bundles, similar to the V-ClPO core structure (Messerschmidt and Wever 1996). The vanadium metal site is located at the bottom of a 15 Å substrate channel, where both monomer

surfaces of the dimer contribute residues to the substrate channel. The substrate channel has an overall funnel-type shape where the entrance of the channel spans 12 Å and narrows to 8 Å near the vanadium-binding site. The funnel surface is lined with both hydrophilic and hydrophobic amino acids, with hydrophobic residues dominating the surface around the vanadium site.

The vanadium atom at the active site is bound in a trigonal bipyramidal coordination geometry, similar to the vanadium(V) site in V-CIPO (Messerschmidt and Wever 1996; Messerschmidt et al. 1997). Four oxygen atoms and N^{ε2} of His-486 coordinate vanadium bound as hydrogen vanadate. An intricate hydrogen bond network to the vanadate cofactor acts to neutralize the negative charge of vanadate. Protein residues (Ser-416, Gly-417, Lys-341, Arg-349, and Arg-480) act as proton donors to the equatorial vanadate oxygens and constitute the central part of the rigid vanadate-binding site [Figure 1.11]. Histidine 418 forms a hydrogen bond to the apical oxygen of vanadate and to the carboxyl O^{δ1} of Asp-278. Histidine-418, like His-404 in V-CIPO, is proposed to function as an acid/base ligand in the overall catalytic cycle. The active site of V-BrPO also contains an extra histidine residue, His-411, not present in the V-CIPO structures. His-411 is within hydrogen bond distance to one of the vanadate oxygen atoms and may participate as a proton donor/acceptor during enzymatic turnover (Colpas et al. 1996; Renirie et al. 2000a).



Figure 1.10: Ribbon-type representation of the V-BrPO homodimer of *A. nodosum*. α -Helices are shown in red, β -strands are shown in green and coils are shown in yellow. Figure was drawn in Swiss-PDB viewer and rendered with gl_render and POV-ray software.



Figure 1.11: Vanadium binding site of V-BrPO from *A. nodosum*. Figure was drawn with Swiss-PDB viewer and rendered with gl_render and POV-ray software.

The structure of the V-BrPO from the marine red alga *C. officinalis* is a homo-dodecamer with a molecular weight of 740 KDa, where approximate dimensions of a single subunit measures 85 Å x 56 Å x 55 Å (Isupov et al. 2000). The dodecamer structure measures ~150 Å in diameter with the 12 subunits arranged in a 23 cubic point group symmetry [Figure 1.12]. The secondary structure is dominated by α -helices and a few β -strands arranged in two four-helix bundles similar to V-BrPO from *A. nodosum*. Each subunit contains two cysteine residues, which do not participate in disulfide bridge formation. Approximately 33% of each subunit is buried in contacts with neighboring subunits, and makes at least one hydrogen bond with nine other subunits within the dodecamer. In addition, each subunit contains a divalent cation-binding site occupied by Mg^{2+} that binds close to the subunit interface. The divalent cations appear to be necessary to form the dimeric structure for the active site cavity.

The vanadium-binding site is formed from residues from two different subunits, suggesting that a dimeric structure is required for full activity even though all vanadate-binding residues are from a single subunit. The vanadium-binding site is positioned at the bottom of a cavity, which is 20 Å deep and 14 Å wide. The native structure was solved with phosphate in place of vanadate at the metal binding site. Amino acid residues proposed to coordinate vanadium are conserved within the class of V-BrPOs. Amino acid residues Ser-483, Gly-484, Lys-398, Arg-406, and Arg-545 are in position to form hydrogen bonds to the equatorial vanadate oxygens [Figure 1.13]. Histidine-551 is placed to directly coordinate vanadium in the axial

position, and the catalytic histidine, His-485 is in position to form a hydrogen bond to the apical vanadate oxygen. V-BrPO from *C. officinalis* also contains the extra histidine residue in proximity to the vanadate-binding site, His-478. Based on the X-ray crystal structure for V-BrPO from both *A. nodosum* and *C. officinalis*, a mechanism for halide oxidation is proposed to be similar to V-ClPO. The presence of the extra histidine in proximity to the active site, and the intricate hydrogen bond network around the monoperoxo-vanadium intermediate works to tune the potential for either chloride or bromide oxidation (Scheme 1.4, adapted from (Weyand et al. 1999)).

Interestingly, comparison of the structures of V-BrPO from *A. nodosum* and *C. officinalis* shown only five residues, not including vanadate binding residues, out of the 17 lining the substrate cavity are conserved between the two structures, and none of these five residues are conserved in the V-ClPO structure (Weyand et al. 1999; Isupov et al. 2000). Also, V-BrPO from *C. officinalis* has only three charged residues (Glu-124, Arg-395, Asp292) within 7.5 Å of the vanadate-binding site, where hydrophobic patches dominate the remainder of the substrate cavity (Isupov et al. 2000). The hydrophobic patches of residues and few charged residues likely influence substrate specificity as well as provide binding sites for organic substrates.

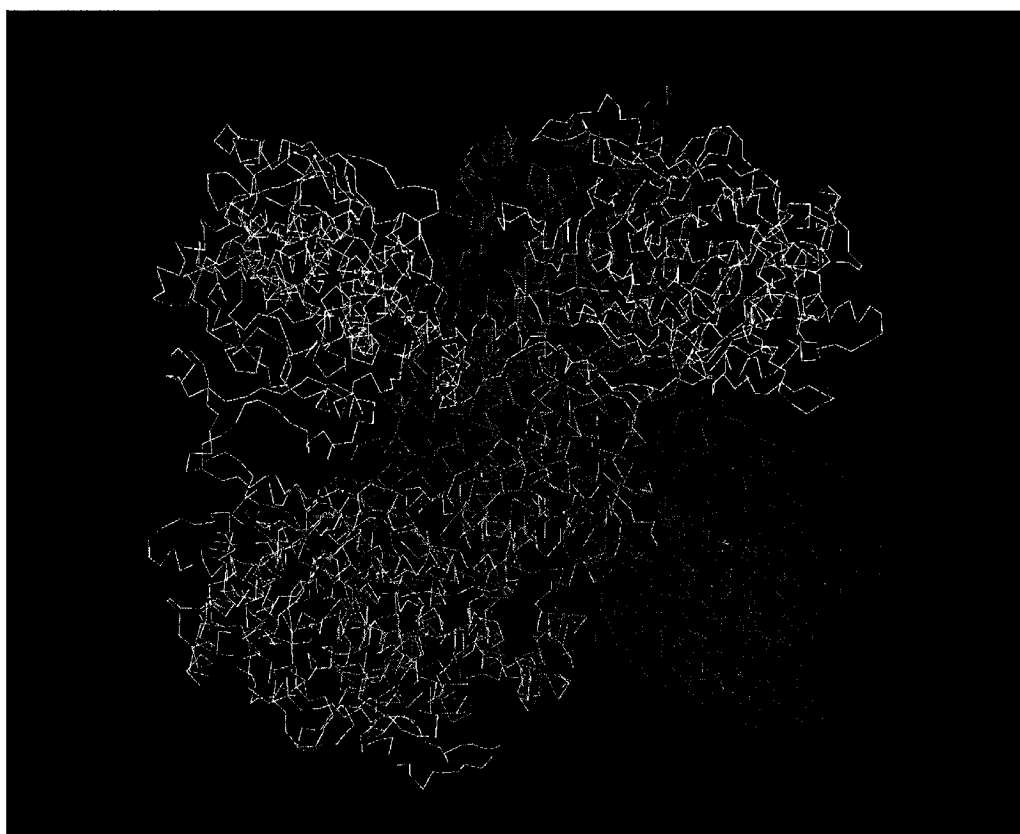


Figure 1.12: A diagram showing the C_{α} backbone of V-BrPO (*C. officinalis*) dodecamer. Figure was drawn with Swiss-PDB viewer and rendered with gl_render and POV-ray software.

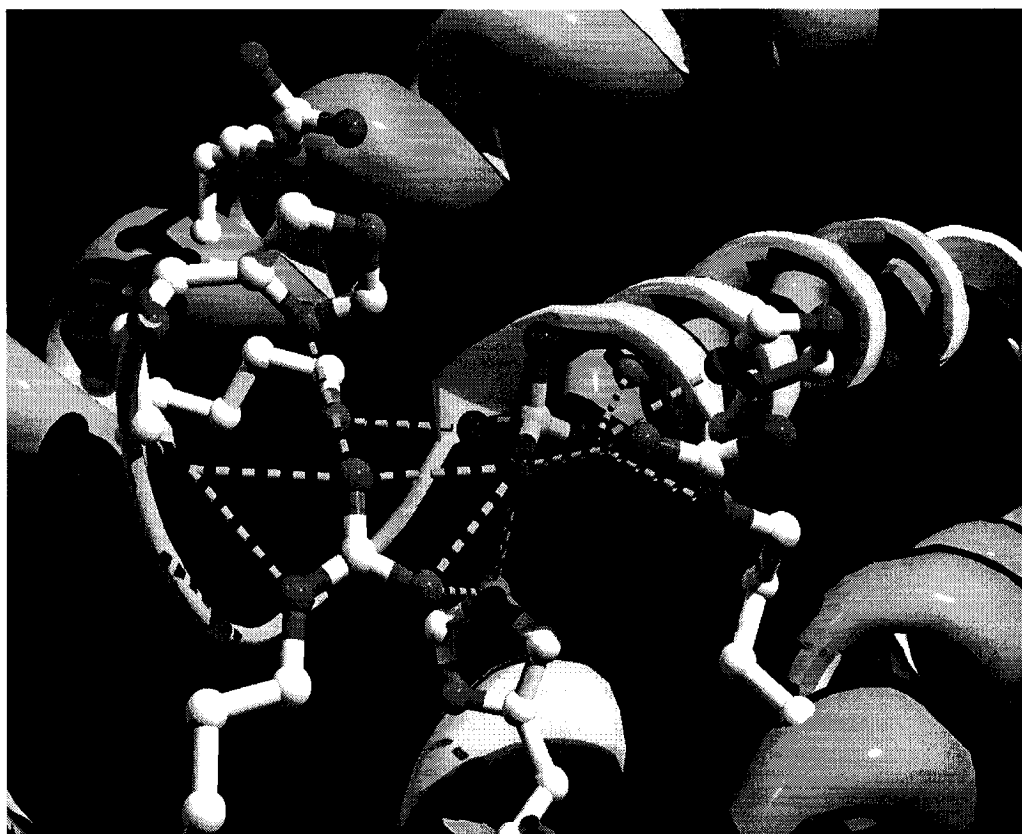
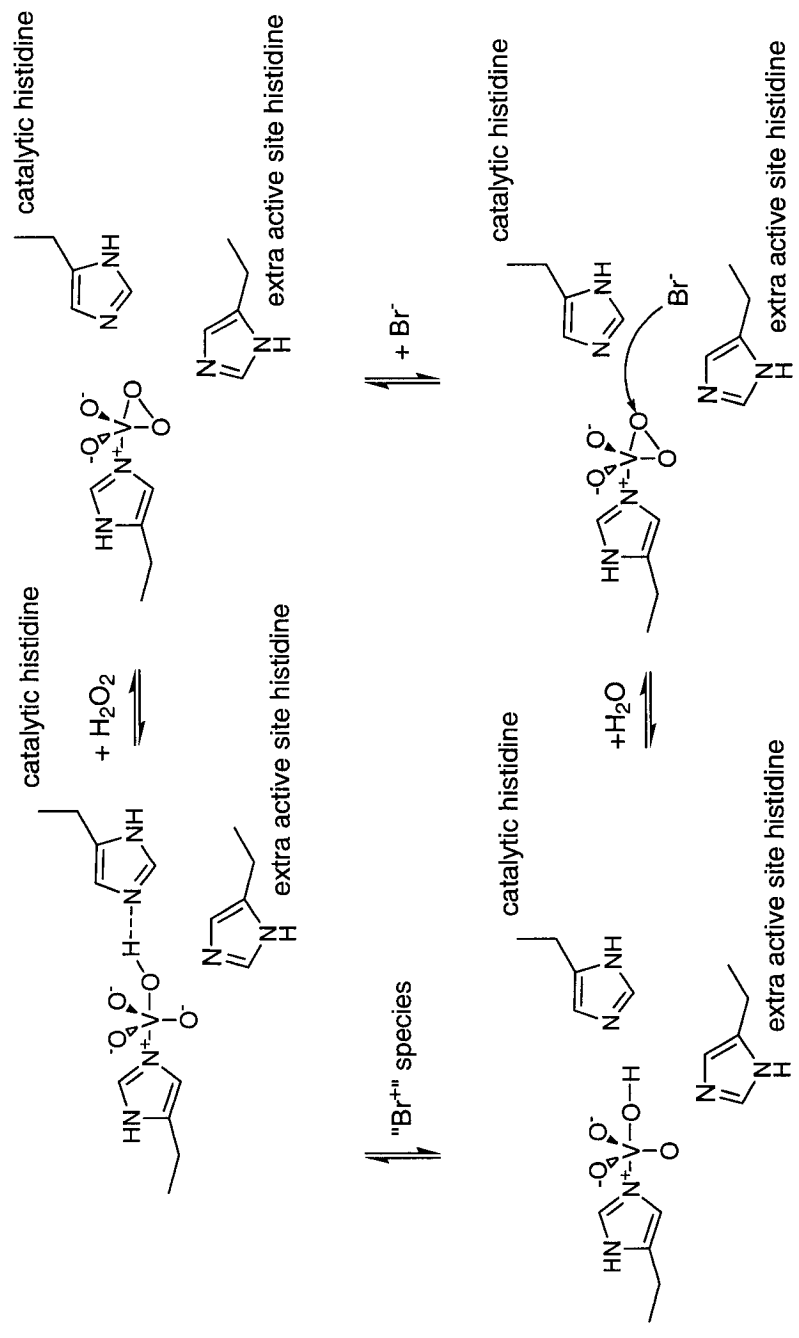


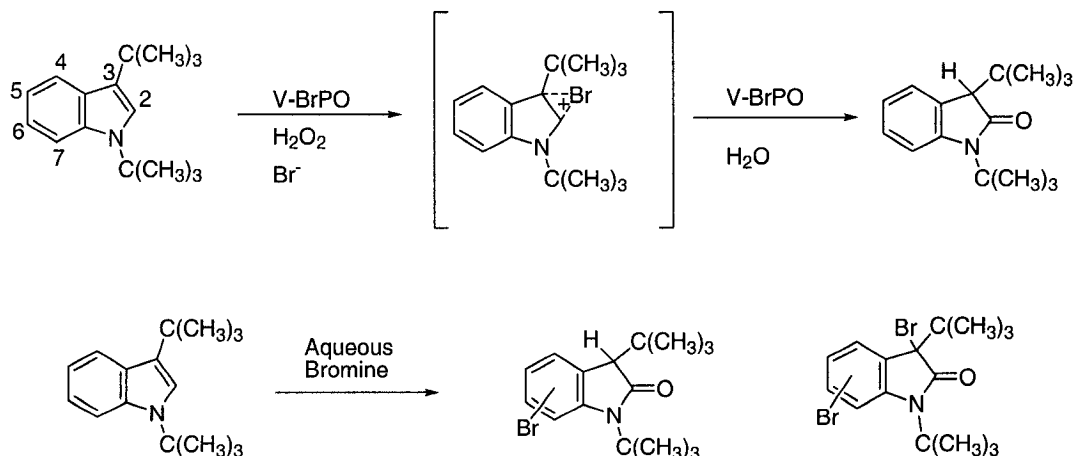
Figure 1.13: Vanadium binding site of V-BrPO from *C. officinalis*. A phosphate molecule occupies the vanadium site. Figure was drawn with Swiss-PDB viewer and rendered with gl_render and POV-ray software.



Scheme 1.4: Proposal of a common reaction mechanism for bromide oxidation by vanadium bromoperoxidases.

The selectivity of V-BrPOs. Initial investigations into the reactivity of V-BrPOs with various substrates such as anisole or prochiral aromatic compounds failed to detect any regio or stereoselectivity (Itoh et al. 1987; Itoh et al. 1988; Krenn et al. 1989). These results suggested that V-BrPO produces a diffusible oxidized bromine intermediate such as hypobromite, bromine or tribromide (de Boer and Wever 1988). However, competitive kinetics studies comparing the bromination of indole substrates by the V-BrPO/H₂O₂/Br⁻ system to bromination by aqueous bromine (i.e., the equilibrium mixture of HOBr = Br₂ = Br₃⁻) demonstrated that V-BrPO-catalyzed reactions were not consistent with a freely diffusible brominating intermediate. Vanadium bromoperoxidase catalyzed the preferential bromination of indole and terpene substrates when competed with equal molar mixtures of phenol red or MCD, whereas the same reactions performed with aqueous bromine under identical reaction conditions resulted in the simultaneous bromination of all substrates present in solution (Martinez et al. 2001) (Tschirret-Guth and Butler 1994; Butler et al. 1998b). Subsequently, fluorescence quenching of the substrate 2-phenylindole by V-BrPO established for the first time a specific enzyme-substrate interaction (Butler et al. 1998b).

The ability of V-BrPO to bind certain organic substrates revisited questions regarding whether the enzyme could catalyze stereospecific or regiospecific halogenation reactions with appropriate starting substrates. Reaction with the indole derivative 1,3-di-*tert*-butylindole and V-BrPO produced a regiospecific



Scheme 1.5: Reaction scheme for the bromination of 1,3-di-tert-butylindole by V-BrPO and aqueous bromine.

bromination to a single isolated product, 1,3-di-*tert*-butyl-2-indolinone (Scheme 1.5) (Martinez et al. 2001). Reactions with aqueous bromine were not regioselective and many products were obtained. The observed selectivity was attributed to 1,3-di-*tert*-butylindole orienting specifically within the active site cleft of V-BrPO, likely along a hydrophobic patch of residues. The regiospecific bromination of 1,3-di-*tert*-butylindole suggest the presence of an enzyme-trapped or enzyme-bound brominating intermediate and not a freely diffusible brominating species.

In addition to regioselective halogenation reactions V-BrPO also catalyzes the enantioselective oxidation of sulfides to sulfoxides (Andersson et al. 1997; Andersson and Allenmark 1998; ten Brink et al. 1998). The direct oxidation of

sulfides occurs in the absence of halides, with the slow addition of hydrogen peroxide (over the course of 2 – 3 days). For example, V-BrPO from *A. nodosum* converts methyl phenyl sulfide to the (*R*)-enantiomer (91% ee), while V-BrPO from *Corallina pilulifera* produces the (*S*)-enantiomer (55% ee) (Andersson et al. 1997; ten Brink et al. 1998; ten Brink et al. 1999). However, the selectivity of sulfoxidation is exclusive to V-BrPO since V-ClPO catalyzes the racemic mixture of the sulfoxide. Kinetic resolution experiments with racemic non-aromatic cyclic thioethers and V-BrPO from *A. nodosum* show that V-BrPO has a kinetic preference for conversion of the (*R*)-enantiomer to the corresponding sulfoxide (ten Brink et al. 1999). V-BrPO from *C. officinalis* also catalyzes the selective sulfoxidation of aromatic sulfides containing a *cis*-positioned carboxyl group to the (*S*)-sulfoxide with 95% enantioselectivity (Andersson and Allenmark 1998).

Given the observed regioselective halogenation reactions and the stereoselective sulfoxidation reactions catalyzed by V-BrPOs a picture is emerging in which subtle differences in the active site channel influence the outcome of regioselective and stereoselective products. Chapter Three explores the ability of V-BrPO from marine red algae to catalyze the enantioselective bromination of terpene substrates towards the production of brominated marine natural products.

Comparative aspects of vanadium haloperoxidases and phosphatidic acid phosphatases:

The vanadium-binding sites of the vanadium haloperoxidases show amino acid sequence identity to an unrelated group of enzymes, the acid phosphatases. The

similarity between the VHPOs and acid phosphatase was first suggested by amino acid sequence alignments (Hemrika et al. 1997; Neuwald 1997; Stukey and Carman 1997; Littlechild et al. 2002). The acid phosphatases that share sequence motif similarity include the type 2 phosphatidic acid phosphatases, bacterial acid phosphatases, mammalian glucose-6-phosphatases and the *Drosophila* developmental protein wunen (Neuwald 1997; Stukey and Carman 1997). Amino acid alignments indicate a perfectly conserved motif (GSYPSGHT), that is similar to the vanadium binding region in V-CIPO and V-BrPO, P[S/A]YPSGHAT. In addition, the histidine residue covalently bound to the vanadate cofactor in the VHPOs are also conserved in the acid phosphatase family.

Vanadium is a known competitive inhibitor of many phosphate-metabolizing enzymes and phosphate inhibits remetallation of VHPOs by competition for the oxyanion binding site (Soedjak et al. 1991b). Sequence and structural data suggest that VHPOs may have phosphatase activity or acid phosphatases may exhibit haloperoxidase activity. Recombinant apo-vanadium chloroperoxidase was subsequently shown to function as an acid phosphatase in the cleavage of *para*-nitrophenylphosphate to *para*-nitrophenol (Hemrika et al. 1997). Apo-rV-CIPO maximal turnover of *para*-nitrophenylphosphate was 1.7 min^{-1} , which is 10,000 times slower than the reported turnover rates for acid phosphatases (i.e., $10^2 - 10^3 \text{ s}^{-1}$). Recently, the vanadate substituted acid phosphatase from *Shigella flexneri* and *Salmonella enterica* ser. *typhimurium* was shown to catalyze the oxidation of bromide (Tanaka et al. 2002). The vanadate-substituted phosphatases had a $K_m^{\text{Br}^-}$ in

the range of 160 – 350 mM, and $K_m^{H_2O_2}$ in the range of 100 – 150 μ M, with turnover values of 3.4 min^{-1} and 33 min^{-1} for *Shigella* and *Salmonella*, respectively. It is clear that apo-V-ClPO and the studied acid phosphatases are not optimized for the biomimetic phosphatase and haloperoxidase activities. Even though the activities of these unrelated enzymes may not be optimized for alternative chemistries, the structural and mechanistic comparisons between the VHPOs and acid phosphatases will hopefully provide insight into the evolution of these different enzyme classes designed to coordinate similar oxyanions.

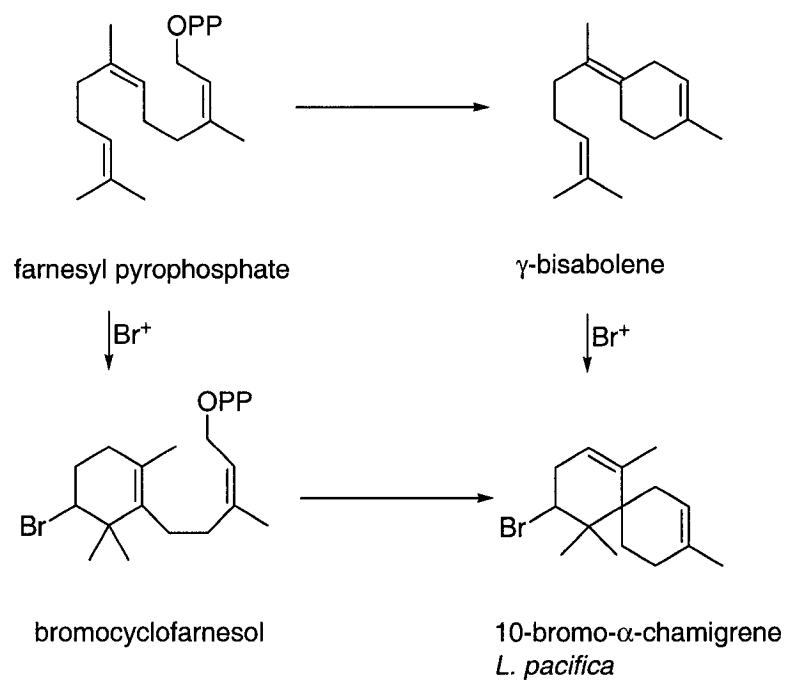
Vanadium bromoperoxidase and the biosynthesis of halogenated marine natural products:

An understanding of the biosynthesis of halogenated marine natural products is valuable to understanding the mechanism of action of halogenating enzymes, as well as the role of halogenated metabolites within the marine environment. Many of the biosynthetic routes proposed are for halogenated structural types found primarily within red algae (Rhodophyta), particularly the halogenated sesquiterpenes and acetogenins. Many of the proposed biosynthetic schemes are supported by biomimetic studies and enzyme-catalyzed halogenation reactions.

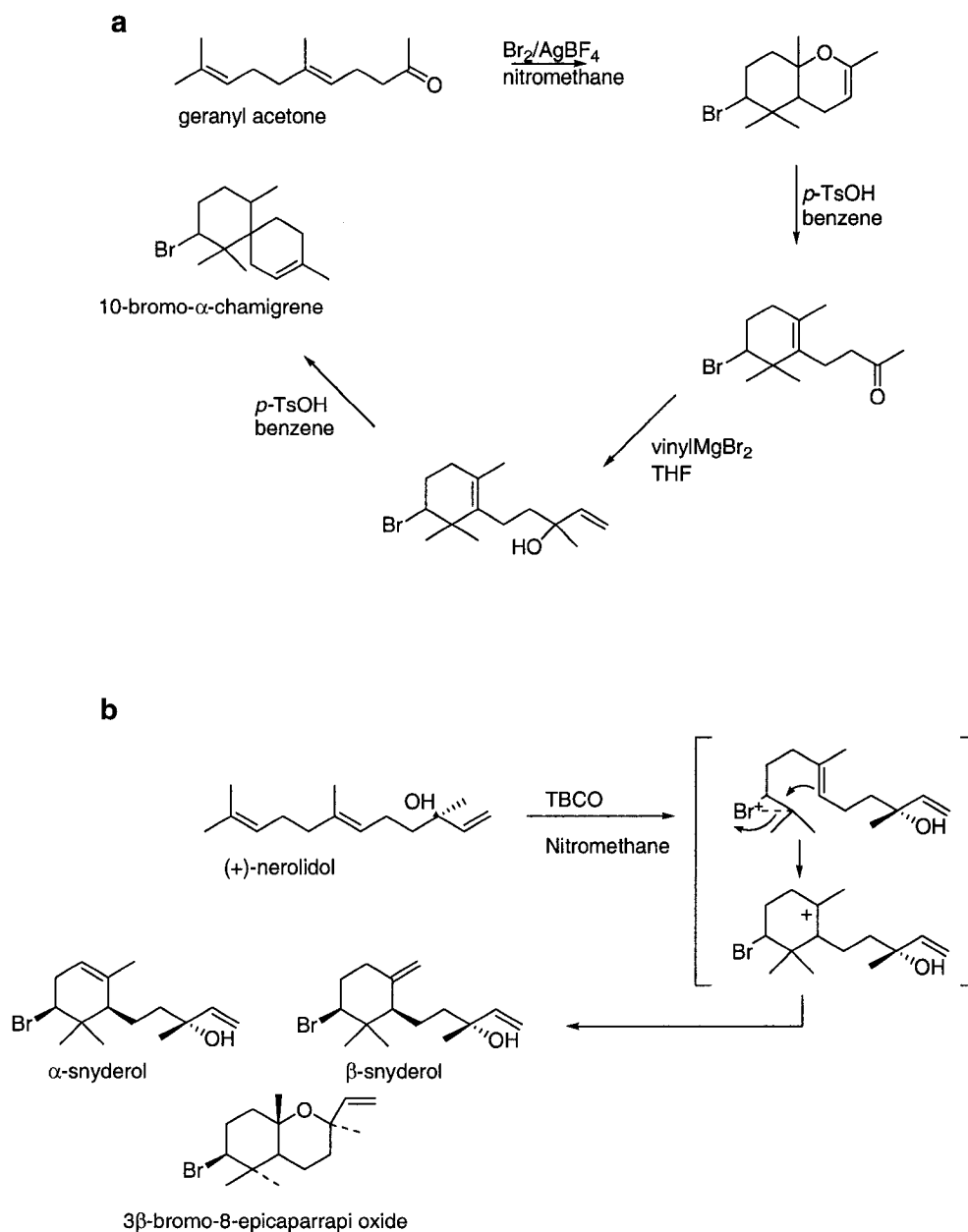
Biomimetic syntheses of halogenated marine natural products. Among the halogenated natural products isolated from marine algae, one of the largest and most varied groups are the halogenated sesquiterpenes, which include the halogenated chamigrenes isolated from the red algal genus *Laurencia*. Over the years several biomimetic syntheses have been proposed, where the most important step in any

biomimetic scheme is the bromonium-ion initiated cyclization of a terpenoid precursor.

For example, a quarter of a century ago Faulkner and Fenical proposed two distinct biosynthetic routes to the fundamental halogenated chamigrene skeleton from the sesquiterpene farnesyl pyrophosphate, by way of either γ -bisabolene or brominated monocyclofarnesol (Scheme 1.6) (Wolinsky and Faulkner 1976) (Fenical 1975; Faulkner 1976). Faulkner applied the biosynthetic scheme involving a brominated monocyclofarnesol intermediate when he used the bromonium-ion induced cyclization of geranyl acetone in the biomimetic synthesis of 10-bromo- α -chamigrene (Scheme 1.7) (Wolinsky and Faulkner 1976). Similarly, Kato and coworkers used the brominating agent 2,4,4,6-tetrabromocyclohexa-2,5-dienone (TBCO) in nitromethane to direct the cyclization of nerolidol to the brominated marine natural products α - and β -snyderol, and 3 β -bromo-8-epicaparrapi oxide (Scheme 1.7) (Kato et al. 1976; Kato et al. 1980). Prestwich and coworkers also used TBCO in nitromethane in the first enantiospecific synthesis of the brominated marine natural product (-)-aplysistatin derived from (*R*)-(+)-malic acid (Shieh and Prestwich 1982).



Scheme 1.6: Proposed biosynthetic scheme for the bromonium ion initiated cyclization of farnesylpyrophosphate to the marine natural product 10-bromo- α -chamigrene.

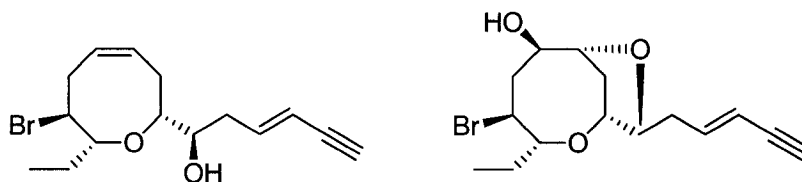


Scheme 1.7: Biomimetic syntheses of brominated marine natural products. (a) Biomimetic bromination and cyclization of geranyl acetone to 10-bromo- α -chamigrene (Wolinsky and Faulkner 1976). (b) Biomimetic bromination of (+)-nerolidol by TBCO, generating marine natural products α / β -snyderol and 3 β -bromo-8-epicaparrapi oxide (Kato et al. 1980).

While biomimetic reactions are useful tools in the synthesis of halogenated marine natural products, many of the reactions suffer from a lack of specificity in bromine-carbon bond formation.

In addition to brominated sesquiterpenes, biomimetic syntheses of halogenated acetylenes or acetogenins have also been studied. The halogenated cyclic structures of this group of marine natural products have features such as varied oxane ring sizes, enyne or allenic side chains, and at least one bromine atom (Erickson 1983). The lauroxocanes are the largest class of cyclized acetogenins and contain the laurencin and laureatin structural types [Figure 1.14]. The bromoetherification functionality found in the halogenated acetogenins fascinates organic chemists with respect to construction of medium ring ethers. Highly labile *cis*- and *trans*-laurediols isolated from *Laurencia* are assumed to be the common biogenetic precursor of the brominated eight-membered cyclic ethers (Fukuzawa et al. 1990a; Fukuzawa et al. 1990b). Murai and colleagues have explored the use of a commercial lactoperoxidase and natural laurediols in the biomimetic one-step synthesis of laurencin and laureatin natural products (Scheme 1.8) (Fukuzawa et al. 1990a). The yield of brominated cyclic products was extremely low, but established a mechanism of bromonium-ion initiated cyclization of precursors to the eight-membered bromoether functionality.

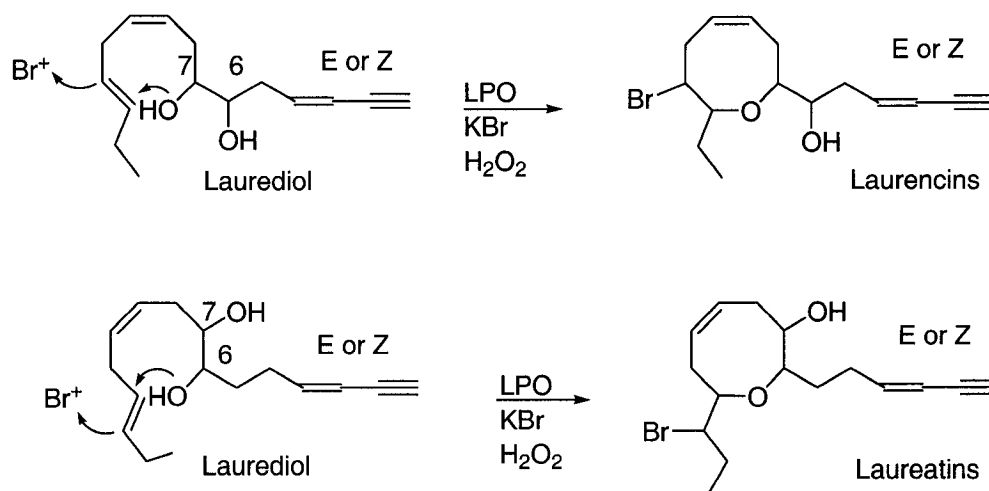
Laurencins



Laureatins



Figure 1.14: Halogenated C15 acetogenins isolated from the marine red alga *Laurencia*.

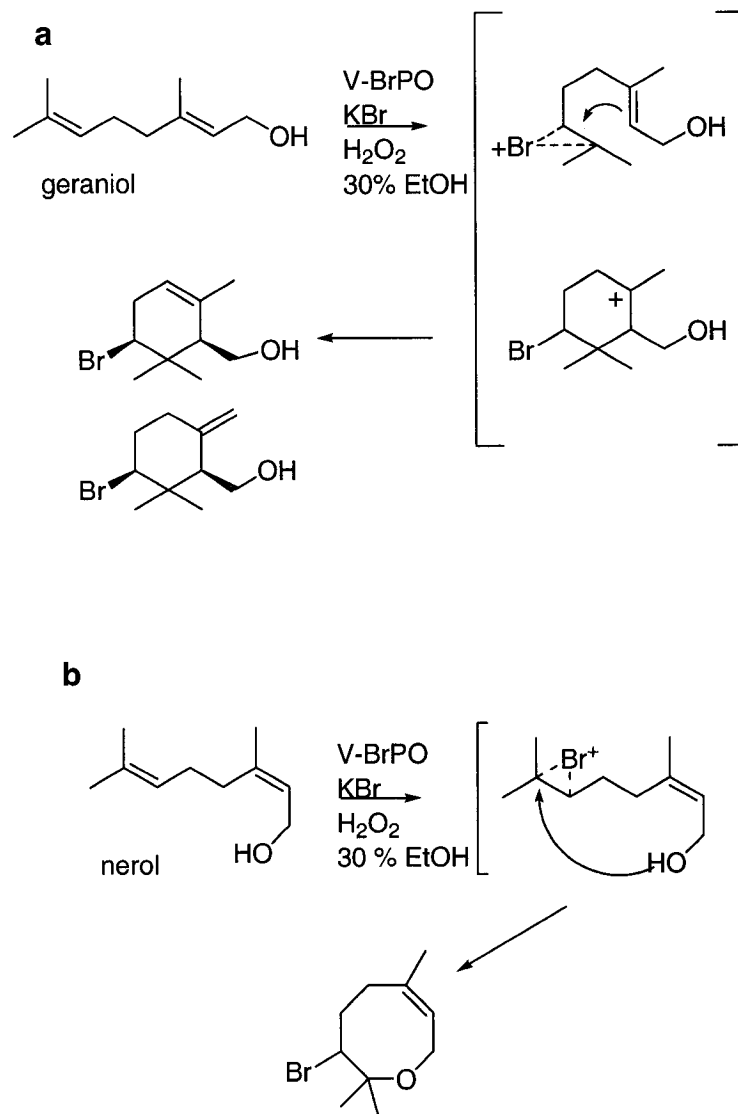


Scheme 1.8: Biomimetic bromination and cyclization of laurediol to laurencin and laureatin natural products by lactoperoxidase.

Haloperoxidases and the syntheses of halogenated marine natural products.

The route by which brominated marine natural products are made within algae is still unclear, but based on biomimetic approaches, appears to require a source of positive bromine in a non-nucleophilic environment to direct the cyclization of substrates.

The active site of V-BrPO includes both of these traits. V-BrPO reacts with monoterpenes geraniol and nerol (Chapter 3) resulting in the formation of brominated monocyclic alcohols from geraniol, and an eight-membered bromocyclic ether from nerol (Scheme 1.9) (Carter-Franklin et al. 2003). The reactions are performed in mixtures of buffers and organic cosolvents (ethanol, isopropanol, 1-propanol), and produce brominated cyclized products despite the presence of excess nucleophiles (i.e., water) to quench bromonium-ion intermediates. In addition, formation of the brominated cyclized monoterpenes appears to be exclusive to V-BrPO, where control reactions with aqueous bromine does not produce brominated cyclized terpenes (Carter-Franklin et al. 2003). Chapter Three addresses the reactivity of V-BrPO isolated from marine algae that produce halogenated marine natural products and the role of V-BrPO in the biosynthesis of chiral halogenated terpenes.



Scheme 1.9: Proposed biosynthetic scheme for V-BrPO bromination and cyclization of monoterpenes (a) geraniol and (b) nerol.

References

- Allen, R. M., M. J. Homer, R. Chatterjee, P. W. Ludden, G. P. Roberts and V. K. Shah (1993). "Dinitrogenase Reductase-Dependent and MgATP-Dependent Maturation of Apo-Dinitrogenase from *Azotobacter vinelandii*." *J. Biol. Chem.* **268**: 23670-23674.
- Andersson, M. and S. Allenmark (1998). "Asymmetric Sulfoxidation Catalyzed by a Vanadium Bromoperoxidase: Substrate Requirements of the Catalyst." *Tetrahedron* **54**: 15293-15304.
- Andersson, M., A. Willetts and S. Allenmark (1997). "Asymmetric Sulfoxidation Catalyzed by a Vanadium-Containing Bromoperoxidase." *J. Org. Chem* **62**: 8455-8458.
- Arber, J. M., B. R. Dobson, R. R. Eady, S. S. Hasnain, C. D. Garner, T. Matsushita, M. Nomura and B. E. Smith (1989). "Vanadium K-Edge X-ray Absorption Spectroscopy of the Functioning and Thionine-Oxidized Forms of the VFe-Protein of the Vanadium Nitrogenase from *Azotobacter chroococcum*." *Biochem. J.* **258**: 733-738.
- Arber, J. M., B. R. Dobson, R. R. Eady, P. Stevens, S. S. Hassain, C. D. Garner and B. E. Smith (1987). "Vanadium K-Edge X-ray Absorption Spectrum of the VFe Protein of the Vanadium Nitrogenase of *Azotobacter chroococum*." *Nature* **325**: 372-374.
- Berry, R. E., E. M. Armstrong, R. L. Beddoes, D. Collison, S. N. Ertok, M. Helliwell and C. D. Garner (1999). "The Structural Characterization of Amavadin." *Angew. Chem. Int. Ed.* **38**: 795-797.
- Butler, A. (1990). The Coordination and Redox Chemistry of Vanadium in Aqueous Solution. Vanadium in Biological Systems. N. D. Chasteen, Kluwer Academic: 25-49.
- Butler, A. (1998a). "Vanadium Haloperoxidases." *Curr. Opin. Chem. Biol.* **2**: 279-285.
- Butler, A., R. A. Tschirret-Guth and M. T. Simpson (1998b). Reactivity of Vanadium Bromoperoxidase. Vanadium Compounds: Chemistry, Biochemistry and Therapeutic Applications. A. S. Tracey and D. C. Crans, American Chemical Society, ACS Symposium Series. **711**: 202-215.

- Carter, J. N., K. E. Beatty, M. T. Simpson and A. Butler (2002). "Reactivity of Recombinant and Mutant Vanadium Bromoperoxidase from the Red Alga *Corallina officinalis*." *J. Inorg. Biochem.* **91**: 59-69.
- Carter-Franklin, J., J. D. Parrish, R. A. Tschirret-Guth, R. D. Little and A. Butler (2003). "Vanadium Haloperoxidase-Catalyzed Bromination and Cyclization of Terpenes." *J. Am. Chem. Soc.* **125**: 3688-3689.
- Chatterjee, R., P. W. Ludden and V. K. Shah (1997). "Characterization of VNFG, the Delta Subunit of the VNF-encoded Apo-Dinitrogenase from *Azotobacter vinelandii*: Implications for its Role in the Formation of Functional Dinitrogenase 2." *J. Biol. Chem.* **272**: 3758-3765.
- Chen, J., J. Christiansen, C. Tittsworth, B. J. Hales, S. J. George, D. Coucouvanis and S. P. Cramer (1993). "Iron EXAFS of *Azotobacter vinelandii* Nitrogenase Mo-Fe and V-Fe Proteins." *J. Am. Chem. Soc.* **115**: 5509-5515.
- Clague, M. J., N. L. Keder and A. Butler (1993). "Biomimics of Vanadium Bromoperoxidase: Vanadium (V) Schiff Base-Catalyzed Oxidation of Bromide by Hydrogen Peroxide." *Inorg. Chem.* **32**: 4754-4761.
- Collier, R. W. (1984). "Particulate and Dissolved Vanadium in the North Pacific Ocean." *Nature* **309**: 441-444.
- Colpas, G. J., B. J. Hamstra, J. W. Kampf and V. L. Pecoraro (1996). "Functional Models for Vanadium Haloperoxidases: Reactivity and Mechanism of Halide Oxidation." *J. Am. Chem. Soc.* **118**: 3469-3478.
- de Boer, E. and R. Wever (1988). "The Reaction Mechanism of the Novel Vanadium-Bromoperoxidase. A Steady-State Kinetic Analysis." *J. Biol. Chem.* **236**: 12326-12332.
- Dilworth, M. J. and R. R. Eady (1991). "Hydrazine is a Product of Dinitrogen Reduction by the Vanadium Nitrogenase from *Azotobacter chroococcum*." *Biochem. J.* **277**: 465-468.
- Erickson, K. L. (1983). Constituents of *Laurencia*. Marine Natural Products. P. J. Scheuer., Academic Press Inc. **V**: 131-257.
- Everett, R. and A. Butler (1989). "Bromide-Assisted Hydrogen Peroxide Disproportionation Catalyzed by Vanadium Bromoperoxidase: Absence of Direct Catalase Activity and Implications for the Catalytic Mechanism." *Inorg. Chem.* **28**: 393-395.

Everett, R. R., J. R. Kanofsky and A. Butler (1990b). "Mechanistic Investigations of the Novel Non-Heme Vanadium Bromoperoxidases - Evidence For Singlet Oxygen Production." *J. Biol. Chem.* **265**: 4908-4914.

Everett, R. R., H. S. Soedjak and A. Butler (1990a). "Mechanism of Dioxygen Formation Catalyzed By Vanadium Bromoperoxidase - Steady State Kinetic Analysis and Comparison to the Mechanism of Bromination." *J. Biol. Chem.* **265**: 15671-15679.

Fallik, E., P. G. Hartel and R. L. Robson (1993). "Presence of Vanadium Nitrogenase in *Azotobacter paspali*." *Appl. Environ. Microbiol.* **59**: 1883-1886.

Faulkner, D. J. (1976). "Biomimetic Synthesis of Marine Natural Products." *Pure & Appl. Chem.* **48**: 28-28.

Faulkner, D. J. (1998). "Marine Natural Products." *Nat. Product Rep.* **15**: 113-158.

Fenical, W. (1975). "Halogenation in the Rhodophyta, A Review." *J. Phycol.* **11**: 245-259.

Frank, P., K. Kustin, W. E. Robinson, L. Linebaugh and K. O. Hodgson (1995). "Nature and Ligand of Vanadium within Whole-Blood Cells and Henze Solution from the Tunicate *Ascidia ceratodes*, as Investigated by Using X-ray Absorption Spectroscopy." *Inorg. Chem.* **34**: 5942-5949.

Fukuzawa, A., M. Aye and A. Murai (1990b). "A Direct Enzymatic Synthesis of Laurencin from Laurediol." *Chem. Lett.*: 1579-1580.

Fukuzawa, A., M. Aye, M. Nakamura, M. Tamura and A. Murai (1990a). "Biosynthetic Formation of Cyclic Bromo-Ethers Initiated by Lactoperoxidase." *Chem. Lett.*: 1287-1290.

Gailus, H., C. Woitha and D. Rehder (1994). "Dinitrogen Vanadates: Synthesis, Reactions and Conditions for Their Stability." *J. Chem. Soc., Dalton Trans.* **23**: 3471-3477.

George, G. N., C. L. Coyle, B. J. Hales and S. P. Cramer (1988). "X-ray Absorption of *Azotobacter vinelandii* Vanadium Nitrogenase." *J. Am. Chem. Soc.* **110**: 4057-4059.

Gribble, G. W. (1998). "Naturally Occurring Organohalogen Compounds." *Acc. Chem. Res.* **31**(3): 141-152.

Gshwend, P. M. (1989). *Science* **227**: 1033-1035.

- Hager, L. P., D. R. Morris, F. S. Brown and H. Eberwein (1966). "Chloroperoxidase: Utilization of Halogen Anions." *J. Biol. Chem.* **241**: 1769-1777.
- Hales, B. J., E. E. Case, J. E. Morningstar, M. F. Dzeda and L. A. Mauterer (1986a). "Isolation of a New Vanadium Containing Nitrogenase from *Azotobacter vinelandii*." *Biochemistry* **25**: 7253-7255.
- Hales, B. J., D. J. Langosch and E. E. Case (1986b). "Isolation and Characterization of a 2nd Nitrogenase Fe-Protein from *Azotobacter vinelandii*." *J. Biol. Chem.* **261**: 5301-5306.
- Harvey, I., J. M. Arber, R. R. Eady, B. E. Smith, C. D. Garner and S. S. Hasnain (1990). "Iron K-Edge X-ray Absorption Spectroscopy of the Fe-Vcofactor of the Vanadium Nitrogenase from *Azotobacter chroococcum*." *Biochem. J.* **266**: 929-931.
- Hemrika, W., R. Renirie, H. L. Dekker, P. Barnett and R. Wever (1997). "From Phosphatases to Vanadium Peroxidases: A Similar Architecture of the Active Site." *Proc. Natl. Acad. Sci. USA* **94**: 2145-2149.
- Hemrika, W., R. Renirie, S. Macedo-Ribeiro, A. Messerschmidt and R. Wever (1999). "Heterologous Expression of the Vanadium-Containing Chloroperoxidase from *Curvularia inaequalis* in *Saccharomyces cerevisiae* and Site-Directed Mutagenesis of the Active Site Residues His496, Lys353, Arg360, and Arg490." *J. Biol. Chem.* **274**: 23820-23827.
- Isupov, M. N., A. R. Dalby, A. A. Brindley, Y. Izumi, T. Tanabe, G. N. Murshudov and J. A. Littlechild (2000). "Crystal Structure of Dodecameric Vanadium-Dependent Bromoperoxidase from the Red Algae *Corallina officinalis*." *J. Mol. Biol.* **299**: 1035-1049.
- Itoh, N., A. Hasan, Y. Izumi and H. Yamada (1988). "Substrate-Specificity, Regiospecificity and Stereospecificity of Halogenation Reactions Catalyzed by Non-Heme-Type Bromoperoxidase of *Corallina pilulifera*." *Eur. J. Biochem.* **172**: 477-484.
- Itoh, N., Y. Izumi and H. Yamada (1987). "Characterization of Nonheme Iron and Reaction-Mechanism of Bromoperoxidase in *Corallina pilulifera*." *J. Biol. Chem.* **262**: 11982-11987.
- Joerger, R. D., T. M. Loveless, L. A. Mitchenal, B. H. Simon and P. E. Bishop (1990). "Nucleotide Sequences and Mutational Analysis of the Structural Genes for Nitrogenase-2 of *Azotobacter vinelandii*." *J. Bacteriol.* **172**: 3400-3408.

Kato, T., I. Ichinose, A. Kamoshida and Y. Kitahara (1976). "Cyclization of Polyenes. Biogenetic-Type Synthesis of Snyderols." J.C.S. Chem. Comm.: 518-519.

Kato, T., K. Ishii, I. Ichinose, Y. Nakai and T. Kumagai (1980). "Brominative Cyclization of Nerolidol and Geranyl-Linalool." J.C.S. Chem. Comm.: 1106-1108.

Krenn, B. E., Y. Izumi, H. Yamada and R. Wever (1989). "A Comparison of Different (Vanadium) Bromoperoxidases - the Bromoperoxidase from *Corallina pilulifera* is also a Vanadium Enzyme." Biochem. et Biophys. Acta **998**: 63-68.

Littlechild, J., E. Garcia-Rodriguez, A. Dalby and M. Isupov (2002). "Structural and Functional Comparisons Between Vanadium Haloperoxidases and Acid Phosphatase Enzymes." J. Mol. Recognit. **15**: 291-296.

Macedo-Ribeiro, S., W. Hemrika, R. Renirie, R. Wever and A. Messerschmidt (1999). "X-ray Crystal Structures of Active Site Mutants of the Vanadium-Containing Haloperoxidase for the Fungus *Curvularia inaequalis*." J. Biol. Inorg. Chem. **4**: 209-219.

Martinez, J. S., G. L. Carroll, R. A. Tschirret-Guth, G. Altenhoff, R. D. Little and A. Butler (2001). "On the Regiospecificity of Vanadium Bromoperoxidase." J. Am. Chem. Soc. **123**: 3289-3294.

Mendz, G. L. (1991). "Stimulation of Mutases and Isomerases by Vanadium." Archives of Biochemistry and Biophysics **291**: 201-211.

Messerschmidt, A., L. Prade and R. Wever (1997). "Implications for the Catalytic Mechanism of the Vanadium-Containing Enzyme Chloroperoxidase from the Fungus *Curvularia inaequalis* by the X-ray Structures of the Native and Peroxide Form." Biol. Chem. **378**: 309-315.

Messerschmidt, A. and R. Wever (1996). "X-ray Structure of a Vanadium-Containing Enzyme: Chloroperoxidase from the Fungus *Curvularia inaequalis*." Proc. Natl. Acad. Sci. USA **93**: 392-396.

Miller, R. W. and R. R. Eady (1988). "Molybdenum and Vanadium Nitrogenase of *Azotobacter chroococcum*: Low Temperature Favors N₂ Reduction by Vanadium Nitrogenase." Biochem. J. **256**: 429-432.

Morningstar, J. E., M. K. Johnson, E. E. Case and B. J. Hales (1987). "Characterization of the Metal Clusters in the Nitrogenase Molybdenum-Iron and Vanadium-Iron Proteins of *Azotobacter vinelandii* Using Magnetic Circular Dichroism Spectroscopy." Biochemistry **26**: 1795-1800.

- Neuwald, A. F. (1997). "An Unexpected Structural Relationship Between Integral Membrane Phosphatases and Soluble Haloperoxidases." *Protein Science* **6**: 1764-1767.
- Nriagu, J. O. (1998). *Vanadium in the Environment. Advances in Environmental Science*. J. O. Nriagu. New York, John Wiley and Sons. **30**.
- Ravi, N., V. Moore, S. Lloyd, B. J. Hales and B. H. Huynh (1994). "Mossbauer Characterization of the Metal Clusters in *Azotobacter vinelandii* Nitrogenase V-Fe Protein." *J. Biol. Chem.* **269**: 20920-20924.
- Rehder, D. (1995). *Vanadium and Its Role in Life, Metal Ions in Biological Systems*. H. Sigel and A. Sigel, New York, Marcel Dekker. **31**.
- Rehder, D. (2003). "Biological and Medicinal Aspects of Vanadium" *Inorg. Chem. Comm.* **6**: 604-617.
- Renirie, R., W. Hemrika and R. Wever (2000a). "Peroxidase and Phosphatase Activity of Active-Site Mutants of Vanadium Chloroperoxidase from the Fungus *Curvularia inaequalis*. Implications for the Catalytic Mechanisms." *J. Biol. Chem.* **275**: 11650-11657.
- Robson, R. L., R. R. Eady, T. H. Richardson, R. W. Miller, M. Hawkins and J. R. Postgate (1986). "The Alternative Nitrogenase of *Azotobacter chroococcum* is a Vanadium Enzyme." *Nature* **322**: 388-390.
- Robson, R. L., P. R. Woodley, R. N. Pau and R. R. Eady (1989). "Structural Genes for the Vanadium Nitrogenase from *Azotobacter chroococcum*." *EMBO J.* **8**: 1217-1224.
- Rush, J. D. and B. H. J. Bielski (1985). "Kinetics of the Reactions of HO₂ with Oxyvanadium and Peroxyvanadium Compounds: A Pulse Radiolysis and Stopped-Flow Study." *J. Phys. Chem.* **89**: 1524-1528.
- Ruttimann-Johnson, C., R. Chatterjee, V. K. Shah and P. W. Ludden (1998). *Vanadium Compounds: Chemistry, Biochemistry, and Therapeutic Applications*. A.C. S. Series. **711**: 228-240.
- Shieh, H. and G. D. Prestwich (1982). "Chiral, Biomimetic Total Synthesis of (-)-Aplysistatin." *Tetrahedron Lett.* **23**: 4643-4646.
- Simons, B. H., P. Barnett, E. Vollenbroek, H. L. Dekker, A. O. Muijsers, A. Messerschmidt and R. Wever (1995). "Primary Structure and Characterization of the

- Vanadium Chloroperoxidase from the Fungus *Curvularia inaequalis*." *Eur. J. Biochem.* **229**: 566-574.
- Soedjak, H. S. and A. Butler (1991a). "Mechanism of Dioxygen Formation Catalyzed By Vanadium Bromoperoxidase From *Macrocystis pyrifera* and *Fucus distichus* - Steady State Kinetic Analysis and Comparison to the Mechanism of V-BrPO From *Ascophyllum nodosum*." *Biochim. Biophys. Acta* **1079**: 1-7.
- Soedjak, H. S., R. R. Everett and A. Bulter (1991b). "The Novel Non-Heme Vanadium Bromoperoxidase from Marine Algae: Phosphate Inactivation." *J. Indust. Microbiol.* **8**: 37-44.
- Soedjak, H. S., J. V. Walker and A. Butler (1995). "Inhibition and Inactivation of Vanadium Bromoperoxidase By the Substrate Hydrogen Peroxide and Further Mechanistic Studies." *Biochemistry* **34**: 12689-12696.
- Stukey, J. and G. M. Carman (1997). "Identification of a Novel Phosphatase Sequence Motif." *Protein Science* **6**: 469-472.
- Tanaka, N., V. Dumay, Q. Liao, A. J. Lange and R. Wever (2002). "Bromoperoxidase Activity of Vanadate-Substituted Acid Phosphatases from *Shigella flexneri* and *Salmonella enterica* ser. *typhimurium*." *Eur. J. Biochem.* **269**: 2162-2167.
- Taylor, S. W., B. Kammerer and E. Bayer (1997). "New Perspectives in the Chemistry and Biochemistry of the Tunichromes and Related Compounds." *Chem. Rev.* **97**: 333-346.
- ten Brink, H. B., H. L. Holland, H. E. Schoemaker, H. van Lingen and R. Wever (1999). "Probing the Scope of the Sulfoxidation Activity of Vanadium Bromoperoxidase from *Ascophyllum nodosum*." *Tetrahedron Asymm.* **10**: 4563-4572.
- ten Brink, H. B., A. Tuynman, H. Dekker, W. Hemrika, Y. Izumi, T. Oshiro, H. E. Schoemaker and R. Wever (1998). "Enantioselective Sulfoxidation Catalyzed by Vanadium Haloperoxidases." *Inorg. Chem.* **37**: 6780-6784.
- Tschirret-Guth, R. A. and A. Butler (1994). "Evidence for Organic Substrate Binding to Vanadium Bromoperoxidase." *J. Am. Chem. Soc.* **116**(1): 411-412.
- Van Schijndel, J., P. Barnett, J. Roelse, E. Vollenbroek and R. Wever (1994). "The Stability and Steady-State Kinetics of Vanadium Chloroperoxidase from the Fungus *Curvularia inaequalis*." *Eur. J. Biochem.* **225**: 151-157.

Van Schijndel, J., E. Vollenbroek and R. Wever (1993). "The Chloroperoxidase from the Fungus *Curvularia inaequalis*: A Novel Vanadium Enzyme." *Biochim. Biophys. Acta* **1161**: 249-256.

Walker, J. V. (1998). Investigations of the Mechanism and Reactivity of Vanadium Bromoperoxidase Isolated from the Marine Brown Alga *Ascophyllum nodosum*. Ph.D. Thesis, University of California, Santa Barbara.

Weyand, M., H. Hecht, M. Kiesz, M. F. Liaud, H. Vitler and D. Schomburg (1999). "X-Ray Structure Determination of a Vanadium-Dependent Haloperoxidase from *Ascophyllum nodosum* at 2.0 Å Resolution." *J. Mol. Biol.* **293**: 595-611.

Wolinsky, L. E. and D. J. Faulkner (1976). "A Biomimetic Approach to the Synthesis of *Laurencia* metabolites. Synthesis of 10-Bromo-Alpha-Chamigrene." *J. Org. Chem.* **41**: 597-600.

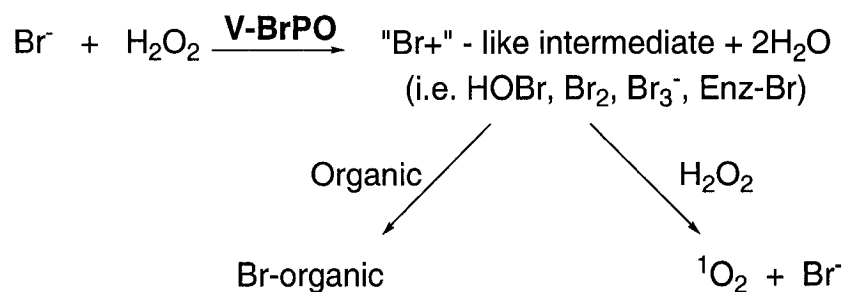
Chapter Two

cDNA Cloning of V-BrPO from Marine Algae (Rhodophyta) and Kinetic Characterization

Introduction

Vanadium bromoperoxidases (V-BrPO) are enzymes that catalyze halide oxidation by hydrogen peroxide. These enzymes, isolated from the major classes of marine algae, are thought to function in the biosynthesis of halogenated marine natural products (Faulkner 1998; Gribble 1998). The scope of which ranges from halogenated indoles, terpenes, and acetogenins to volatile halogenated hydrocarbons. In many cases the halogenated compounds are of pharmacological interest due to their biological activities (e.g., anti-microbial, anti-fungal, anti-inflammatory, anti-viral)(Faulkner 2000).

Catalytically active vanadium bromoperoxidase requires one equivalent of vanadium (V) per subunit of enzyme. Using vanadium as the cofactor, V-BrPO catalyzes the two-electron oxidation of bromide and iodide by hydrogen peroxide in a substrate-inhibited bi bi ping pong mechanism (de Boer and Wever 1988; Everett et al. 1990a). The oxidized halogen intermediate can halogenate an appropriate organic substrate or oxidize a second equivalent of hydrogen peroxide to produce dioxygen in the singlet excited state (Scheme 2.1) (Everett and Butler 1989; Everett et al. 1990b). Bromination of organic substrates by V-BrPO proceeds through an electrophilic (i.e., Br^+) rather than a radical (Br^\bullet) process (Soedjak et al. 1995).



Scheme 2.1

Recently the X-ray crystal structure of native V-BrPO from the brown alga *Ascophyllum nodosum* (AnV-BrPO) and the red alga *Corallina officinalis* (CoV-BrPO) have been solved to 2.0 Å and 2.3 Å resolution respectively (Weyand et al. 1999; Isupov et al. 2000). The vanadium (V) atom in the X-ray structure of AnV-BrPO has a trigonal bipyramidal coordination geometry similar to the vanadium (V) site in vanadium chloroperoxidase (V-CIPO) (Weyand et al. 1999). Vanadium (V) in the form of vanadate ion, is axially coordinated by a histidine residue (His⁴⁸⁶) (AnV-BrPO). The negatively charged cofactor is neutralized by several hydrogen bond interactions from side chain residues at the active site. The protein residues (Ser⁴¹⁶, Gly⁴¹⁷, Lys³⁴¹, Arg³⁴⁹ N^{η1}, N^{η2}, Arg⁴⁸⁰ N^{η2}, His⁴¹⁸) act as proton donors to vanadate and constitute the central part of a rigid oxyanion binding site. The vanadate binding residues in CoV-BrPO were shown to be identical to residues

identified in *AnV*-BrPO, even though the structure was solved with inorganic phosphate in place of vanadate (Isupov et al. 2000).

The active sites of V-BrPO for both *C. officinalis* and *A. nodosum* contain an additional histidine residue not present in V-ClPO (i.e., His⁴⁷⁸ *CoV*-BrPO, sequence reported by Isupov et al., and His⁴¹¹ *AnV*-BrPO). The additional histidine residue is not coordinated to the vanadate cofactor, but is within hydrogen bonding distance to one of the vanadate oxygen atoms. It has been proposed that the extra histidine influences the activated peroxovanadate intermediate by decreasing its susceptibility to nucleophilic attack by chloride. The extra histidine residue may act as a proton donor/acceptor during the enzyme reaction, thus giving rise to the observed differences in catalytic activities of V-ClPO and V-BrPO (Hemrika et al. 1999; Weyand et al. 1999; Renirie et al. 2000a). However, the precise role of the extra histidine residue has not been fully determined.

In an effort to probe the role of certain active site residues and to elucidate the functional significance of the extra histidine residue at the active site we have cloned V-BrPO from the red alga *C. officinalis*. Reported herein is the first true sequence for the full-length cDNA of r*CoV*-BrPO, the deduced amino acid sequence, and the bacterial expression system used to obtain recombinant enzyme. Kinetic parameters for the recombinant protein were determined and found similar to the native enzyme. Also reported is the first mutational study on the active site of *CoV*-BrPO. As an initial approach to understanding the function of the additional histidine residue and its influence on halide oxidation (i.e., His⁴⁸⁰ r*CoV*-BrPO; this

work, as translated from the full nucleotide sequence), the effects of mutating the residue His⁴⁸⁰ to an alanine was examined. In addition to cloning V-BrPO from *C. officinalis*, marine red algae reported to produce halogenated marine natural products of pharmacological importance (*Plocamium*, *Laurencia*, and *Delisea*) were screened for V-BrPO activity and the V-BrPO genes cloned and characterized.

Methods and Materials

cDNA library construction and cloning of V-BrPO (*C. officinalis*):

Corallina officinalis was collected in April of 1998 off the coast of Santa Barbara, California and frozen at -80°C.

Total RNA was prepared from the alga by phenol/SDS extraction methods, and poly(A)⁺ RNA was further isolated using the PolyAtract mRNA isolation system (Promega). A double stranded cDNA library was prepared from poly(A)⁺ RNA (5 µg), using the Zap cDNA Synthesis Kit and the Zap cDNA Cloning Kit according to manufacturer's instructions (Stratagene).

Polymerase chain reaction (PCR) amplifications with oligonucleotides designed from the known nucleotide sequences of VBPO1 and VBPO2 from *Corallina pilulifera* were performed using cDNA prepared from total isolated mRNA. The upstream primer sequence used, (5'-GCCGAGGGCAGCCCATTCATCC-3') codes for the amino acid sequence [AEGSPFHP] from VBPO1 (Shimonishi et al. 1998). The downstream primer, (5'-AAGTAGTGAACACCTGCCATGTT-3') codes for the amino acid sequence [NMAGVHYF] from VBPO1 (Shimonishi et al. 1998). The temperature profile was 94 °C for 0.5 minutes, 51 °C for 0.5 minutes and 68 °C for 2.0 minutes for 25 cycles in a Perkin Elmer thermocycler. The PCR reactions were performed using high fidelity *pfu* Turbo DNA polymerase (Stratagene).

The single fragment obtained by PCR amplifications was used to probe a cDNA library from *C. officinalis*. One million clones were screened by plaque hybridization with a 3'-end labeled oligonucleotide. The oligonucleotide probe (5'-GCCGAGGGCAGCCCATTCCATCCGTCCTAC-3') was labeled with fluorescein-11-dUTP using terminal transferase (ECL 3'-oligolabelling module, AP Biotech). Phage plaques were transferred to nylon membranes, and the DNA fixed to the membranes by alkali fixation methods. Following pre-hybridization of the membranes for two hours at 45 °C in a solution containing 5 x SSC (0.750 M NaCl, 0.075 M sodium citrate pH 7.0), 0.02% w/v SDS, 100 µg salmon sperm DNA and 5 x Denhardt's solution, the membranes were hybridized overnight at 45 °C with the fluorescein labeled probe.

Membranes were washed several times with 1 x SSC, 0.1% SDS at 57 °C. Membranes were prepared for antibody incubations by blocking the filters at room temperature in 0.1 M Tris-HCl pH 7.5, 0.15 M NaCl and 20-fold dilution of antibody liquid block solution for 60 minutes (AP Biotech). The membranes were incubated overnight at room temperature with a 1/5000 dilution of an anti-fluorescein antibody conjugated to horseradish peroxidase (HRP, AP Biotech) in 0.1 M Tris-HCl pH 7.5, 0.4 M NaCl and 0.5% w/v bovine serum albumin, followed by several washes with the same buffer at room temperature.

Oligonucleotide probe detection was performed using luminol-based substrates (AP Biotech) with the conjugated reporter enzyme, HRP. Chemiluminescent signals were detected using ECLTM HyperfilmTM. Positive clones

were isolated and *in vivo* excision of the cDNA insert-containing pBluescript phagemids were performed. The cloned inserts were sequenced using T3/T7 primers from opposite directions by an automated DNA sequencer (Iowa State University, DNA Sequencing Facility).

Cloning of the 5'-coding region for the V-BrPO gene was performed by PCR amplification with cDNA template using primers designed from the 5'- nucleotide sequences of VBPO1 and VBPO2 and downstream sequence information obtained from cDNA library screening. The forward primer in the reaction was 5'-ATGGGTATTCCAGCTGACAAC-3' and the reverse primer used was 5'-CGTAGCCACCTCAGTCACCAG-3'. The temperature profile of the PCR reaction was 94 °C for 0.5 minutes, 52 °C for 1.0 minute, and 68 °C for 2.5 minutes for 25 cycles. Amplified PCR products were excised from a 0.7% agarose gel and cloned into the pGEM-T easy vector (Promega) for further sequence analysis.

RT-PCR cloning of marine red algae (*Plocamium cartilagineum*, *Laurencia pacifica*, and *Delisea pulchra*):

The marine red alga *Plocamium cartilagineum* was collected in an intertidal zone off the coast of Santa Barbara, California in the Fall of 2001 by Shane Anderson at the Marine Science Institute, UCSB. The marine red alga *Laurencia pacifica* was collected in an intertidal zone off the coast of La Jolla, California in the Fall/Winter of 2001/2002 by Eddie Kisfaludy at UCSD/Scripps. The marine red alga *Delisea pulchra* was collected by Bill Baker (University South Florida) on an

expedition to Antarctica in the Winter of 2002. All algae were stored at -80°C , sealed in double zip-lock freezer bags.

Small-scale isolation of total RNA. Frozen algae was rinsed in doubly deionized water (ddH₂O, Nanopure) followed by air drying at room temperature for 1 hour. Dried algae was frozen with liquid nitrogen and ground to a fine powder with a mortar and pestle. Six hundred milligrams of powdered algae was used with the Qiagen Plant RNeasy Kit (Qiagen) according to the manufacturer's protocols. Isolated total RNA was resuspended in 50 μL of DEPC-treated ddH₂O.

Reverse-Transcriptase Polymerase Chain Reaction. RT-PCR was performed using the One Step RT-PCR kit (Qiagen) according to the manufacturer's protocols. Primers used in the reactions were BPO1, BPO2, For3Full, For02, and FullRev (Table 2.1).

Primer name	Sequence
For3Full	5'ATGGGTATTCCAGCTGACAACCT3'
For02	5'CATGACGACAATGGCGCTATTAT3'
BPO1	5'GCCGAGGGCAGCCCATTCATCC3'
BPO2	5'AAGTAGTGAACACCTGCCATGTT3'
FullRev	5'CAATAAACGUTUGCCTAAGCTGC3'

Table 2.1: Primer sequences used in RT-PCR reactions.

Products from RT-PCR reactions were visualized on 0.7% - 1.5% agarose/TAE gels with ethidium bromide. DNA of interest was excised from the gel and purified using the GIBCO Concert Gel Extraction Kit (GIBCO-BRL) according to the manufacturer's protocol. Purified products were subcloned into the PCR-Script-Amp^r cloning vector (Stratagene) and transformed into Ultracompetent XL-1 Gold *E. coli* cells, all according to manufacturer's protocols. Transformed *E. coli* (at least 10-20 colonies) were grown to confluence, and plasmids isolated using the Plasmid Isolation Kit (BioRad). The presence of the insert of interest was confirmed by restriction digest analysis using PST1. Plasmids harboring the DNA of interest were sequenced by the Iowa State Sequencing Facility. The cloned inserts were sequenced using T3/T7 primers from opposite directions by an automated DNA sequencer.

Nucleotide and protein sequence alignment analyses. Nucleotide sequences of V-BrPO genes were aligned with CLUSTAL W without manual adjustment using the BIOEDIT sequence alignment editor (Hall 1999). The amino acid sequences for cloned V-BrPOs were also aligned using CLUSTAL W. Sequence identity analysis was performed using the GENEDOC program, v.2.5 (Nicholas et al. 1997).

Expression and purification of recombinant CoV-BrPO (*C. officinalis*):

The expression vector pTrcHis2B (Invitrogen) was doubly digested with *NcoI* and *PstI* followed by dephosphorylation of the vector ends. Using PCR, *NcoI* and *PstI* restriction sites were generated at the 5' and 3' ends respectively of the V-BrPO gene. The forward primer used was 5'-

CTAGCCATGGGTATTCCAGCTGAC-3', and the reverse primer was 5'-
TTCCTTCTGCAGCAATAAACGTTGGCCTAA-3'. The restriction sites are
underlined in each primer. The PCR product was doubly digested with *NcoI* and
PstI restriction enzymes to generate the restriction ends on either side of the V-BrPO
gene. Following purification of the gene on a 1% agarose gel, the gene was ligated
to the *NcoI* and *PstI* sites of the pTrcHis2B expression vector. A transformation
reaction of the ligation product was performed into the *E.coli* strain BL21.

A small starter culture of the transformed bacteria with the resultant plasmid
was used to inoculate a 1-liter culture of LB-medium containing 100 µg/ml of
ampicillin. Recombinant expression was induced with 1 mM IPTG after 6 hours of
growth at 37 °C. Protein expression experiments were performed at 20 °C, 30 °C
and 37 °C for various lengths of time to optimize protein expression levels.

The induced cells were harvested by centrifugation at 5000 x g for 20
minutes at 4 °C followed by resuspension of the cells in 50 mM Tris-SO₄ buffer (pH
8.0) with 1 mM NH₃VO₃. Cell lysis was performed using lysozyme treatment (100
ug/ml) followed by sonication.

Soluble protein was purified by modification of the protocol described for
recombinant V-BrPO from *C. pilulifera* (Shimonishi et al. 1998). In all anion
exchange purification steps KBr salt was used instead of NaCl. Active fractions
eluting from the DEAE FF anion exchange column were heat shock treated at 65 °C
for 20 minutes followed by immediate centrifugation at 16,000 x g. The supernatant

was used in all subsequent purification steps. In addition, the gel filtration resin Superose 6 (Pharmacia) was used in FPLC as a last purification step.

Production of mutant H480A (from recombinant CoV-BrPO):

Mutant H480A was produced using the Quickchange Site-directed Mutagenesis Kit (Stratagene). The mutation was made directly in the pTrc2.CVBPO expression vector according to the Quickchange protocol using the primers 5'-TCGCCGAGGGCAGCCCATTCGCCCCGTCCTACGGAAGCGGCCA-3' and the complementary primer 5'-TGGCCGCTTCCGTAGGACGGGGCGAATGGGCTGCCCTCGGCGA-3'. After confirming the presence of the desired mutation by sequencing, the vector was transformed into the *E. coli* strain BL21 for expression experiments. Purification of mutant H480A was as described for rCoV-BrPO.

Purification of native V-BrPO from marine red algae (*Plocamium cartilagineum*):

Approximately 300 grams of algae were ground in a cooled mortar and pestle with liquid nitrogen to obtain a fine red powder. Two volume equivalents of 0.1 M Tris-buffer pH 8.0 was added to the powdered algae and blended at high speed at 4 °C for 10 minutes (commercial Waring Blender). Crude extracts were centrifuged at 6000 rpm for 30 minutes, and the supernatants retained. Remaining algal pellets were rehomogenized two more times followed by centrifugation. The pooled supernatants were concentrated on an Amicon stir-cell with a 30 kDa cut-off filter membrane. The concentrated supernatants were batch loaded onto 200 mL of DEAE FF resin (Pharmacia). Protein was eluted by step-gradient using 1M NaCl in

0.1 M Tris-SO₄ pH 8.0. Bromoperoxidase activity of collected fractions was determined by standard monochlorodimedone (MCD) assay (see below). In some cases bromoperoxidase activity was determined by bromination of phenol red to bromophenol blue, or by using the triiodide assay. Haloperoxidase activity eluted within the 0.3 - 0.5 M NaCl fraction. Fractions showing haloperoxidase activity were further purified by Superose-6 gel filtration in 0.1 M Tris-HCl pH 8.0, and by Mono Q anion exchange chromatography (same buffers as was used for DEAE FF). The final yield of V-BrPO was 300 units of bromoperoxidase activity as determined by MCD activity.

Demetallation/remetallation of purified V-BrPO. The role of vanadium in the haloperoxidase enzyme purified from *P. cartilagineum* was determined by removal of bound metal cofactors by overnight dialysis with 0.1 M citrate/phosphate buffer (pH 3.9) at 4°C (with or without 5 mM EDTA). Following dialysis the samples were reconstituted in buffer (0.1 M Tris-HCl pH 8.0; with or without 1 mM NH₄VO₃) by repetitive washing, and subsequently assayed for MCD bromination.

Conditions for steady state kinetic analysis of native, recombinant, and mutant V-BrPOs:

The reaction buffer for the steady state kinetic analysis of MCD bromination consisted of 80 mM sodium phosphate at pH 6.50 with varied concentrations of potassium bromide (0.500 mM – 50 mM) and sufficient sodium sulfate to give a final ionic strength of 0.8 M. The hydrogen peroxide concentrations were varied from 5 μM to 5 mM. All reactions were performed at 25 °C. The concentration of

hydrogen peroxide was determined spectrophotometrically by the formation of triiodide (I_3^-) as described (Bjorksten 1968).

Iodoperoxidase activity for mutant H480A was measured by following the conversion of I^- to I_3^- by hydrogen peroxide at 350 nm ($\epsilon_M = 26,400 \text{ cm}^{-1} \text{ M}^{-1}$). Enzyme-free reactions were used as background controls. The enzyme activity was determined indirectly by measuring the consumption of H_2O_2 . The reaction buffer consisted of 80 mM sodium phosphate pH 6.5 with varied concentrations of potassium iodide (0.250 mM – 100 mM). The hydrogen peroxide concentrations were varied from 5 μM to 800 μM . All reactions were performed at 25 °C. In addition, steady state kinetic reactions for mutant H480A were performed in the presence of excess vanadate (100 μM) to account for possible alterations of protein-cofactor interaction introduced by the mutation.

Steady state kinetic analysis:

The initial rates, v , as a function of hydrogen peroxide or bromide/iodide concentrations were fit to the Michaelis-Menten expression of the form $v = V[H_2O_2]/(K + [H_2O_2])$ by an iterative process, where V and K are functions of K_m^{halide} and $K_m^{H_2O_2}$ (Cleland 1979). The kinetic parameters, K_m^{halide} and $K_m^{H_2O_2}$ were obtained from appropriate fits of initial rate data as a function of hydrogen peroxide and bromide/iodide concentrations using Cleland's programs PINGPONG (Cleland 1979). All measurements were performed in duplicate or triplicate. Results

presented are the least square fits to the data and not the best fit by the PINGPONG program.

Kinetic Derivations. The rate equation for an enzyme-catalyzed ping-pong reaction with two substrates (H_2O_2 and Br^-) is

$$v = \frac{V[\text{H}_2\text{O}_2][\text{Br}^-]}{K_m^{\text{H}_2\text{O}_2}[\text{Br}^-] + K_m^{\text{Br}^-}[\text{H}_2\text{O}_2] + [\text{H}_2\text{O}_2][\text{Br}^-]} \quad \text{eq. 2.1}$$

which can be cast in the form of a rectangular hyperbola for fixed values of $[\text{H}_2\text{O}_2]$:

$$v = \frac{V[\text{Br}^-]}{K + [\text{Br}^-]} \quad \text{eq. 2.2}$$

where

$$V = \frac{V_{\max}}{1 + (K_m^{\text{H}_2\text{O}_2}/[\text{H}_2\text{O}_2])} \quad \text{eq. 2.3}$$

$$K = \frac{K_m^{\text{Br}^-}}{1 + (K_m^{\text{H}_2\text{O}_2}/[\text{H}_2\text{O}_2])} \quad \text{eq. 2.4}$$

Plots of $1/v$ versus $1/[\text{Br}^-]$ are linear and parallel at varying $[\text{H}_2\text{O}_2]$ since

$$\frac{1}{v} = \frac{1}{V} + \frac{K}{V[\text{Br}^-]} \quad \text{eq. 2.5}$$

Enzyme activity assays

In-gel activity staining was performed for native, recombinant and mutant forms of *CoV*-BrPO. SDS-polyacrylamide gel electrophoresis was performed using 10% Ready-Gels (Bio-Rad) under native conditions (in the presence of SDS, but without reducing agent or boiling). Bromoperoxidase activity in the gel was assessed by incubating the gel in 0.1 M sodium phosphate buffer (pH 6.5), 0.1 M KBr, 100 μ M vanadate, 1 mM *o*-dianisidine, and 2 mM H₂O₂.

Specific activity measurements for the bromination of MCD were performed for r*CoV*-BrPO and mutant H480A at varied pH (4.5 – 7.0) in 0.1 M citrate/phosphate buffer. Reactions were performed under conditions of low substrate concentrations (0.5 mM H₂O₂, 5 mM Br⁻) and high substrate concentrations (5 mM H₂O₂, 100 mM Br⁻) in the presence of 100 μ M vanadate. Protein concentrations were determined according to bicinchoninic acid assay purchased from Pierce Chemical Co.

Results

DNA and amino acid sequence analysis of recombinant vanadium bromoperoxidase from marine red algae:

The cloning strategy used to obtain the genes for V-BrPO from marine red algae was prompted by earlier studies which demonstrated that the vanadium-dependent bromoperoxidases from *C. pilulifera* and *C. officinalis* reacted similarly towards antiserum generated against purified V-BrPO from *C. pilulifera* (Itoh et al. 1987). In addition, protein amino acid analyses of other vanadium-dependent haloperoxidases from marine sources have shown high sequence similarity of active site residues associated with the binding site of the vanadate cofactor (Shimonishi et al. 1998; Weyand et al. 1999; Isupov et al. 2000).

The use of primers and DNA probes designed to target the active site sequences of vanadium-dependent haloperoxidases afforded single clones for V-BrPO from the marine red algae *C. officinalis* (*CoV-BrPO*), and *P. cartilagineum* (*PcV-BrPO*), and two different clones from the marine red alga *D. pulchra* (*DpDV-BrPO* and *DpEV-BrPO*). The complete gene sequence for *CoV-BrPO* was constructed using nucleotide sequences obtained from cDNA library screening and PCR experiments. The complete gene sequences for *PcV-BrPO*, *DpDV-BrPO* and *DpEV-BrPO* were constructed from nucleotide sequences obtained from RT-PCR experiments. Sequencing of at least fifteen isolated clones from both directions was performed to check for ambiguities in the gene sequences and the possible presence of isoforms. The clones *CoV-BrPO*, *PcV-BrPO*, *DpDV-BrPO* and *DpEV-BrPO* are

all 1794 nucleotides in length, and the open reading frame of each gene encodes a protein of 598 amino acids [Figures 2.1 – 2.4]. The calculated molecular mass for each protein is 65,458 Da.

The translated amino acid sequences for cloned V-BrPOs (*CoV*-BrPO, *PcV*-BrPO, *DpDV*-BrPO, *DpEV*-BrPO) were examined with respect to other known amino acid sequences of vanadium-dependent bromoperoxidases. Alignments to V-BrPOs isolated from *C. pilulifera* showed greater than 90% sequence identity, with 100% conservation of all active site residues with one exception [Figure 2.5]. Surprisingly, the two clones isolated from *D. pulchra* differ in only three amino acids, where an important amino acid substitution occurs (H553R) in a conserved active site domain.

In addition, alignments of amino acid sequences from the marine brown algae *A. nodosum* and *Fucus distichus* to cloned V-BrPOs are shown [Figure 2.5]. Both V-BrPOs from the brown algae show 31% sequence identity to cloned V-BrPOs (*CoV*-BrPO, *PcV*-BrPO, *DpDV*-BrPO, *DpEV*-BrPO). Shown in black are amino acids that are conserved 100% between all V-BrPOs. The alignments for V-BrPOs amino acid sequences indicate highly conserved consensus sequences, GSPxHPSYxSGHA and LTxxGEI/LNKLAxNxAxGRxMxGxHYxxDxxxxLLLGE. The conserved consensus sequence contains amino acid residues reported to be associated with the anion-binding site of the vanadate cofactor as shown by X-ray crystallography (Messerschmidt and Wever 1996; Weyand et al. 1999; Isupov et al. 2000).

Corallina officinalis

1 ATGGGTATTCCAGCTGACAACTCCAAGTCGCGCCAAGGCTTCATTTCGATACGCGTGTATCTGCGGCCGAGCTCGCACTCGCCCGGGA
M G I P A D N L Q S R A K A S F D T R V S A A E L A L A R G

91 GTTGTGCCATCGCTTGCAAATGGAGAGGAGCTTCTCTACCGCAACCCCTGACCCCTGAGAACGGAGATCCAAGCTTCATCGTTAGCTTCACA
V V P S L A N G E E L L Y R N P D P E N G D P S F I V S F T

181 AAGGCTCTCCCGATGACGACAATGGCGCTATTATTGACCCCGACGACTTCTTGGCCTTCGTTTCGTCGCGATCAATAGTGGAGATGAGAAG
K G L P H D D N G A I I D P D D F L A F V R A I N S G D E K

271 GAGATCGCCGACCTCACATTGGGGCCAGCTCGCGACCCGACACTGGCTTACCAATCTGGCGCTCGGATTTGGCGAATTCCTCGAGCTC
E I A D L T L G P A R D P D T G L P I W R S D L A N S L E L

361 GAAGTGCAGGATGGGAAAACAGCTCTGCCGGTCTCACCTTCGACCTGGAGGGCCCGGACGCGCAGTCGATGGCCATGCCACCGGGCGCT
E V R G W E N S S A G L T F D L E G P D A Q S I A M P P A P

451 GTGCTCACGAGCCCTGAGCTCATCGCCGAGATAGCAGAACTGTACCTGATGGCGCTGGACGCGAAATCGAGTTTAGCGAGTTTATTGTC
V L T S P E L I A E I A E L Y L M A L G R E I E F S E F D S

541 CCAAAGAACGACAGATATATTCATTTCCTATTGATCAGCTTAACGGGCTAGAGTGGTTC AACACGCGCGCAATGCTCGGAGATCCGCT
P K N A E Y I Q F A I D Q L N G L E W F N T P A M L G D P P

631 GCGGAAATCCGTCGCGCTCGCGGTGAGGTGACTGTTCGAAACTTGTTCGCGGTATTCTTCCAGGCTCTGAGGTCGCGCCGATATCAGC
A E I R R R R G E V T V G N L F R G I L P G S E V G P Y L S

721 CAGTACATCATCGTTGGTAGCAAGCAGATTGGCTCCGCGACGGGTGGCAACAAACTCTCGTGAGCCCAATGCCGCTGATGAGTTTGTAT
Q Y I I V G S K Q I G S A T G G N K T L V S P N A A D E F D

811 GGTGAAATCGCCTACGGAAGCATCACCATTAGCCAGCGGGTGCCTATCGCCACGCTGGCGCGACTTTATGACCGACTTGAAGGTATTC
G E I A Y G S I T I S Q R V R I A T P G R D F M T D L K V F

901 CTTGACGTCACGAGCAGCTCGCGACTTCCGAGGCTTTGAGTCGTATGAGCCGGGAGCACGCTCATCCGACGATCCCGCATCTTGGCAGC
L D V Q D A A D F R G F E S Y E P G A R L I R T I R D L A T

991 TGGGTGCACTTTGACGCACTGTACGAGGCTACCTCAATCGCTGCCTGATTCTGTGGCGAACCGGTGCCGTTTCGATCCCAACATCCG
W V H F D A L Y E A Y L N A C L I L L A N R V P F D P N I P

1081 TTCCAGCAGGAGGACAAGCTCGATAACCAGGACGTGTTTGTGAACTTCGGAGACGCACAGTGTGAGTCTGGTGACTGAGGTGGCTACG
F Q Q E D K L D N Q D V F V N F G D A H V L S L V T E V A T

1171 CGCGCTTGAAGGCGGTACGGTACCAGAAGTTTAACATTCATCGCTCGCGCTGCGGCTGAGGCTACCGGTGGTCTGATAGCGTGAACAA
R A L K A V R Y Q K F N I H R R L R P E A T G G L I S V N K

1261 ATCGCAGCGGAGAAGGCGAGAGCGTTTCCCTGAGGTTGACCTTGCTGTGAAGAGCTGAAGATATCCTGGAAAGCTGAAATTAGC
I A A E K G E S V F P E V D L A V E E L E D I L E K A E I S

1351 AATAGGAAACAGAACAATGCTGACGAGATCCCTGACCCCTGATCCTTCATTCCTGTTCCCGCAGGCATTCGCCGAGGGCAGCCCATCCAT
N R K Q N I A D G D P D P D P S F L L P Q A F A E G S P F H

1441 CCGTCTACGGAAGCGGCCACGCTGTGGTTCGTCGGCGCATGTGTGACGATCCCTCAAGCGTTCCTTCGACTCCAACCTCCAGATCGATCAG
P S Y G S G H A V V A G A C V T I L K A F F D S N F Q I D Q

1531 GTGTTTCGAGGTCGACAAAGATGAGGACAAGCTTGTAAGTTCGCTTTCAAGGAACTCTCACTGTTCGCCGTTGAGCTGAACAAGCTCGCC
V F E V D K D E D K L V K S S F K G T L T V A G E L N K L A

1621 GACAATATTGCGATCGGGCGGAACATGGCAGGTGTTCACTACTTCTCTGACCACTCGAGTCAATTCCTGCTGGTGAGCAGGTTCGCGATT
D N I A I G R N M A G V H Y F S D Q F E S I L L G E Q V A I

1711 GGAATCTTGGAGAGCAGAGCTGACGATGAGGAGAACTTCTTCTCAACTGCGGAAGTTTGATGGAATACAATCCAGATCTAA
G I L E E Q S L T Y G E N F F F N L P K F D G T T I Q I *

Figure 2.1: The nucleotide sequence and deduced amino acid sequence of *Corallina officinalis* vanadium bromoperoxidase (accession number AF218810). The nucleotide sequences used in primer design for PCR amplification reactions are listed in Table 2.1. The nucleotide sequences used as a probe to screen the cDNA library are provided in Methods and Materials.

Plocamium cartilagineum

1 ATGGGTATTCCAGCTGACAACCTCCAAAGTCGCGCCAAAGGCTTCATTCGATACGCGTGTATCTGCGGCTGAGCTCGCACTCGCGCGCGGA
M G I P A D N L Q S R A K A S F D T R V S A A E L A L A R G

91 TCTGTACCATCGTTTGCAAATGGAGAGGAGCTTCTCTACCGCAACCCTGACCCCTGATAACGATGATCCAAGCTTCATCGTAGCTTCACA
S V P S F A N G E E L L Y R N P D P D N D D P S F I A S F T

181 AAGGGTCTTCCGCACGACACAATGGCGCTATTATTGACCCCGACGACTTCTTGGCCTTCGTTCTGCGATCAATAGTGGAGATGAGAAG
K G L P H D D N G A I I D P D D F L A F V R A I N S G D E K

271 GAGATCGCCGACCTCACATTGGGGCCAGCTCGCGACCCGGACACTGGCTTACCAATCTGGCGCTCGGATTTGGCGAATTTCTAGAGCTC
E I A D L T L G P A R D P D T G L P I W R S D L A N S L E L

361 GAAGTGCAGGATGGGAAAACAGCTCTGCCGGTCTCACTTTCGATCTGGAGGCGCGACGCGCAGTCGATTCGCATGCCACCGGCGCT
E V R G W E N S S A G L T F D L E G P D A Q S I A M P P A P

451 GTGCTCACGAGCCCTGAGCTCATCGCCGAGATAGCAGAAGTACCTGATGGCGCTTGGACGCGAAATCGGATTTAGCAGTGTGATTC
V L T S P E L I A E I A E L Y L M A L G R E I E F S E F D S

541 CCAAAGAACGAGATATATTGCTATTGATCAGCTTAACGGCTAGAGTGGTCAACACCGCGCAATGCTCGGAGATCCGCCT
P K N A E Y I Q F A I D Q L N G L E W F N T P A M L G D P P

631 GCGAAAATCCGTCGCGCTCGCGGTGAGGTGACTGTGCGAAACTTGTTCGCGGTATTCTTCCAGGCTCTGAGGTGCGCCGTATCTCAGC
A K I R R R R G E V T V G N L F R G I L P G S E V G P Y L S

721 CAGTACATCATCGTTGGTAGCAAGCAGATTGGCTCCGCGAGGTTGGCAGCAAACTCTCGTAGCCCAATGCCGCTGATGAGTTGAT
Q Y I I V G S K Q I G S A T V G S K T L V S P N A A D E F D

811 GGTGAAATCGCCTACGGAAGCATACCATTAGCCAGCGTGTGCGTATCGCCACGCTGGGCGGACTTCATGACCGACTTGAAGGTATTC
G E I A Y G S I T I S Q R V R I A T P G R D F M T D L K V F

901 CTTGACGCTCCAGGACGCTCGGACTTCCGAGGCTTTGAGTCTGATGAGCCGGAGCAGCCTCATCCGGACGATCCGCGATCTTGGCAGC
L D V Q D A A D F R G F E S Y E P G A R L I R T I R D L A T

991 TGGGTGCACTTTGACGCACTGTACGAGGCCACTCAATGCGTGCCTGATTCTGTGGCGAACCAGCGTGCCTTCGATCCCAACATTCCG
W V H F D A L Y E A Y L N A C L I L L A N R V P F D P N I P

1081 TTCCAGCAGGAGGCAAGCTCGATAAACCAGGACGTGTTTGTGAACCTTCGGAGACGCACACGCTGCTGAGTCTGGTGAAGTGGCTAGC
F Q Q E G K L D N Q D V F V N F G D A H V L S L V T E V A T

1171 CGCGCGTTGAAGGCGTACGGTACCAGAAGTTAACATTCATCGTGCCTCGCGCTGAGGCTACCGGTGGTCTGATAGCGTGAACAA
R A L K A V R Y Q K P N I H R R L R P E A T G G L I S V N K

1261 ATCGCAGCGGAGAAGGGCGAGAGCGTTTTCCCTGAGGTTGACCTTGCTGTTGAAGAGCTTGGAGATATCCTGGAGAAAGCTGAATTAGC
I A A E K G E S V F P E V D L A V E E L G D I L E K A E I S

1351 AATAGGAACAGAACATTGCTGACGGAGATCCTGACCCCTGATCCTTCATTCCTGTTGCCGACGGCATTCCGCCAGGGCAGCCATCCAT
N R K Q N I A D G D P D P D P S F L L P Q A F A E G S P F H

1441 CCGTCTACGGAAGCGCCACGCTGTGGTTGCTGGCGCATGTGTGACGATCCTCAAGGCGTCTTTCGACTCCAACCTCCAGATCGATCAG
P S Y G S G H A V V A G A C V T I L K A F F D S N F Q I D Q

1531 GTGTTCCAGGTCGACAAAGATGAGGACAGGCTTGTAAAGTCGCTTTCAAGGGAACCTCTCACTGTTGCCGGTGAAGTGAACAGCTCGCC
V F E V D K D E D R L V K S S F K G T L T V A G E L N K L A

1621 GACAATATTGCGATCGGGCGGAACATGGCAGGTGTTCACTACTTCTCTGACCAGTTCGAGTCAATTCGCTTGGTGAAGCAGGTTGCGATT
D N I A I G R N M A G V H Y F S D Q F E S I L L G E Q V A I

1711 GGAATCTTGAAGAGCAGAGTCTGACGTATGGCGAGAAGTCTTCTTCAACTTCCGGAAGTTGATGGAACATAATCCAGATCTAA
G I L E E Q S L T Y G E N F F F N L P K F D G T T I Q I *

Figure 2.2: The nucleotide sequence and deduced amino acid sequence of *Plocamium cartilagineum* vanadium bromoperoxidase. The nucleotide sequences used in primer design for RT-PCR amplification reactions are shown in Table 2.1.

D. pulchra clone E

```

1   ATGGGTATCCAGCTGACAACCTCCAAAATCGCGCAAGGCTTCATTTCGATACCGGTGTATCTGCGCGGAGCTCGCACTCGCCCGCGGA
   M G I P A D N L Q N R A K A S F D T R V S A A E L A L A R G
91  GTTGTGCCATCGTTTGC AAAATGGAGAGGAGCTTCCCTACCCGACCCCTGACCCCTGAGAACGGTGATCCAAGCTTCATCGCTAGCTTCACA
   V V P S F A N G E E L P Y R D P D P E N G D P S F I A S F T
181 AAGGCTCTCCGCACGACGACAATGGCGCTATTATTGACCCGACGACTTCTTGGCCTTCGTTTCGTGCGATCAATAGTGGAGATGAGAAG
   K G L P H D D N G A I I D P D D F L A F V R A I N S G D E K
271 GAGATCGCCGACCTCACATTTGGGACCAGCTCGCGACCCGACACTGGCTTACCAATCTGGCGCTCGGATTTGGCGAATTCCTCGAGCTC
   E I A D L T L G P A R D P D T G L P I W R S D L A N S L E L
361 GAAGTGCAGGATGGGCCAACAGCTCTGCCGGTCTCACCTTCGACCTGGAGGGCCCGGACGCGCAGTCGATTGCCATGCCACCCGGCGCCT
   E V R G W A N S S A G L T F D L E G P D A Q S I A M P P A P
451 GTGCTCACGACCCCTGAGCTCATCGCCGAGATAGCAGAAGTGTACCTGATGGCACTTGGACGCGAAATCGAGTTTAGCGAGTTTGATTCC
   V L T S P E L I A E I A E L Y L M A L G R E I E F S E F D S
541 CCAAAGAACGACAGATATATTCAGTTTGCCTATTCATCAGCTTAACGGCTAGAGTGGTCAACACGCCGGAATGCTCGGAGACCCGCCT
   P K N A E Y I Q F A I D Q L N G L E W F N T P A M L G D P P
631 GCGGAAATCCGTCGCGCTCGCGGTGAGGTGACTGTCGAAAACCTTGTTCGCGGTATTCTTCCAGGCTCTGAGGTCGCGCCGCTATCTCAGC
   A E I R R R R G E V T V G N L F R G I L P G S E V G P Y L S
721 CAGTACATCATCGTTGGTAGCAAGCAGATTGGCTCCGCGACGGTTGGCAGCAAACTCTCGTGAGCCCAATGCCGCTGATGAGTTTGTAT
   Q Y I I V G S K Q I G S A T V G S K T L V S P N A A D E F D
811 GGTGAAATCGCCTACGGAAGCATACCATTAGCCAGCGTGTGCGTATCGCCACGCTGGGCGGACTTCATGACCCGACTTGAAGGTATTC
   G E I A Y G S I T I S Q R V R I A T P G R D F M T D L K V F
901 CTTTACGTCAGGACGCTGCGGACTTCCGANGCTTTGAGTCGTATGAGCCGGGAGCAGCCCTCATCCGACGATCCCGGATCTTGGCAGG
   L Y V Q D A A D F R X F E S Y E P G A R L I R T I R D L A T
991 TGGGTGCACCTTACCGCAGTACGAGGCCCTACCTCAATGCGTGCCTGATCTGTTGGCGAACCCGTCGCGCTTCGATCCCAACATCCG
   W V H F D A L Y E A Y L N A C L I L L A N R V P F D P N I P
1081 TTCCAGCAGGAGGACAAGCTCGATAACCAGGACGTGTTTGTGAACTTCGGAGACGCACAGTGTGAGTCTGGTGACTGAGTGGCTACG
   F Q Q E D K L D N Q D V F V N F G D A H V L S L V T E V A T
1171 CGCGCGTTGAAGCGGTACGGTACCAGAAGTTTAACATTCATCGTCCGCTCGCGCTGAGGCTACCGGTGGTCTGATTAGCGTGAACAAA
   R A L K A V R Y Q K F N I H R R L R P E A T G G L I S V N K
1261 ATCCGACGGGAGAAGGCGAGAGCGTTTTCCCTGAGGTTGACCTTGTGTTGAAGAGCTTGGAGATATCTGGAGAAAGCTGAAATTAGC
   I A A E K G E S V F P E V D L A V E E L G D I L E K A E I S
1351 AATAGGAACAGAACATTTGCTGACGGAGATCCTGACCCCTGATCCTTCATTCCTGTTGCGCAGGCATTGCGCGAGGCGAGCCATCCAT
   N R K Q N I A D G D P D P D P S F L L P Q A F A E G S P F H
1441 CCGTCTACGGAAGCGCCACGCTGTGGTTGCTGGCGCATGTGTGACGATCCTCAAGGCGTTCTTCGACTCCAACCTCCAGATCGATCAG
   P S Y G S G H A V V A G A C V T I L K A F F D S N F Q I D Q
1531 GTGTTCCAGGTCGACAAAGATGAGGACAAGCTTGTAAAGTCGTTTCAAGGGAACCTCACTGTGCGCGTGAGCTGAACAAGCTCGCC
   V F E V D K D E D K L V K S S F K G T L T V A G E L N K L A
1621 GACAATATTGCGACCGGGCGGAACATGGCAGGTGTTGCTACTTCTCTGACCAGTTCGAGTCAATTCTGCTTGGTGGAGCAGTTGGCGATT
   D N I A T G R N M A G V R Y F S D Q F E S I L L G E Q V A I
1711 GGAATCTTGAAGAGCAGAGTCTGACGTATGGCGAGAACTTCTTCTCAACTTGGCGAAGTTTGTGGAACATAATCCAGATCTAA
   G I L E E Q S L T Y G E N F F F N L P K F D G T T I Q I *

```

Figure 2.3: The nucleotide sequence and deduced amino acid sequence of *Delisea pulchra* (clone E) vanadium bromoperoxidase. The nucleotide sequences used in primer design for RT-PCR amplification reactions are shown in Table 2.1.

Delisea pulchra.D

```

1   ATGGGTATTCAGCTGACAACCTCCAAAATCGCGCCAAGGCTTCATTCGATACGCGTGTATCTGCGGCCGAGCTCGCACTCGCCCGGGA
   M G I P A D N L Q N R A K A S F D T R V S A A E L A L A R G
91  CTTGTGCCATCGTTTGCAAATGGAGAGGAGCTTCCCTACC CGCACCTGACCTGAGAACGGTGATCCAAGCTTCATCGCTAGCTTCACA
   V V P S F A N G E E L P Y R D P D P E N G D P S F I A S F T
181 AAGGGTCTTCGACGACGACAATGGCGTATTATTGACCCGACGACTTCTTGGCCTTCGTTGCGATCAATAGTGGAGATGAGAAG
   K G L P H D D N G A I I D P D D F L A F V R A I N S G D E K
271 GAGATCGCCGACCTCACATTGGGGCCAGCCCGACCCGGACACTGGCTTACCAATCTGGCGCTCGGATTTGGCGAATTCTCTCGAGCTC
   E I A D L T L G P A R D P D T G L P I W R S D L A N S L E L
361 GAAGTGGAGGATGGGCCAACAGCTCTGCCGCTCTCACCTTCGACCTGGAGGGCCCGGACGCGAGTCGATTGCCATGCCACCGGCGCT
   E V R G W A N S S A G L T F D L E G P D A Q S I A M P P A P
451 GTGTCACGAGCCCTGAGTCATCGCCGAGATAGCAGAACTGACCTGATGGCACTTGGACGCGAAATCGAGTTTAGCGAGTTGATTCC
   V L T S P E L I A E I A E L Y L M A L G R E I E F S E F D S
541 CCAAAGAACGCAGAGTATATTGCTATTGATCAGCTTAACGGGCTAGAGTGGTTCAACACGCGGCAATGCTCGGAGACCCGCT
   P K N A E Y I Q F A I D Q L N G L E W F N T P A M L G D P P
631 GCGGAAATCCGTCGCGCTCGCGGTGAGGTGACTGTCGGAACCTTGTCCGCGGTATTCTCCAGGCTCTGAGGTGCGGCCGCTATCTCAGC
   A E I R R R R R G E V T V G N L F R G I L P G S E V G P Y L S
721 CAGTACATCATCGTTGGTAGCAAGCAGATTGGCTCCGCGAGGTTGGCAGCAAACTCTCGTGAGCCCAATGCCGCTGATGAGTTTGAT
   Q Y I I V G S K Q I G S A T V G S K T L V S P N A A D E F D
811 GGTGAAATCGCCTACGGAAGCATCACCATAGCCAGCGTGTGCGTATCGCCACGCTGGCGCGACTTCATGACCCGACTGAAGGTATTC
   G E I A Y G S I T I S Q R V R I A T P G R D F M T D L K V F
901 CTTGACGCTCCAGGACGCTCGGACTTCCGAGGCTTTGAGTCGATGAGCCGGGAGCACGCTCATCCGGACGATCCGCGATCTTGCAGC
   L D V Q D A A D F R G F E S Y E P G A R L I R T I R D L A T
991 TGGGTGCACTTTGACGCACTGTACGAGGCTACCTCAATGCGTGCCTGATTCTGTGGCAACCGGCTGCCGTTGATCCCAACATCCG
   W V H F D A L Y E A Y L N A C L I L L A N R V P F D P N I P
1081 TTCCAGCAGGAGGACAAGCTCGATAACCAGGACGTGTTTGTGAACTTCGGAGACGCACAGTGTGAGTCTGGTACTGAGGTGGCTACG
   F Q Q E D K L D N Q D V F V N F G D A H V L S L V T E V A T
1171 CGCGCGTTGAAGGCGGTACGGTACCAGAAGTTAACATTTCGTCGCTCGGCTGAGGCTACCGGTGCTGATTAGCGTGAACAAA
   R A L K A V R Y Q K F N I H R R L R P E A T G G L I S V N K
1261 ATCCGACGCGAGAAGGCGGAGAGCGTTTTCCCTGAGGTTGACCTTGCTGTGAAGAGCTTGGAGATATCCTGGAGAAGCTGAAATTAGC
   I A A E K G E S V F P E V D L A V E E L G D I L E K A E I S
1351 AATAGGAAACAGAACATTGCTGACGGAGATCCTGACCTGATCCTTATTCTGTTGCCGAGGCTTTCGCGGAGGGCAGCCATTCCAT
   N R K Q N I A D G D P D P D P S F L L P Q A F A E G S P F H
1441 CCGTCTACGGAAGCGGCCACGCTGTGGTTGCTGGCGCATGTGTGACGATCCTCAAGGCGTTCTTCGACTCCAATTCCAGATCGATCAG
   P S Y G S G H A V V A G A C V T I L K A F F D S N F Q I D Q
1531 GTGTTGAGGTCGACAAAGATGAGGACAAGCTTGTAAAGTCGCTTTCAAGGGAAGCTCACTGTTGCGGTTGAGTGAACAAGCTCGCC
   V F E V D K D E D K L V K S S F K G T L T V A G E L N K L A
1621 GACAATATTGCGATCGGGCGGAACATGGCAGGTGTTCACTACTTCTGACCAGTTCGAGTCAATTCGCTTGGTGAGCAGGTTCGAGT
   D N I A I G R N M A G V H Y F S D Q F E S I L L G E Q V A I
1711 GGAATCTTGAAGAGCAGAGTCTGACGTATGGCGAGAAGCTTCTTCAACTTGGCGAAGTTTGATGGAACTACAATCCAGATCTAA
   G I L E E Q S L T Y G E N F F F N L P K F D G T T I Q I *

```

Figure 2.4: The nucleotide sequence and deduced amino acid sequence of *Delisea pulchra* (clone D) vanadium bromoperoxidase. The nucleotide sequences used in primer design for RT-PCR amplification reactions are shown in Table 2.1.

C. officinalis : ----- : -
A. nodosum : ----- : -
C. pilulifera-2 : ----- : -
C. pilulifera-1 : ----- : -
F. distichus : MLCHAADTRGSPMPD TGVLRLLTSEQRAKWRRQLEGEKSLGFHPSETPYIKYLEGSET : 60
P. cartilagineum : ----- : -
D. pulchra-E : ----- : -
D. pulchra-D : ----- : -

C. officinalis : ----- : -
A. nodosum : ----- : -
C. pilulifera-2 : ----- : -
C. pilulifera-1 : ----- : -
F. distichus : WKKVKLP TDGISASKILGKIMARVRIATALAVVLAAPCLAFDEVTASGVFPEEHKHTGEG : 120
P. cartilagineum : ----- : -
D. pulchra-E : ----- : -
D. pulchra-D : ----- : -

C. officinalis : -MGIFADNLQSRKASFDTRVSAEELALARGVVPSPANGSELLYRNPDPENGDPSFIASF : 59
A. nodosum : ---XTCSTSDDDADDPFPNERDDEAFASRVAAAKRELEGTGTVCQIN---NGETDLAAKF : 54
C. pilulifera-2 : -MGIFADNLQSRKASFDTRVAAEELALARGVVPSPANGSELLYRN--CETGDPSTIASF : 57
C. pilulifera-1 : -MGIFADNLQSRKASFDTRVAAEELALNRGVVPSPANGSELLYRNPPDNDPSTIASF : 59
F. distichus : RHLQTCTSDDDALDPAPNFRDINVAFASTRDAARRERDGTGTVCQIT---NGETDLATMF : 177
P. cartilagineum : -MGIFADNLQSRKASFDTRVSAEELALARGVVPSPANGSELLYRNPPDNDPSTIASF : 59
D. pulchra-E : -MGIFADNLQSRKASFDTRVSAEELALARGVVPSPANGSELPYRDPDPENGDPSFIASF : 59
D. pulchra-D : -MGIFADNLQSRKASFDTRVSAEELALARGVVPSPANGSELPYRDPDPENGDPSFIASF : 59

C. officinalis : TKGLPHDDNGAIIIDDDFLAFVRAINSGDEKEIADLTLC-PARDPDTGLPIWRSDLANSI : 118
A. nodosum : HKSLPHDELIC-QVDADAFALIEDCHLNGDLSICEDVPGNSECDP-----VG--- : 100
C. pilulifera-2 : TKGLPHDDNGAIIIDDDFLAFVRAINSGDEKEIADLTLC-PARDPETGLPIWRSDLANSI : 116
C. pilulifera-1 : TKGLPHDDNGAIIIDDDFLAFVRAINSGDEKEIADLTLC-PARDPETGLPIWRSDLANSI : 118
F. distichus : HKSLPHDELIC-QVTADDFALIEDCHLNGDLSICEDVPG-----DP-----AG--- : 219
P. cartilagineum : TKGLPHDDNGAIIIDDDFLAFVRAINSGDEKEIADLTLC-PARDPDTGLPIWRSDLANSI : 118
D. pulchra-E : TKGLPHDDNGAIIIDDDFLAFVRAINSGDEKEIADLTLC-PARDPDTGLPIWRSDLANSI : 118
D. pulchra-D : TKGLPHDDNGAIIIDDDFLAFVRAINSGDEKEIADLTLC-PARDPDTGLPIWRSDLANSI : 118

C. officinalis : ELEVRGWNSSAGLTFDLEGPDAQSIAMPPAPVLTSPELAEIAELYLMALGREIEFSEF : 178
A. nodosum : ---RLVNPTAAFAIDISGPAFSATTIPPVPTLSPELAAQLAEVYWMALARDVPPMQY : 155
C. pilulifera-2 : ELEVRGWNSSAGLTFDLEGPDAQSVAMPPAPVLTSPELAEIAELYLMALGRDIEFSEF : 176
C. pilulifera-1 : ELEVRGWNSSAGLTFDLEGPDAQSIAMPPAPVLTSPELAEIAELYLMALGREIEFSEF : 178
F. distichus : ---RLVNPTAAFAIDISGPAFSATTIPPVPTLSPELAAQLAEVYWMALARDVPPMQY : 274
P. cartilagineum : ELEVRGWNSSAGLTFDLEGPDAQSIAMPPAPVLTSPELAEIAELYLMALGREIEFSEF : 178
D. pulchra-E : ELEVRGWNSSAGLTFDLEGPDAQSIAMPPAPVLTSPELAEIAELYLMALGREIEFSEF : 178
D. pulchra-D : ELEVRGWNSSAGLTFDLEGPDAQSIAMPPAPVLTSPELAEIAELYLMALGREIEFSEF : 178

C.officinalis : DSPKNAEYIQFAIDQLNGLEWFNTPAMLGPPAEIRRRRGEVTVGNLFRGILPGSEVGPY : 238
A.nodosum : GDDITVTAAANLAGMGGFPNLDVAVTIGSDGTVDP-----LSQLFRATFVGVETGPF : 207
C.pilulifera-2 : ESPKNAAFIRSAIERLNGLEWFNTPAKLGPPAEIRRRRGEVTVGNLFRGILPGSEVGPY : 236
C.pilulifera-1 : DSPKNAEYIQFAIDQLNGLEWFNTPAKLGPPAEIRRRRGEVTVGNLFRGILPGSEVGPY : 238
F.distichus : GDEITTTAAANLAGMGGFPNLDVAVTIGSDGTVDP-----FSQLFRATFVGVETGPF : 326
P.cartilagineum : DSPKNAEYIQFAIDQLNGLEWFNTPAMLGPPAEIRRRRGEVTVGNLFRGILPGSEVGPY : 238
D.pulchra-E : DSPKNAEYIQFAIDQLNGLEWFNTPAMLGPPAEIRRRRGEVTVGNLFRGILPGSEVGPY : 238
D.pulchra-D : DSPKNAEYIQFAIDQLNGLEWFNTPAMLGPPAEIRRRRGEVTVGNLFRGILPGSEVGPY : 238

C.officinalis : LSQYIIVGSKOIGSATVGNKTLVSPNAAEFDGGETAYGSSITISQVRVRIATPGRDFMMDLK : 298
A.nodosum : ISQLLVN-----SFTIDSIITVEPKQETFAPDVNYMVD : 241
C.pilulifera-2 : LSQYIIVGSKOIGSATVGNKTLVSPNAAEFDGGETAYGSSITISQVRVRIATPGRDFMMDLK : 296
C.pilulifera-1 : LSQYIIVGSKOIGSATVGNKTLVSPNAAEFDGGETAYGSSITISQVRVRIATPGRDFMMDLK : 298
F.distichus : VSQLLVN-----SFTIDAIITVEPKQETFAPDLNYMVD : 360
P.cartilagineum : LSQYIIVGSKOIGSATVGNKTLVSPNAAEFDGGETAYGSSITISQVRVRIATPGRDFMMDLK : 298
D.pulchra-E : LSQYIIVGSKOIGSATVGNKTLVSPNAAEFDGGETAYGSSITISQVRVRIATPGRDFMMDLK : 298
D.pulchra-D : LSQYIIVGSKOIGSATVGNKTLVSPNAAEFDGGETAYGSSITISQVRVRIATPGRDFMMDLK : 298

C.officinalis : VFLLVQDAADFRCFESYEFGARLIRTRDLATWVHFDALYEAYLNAACLILLANRVFFDEN : 358
A.nodosum : EWLNIQNGGPPAGEELLDDELRFVFNARDLARVFTDNINTEAYRGALILLGLDAFNFRAG : 301
C.pilulifera-2 : VFLLVQDGAADFRCFESYEFGARLIRTRDLATWVHFDALYEAYLNAACLILLANRVFFDEN : 356
C.pilulifera-1 : VFLLVQDAADFRCFESYEFGARLIRTRDLATWVHFDALYEAYLNAACLILLANRVFFDEN : 358
F.distichus : EWLNIQNGGPPAGEELDEELRFIRNARDLARVSVFNINTEAYRGSLLILLGLGAFSEFG : 420
P.cartilagineum : VFLLVQDAADFRCFESYEFGARLIRTRDLATWVHFDALYEAYLNAACLILLANRVFFDEN : 358
D.pulchra-E : VFLLVQDAADFRCFESYEFGARLIRTRDLATWVHFDALYEAYLNAACLILLANRVFFDEN : 358
D.pulchra-D : VFLLVQDAADFRCFESYEFGARLIRTRDLATWVHFDALYEAYLNAACLILLANRVFFDEN : 358

C.officinalis : IFFQEDKLDNODVFNFGDAHVLSLVTEVATRAKAVRYQKFNHRRRLRPEARGGGLISV : 418
A.nodosum : VNGPFLD-IDRQACFVNFGISHYFRLLIG-AAELAQRSSWYQKWVHRFARPEALGGTLEH : 359
C.pilulifera-2 : IFFQEDKLDNODVFNFGSAHVLSLVTEVATRAKAVRYQKFNHRRRLRPEARGGGLISV : 416
C.pilulifera-1 : IFFQEDKLDNODVFNFGSAHVLSLVTEVATRAKAVRYQKFNHRRRLRPEARGGGLISV : 418
F.distichus : INGPFLD-IDRQACFVNFGTSHYFRLLIG-AAELAQRASCYQKWVHRFARPEALGGTLEH : 478
P.cartilagineum : IFFQEDKLDNODVFNFGDAHVLSLVTEVATRAKAVRYQKFNHRRRLRPEARGGGLISV : 418
D.pulchra-E : IFFQEDKLDNODVFNFGDAHVLSLVTEVATRAKAVRYQKFNHRRRLRPEARGGGLISV : 418
D.pulchra-D : IFFQEDKLDNODVFNFGDAHVLSLVTEVATRAKAVRYQKFNHRRRLRPEARGGGLISV : 418

C.officinalis : NKIAAEKG-ESVFPVVDLAVEEEDILEKAEISNRKQNIADGDEDDPDSFLLPQAFAGS : 477
A.nodosum : TIKG-----E-LNADFDLSLENAELKRVAAINAAQN-----PNNEVTYLLPQAIQEGS : 408
C.pilulifera-2 : NKKSFLAGSDIIFPEVSELVEEISSIIDDVAESNEKQNRADGIVSPDKSFLLPQAFAGS : 476
C.pilulifera-1 : NKIAPQKG-ESVFPVVDLAVEEEDILEKAEISNRKQNIADGDEDDPDSFLLPQAFAGS : 477
F.distichus : TIAG-----D-LDADFDSLENDLKRVAETNAAQN-----PNNEVTYLLPQAIQVGS : 527
P.cartilagineum : NKIAAEKG-ESVFPVVDLAVEEEDILEKAEISNRKQNIADGDEDDPDSFLLPQAFAGS : 477
D.pulchra-E : NKIAAEKG-ESVFPVVDLAVEEEDILEKAEISNRKQNIADGDEDDPDSFLLPQAFAGS : 477
D.pulchra-D : NKIAAEKG-ESVFPVVDLAVEEEDILEKAEISNRKQNIADGDEDDPDSFLLPQAFAGS : 477

```

C.officinalis : PEHPSYSGHAVVAGACVTILKAFDSDN-FQIDQVFEVDRDQEDKLVKSSFKG-RLTVAGE : 535
A.nodosum : PTHPSYPSGHATQNGAFATVLKALIGLDRGGDCYPDPVYDIDGLKLIDFRGSCLTPEGE : 468
C.pilulifera-2 : PEHPSYSGHAVVAGACVTILKAFDAN-FQIDKVFVVDLQEDKLVKSSFKG-RLTVAGE : 534
C.pilulifera-1 : PEHPSYSGHAVVAGACVTILKAFDSG-IEIDQVFEVDRDQEDKLVKSSFKG-RLTVAGE : 535
F.distichus : PTHPSYPSGHATQNGAFATVLKALIGLDRGGECPNPFVPSIDGLLELINFEGACLTPEGE : 587
P.cartilagineum : PEHPSYSGHAVVAGACVTILKAFDSDN-FQIDQVFEVDRDQEDKLVKSSFKG-RLTVAGE : 535
D.pulchra-E : PEHPSYSGHAVVAGACVTILKAFDSDN-FQIDQVFEVDRDQEDKLVKSSFKG-RLTVAGE : 535
D.pulchra-D : PEHPSYSGHAVVAGACVTILKAFDSDN-FQIDQVFEVDRDQEDKLVKSSFKG-RLTVAGE : 535

C.officinalis : LNKLAENIATGRNMAGVHYFSDQFESILLGEOVAIGILEEQSLTYGENFFNLPKFDGTT : 595
A.nodosum : LNKLAENVAFGROMLGIHYRFDGIQCLLLGETITVRLHQEIMTFAEESTFEFRLFTCEV : 528
C.pilulifera-2 : LNKLAENVAFGROMLGIHYRFDQFESILLGEOVAIGILEEQSLTYGENFFNLPKFDGTT : 594
C.pilulifera-1 : LNKLAENIATGRNMAGVHYFSDQFESILLGEOVAIGILEEQSLTYGENFFNLPKFDGTT : 595
F.distichus : LNKLAENVAFGROMLGIHYRFDGIQCLLLGETITVRLHQEIMTFAEESTFEFRLFTCEV : 647
P.cartilagineum : LNKLAENIATGRNMAGVHYFSDQFESILLGEOVAIGILEEQSLTYGENFFNLPKFDGTT : 595
D.pulchra-E : LNKLAENIATGRNMAGVHYFSDQFESILLGEOVAIGILEEQSLTYGENFFNLPKFDGTT : 595
D.pulchra-D : LNKLAENIATGRNMAGVHYFSDQFESILLGEOVAIGILEEQSLTYGENFFNLPKFDGTT : 595

C.officinalis : IQI----- : 598
A.nodosum : IKLFQDGTFTIDGFKCPLVYTGVENCV- : 556
C.pilulifera-2 : IQI----- : 597
C.pilulifera-1 : IQI----- : 598
F.distichus : IKLFQDGTFSIDGDMCSGLVYTGVAQCQA : 676
P.cartilagineum : IQIXX----- : 600
D.pulchra-E : IQI----- : 598
D.pulchra-D : IQI----- : 598

```

Figure 2.5: Alignment of the amino acid sequence of vanadium bromoperoxidase for *Corallina officinalis* with other known sequences of V-BrPOs. The sequences obtained from GenBank were aligned using ClustalW Multiple Alignment program and displayed using GeneDoc. Sequence identity analysis was performed using GeneDoc. *C. officinalis* translated from nucleotide sequence, accession number AF218810, *C. pilulifera*-1, accession number BAA31261; *C. pilulifera*-2, accession number BAA31262; *A. nodosum* V-BrPO, accession number 1QI9A-B; *Fucus distichus* V-BrPO, accession number AAC35279; *P. cartilagineum*, *D. pulchra*-E (Clone E), *D. pulchra*-D (clone D).

Expression of recombinant CoV-BrPO and H480A in *E.coli*:

For initial expression experiments of CoV-BrPO in *E.coli*, the gene was inserted into the vector pTrcHis2B (Invitrogen) under the control of a *trc* promoter.

Expression experiments were performed at various temperatures to optimize the amount of soluble protein produced. Experiments performed at 37 °C produced minimal amounts of soluble protein and the majority of expressed protein formed inclusion bodies [Figure 2.6]. Alteration of the growth temperature following induction proved to be important in order to increase the ratio of soluble to insoluble protein. Optimal soluble expression conditions V-BrPO were 16 hours at 20 °C – 25 °C, following induction with 1 mM IPTG.

rCoV-BrPO is produced as the apo-protein in *E.coli*, and requires the addition of vanadium during the purification procedures. Purification of the enzyme from bacterial cell lysates was similar to the procedure described for recombinant V-BrPO from *C. pilulifera*, and produced approximately 0.1 - 0.3 mg of purified protein per liter of culture with specific activities around 150 - 200 $\mu\text{mol MCD}$ brominated/min/mg.

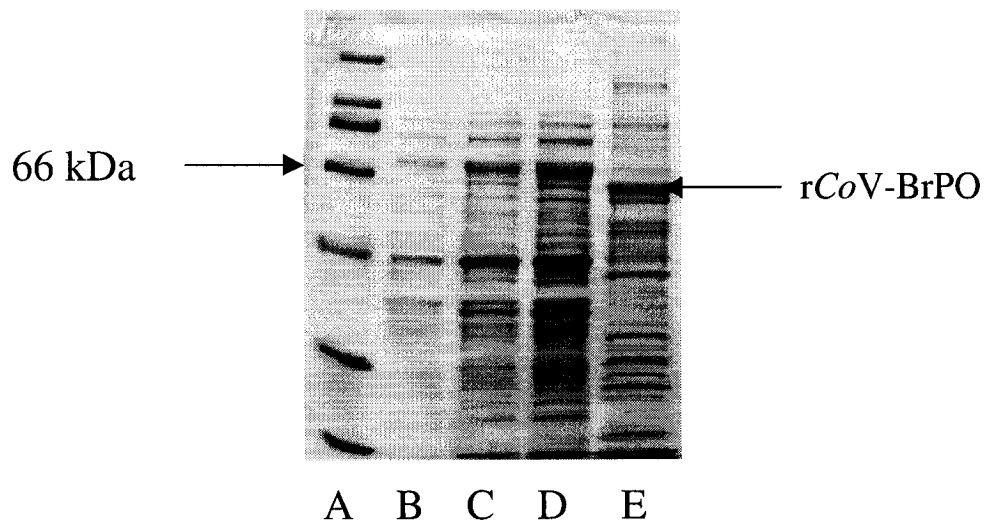


Figure 2.6: Reducing SDS-PAGE 10% gel (ReadyGels, Biorad) of *E. coli* expression experiments for rCoV-BrPO. Lane A, molecular weight marker. Lane B, post-induction time = 0 hrs (soluble protein). Lane C, post-induction time = 4 hrs (soluble protein). Lane D, post-induction time = 8 hrs (soluble protein). Lane E, post-induction time = 8 hrs (insoluble protein).

Kinetic analyses for recombinant CoV-BrPO and mutant H480A:

Recombinant CoV-BrPO. The steady state rates of MCD bromination by rCoV-BrPO were investigated as a function of hydrogen peroxide concentration (5 μM – 200 μM) and bromide concentration (0.500 mM – 5 mM) at pH 6.5. Plots of the initial rates of MCD bromination versus hydrogen peroxide and bromide concentrations showed typical Michaelis-Menten type saturation kinetic behavior.

Double reciprocal plots of the initial steady state rates of MCD-bromination versus hydrogen peroxide concentrations at low fixed bromide concentrations (0.500 mM – 2.00 mM) produced a set of parallel lines [Figure 2.7]. Parallel lines were also observed for initial steady state rates versus bromide concentrations at fixed hydrogen peroxide concentrations (5 μ M – 50 μ M) [Figure 2.8]. The parallel plots are consistent with the bi bi ping pong mechanism reported previously for the class of vanadium-dependent haloperoxidases (VHPOs)(de Boer and Wever 1988; Everett et al. 1990a; Soedjak and Butler 1991).

The values of K_m^{Br} and $K_m^{\text{H}_2\text{O}_2}$ for rCoV-BrPO at pH 6.5 were determined from the best fit using Cleland's PINGPONG program (Cleland 1979). The calculated values for K_m^{Br} and $K_m^{\text{H}_2\text{O}_2}$ were 1.20 mM and 17.0 μ M respectively (Table 2.2). The kinetic constants for native V-BrPO from *C. officinalis*, (isolated and purified from the same batch of alga as the mRNA for V-BrPO), were similar to values from the recombinant enzyme, i.e. K_m^{Br} of 1.29 mM and $K_m^{\text{H}_2\text{O}_2}$ of 27 μ M, showing explicitly that the native and recombinant proteins behave similarly [Figure 2.9, Figure 2.10]. The pH optimum and kinetic constants reported previously for native V-BrPO isolated from *C. officinalis* are in agreement with the values reported here (Table 2.2) (Sheffield et al. 1993).

Bromoperoxidase activity of mutant H480A. Kinetic analysis of the haloperoxidase activity for mutant H480A was performed to evaluate the affect the

mutation had on overall catalysis. rCoV-BrPO was used as a comparative wild type control in the measurements. When the haloperoxidase activity of mutant H480A

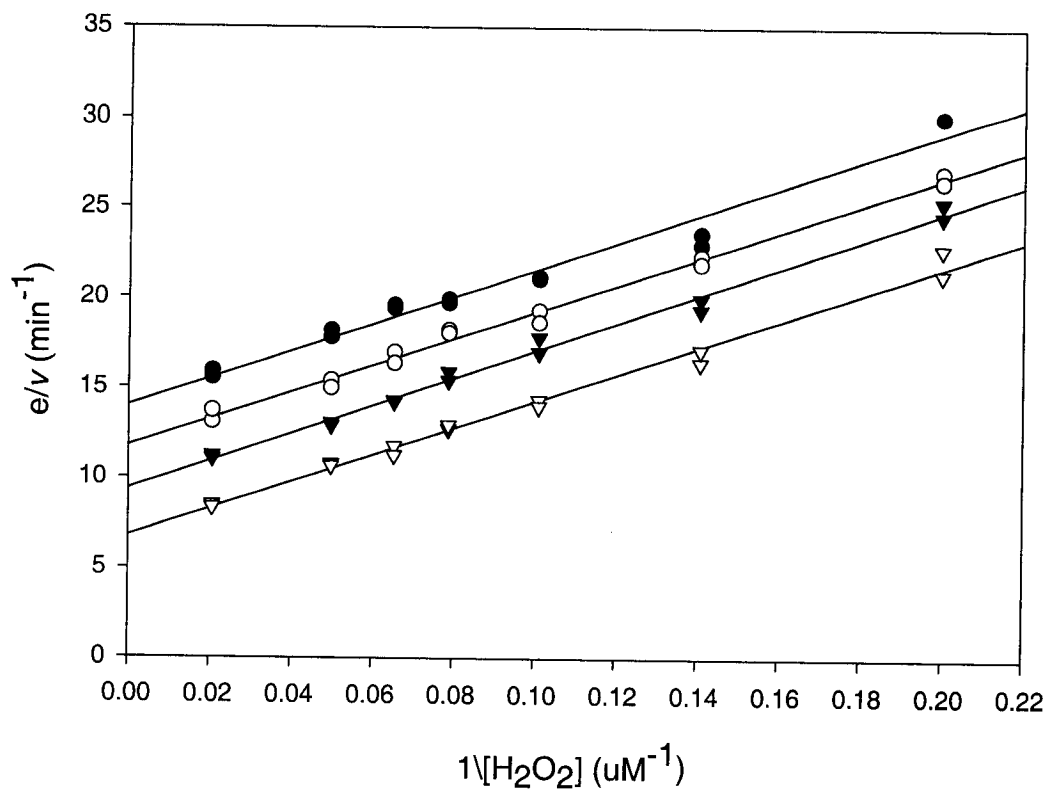


Figure 2.7: Primary double reciprocal plot of the rate of MCD bromination as a function of hydrogen peroxide concentration at fixed, low bromide concentrations at pH 6.50 for rCoV-BrPO; ● 0.500 mM Br⁻, ○ 0.750 mM Br⁻, ▼ 1.00 mM Br⁻, ▽ 2.00 mM Br⁻. Each line is the linear least squares fit to data.

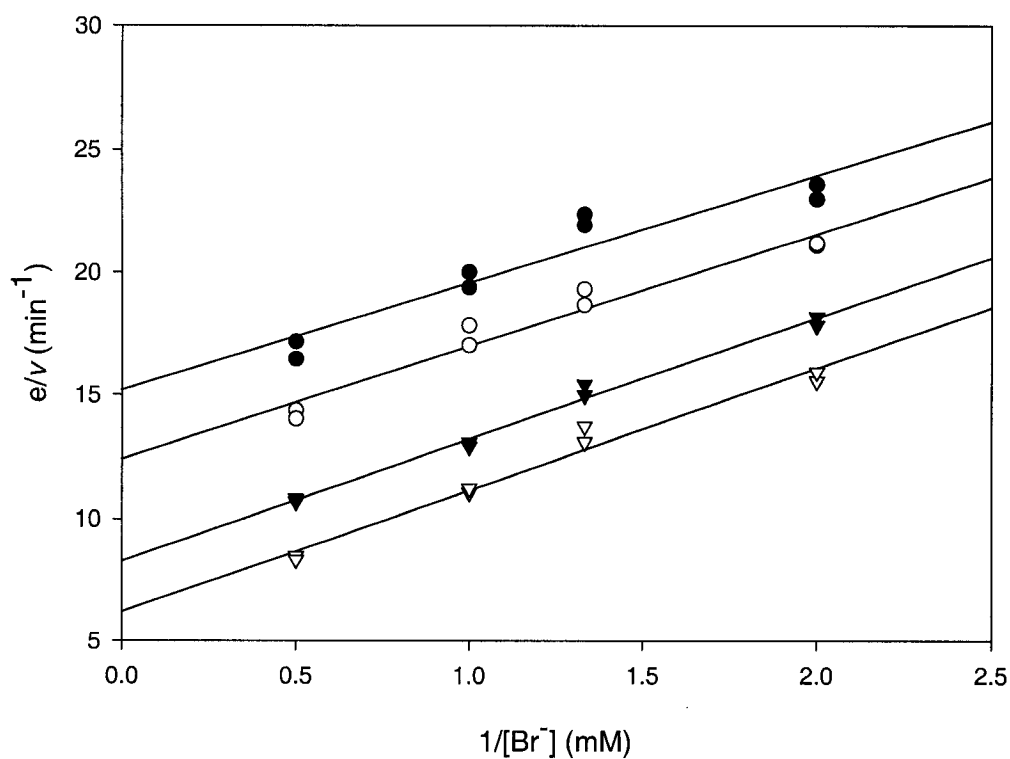


Figure 2.8: Primary double reciprocal plot of the rate of MCD bromination as a function of bromide concentration at fixed, low H_2O_2 concentrations at pH 6.50 for $r\text{CoV-BrPO}$; \bullet $7.1 \mu\text{M H}_2\text{O}_2$, \circ $9.9 \mu\text{M H}_2\text{O}_2$, \blacktriangledown $20 \mu\text{M H}_2\text{O}_2$, ∇ $48.6 \mu\text{M H}_2\text{O}_2$. Each line is the linear least squares fit to data.

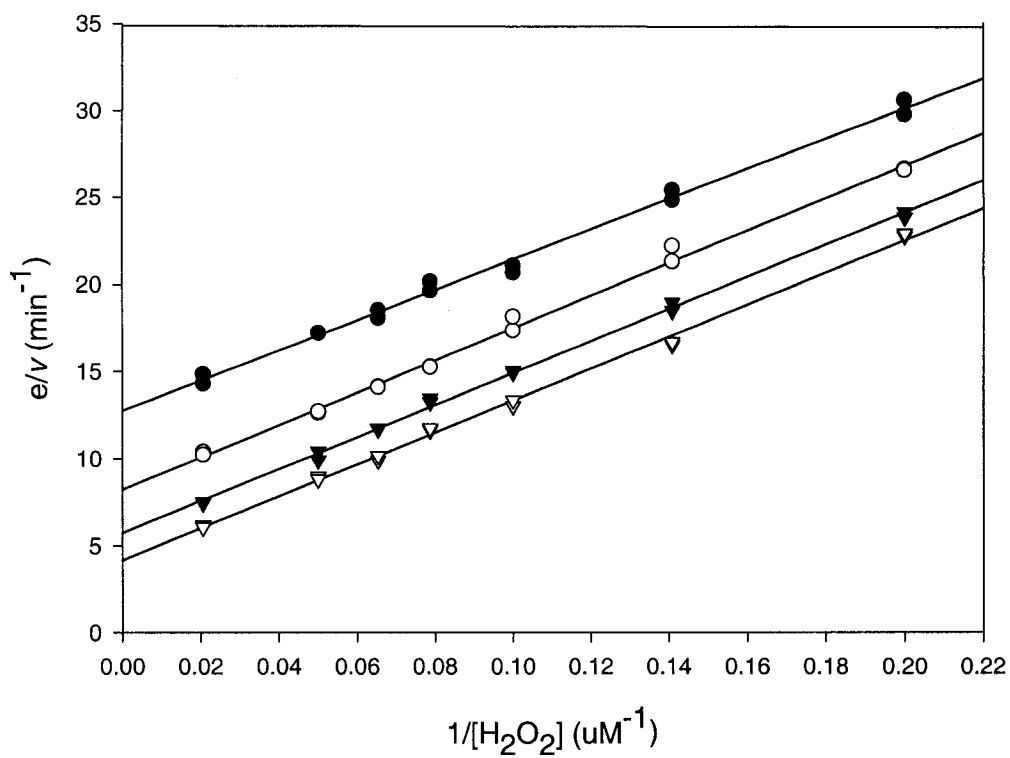


Figure 2.9: Primary double reciprocal plot of the rate of MCD bromination as a function of hydrogen peroxide concentration at fixed, low bromide concentrations at pH 6.50 for native CoV-BrPO; ● 0.500 mM Br⁻, ○ 1.00 mM Br⁻, ▼ 2.00 mM Br⁻, ▽ 5.00 mM Br⁻. Each line is the linear least squares fit to data.

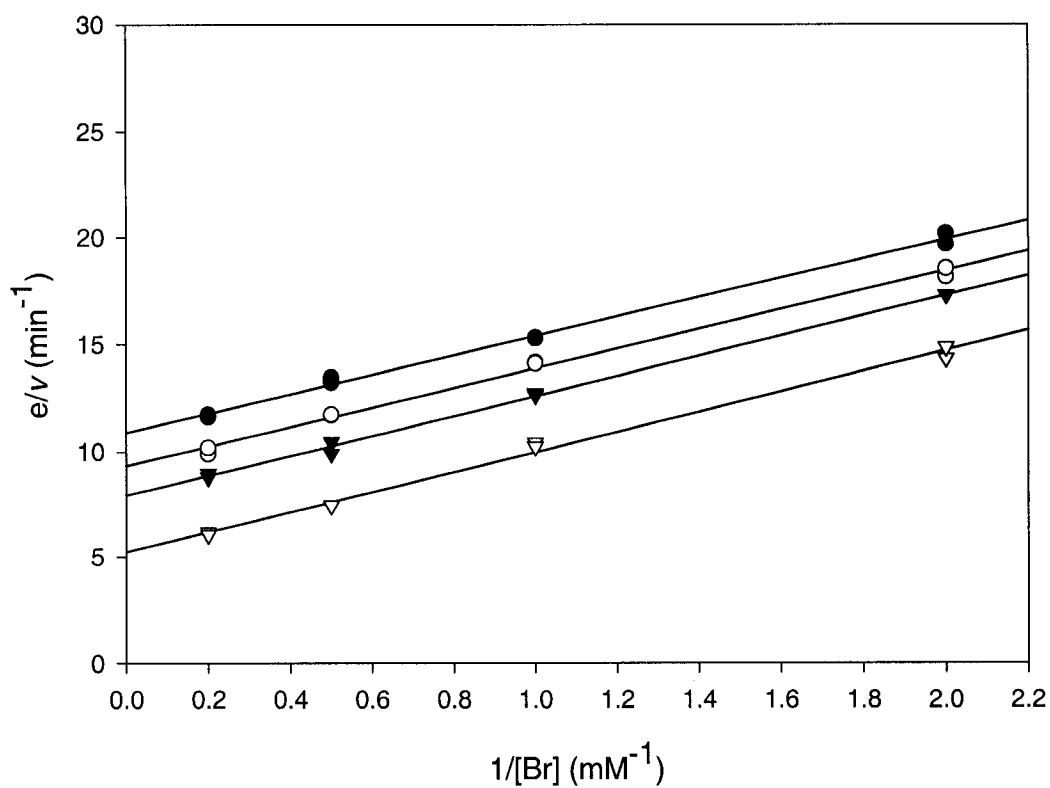


Figure 2.10: Primary double reciprocal plot of the rate of MCD bromination as a function of bromide concentration at fixed, low H₂O₂ concentrations at pH 6.50 for native CoV-BrPO; ● 12.7 μM H₂O₂, ○ 15.3 μM H₂O₂, ▼ 20 μM H₂O₂, ▽ 48.6 μM H₂O₂. Each line is the linear least squares fit to data.

V-BrPO	K_m^{Br} (mM)	$K_m^{\text{H}_2\text{O}_2}$ (μM)	$K_m^{\text{I}^-}$ (mM)
rCoV-BrPO	1.2	17.0	
Native	1.29	27	
CoV-BrPO			
H480A		200	33
<i>P. canaliculata</i> ^a		110	2.1
PcI			
<i>P. canaliculata</i> ^a		200	2.4
PcII			
<i>S. polyschides</i> ^b		478	3.25
SpV1			
<i>A. nodosum</i> ^c	25.8	113	0.82
CoV-BrPO ^d	1	60	
<i>P. cartilagineum</i>	10	90	
<i>C. pilulifera</i> ^e	11	92	

Table 2.2: Kinetic parameters obtained from the rates of MCD bromination and triiodide formation at pH 6.5; kinetic parameters were obtained using the PINGPONG program.

^a from M. Almeida (2001 a)

^b from M. Almeida (2001 b)

^c from H. Vilter (1983)

^d from D. J. Sheffield (1993)

^e from N. Itoh (1986)

was measured at pH 6.5 using chloride, bromide and iodide as substrates it was found that H480A showed no chloroperoxidase activity, but retained the ability to oxidize bromide and iodide. The specific activity of H480A for bromide oxidation was 4% (i.e., 6.3 $\mu\text{mol MCD brominated}/\text{min}/\text{mg}$) of the rCoV-BrPO activity at the same pH (i.e., 6.5) in the presence of excess vanadium cofactor (100 μM). Excess vanadium was included in the haloperoxidase reactions to compensate for possible alterations in enzyme-cofactor interactions introduced by the mutation. When purified native CoV-BrPO, rCoV-BrPO, and mutant H480A were analyzed by native PAGE and in-gel activity assays performed with substrates bromide, hydrogen peroxide, and *o*-dianisidine [Figure 2.11], it was shown that rCoV-BrPO (lane 2) and mutant H480A (lane 3) ran similarly in the gel to native CoV-BrPO (lane 1). The similar migrations of the enzymes in the gel suggest the recombinant and mutant form of rCoV-BrPO retain a similar structure to native CoV-BrPO. In addition, lane 3 of the native gel analysis revealed that the mutant H480A had substantially less bromoperoxidase activity than native CoV-BrPO and rCoV-BrPO under the conditions of incubation.

Specific activity measurements for H480A and rCoV-BrPO, as a function of pH, were performed to determine the pH optimum of haloperoxidase activity [Figure 2.12]. Recombinant CoV-BrPO showed optimal bromoperoxidase activity around pH 6.0 using both low substrate concentrations (0.5 mM H_2O_2 , 5 mM Br^-) and high substrate concentrations (5 mM H_2O_2 , 100 mM Br^-). Mutant H480A showed

maximum bromoperoxidase activity between pH 6.0 - 6.5 under conditions of high substrate concentrations (5 mM H₂O₂ and 100 mM Br⁻), but with reduced specific activity when compared to rCoV-BrPO [Figure 2.12]. At all the pH values tested, mutant H480A bromoperoxidase activity did not have bromoperoxidase activity using low substrate concentrations (0.5 mM H₂O₂, 5mM Br⁻).

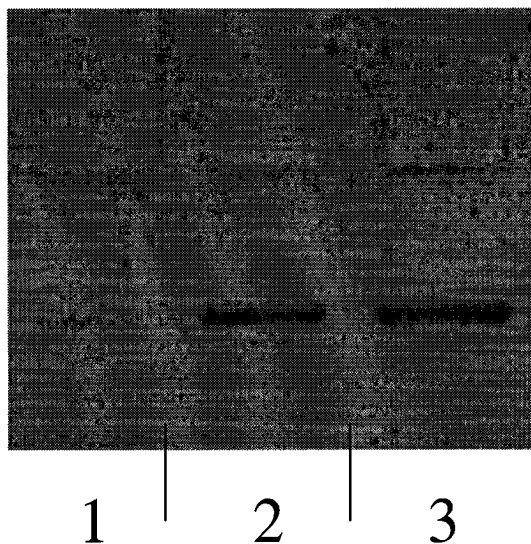


Figure 2.11: In-gel activity analysis of V-BrPO isolated from *C. officinalis* or *E. coli* (recombinant protein). Purified protein was separated on 10% SDS-polyacrylamide gels under native conditions. The proteins were visualized in the gel by activity staining with *o*-dianisidine, bromide, and hydrogen peroxide at pH 6.5. Lane 1, mutant H480A (36µg); Lane 2, native V-BrPO from *C. officinalis* (1µg); Lane 3, rCoV-BrPO (1µg).

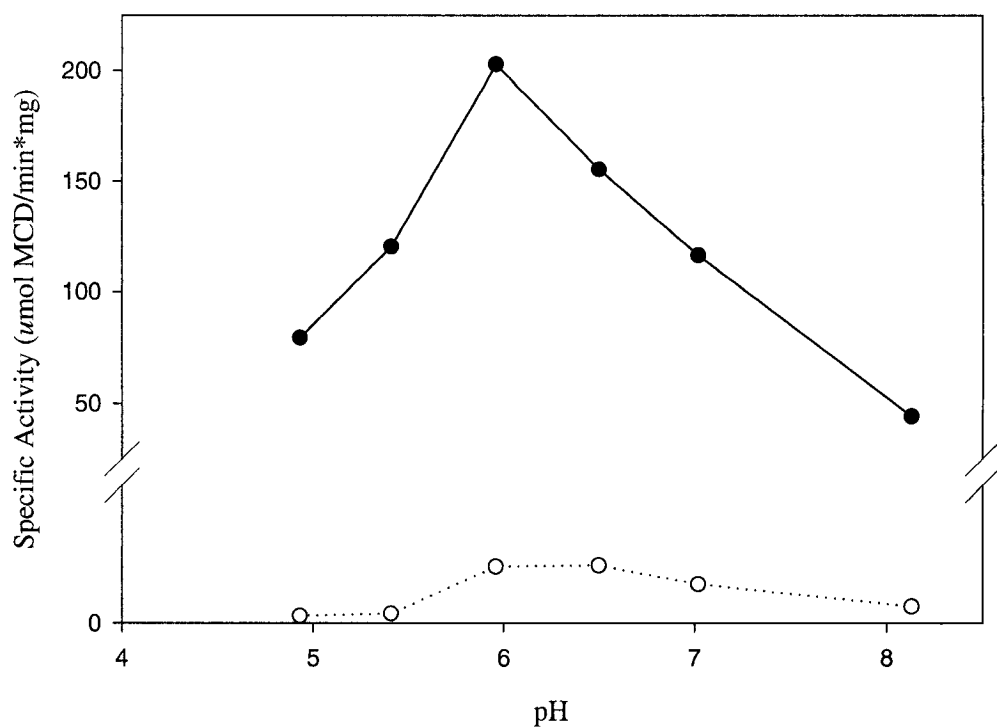


Figure 2.12: Specific activity measurements of (●) rCoV-BrPO and (○) mutant H480A as a function of pH. Reaction conditions were 3 nM rCoV-BrPO or 225 nM H480A, 100 mM bromide, 5 mM H₂O₂, and 100 μM vanadate. The reaction rates were determined in duplicate. The buffers used are listed in Materials and Methods.

Iodoperoxidase activity of mutant H480A. The severely reduced bromoperoxidase activity of H480A prompted the kinetic analysis of iodide oxidation. The steady state rate of triiodide formation by H480A was examined as a function of hydrogen peroxide (10 μM – 500 μM) and iodide (1 mM – 50 mM) at pH 6.5. Plots of initial rates of triiodide formation versus hydrogen peroxide concentrations or iodide concentrations showed saturation-type Michealis-Menten kinetics [Figure 2.13, 2.14]. Double reciprocal plots of the initial steady state rates of triiodide formation versus hydrogen peroxide produced a set of parallel lines [Figure 2.15]. Parallel lines were also observed for initial steady state rates versus iodide concentrations at fixed hydrogen peroxide concentrations [Figure 2.16]. Using Cleland's PING PONG kinetic program the calculated kinetic constants for hydrogen peroxide, $K_m^{\text{H}_2\text{O}_2}$, and iodide, $K_m^{\text{I}^-}$, was 200 μM and 33 mM, respectively (Table 2.2).

Effects of the vanadium (V) cofactor on the haloperoxidase activity of mutant H480A. The reduced specific activity of H480A was considered with respect to protein-metal interactions. Without the availability of a crystal structure of the mutated active site it seemed conceivable that mutation of H480 could affect enzyme-cofactor interactions by altering hydrogen bond interactions to the cofactor, or by inducing changes in the electrostatic distribution potential at the active site. During the purification procedure for rCoV-BrPO and mutant H480A from *E. coli*, the apo-enzymes were activated with vanadate (1 mM) at pH 8.3. Formation of the

rCoV-BrPO holoenzyme was indicated by no further increases in haloperoxidase activity upon incubation in the presence of excess cofactor. Mutant H480A, following activation with vanadate and purification, exhibited variable haloperoxidase activity depending on the presence or absence of excess cofactor in reaction solutions [Figure 2.17]. The rate of MCD bromination by mutant H480A increased when added excess cofactor was present in the reaction versus reactions in the absence of excess cofactor [Figure 2.17 trace a & b]. Reactions where mutant H480A and excess vanadate were pre-incubated prior to the addition of bromide and hydrogen peroxide did not further increase the reaction rate [Figure 2.17 trace c]. The lack of change in the reaction rate of pre-incubated samples of H480A and vanadate suggests the increased activity in the presence of excess cofactor is not dependent on equilibrium being reached between mutant H480A and excess vanadate in solution. However, when mutant H480A was pre-incubated with excess vanadate and hydrogen peroxide prior to the addition of bromide an increase in the reaction rate was observed [Figure 2.17 trace d]. The enhanced reaction rate suggest that the increase in activity for H480A is a combined effect of vanadate and the first substrate in the catalytic cycle, hydrogen peroxide. Although the specific activity of bromide and iodide oxidation is marginally improved in the presence of excess cofactor, the haloperoxidase activity of H480A is still only a small percentage of recombinant CoV-BrPO activity.

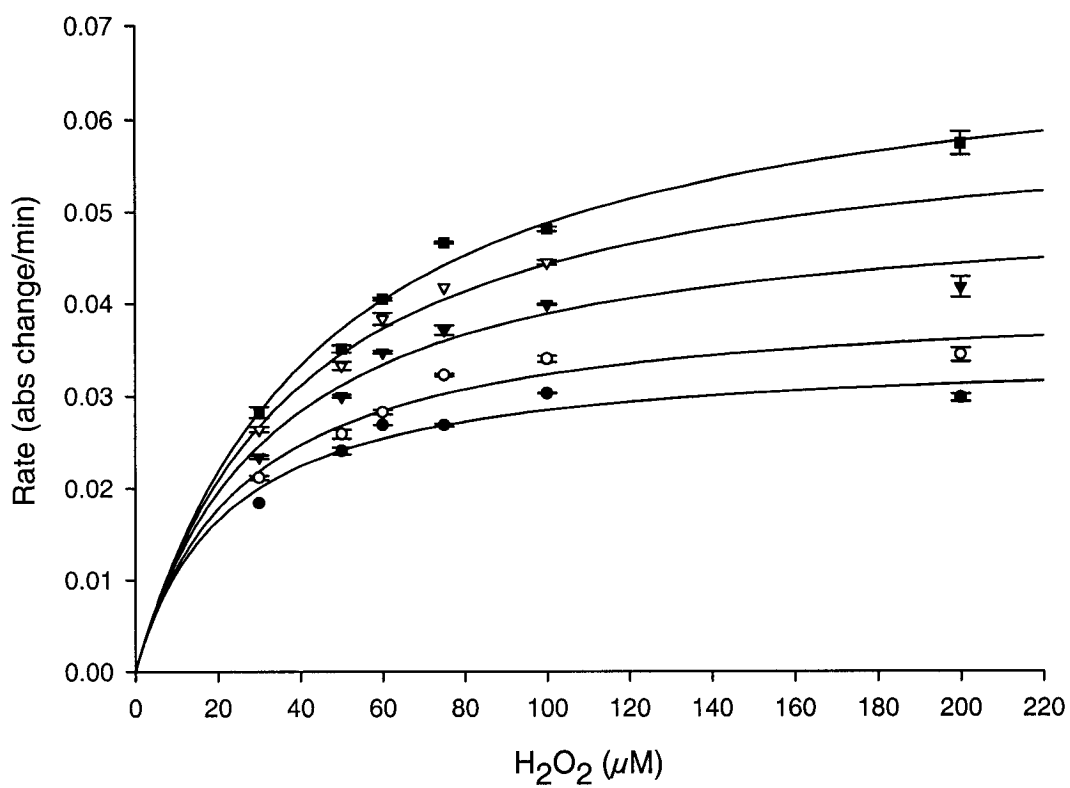


Figure 2.13: Saturation kinetic plot of the rate of triiodide formation vs. H₂O₂ concentration at fixed low iodide concentrations at pH 6.5 for H480A; ● 5 mM I⁻, ○ 6 mM I⁻, ▼ 8 mM I⁻, ▽ 10 mM I⁻, ■ 12 mM I⁻.

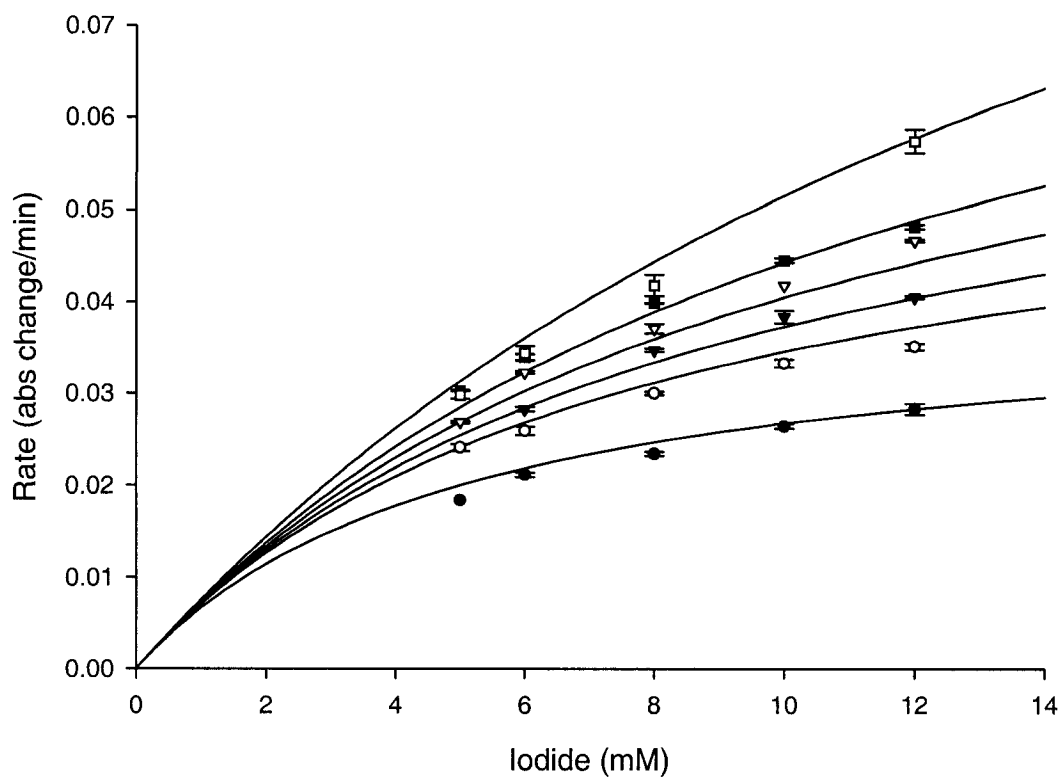


Figure 2.14: Saturation kinetic plot of the rate of triiodide formation vs. iodide concentration at fixed low H₂O₂ concentrations at pH 6.5 for H480A; ● 30 μM H₂O₂, ○ 50 μM H₂O₂, ▼ 60 μM H₂O₂, ▽ 75 μM H₂O₂, ■ 100 μM H₂O₂, □ 200 μM H₂O₂.

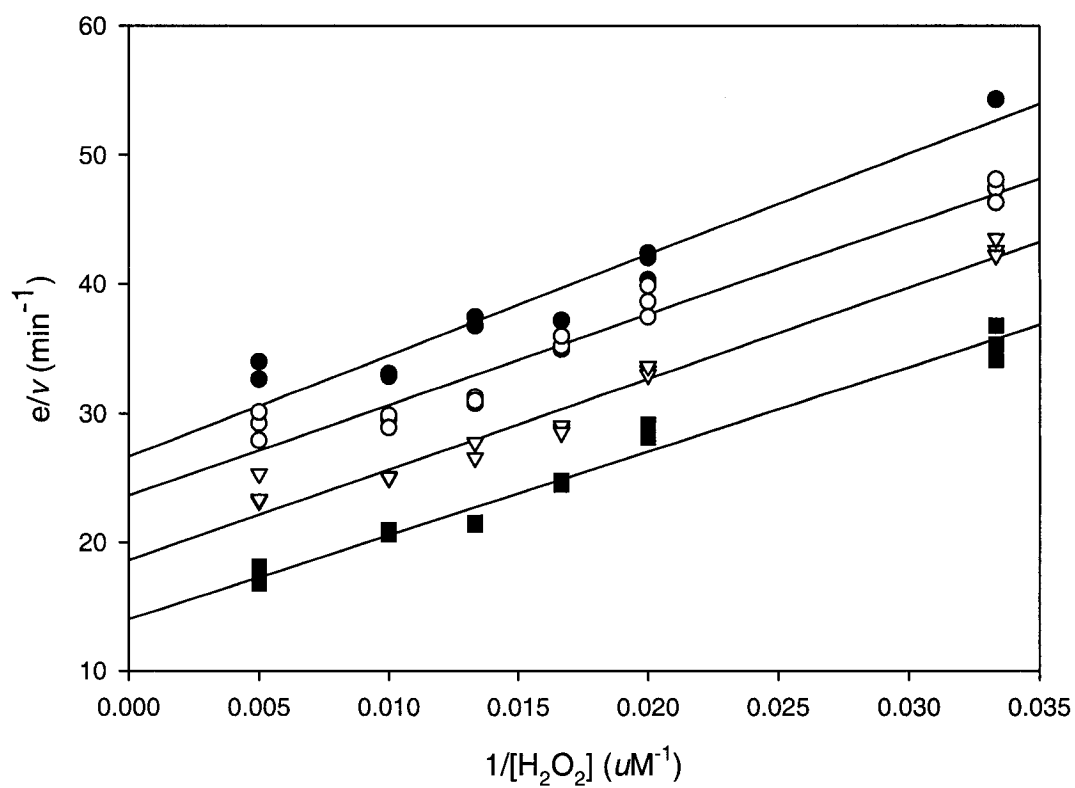


Figure 2.15: H480A Primary double-reciprocal plot of the rate of triiodide formation as a function of hydrogen peroxide concentration at fixed, low iodide concentrations at pH 6.50. ● 5 mM I⁻, ○ 6 mM I⁻, ▽ 10 mM I⁻, ■ 12 mM I⁻. Each line is the linear least squares fit to data.

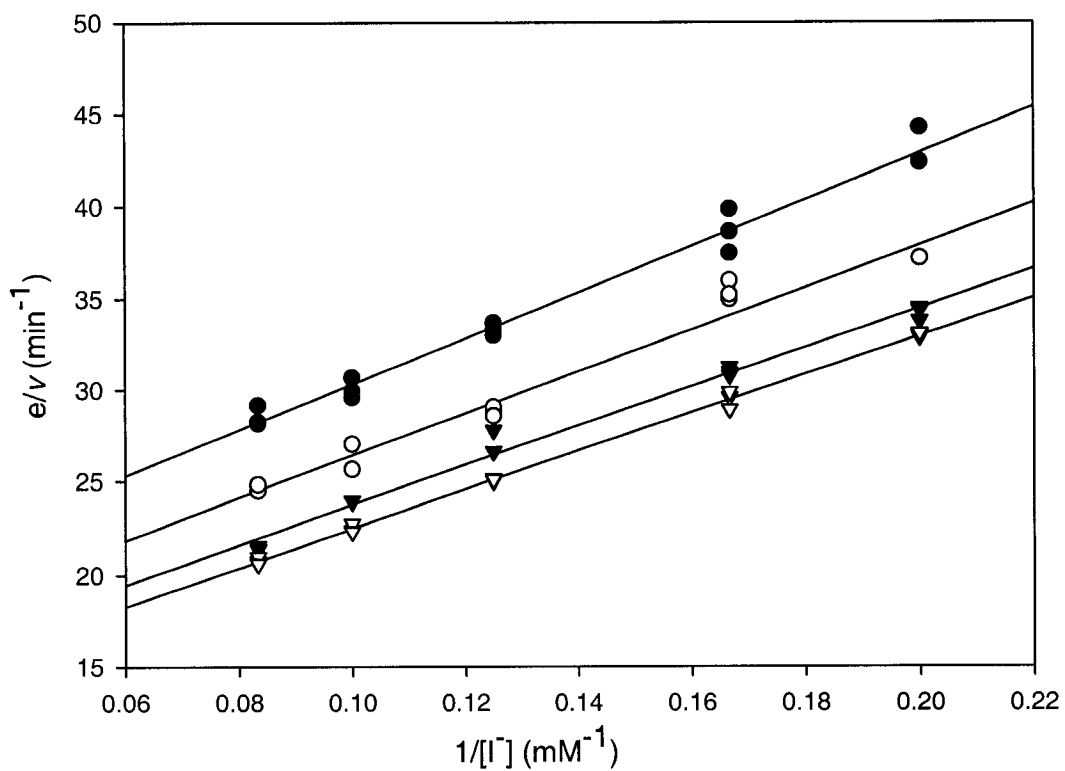


Figure 2.16: H480A Primary double-reciprocal plot of the rate of triiodide formation as a function of iodide concentration at fixed, low H_2O_2 concentrations at pH 6.50. \bullet 50 μM I^- , \circ 60 μM I^- , \blacktriangledown 75 μM I^- , ∇ 100 μM I^- . Each line is the linear least squares fit to data.

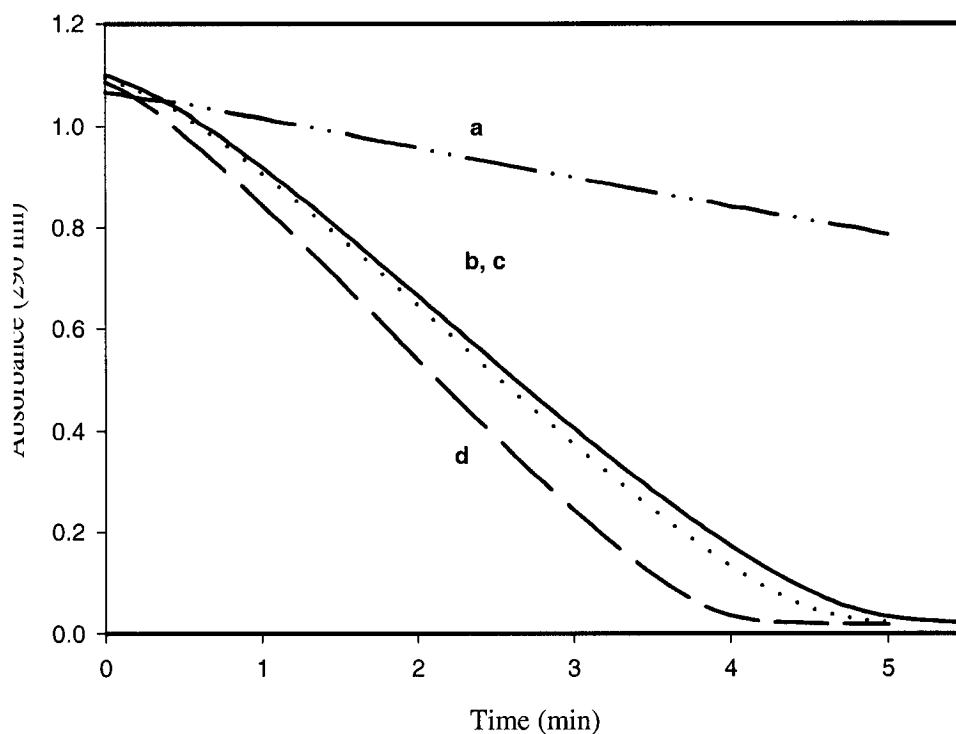


Figure 2.17: Improved specific activity of mutant H480A in the presence of excess vanadate and hydrogen peroxide.
 Trace a: MCD activity assay containing H480A (550 nM), 50 mM phosphate buffer pH 6.50, 100 mM KBr, and 5 mM H₂O₂.
 Trace b: MCD activity assay containing H480A (550 nM), 50 mM phosphate buffer pH 6.50, 100 mM KBr, 5 mM H₂O₂, and 100 μM vanadate.
 Trace c: Same conditions as trace b; reaction was initiated by the addition of hydrogen peroxide following a ten minute pre-incubation of the enzyme and 100 μM vanadate.
 Trace d: Same conditions as trace b; reaction was initiated by the addition of halide following a ten minute pre-incubation of the enzyme, vanadate, and hydrogen peroxide.

Vanadium bromoperoxidase from the marine red alga *Plocamium cartilagineum*:

Isolation. A vanadium-dependent bromoperoxidase was isolated from the marine red alga *P. cartilagineum*. Initially, supernatants of cell-free extracts of *P. cartilagineum* were negative for bromoperoxidase activity by MCD assay, and showed only weak iodoperoxidase activity by triiodide assay. Subsequent fractionation of crude extracts by anion-exchange chromatography (DEAE FF) afforded fractions with bromoperoxidase activity by MCD assay and bromination of phenol red activity assay. Additional purification by size exclusion chromatography (Sephacryl-300 and/or Superose 6 resin) produced active enzyme within the same elution profile as native V-BrPO from *C. officinalis*. As a last purification step MonoQ anion-exchange resin (linear gradient of 0 – 1 M NaCl over 30 minutes, 0.5 ml/min optimum) was used, and produced active enzyme used in steady state kinetic analyses. The monomer molecular weight of native *PcV*-BrPO was estimated by SDS-PAGE as 66 000 Da [Figure 2.18].

The vanadium dependence of the purified *PcV*-BrPO was evaluated by demetallation/remetallation experiments. MCD bromination of purified *PcV*-BrPO was initially determined prior to demetallation [Figure 2.19-a]. Purified *PcV*-BrPO was dialyzed with 0.1 M citrate/phosphate buffer (pH 3.9) at 4 °C for 24 hours, followed by reconstitution of the enzyme with 0.1 M Tris-HCl pH 8.0, and MCD activity assessed (58% of original activity remained) [Figure 2.19-b]. In addition, purified enzyme was dialyzed with 0.1 M citrate/phosphate buffer (pH 3.9)

containing 5 mM EDTA. Following reconstitution in 0.1 M Tris-HCl, the MCD activity of the demetallated enzyme was only 41% of the original purified enzyme [Figure 2.19-c]. Enzymatic activity could be restored when demetallated enzyme was reconstituted in 0.1 M Tris-HCl containing 1 mM NH_4VO_3 (90% of original activity restored) [Figure 2.19-d].

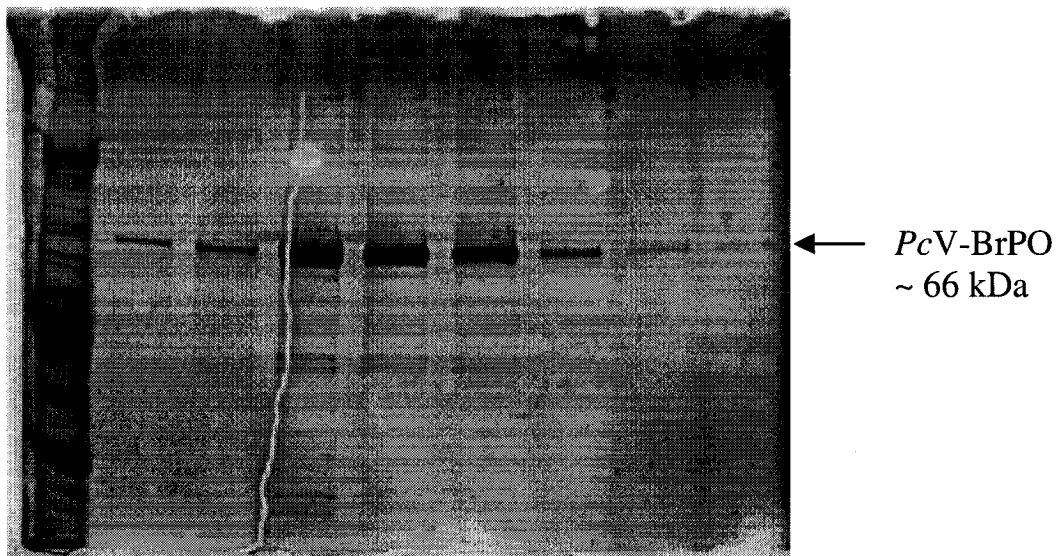


Figure 2.18: Reducing SDS-PAGE 7% gel (ReadyGel, Biorad) of fractions eluting from a MonoQ anion exchange column for purified native *PcV-BrPO*. *PcV-BrPO* has an approximate molecular weight of 66 kDa. Lane 1, silver stained molecular weight marker.

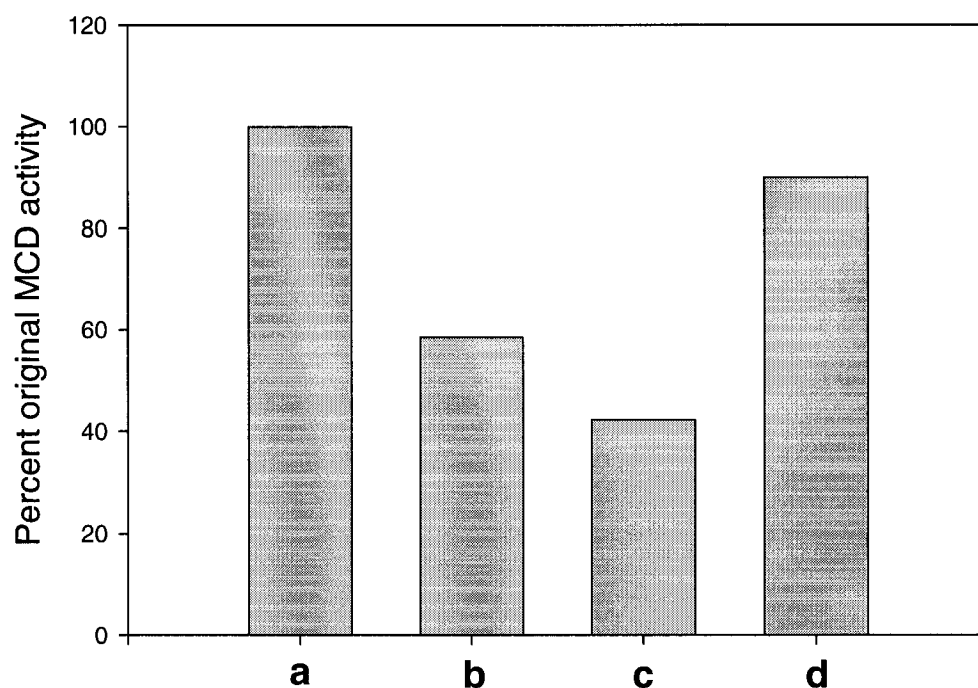


Figure 2.19: Vanadium dependence of the bromoperoxidase isolated from the marine red alga *Plocamium cartilagineum*. (a) native PcV-BrPO original MCD activity prior to demetallation. (b) native PcV-BrPO MCD activity relative to (a), dialyzed with phosphate buffer pH 3.9 (without EDTA). (c) native PcV-BrPO MCD activity relative to (a), dialyzed with phosphate buffer pH 3.9 and 5 mM EDTA. (d) native PcV-BrPO MCD activity relative to (a), dialyzed with phosphate buffer pH 3.9, 5 mM EDTA, and remetallation with 1 mM NH_4VO_3 .

Steady state kinetic analysis. The steady state rates of MCD bromination by native *PcV*-BrPO were investigated as a function of hydrogen peroxide concentration (5 μM – 200 μM) and bromide concentration (0.500 mM – 5 mM) at pH 6.5. Plots of the initial rates of MCD bromination versus hydrogen peroxide and bromide concentrations showed typical Michaelis-Menten type saturation kinetic behavior [Figure 2.20, 2.21].

Double reciprocal plots of the initial steady state rates of MCD-bromination versus hydrogen peroxide concentrations at low fixed bromide concentrations (0.500 mM – 2.00 mM) produced a set of parallel lines [Figure 2.22]. Parallel lines were also observed for initial steady state rates versus bromide concentrations at fixed hydrogen peroxide concentrations (5 μM – 50 μM) [Figure 2.23]. The parallel plots are consistent with a bi bi ping pong mechanism (de Boer and Wever 1988; Everett et al. 1990a; Soedjak and Butler 1991).

The values of K_m^{Br} and $K_m^{\text{H}_2\text{O}_2}$ for *PcV*-BrPO at pH 6.5 were determined from the best fit using Cleland's PINGPONG program (Cleland 1979). The calculated value for K_m^{Br} and $K_m^{\text{H}_2\text{O}_2}$ are 10 mM and 90.0 μM , respectively (Table 2.2).

Inhibition of *P. cartilagineum* V-BrPO catalyzed bromination of MCD by hydrogen peroxide. Addition of native *PcV*-BrPO to a solution of bromide (25 mM), hydrogen peroxide and MCD induces the bromination of MCD in competition with dioxygen formation via the bromide-assisted disproportionation of hydrogen

peroxide (see Scheme 1). At high concentrations of hydrogen peroxide (i.e., $[H_2O_2] \gg K_m^{H_2O_2}$) the rate of MCD bromination decreases as shown in Figure 2.24 for pH 5.91 – 7.04. Under conditions of steady-state studies (i.e., turnover for at least 10 minutes), the decreased rate of MCD bromination is due to inhibition of native *PcV*-BrPO (Soedjak et al. 1995). At high concentrations of bromide (i.e., $[Br^-] \gg K_m^{Br}$) the rate of MCD bromination slowly increases as shown in Figure 2.25 for pH 5.91 – 7.04. Under conditions of steady state studies, native *PcV*-BrPO is more tolerant to higher concentrations of bromide than hydrogen peroxide.

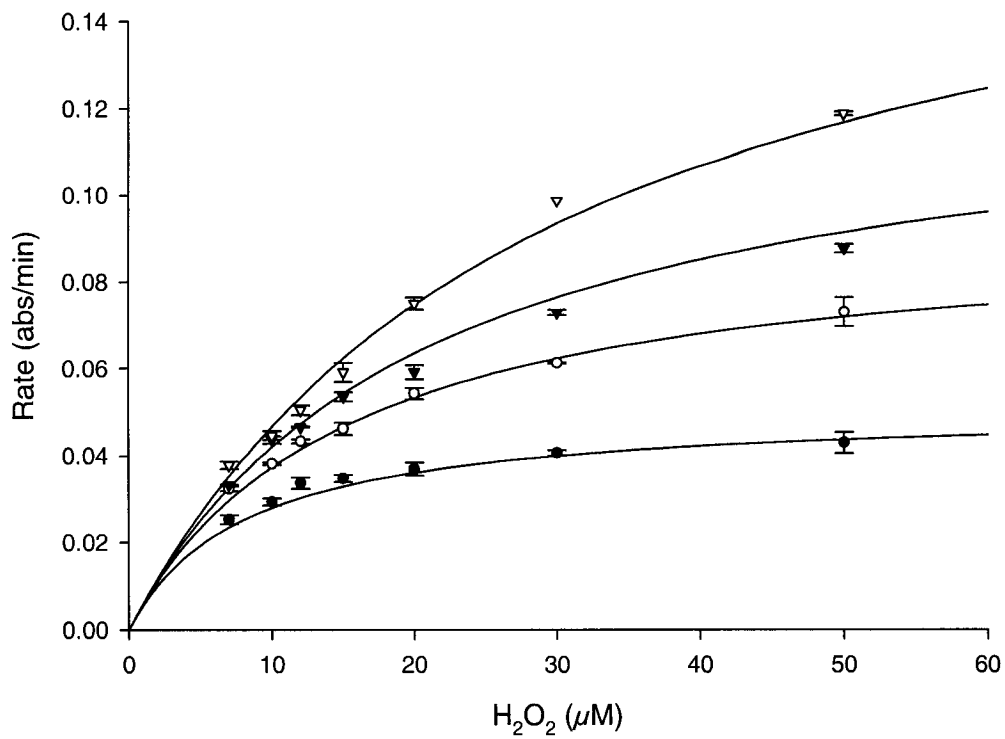


Figure 2.20: Saturation kinetic plot of the rate of MCD bromination vs. H₂O₂ concentration at fixed low bromide concentrations at pH 6.5 for V-BrPO (*P. cartilagineum*); ● 1 mM Br⁻, ○ 2 mM Br⁻, ▼ 3 mM Br⁻, ▽ 5 mM Br⁻.

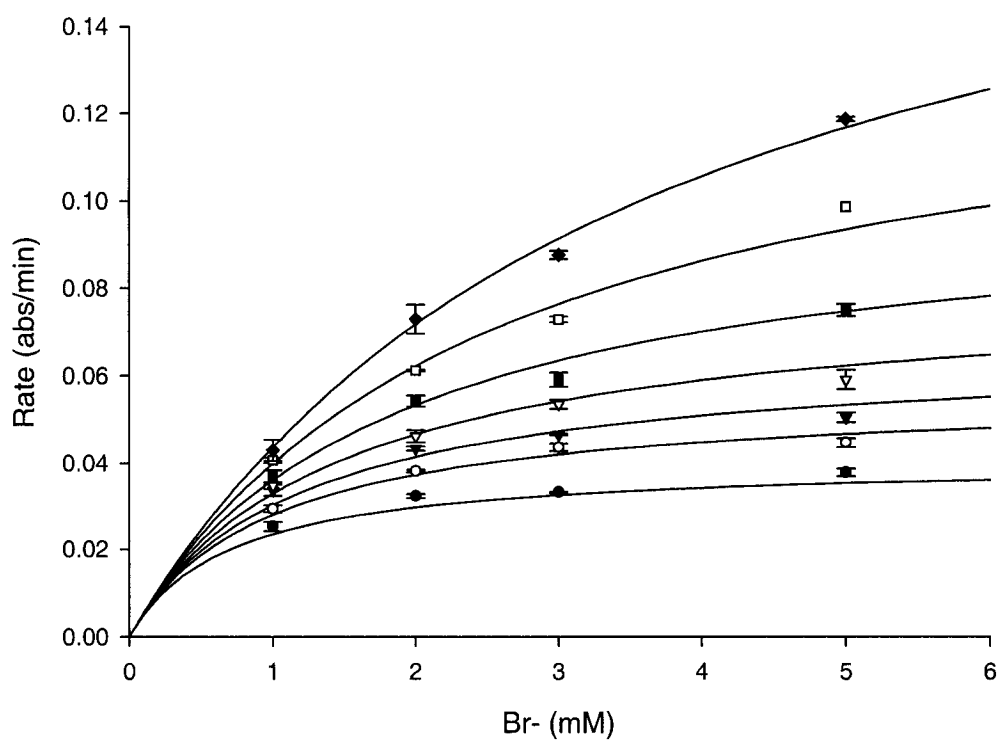


Figure 2.21: Saturation kinetic plot of the rate of MCD bromination vs. bromide concentration at fixed low H₂O₂ concentrations at pH 6.5 for V-BrPO (*P. cartilagineum*); • 7 μM H₂O₂, ○ 10 μM H₂O₂, ▼ 12 μM H₂O₂, ▽ 15 μM H₂O₂, ■ 20 μM H₂O₂, □ 30 μM H₂O₂, ◆ 50 μM H₂O₂.

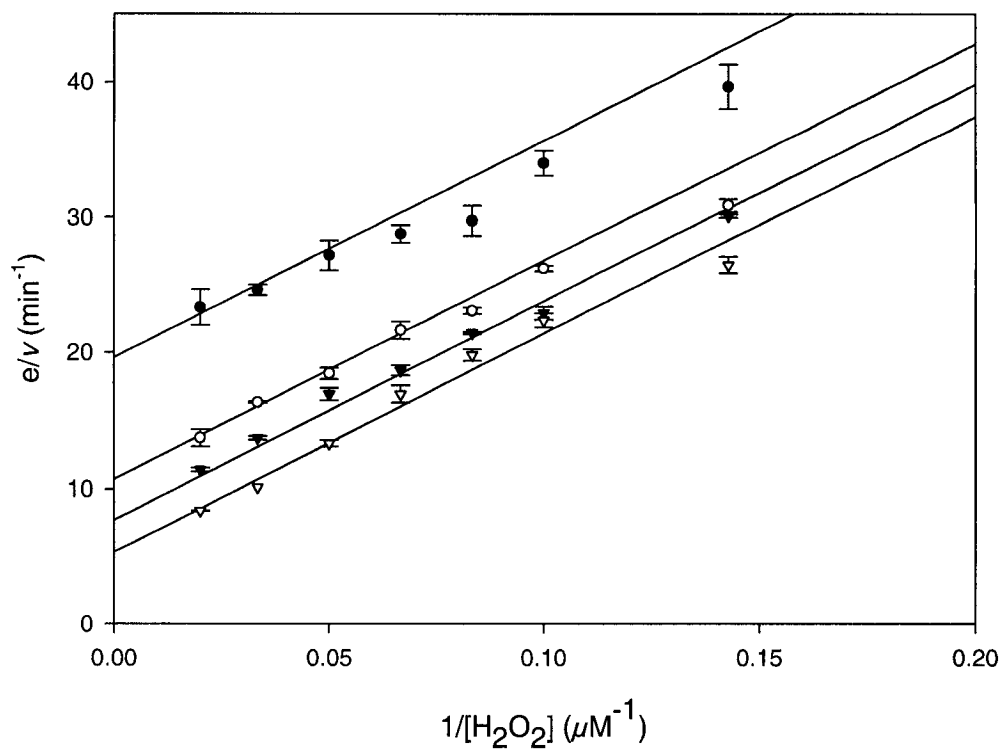


Figure 2.22: Primary double reciprocal plot of the rate of MCD bromination as a function of hydrogen peroxide concentration at fixed, low bromide concentrations at pH 6.50 for V-BrPO (*P. cartilagineum*); ● 1.00 mM, ○ 2.00 mM Br⁻, Br⁻, ▼ 3.00 mM Br⁻, ▽ 5.00 mM Br⁻. Each line is the linear least squares fit to data.

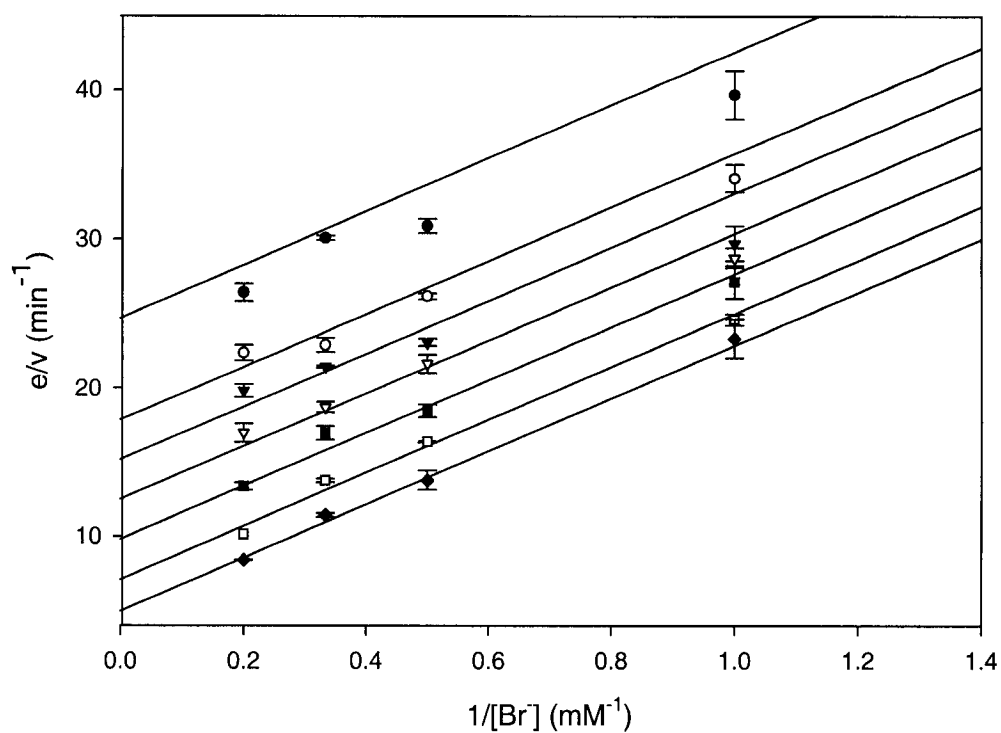


Figure 2.23: Primary double reciprocal plot of the rate of MCD bromination as a function of bromide concentration at fixed, low H_2O_2 concentrations at pH 6.50 for V-BrPO (*P. cartilagineum*); \bullet $7 \mu\text{M H}_2\text{O}_2$, \circ $10 \mu\text{M H}_2\text{O}_2$, \blacktriangledown $12 \mu\text{M H}_2\text{O}_2$, ∇ $15 \mu\text{M H}_2\text{O}_2$, \blacksquare $20 \mu\text{M H}_2\text{O}_2$, \square $30 \mu\text{M H}_2\text{O}_2$, \blacklozenge $50 \mu\text{M H}_2\text{O}_2$. Each line is the linear least squares fit to data.

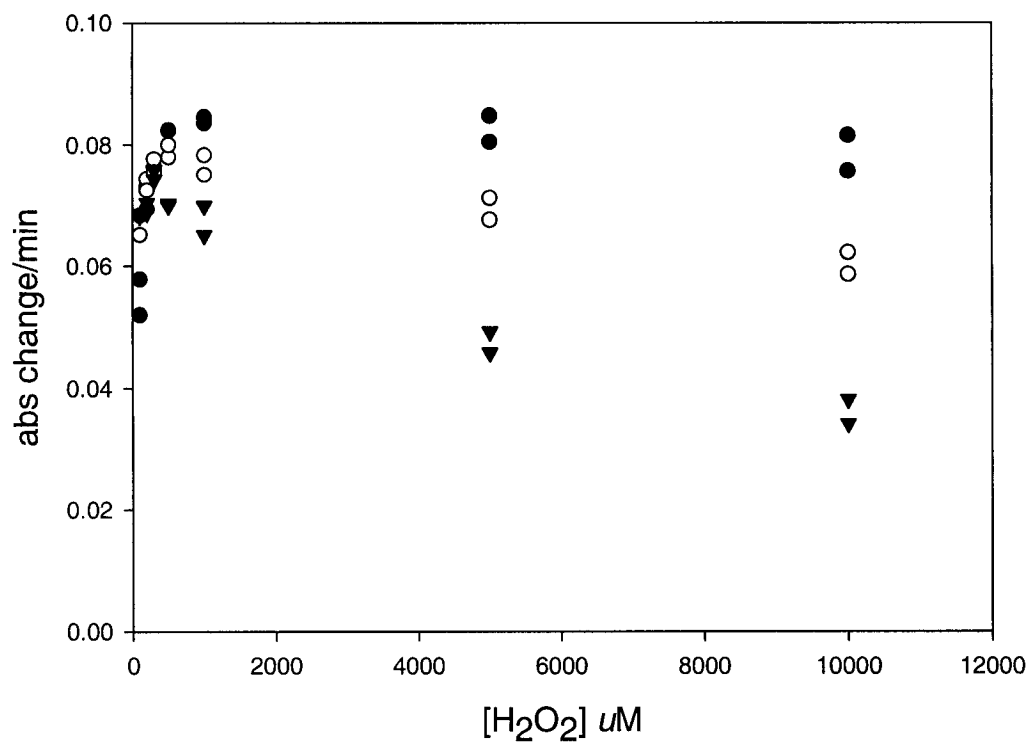


Figure 2.24: Saturation kinetic plot of the rates of MCD bromination vs. H_2O_2 concentrations as a function of pH at constant bromide concentration (25 mM) for V-BrPO (*P. cartilagineum*); ● pH 5.91, ○ pH 6.46, ▼ pH 7.04.

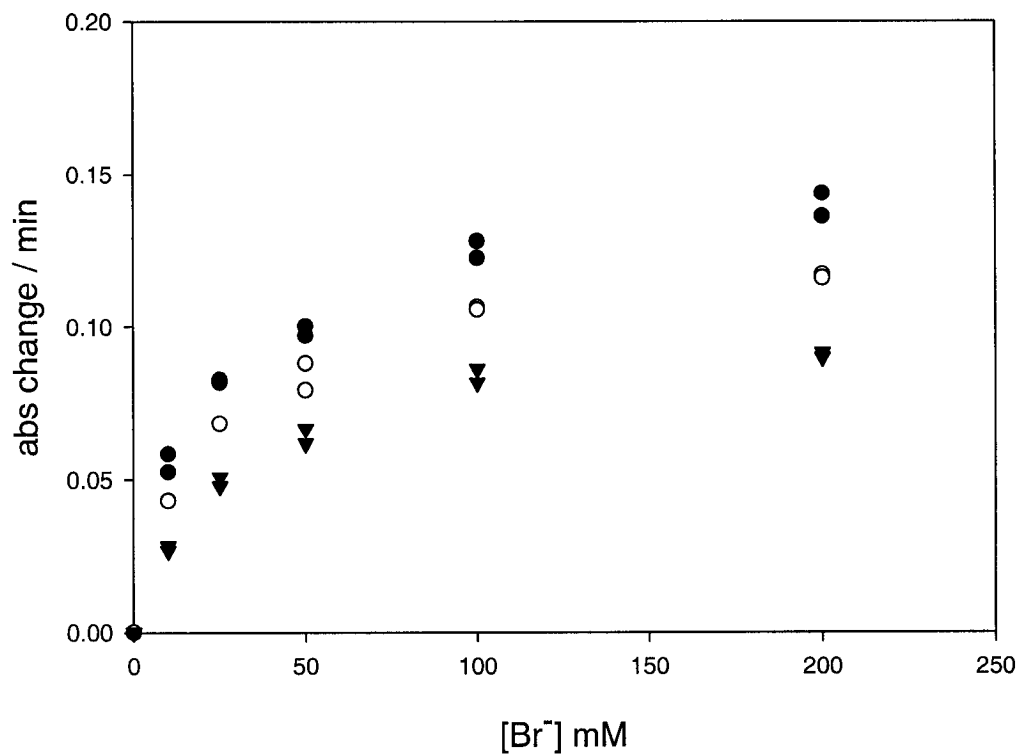


Figure 2.25: Saturation kinetic plot of the rates of MCD bromination vs. bromide concentrations as a function of pH at constant H_2O_2 concentration (5 mM) for V-BrPO (*P. cartilagineum*); ● pH 5.91, ○ pH 6.46, ▼ pH 7.04.

Discussion

Sequence analyses of cloned V-BrPOs:

The active site architectures of vanadium dependent haloperoxidases are strikingly similar, yet the differences in halide specificity between V-BrPO and V-ClPO are unaccounted for. One distinguishing difference in active site architecture around the vanadate cofactor for V-BrPO and V-ClPO is an additional histidine residue in V-BrPO in proximity to the vanadate-binding site, where the histidine residue is replaced with a phenylalanine in V-ClPO [Figure 2.26]. To date, all characterized V-BrPOs display the same vanadium binding site motif:

YQKF[N/Q][I/V]HRxx**R**PEA, P[S/A]YPSGHAT,

GE[L/I]NKLA[D/V]N[I/V]A[I/F]**GR**[N/Q]M[A/L]GV**HY** (vanadate coordinating residues are shown in bold). PCR primers were designed based on the conserved vanadium binding site motif and used successfully to screen different species of red algae (*C. officinalis*, *P. cartilagineum*, *L. pacifica*, and *D. pulchra*) for the presence of vanadium bromoperoxidase. Full-length sequences for V-BrPO were obtained from *C. officinalis*, *P. cartilagineum*, and *D. pulchra* using PCR primers designed from the 5'- and 3'- encoding regions of V-BrPO from *C. pilulifera* (Shimonishi et al. 1998). Partial sequences for V-BrPO from the marine alga *L. pacifica* were obtained. Jessica Martin (Butler Lab, UCSB) is currently finishing the 5'-region of the gene.

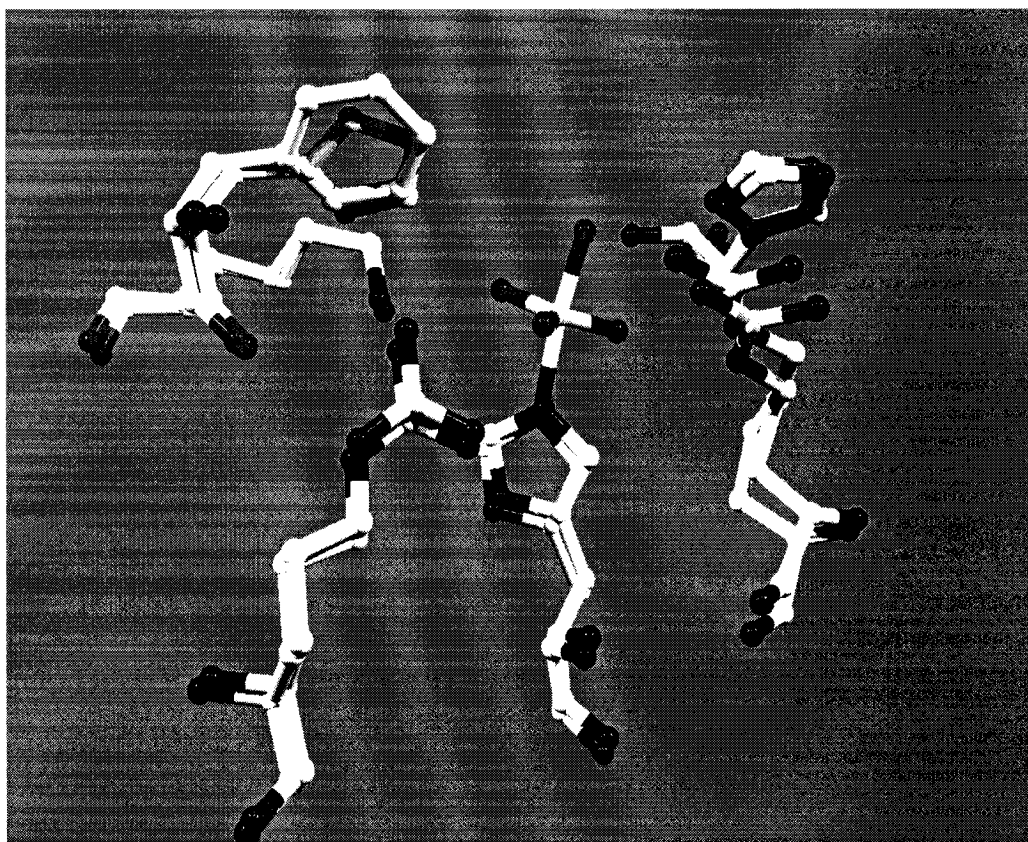


Figure 2.26: Active site superposition of vanadium bromoperoxidase (*C. officinalis*) and vanadium chloroperoxidase (*C. inaequalis*) near the V-CIPO vanadate cofactor based on secondary structural alignments. Figure was created with Swiss-PDB-Viewer and gl_rendered with POV-ray.

The sequence similarity for the V-BrPO genes and amino acid composition from the marine red algae suggest a common genetic origin. The marine algae examined in this study (4 total) are all members of the same phyla Rhodophyta, but each belongs to a different order [Figure 2.27]. Interestingly, V-BrPO appears to be prevalent in many different marine red algae, prompting the question as to its *in vivo* function. Vanadium bromoperoxidase has been proposed to function in the production of oxidized halides (i.e., hypobromite, bromine or tribromide) as a microbial deterrent, in the production of volatile halogenated hydrocarbons, or in the biosynthesis of halogenated metabolites (Fenical 1975; de Boer and Wever 1988). It is probable that V-BrPO participates in all of the above functions, but determining the specific function of V-BrPO in different species of alga will have to await expression profiling experiments designed to understand why, when, and where V-BrPO performs its chemistry.

In addition to the high sequence identity between different V-BrPOs from marine red algae, V- BrPO also has sequence homology with a family of acid phosphatases, including soluble and membrane-bound isoforms of phosphatidic acid phosphatases (PAP) (Hemrika et al. 1997c; Renirie et al. 2000a; Littlechild et al. 2002). The PAP family have a perfectly conserved sequence motif (GSYPSGHT), that is similar to the vanadate binding region of haloperoxidases, P[S/A]YPSGHAT. The mutated isoform of V-BrPO cloned from *D. pulchra* (amino acid change at the axial ligand histidine to an arginine residue H553R; *DpEV*-BrPO) likely does not

possess vanadium haloperoxidase activity, but may function as a phosphatase enzyme within the alga. Experiments to answer this question are being explored by Jessica Martin.

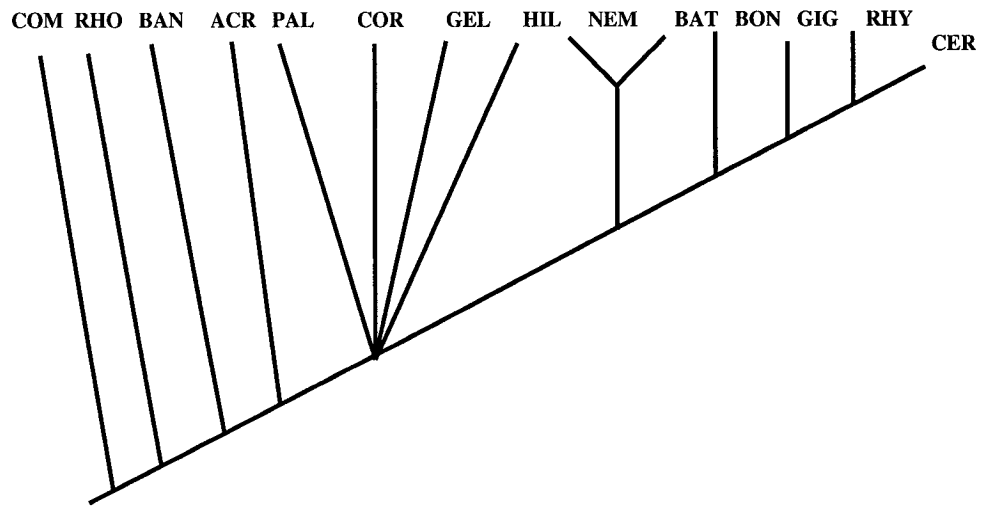


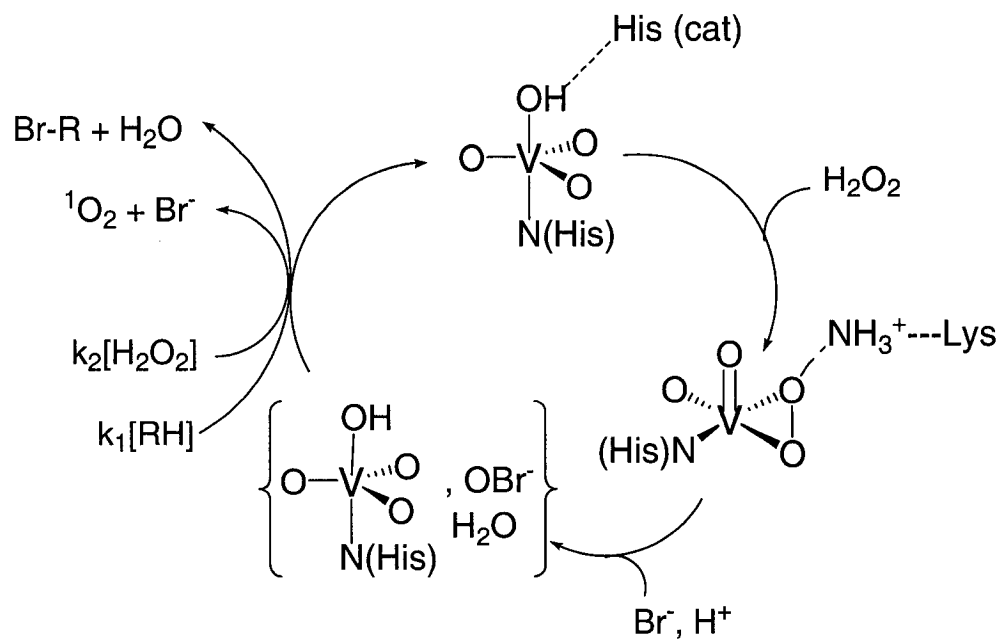
Figure 2.27: Cladogram showing consensus tree for orders of marine red algae. Note: figure redrawn from Gabrielson et al. (1985). COM = Compsopogonales, RHO = Rhodochaetales, BAN = Bangiales, ACR = Acrochaetales, NEM = Nemiales, BAT = Batrachospermales, COR = Corallinales, HIL = Hildenbrandiales, GEL = Gelidiales, PAL = Palmariales, GIG = Gigartinales, BON = Bonnemaisoniales, RHY = Rhodymeniales, CER = Ceramiales. Vanadium bromoperoxidase from the marine red alga *Corallina officinalis* (CoV-BrPO) belongs to the order Corallinales. Vanadium bromoperoxidase from the red alga *Laurencia pacifica* (LpV-BrPO) belongs to the order Ceramiales. Vanadium bromoperoxidase from the marine red alga *Plocamium cartilagineum* (PcV-BrPO) belongs to the order Gigartinales. Vanadium bromoperoxidase from the marine red alga *Delisea pulchra* (DpV-BrPO) belongs to the order Bonnemaisoniales.

Kinetic analyses of recombinant CoV-BrPO:

V-BrPO from the red alga *C. officinalis* was cloned and kinetically characterized. The cloned gene for rCoV-BrPO was used to study the active site mutant H480A in an effort to understand the role of this residue in the activation of H₂O₂ and the oxidation of halides. Steady state kinetic analysis of rCoV-BrPO for bromide oxidation indicated that V-BrPO performs according to a substrate-inhibited bi bi ping pong mechanism, as was previously reported for this class of enzymes. The substrate kinetic parameters for bromoperoxidase-catalyzed reactions by rCoV-BrPO were similar to reported values for other vanadium-dependent haloperoxidases from marine algae (Itoh et al. 1986; Sheffield et al. 1993). Steady-state kinetic analyses support the proposed mechanism where hydrogen peroxide first coordinates the vanadate cofactor to form the peroxovanadate intermediate prior to oxidation of the halide (Scheme 2.2).

Bromoperoxidase activity of mutant H480A:

Mutation of the extra-histidine residue in rCoV-BrPO significantly decreased activity towards bromide oxidation, and essentially transformed H480A into a vanadium-dependent iodoperoxidase. The low residual bromoperoxidase



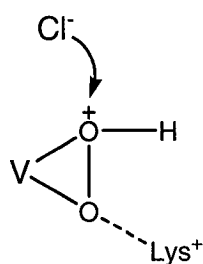
Scheme 2.2: Proposed catalytic cycle for vanadium dependent haloperoxidases.

activity for H480A was only observed under conditions of increased enzyme and substrate concentrations. Similar results were observed for the V-CIPO active site mutant R360A involved in charge neutralization of the vanadate cofactor (Hemrika et al. 1999). Mutant R360A possessed residual chloroperoxidase activity but retained the ability to oxidize bromide, and demonstrated high substrate kinetic constants. The decreased chloroperoxidase activity for the R360A mutant was attributed to a weakened activation of the bound peroxide species (Hemrika et al. 1999). The pH dependence on bromoperoxidase activity for H480A as compared to rCoV-BrPO suggests that the extra histidine residue does not govern the pH at which overall catalysis occurs.

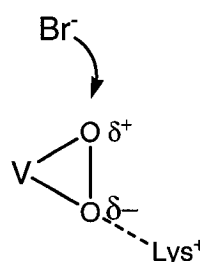
Mutant H480A iodoperoxidase activity:

The value of $K_m^{H_2O_2}$ in the iodoperoxidase reaction for H480A, $K_m^{H_2O_2} = 200 \mu\text{M}$, was similar to $K_m^{H_2O_2}$ for vanadium-iodoperoxidases from the brown algae *Pelvetia canaliculata* and *Saccorhiza polyschides* (PcI $K_m^{H_2O_2} 110 \mu\text{M}$, PcII $K_m^{H_2O_2} 200 \mu\text{M}$ and SpV₁ $K_m^{H_2O_2} 478 \mu\text{M}$) (Vilter 1983a; Vilter 1983b; Almeida et al. 1998; Almeida et al. 2000). In contrast, $K_m^{I^-}$ for H480A was greater than $K_m^{I^-}$ for both native vanadium iodoperoxidases and vanadium bromoperoxidases (Vilter 1983a; Vilter 1983b). The increased value of $K_m^{I^-}$ for H480A suggest that mutation of the extra-histidine residue weakens activation of the bound peroxide species for oxidation by halides. Previous speculations are that the extra histidine present in V-BrPO contributes to the observed differences in oxidative power between V-CIPO

and V-BrPO. The extra histidine is proposed to alter the protonation state of the bound peroxide that would be attacked by the incoming halide ion (Hemrika et al. 1999; Weyand et al. 1999; Renirie et al. 2000a). The peroxovanadate moiety in V-ClPO is predicted to be protonated, whereas the extra histidine in V-BrPO is predicted to prevent protonation of the bound peroxide (Scheme 2.3) (Hemrika et al. 1999; Renirie et al. 2000a). Model studies of vanadium (V) complexes with hydrogen peroxide also imply that the protonation state of the bound peroxide species is important in the mechanism of halide oxidation by VHPOs (Colpas et al. 1996; Hamstra et al. 1998). The kinetics of iodide oxidation by H480A suggest the presence of the extra histidine at the active sites of V-BrPOs is necessary for the formation of the peroxovanadate intermediate as well as the effective activation of the bound peroxide towards halide oxidation.



Strongly oxidizing protonated form of the side-on bound peroxide



Less oxidizing unprotonated form of the side-on bound peroxide

Scheme 2.3: Protonation of the side-on bound peroxide that is postulated to be attacked by the incoming halide; a possible explanation for the difference in reactivity between V-ClPO and V-BrPO.

Mutant H480A possessed similar specific activity values for iodoperoxidase activity when compared to vanadium iodoperoxidase from *Laminaria ochroleuca* and *S. polyschides* at the same pH, where specific activities ranged from 0.5 U/mg to 5 U/mg (Almeida et al. 2001). The similar specific activity of H480A and iodoperoxidases raises questions regarding the active site coordination of the vanadate cofactor for classical vanadium iodoperoxidases. Currently, primary amino acid sequence data is not available for vanadium iodoperoxidases, thus it is unclear what the structural and mechanistic differences are between vanadium bromoperoxidases and vanadium iodoperoxidases. The iodoperoxidase activity observed for mutant H480A suggests that there are primary residues at the active sites of vanadium iodoperoxidases that may differ from the normally conserved consensus sequence for vanadium haloperoxidases.

Effects of the vanadium (V) cofactor on the haloperoxidase activity of mutant H480A:

The improved specific activity of mutant H480A in the presence of added vanadate and peroxovanadate cofactor suggests mutation of the histidine alters the interaction of vanadate at the active site of the enzyme. A likely result of the histidine mutation is a change in the electrostatic potential around the active site, thereby reducing the charge neutralization of the vanadate cofactor. The improved haloperoxidase activity observed following pre-incubation of the enzyme with vanadate and hydrogen peroxide implies that only a fraction of H480A is in the

holoform of the enzyme, and a more complete formation of the activated enzyme is achieved in presence of a pre-formed peroxovanadate complex. The improved haloperoxidase activity of H480A is similar to cofactor incubations with mutant H404A from V-CIPO, where H404A also showed increased haloperoxidase activity upon pre-incubation with vanadate and hydrogen peroxide (Renirie et al. 2000a). It is conceivable that the improved halogenating activity observed following pre-incubation with vanadate and hydrogen peroxide reflects a greater stability of a peroxovanadate species over vanadate at the mutated active site. X-ray crystal structure analysis of V-CIPO peroxovanadate structure showed hydrogen peroxide side-on bound to vanadate in a distorted tetrahedral conformation, which is different than the trigonal bipyramidal structure of the native holoenzyme (Messerschmidt and Wever 1996; Messerschmidt et al. 1997).

Isolation and characterization of V-BrPO from *Plocamium cartilagineum*:

A vanadium-dependent bromoperoxidase was isolated and cloned from the marine red alga *P. cartilagineum*. Previous attempts by other researchers to identify a haloperoxidase from this alga were not successful (Moore and Okuda 1996). Our initial attempts at detecting bromination of MCD in the cell-free extracts of the alga were not successful. Marginal bromoperoxidase activity was only detected in partially purified extracts from anion-exchange chromatography, although increasingly better bromoperoxidase activity was observed with purified enzyme.



Figure 2.28: Polyhalogenated monoterpenes from the red alga *Plocamium cartilagineum* (Mynderse 1963).

It has been proposed that V-BrPO participates in the biosynthetic pathways of halogenated marine natural products. *P. cartilagineum* produces polyhalogenated monoterpenes that exhibit feeding deterrent and anti-microbial properties [Figure 2.28] (Mynderse and Faulkner 1963) The biosyntheses of such halogenated natural products have not been elucidated. It is proposed that the lack of detectable bromoperoxidase activity in crude extracts of *Plocamium* may be a result of competing organic substrates present within the extracts that are preferentially brominated instead of MCD. Bromination of MCD becomes detectable as competing endogenous organic substrates are removed during subsequent purification steps. Preferential bromination of certain organic compounds by V-BrPO is well documented (Tschirret-Guth and Butler 1994; Martinez et al. 2001)

Steady state kinetic analysis of native *PcV*-BrPO for bromide oxidation indicates that *PcV*-BrPO performs according to a substrate-inhibited bi bi ping pong mechanism. The substrate kinetic parameters for bromoperoxidase-catalyzed reactions by *PcV*-BrPO are similar to reported values of other vanadium-dependent haloperoxidases from marine red algae (Sheffield et al. 1993; Carter et al. 2002). The $K_m^{\text{H}_2\text{O}_2}$ and $K_m^{\text{Br}^-}$ are identical to reported values for V-BrPO isolated from *C. pilulifera* (Table 2.2) (Itoh et al. 1986).

In summary, the consensus sequences found for V-BrPO from marine sources and their similar architecture to the active sites of V-ClPO has provided a framework to obtain and characterize the recombinant forms of V-BrPO from marine red algae. The active site mutation analysis of *CoV*-BrPO is the first report of its kind. The full-length sequences reported for V-BrPO from the marine red algae *C. officinalis*, *P. cartilagineum*, and *D. pulchra* are the first V-BrPO sequences reported from these species of red algae.

Mutation of the extra histidine residue (H480A) present in *rCoV*-BrPO showed the importance of this residue in the oxidation of halides by hydrogen peroxide. The mutated enzyme was essentially transformed into a vanadium-dependent iodoperoxidase. Iodoperoxidase activity of mutant H480A showed the mutant bound H_2O_2 ten times less tightly than native and recombinant *CoV*-BrPO. In addition, mutant H480A showed a greater $K_m^{\text{I}^-}$ value than what is observed for other reported vanadium haloperoxidases. The extra-histidine residue present in V-

BrPOs likely contributes to the intricate balance of charges and hydrogen bond networks present in vanadium haloperoxidases that enable the activation of hydrogen peroxide for the oxidation of halides. However, a picture is emerging where by the differences in V-BrPO and V-CIPO activity are not as simple as replacement of one amino acid for another. The subtle differences in the architecture surrounding the vanadium sites in these two enzymes provide a finely tuned distribution of charges, which reflects the ability to oxidize specific halides. It is expected that the continued investigations of site-directed mutants of V-BrPO and the generation of laboratory evolved mutants of V-BrPO will contribute to the understanding of the mechanistic differences between vanadium- chloro, bromo, and iodoperoxidases.

References

- Almeida, M., S. H. Filipe, M. Maia, M.F., R. Melo, N. Severino, J. A. L. da Silva, J. J. R. Frausto da Silva and R. Wever (2001). "Vanadium Haloperoxidases from Brown Algae of the Laminariaceae Family." *Phytochemistry* **57**: 633-642.
- Almeida, M., M. Humanes, R. Melo, J. A. Silva, J. J. R. Frausto da Silva, H. Vilter and R. Wever (1998). "Saccorhiza Phaeophyceae (phaeophyceae; Phyllariaceae) a New Source for Vanadium-Dependent Haloperoxidases." *Phytochemistry* **48**: 229-239.
- Almeida, M. G., M. Humanes, R. Melo, J. A. Silva, J. J. R. Frausto da Silva and R. Wever (2000). "Purification and Characterization of Vanadium Haloperoxidases from the Brown Alga *Pelvetia canaliculata*." *Phytochemistry* **54**: 5-11.
- Bjorksten, F. (1968). "A Kinetic Study of the Horseradish Peroxidase-Catalyzed Oxidation of Iodide." *Eur. J. Biochem.* **5**: 133-142.
- Carter, J. N., K. E. Beatty, M. T. Simpson and A. Butler (2002). "Reactivity of Recombinant and Mutant Vanadium Bromoperoxidase from the Red Alga *Corallina officinalis*." *J. Inorg. Biochem.* **91**: 59-69.
- Cleland, W. (1979). "Statistical Analysis of Enzyme Kinetic Data." *Methods Enzymol.* **63**: 103-138.
- Colpas, G. J., B. J. Hamstra, J. W. Kampf and V. L. Pecoraro (1996). "Functional Models for Vanadium Haloperoxidases: Reactivity and Mechanism of Halide Oxidation." *J. Am. Chem. Soc.* **118**: 3469-3478.
- de Boer, E. and R. Wever (1988). "The Reaction Mechanism of the Novel Vanadium-Bromoperoxidase. A Steady-State Kinetic Analysis." *J. Biol. Chem.* **263**: 12326-12332.
- Everett, R. and A. Butler (1989). "Bromide-Assisted Hydrogen Peroxide Disproportionation Catalyzed by Vanadium Bromoperoxidase: Absence of Direct Catalase Activity and Implications for the Catalytic Mechanism." *Inorg. Chem.* **28**: 393-395.
- Everett, R. R., J. R. Kanofsky and A. Butler (1990b). "Mechanistic Investigations of the Novel Non-Heme Vanadium Bromoperoxidases - Evidence For Singlet Oxygen Production." *J. Biol. Chem.* **265**: 4908-4914.
- Everett, R. R., H. S. Soedjak and A. Butler (1990a). "Mechanism of Dioxygen Formation Catalyzed By Vanadium Bromoperoxidase - Steady State Kinetic

- Analysis and Comparison to the Mechanism of Bromination." *J. Biol. Chem.* **265**: 15671-15679.
- Faulkner, D. J. (1998). "Marine Natural Products." *Nat. Prod. Rep.* **15**: 113-158.
- Faulkner, D. J. (2000). "Marine Pharmacology." *Antonie van Leeuwenhoek* **77**: 135-145.
- Fenical, W. (1975). "Halogenation in the Rhodophyta, A Review." *J. Phycol.* **11**: 245-259.
- Gribble, G. W. (1998). "Naturally Occurring Organohalogen Compounds." *Acc. Chem. Res.* **31**: 141-152.
- Hall, T. A. (1999). "BioEdit: A User-Friendly Biological Sequence Alignment Editor and Analysis Program for Windows 95/98/NT." *Nucl. Acids Symp. Ser.* **41**: 95-98.
- Hamstra, B. J., G. J. Colpas and V. L. Pecoraro (1998). "Reactivity of Dioxovanadium (V) complexes with Hydrogen Peroxide: Implications for Vanadium Haloperoxidase." *Inorg. Chem.* **37**: 949-955.
- Hemrika, W., R. Renirie, H. L. Dekker, P. Barnett and R. Wever (1997c). "From Phosphatases to Vanadium Peroxidases: A Similar Architecture of the Active Site." *Proc. Natl. Acad. Sci. USA* **94**: 2145-2149.
- Hemrika, W., R. Renirie, S. Macedo-Ribeiro, A. Messerschmidt and R. Wever (1999). "Heterologous Expression of the Vanadium-Containing Chloroperoxidase from *Curvularia inaequalis* in *Saccharomyces cerevisiae* and Site-Directed Mutagenesis of the Active Site Residues His496, Lys353, Arg360, and Arg490." *J. Biol. Chem.* **274**: 23820-23827.
- Isupov, M. N., A. R. Dalby, A. A. Brindley, Y. Izumi, T. Tanabe, G. N. Murshudov and J. A. Littlechild (2000). "Crystal Structure of Dodecameric Vanadium-Dependent Bromoperoxidase from the Red Algae *Corallina officinalis*." *J. Mol. Biol.* **299**: 1035-1049.
- Itoh, N., A. K. M. Hasan, Y. Izumi and H. Yamada (1987). "Immunological Properties of Bromoperoxidases in Coralline Algae." *Biochem. Int.* **15**: 27-33.
- Itoh, N., Y. Izumi and H. Yamada (1986). "Characterization of Nonheme Type Bromoperoxidase in *Corallina pilulifera*." *J. Biol. Chem.* **261**: 5194-5200.

Littlechild, J., E. Garcia-Rodriguez, A. Dalby and M. Isupov (2002). "Structural and Functional Comparisons Between Vanadium Haloperoxidases and Acid Phosphatase Enzymes." *J. Mol. Recognit.* **15**: 291-296.

Martinez, J. S., G. L. Carroll, R. A. Tschirret-Guth, G. Altenhoff, R. D. Little and A. Butler (2001). "On the Regiospecificity of Vanadium Bromoperoxidase." *J. Am. Chem. Soc.* **123**: 3289-3294.

Messerschmidt, A., L. Prade and R. Wever (1997). "Implications for the Catalytic Mechanism of the Vanadium-Containing Enzyme Chloroperoxidase from the Fungus *Curvularia inaequalis* by X-ray Structures of the Native and Peroxide Form." *Biol. Chem.* **378**: 309-315.

Messerschmidt, A. and R. Wever (1996). "X-ray Structure of a Vanadium-Containing Enzyme: Chloroperoxidase from the Fungus *Curvularia inaequalis*." *Proc. Natl. Acad. Sci. USA* **93**: 392-396.

Moore, C. A. and R. K. Okuda (1996). "Bromoperoxidase Activity in 94 Species of Marine Algae." *Journal Nat. Toxins* **5**: 295-305.

Mynderse, J. S. and D. J. Faulkner (1963). "Polyhalogenated Monoterpenes from the Red Alga *Plocamium cartilagineum*." *Tetrahedron* **31**: 1963-1967.

Nicholas, K. B., H. B. Nicholas, Jr and D. W. Deerfield, II (1997). *EMBnet News* **4**: 14.

Renirie, R., W. Hemrika and R. Wever (2000a). "Peroxidase and Phosphatase Activity of Active-Site Mutants of Vanadium Chloroperoxidase from the Fungus *Curvularia inaequalis*. Implications for the Catalytic Mechanisms." *J. Biol. Chem.* **275**: 11650-11657.

Sheffield, D. J., T. Harry, A. J. Smith and L. J. Rogers (1993). "Purification and Characterization of the Vanadium Bromoperoxidase from the Macroalga *Corallina officinalis*." *Phytochemistry* **32**: 21-26.

Shimonishi, M., S. Kuwamoto, H. Inoue, R. Wever, T. Ohshiro, Y. Izumi and T. Tanabe (1998). "Cloning and Expression of the Gene for a Vanadium-Dependent Bromoperoxidase from a Marine Macro-Alga, *Corallina pilulifera*." *FEBS Lett.* **428**: 105-110.

Soedjak, H. S. and A. Butler (1991). "Mechanism of Dioxygen Formation Catalyzed By Vanadium Bromoperoxidase From *Macrocystis-Pyrifera* and *Fucus-Distichus* - Steady State Kinetic Analysis and Comparison to the Mechanism of V-Brpo From *Ascophyllum-Nodosum*." *Biochim. Biophys. Acta* **1079**: 1-7.

Soedjak, H. S., J. V. Walker and A. Butler (1995). "Inhibition and Inactivation of Vanadium Bromoperoxidase By the Substrate Hydrogen Peroxide and Further Mechanistic Studies." *Biochemistry* **34**: 12689-12696.

Tschirret-Guth, R. A. and A. Butler (1994). "Evidence for Organic Substrate Binding to Vanadium Bromoperoxidase." *J. Am. Chem. Soc.* **116**: 411-412.

Vilter, H. (1983a). "Peroxidases from Phaeophyceae IV. Fractionation and localization of Peroxidase Isoenzymes in *Ascophyllum nodosum*." *Botanica Marina* **26**: 451-455.

Vilter, H. (1983b). "Peroxidases From Phaeophyceae 3.: Catalysis of Halogenation by Peroxidases from *Ascophyllum nodosum*." *Bot. Mar.* **26**: 429-435.

Weyand, M., H. Hecht, M. Kiesz, M. F. Liaud, H. Vitler and D. Schomburg (1999). "X-ray Structure Determination of a Vanadium-Dependent Haloperoxidase from *Ascophyllum nodosum* at 2.0 Å Resolution." *J. Mol. Biol.* **293**: 595-611.

Chapter Three

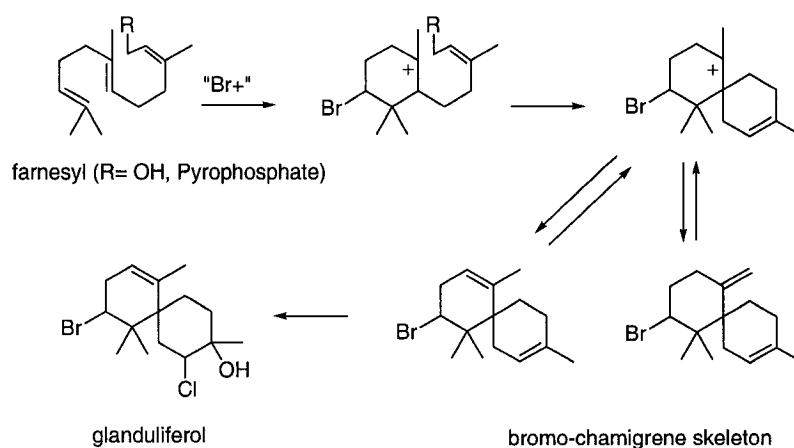
The Role of Vanadium Bromoperoxidase in the Biosynthesis of Halogenated Terpenes

Introduction

Halogenated natural products are the most frequently reported metabolites in marine red algae (Rhodophyceae) (Fenical 1975; Fusetani 2000; Faulkner 2002). The widespread occurrence of halogenated natural products from marine organisms has prompted numerous investigations into the total synthesis and biomimetic synthesis of halogenated marine metabolites, most notably bromine-containing cyclic sesquiterpenes. A quarter of a century ago, Faulkner and Fenical proposed the formation of brominated sesquiterpenes via a bromo-cation active species (Fenical 1975; Faulkner 1976a). Bromination is proposed to occur at the terminal olefin of a farnesyl-derivative, followed by ring closure to a monobromocyclohexadienyl cation. The spiro-compound is formed *via* a cyclization reaction, with elimination of the hydroxyl/pyrophosphate group to form the bromo-chamigrene skeleton. Additional brominated/chlorinated and oxygenated sesquiterpene metabolites are formed *via* skeleton 1,2-rearrangements (Scheme 3.1) (Martin and Darias 1978).

Initial investigations into the biomimetic synthesis of halogenated cyclic terpenes, carried out at a time when the existence of marine haloperoxidases had only been hypothesized, utilized direct bromine-carbon bond formation with successive ring closure of the terpene precursor, or alternatively the indirect incorporation of bromine to the cyclized terpenoid intermediate. Successfully

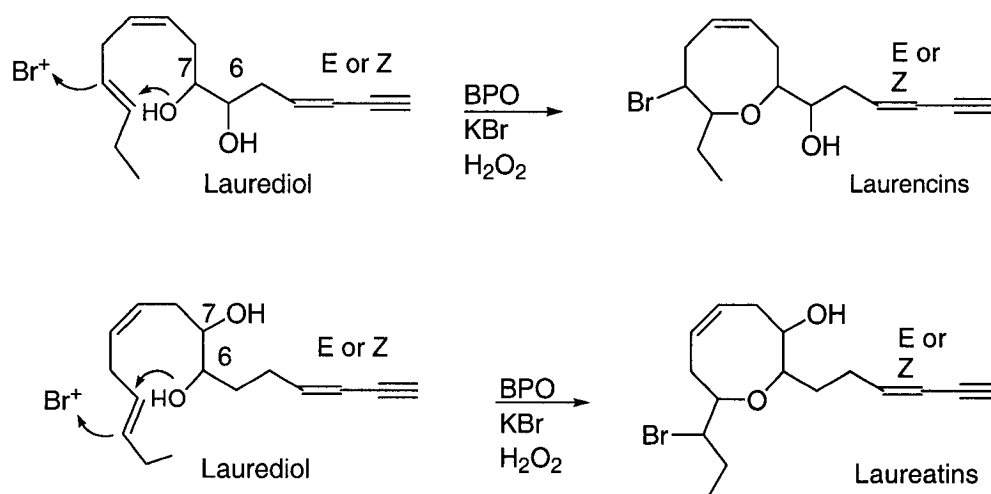
employed reagents include N-bromosuccinimide [van Tamelen, 1966 #42; Gonzalez, 1976 #44], bromine in the presence of Lewis acids such as AlBr_3 , SnBr_4 or AgBF_4 (Wolinsky and Faulkner 1976; Hoye and Kurth 1978), 2,4,4,6-tetrabromocyclohexa-2,5-dienone (TBCO) in the presence of Lewis acids (Kato et al. 1980; Shieh and Prestwich 1982; Gonzalez and Forsyth 2000), and acid-catalyzed cyclization of terpene containing terminal bromohydrins. Mercuric trifluoroacetate or the mercury (II) triflate/*N,N*-dimethylaniline complex have also been used in the synthesis of cyclized brominated terpenes (Hoye and Kurth 1979; Hoye et al. 1981; Gopalan et al. 1992).



Scheme 3.1: Proposed pathway for bromonium-ion induced cyclization of sesquiterpenes.

Biomimetic approaches have provided useful routes for production of halogenated marine metabolites, although little is known about the biosynthesis of brominated cyclic sesquiterpenes within marine algae sources. Previously, Murai and coworkers demonstrated the bromoetherification of (3*E*)- and (3*Z*)-laurediol to (3*E*)- and (3*Z*)-prelauretins using a commercially available lactoperoxidase and a partially purified bromoperoxidase from the red alga *Laurencia nipponica* (Scheme 3.2) (Fukuzawa et al. 1990a; Fukuzawa et al. 1992; Fukuzawa et al. 1994).

Vanadium bromoperoxidase (V-BrPO) is particularly prevalent, having been found in all classes of marine algae (Hemrika et al. 1998; Butler et al. 2001). The active site of V-BrPO contains a single vanadate ion (V^V) coordinated to the



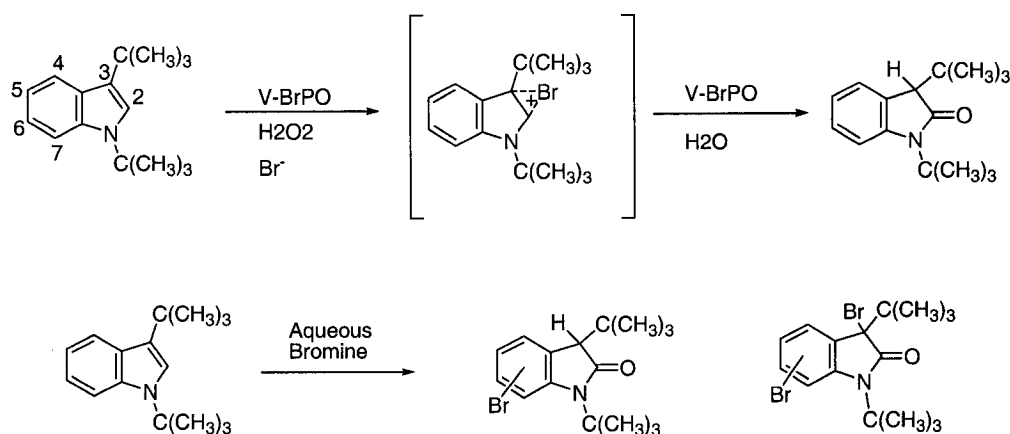
Scheme 3.2: Proposed bromoetherification of laurediol by peroxidase enzymes.

protein scaffold by a single histidine residue at the bottom of a deep active site channel (Weyand et al. 1999; Isupov et al. 2000). V-BrPO catalyzes halide

oxidation by coordination of hydrogen peroxide. The oxidized intermediate can halogenate an appropriate organic substrate or oxidize a second equivalent of hydrogen peroxide, producing dioxygen in the singlet excited state (Everett et al. 1990; Butler and Walker 1993). It has also been established that oxidation of the halide produces a two-electron oxidized halogen species (e.g, Br^+ in the case of Br^- oxidation), and subsequent halogenation of organic substrates proceeds through an electrophilic (Br^+) rather than a radical (Br^\bullet) process (Soedjak et al. 1995).

Early reports on the reactivity of V-BrPO towards prochiral aromatic compounds failed to demonstrate any regio or stereoselectivity upon bromination (Itoh et al. 1987; Itoh et al. 1988; Krenn et al. 1989). The lack of selectivity suggested that V-BrPO produces a diffusible oxidized halogen intermediate such as hypobromite, bromine, or tribromide within the algae (de Boer and Wever 1988). More recently however, V-BrPO was shown to perform regioselective bromination of 1,3-di-*tert*-butylindole yielding 1,3-di-*tert*-butyl-2-indolinone exclusively, while multiple products were observed using aqueous bromine (Scheme 3.3) (Martinez et al. 2001). In addition, competitive bromination kinetics of certain indoles showed that V-BrPO-catalyzed reactions were not consistent with halogenation by a freely-diffusible oxidized species (i.e., $\text{HOBr} = \text{Br}_2 = \text{Br}_3^-$). Also, fluorescence quenching of indoles (2-phenylindole) by V-BrPO established a direct interaction of indoles with V-BrPO (Tschirret-Guth and Butler 1994). In addition to regioselective halogenation of indoles, it has been recently discovered that V-BrPO can catalyze the stereospecific oxidation of bicyclic sulfides to the corresponding sulfoxides with

a high degree of enantioselectivity (>95% ee) (Andersson et al. 1997; Andersson and Allenmark 1998; ten Brink et al. 1998). The stereoselective oxidations were performed in the absence of halide. The sulfoxidation reactions are the only known direct oxygen transfer reaction catalyzed by V-BrPO. Interestingly, the V-BrPO's from *Ascophyllum nodosum* and *Corallina officinalis* direct the oxidation to differing enantiomers of the sulfoxide, while the similar recombinant vanadium chloroperoxidase (V-CIPO) from *Curvalaria inaequalis* catalyzes the production of a racemic sulfoxide mixtures. The different selectivities of the vanadium haloperoxidases (VHPOs) and recent X-ray crystallographic studies suggest subtle differences exist in the substrate channel of these enzymes (Weyand et al. 1999;



Isupov et al. 2000).

Scheme 3.3: Bromination of 1,3-di-tert-butylindole by V-BrPO and aqueous bromine.

Given that V-BrPO can catalyze enantioselective oxidations of selective sulfides, as well as bind certain organic substrates (such as indoles, and presumably the bicyclic sulfides), and perform regioselective halogenation of indoles, it seemed reasonable that V-BrPO could catalyze selective bromination of terpene substrates towards the production of brominated marine natural products. In an attempt to explore the role of vanadium bromoperoxidase in the biosynthesis of brominated marine natural products, we probed the enzyme's ability to selectively brominate and cyclize monoterpenes, sesquiterpenes, terpene analogs and model compounds. Reported herein is the halogenation and cyclization of terpenes by V-BrPO in the production of marine natural products and structures found within brominated natural products, establishing V-BrPO's likely role in the biogenesis of brominated cyclic terpenes from marine organisms.

Methods and Materials

General methods:

Vanadium bromoperoxidase from the marine red algae *Corallina officinalis*, *Plocamium cartilagineum*, and *Laurencia pacificia* were purified as described for *C. officinalis* with minor modifications (Brindley et al. 1998; Carter et al. 2002) (see Chapter 2). Bromoperoxidase activity was determined by monitoring the bromination of 50 μM monochlorodimedone (MCD) spectrophotometrically at 290 nm under conditions of 0.1 M KBr, and 1 mM H_2O_2 in 0.1 M sodium phosphate buffer (pH 6.00). The extinction coefficient at 290 nm between MCD and brominated MCD is $19,900 \text{ cm}^{-1} \text{ M}^{-1}$ (Hager et al. 1966).

^1H NMR and ^{13}C NMR spectra were recorded on a Varian 500 instrument using deuteriochloroform as the solvent (CHCl_3 , standard, $\delta = 7.27$ ppm). Multiplicities are indicated by s (singlet), d (doublet), t (triplet), q (quartet), m (multiplet), a (apparent) or br (broadened). Coupling constants, J , are reported in Hertz. ^{13}C spectra are assigned with either a (+) or (-) symbol to indicate the orientation of the signal using an attached proton test (APT) pulse sequence. Signals with a (+) orientation have either zero or two attached protons; signals with a (-) signal have either one or three attached protons. FTIR spectra were recorded on a JASCO 600 spectrophotometer. Consumption and formation of reaction substrates and products were monitored using a Hewlett-Packard 5890-series II gas chromatograph coupled with a Hewlett-Packard 592-A-EI gas chromatograph.

Chiral gas chromatography analysis was performed using a Cyclosil B capillary column (J & W Scientific).

Aqueous bromine was prepared by dilution of bromine vapors in 0.1 M NaOH and standardized by tri-iodide formation (I_3^- ; λ_{\max} 353 nm, $\Delta\epsilon = 26,600 \text{ cm}^{-1} \text{ M}^{-1}$ determined in 0.1 M citrate-phosphate buffer with 0.05 M KI (pH 4.5). The predominant species in solution at pH 6 – 7 is HOBr; however, multiple oxidized bromine species are present in solution which are best represented as $OBr^- = HOBr = Br_2 = Br_3^-$ (Ziderman 1972). This reaction mixture will be referred to as “aqueous bromine” throughout this chapter.

Reversed-phase HPLC was used to ultra-purify product from reactions with V-BrPO or aqueous bromine as well as for retention time analysis. A C_{18} column (semi-preparative 250 x 10 mm or analytical 250 x 4.5 mm, ODS-AQ, YMC Inc.) was used on a Waters HPLC system equipped with two Waters 515 pumps. Products were eluted using gradient mixtures of acetonitrile and water, and the UV absorbance (214 nm) of the eluent was measured with a dual wavelength detector. When necessary, normal-phase HPLC was performed to ultra-purify products that eluted as overlapping peaks in reversed-phase mode. A HPLC silica column (semi-preparative 250 x 10 mm, YMC-Sil, YMC Inc.) was used and products were eluted isocratically with 0.3% isopropanol/hexanes. The UV absorbance of the eluent was measured at 214 nm.

Flash column chromatography was performed using 230 - 400 mesh silica gel (EM Science) and mixtures of ether and pentane as eluent. All *trans* (+)-nerolidol

was purchased from Indofine Chemical Company and used as received. Linalool, nerol, geraniol, geranyl acetate and geranyl acetone were used as received from Aldrich-Sigma Chemical Company. Compounds *cis*-5-octene-1-ol, and *cis*-3-nonene-1-ol were used as received from Alfa Aesar chemical company. TBCO was used as obtained from Acros.

V-BrPO catalyzed reactions (product profile analysis):

Linalool. Linalool (0.5 mM) (**1**) predissolved in ethanol was added to 0.15 M phosphate solution (pH 5.7) containing 30% v/v ethanol and 40 mM KBr. Enzymatic reactions containing 23 nM V-BrPO were initiated by addition of 1 or 2 mol equivalents of H₂O₂ in relation to linalool concentration. Reactions were extracted with 2 vol each of hexanes, brine, and dried by passage through a short plug of MgSO₄. Organic extracts were used directly for analysis by gas chromatography mass spectrometry (GC-MS). Brominated ethereal products **2** and **3** have been reported (Gonzalez and Forsyth 2000).

Kinetic resolution of linalool with V-BrPO. Racemic linalool (1 mg, 6 mM) was predissolved in 600 µl of isopropyl alcohol, and added to 394 µl of 0.05 M phosphate buffer (pH 6.0) and 40 mM KBr (final volume 1 ml). Vanadium bromoperoxidase was added (9 nM) and the reaction initiated by the single batch addition of H₂O₂ to final concentration of 1, 3, 6, or 12 mM. Reactions were incubated for 1 hour in the dark. At the completion of 1 hour, 1 milligram of geranyl acetone was added quantitatively as an internal standard. The mixture was extracted with 2 vol methylene chloride, followed by 30 seconds of vortexing, and 2 minutes

of centrifugation on a tabletop centrifuge at 1380 x *g*. The organic layer was used directly for GC-MS and chiral GC analysis. The percent conversion of linalool was determined from the raw area under the peak of remaining linalool relative to the raw area under the peak for geranyl acetone as the internal standard. The relative amounts of remaining *R*- and *S*-linalool were determined using a CyclosilB capillary chiral GC column using an isotherm of 125 °C.

Nerol. Nerol (**4**) (0.5 mM) predissolved in ethanol, was added to a 0.15 M phosphate solution (pH 5.7) containing 30% v/v ethanol and 40 mM KBr (final pH of the solution, 6.5). Enzymatic reactions containing 23 nM V-BrPO were initiated by addition of 1 or 2 mol equivalents of H₂O₂ (controlled addition via syringe pump, 1 equiv per hour) with respect to the terpene concentration. Product profile analysis was performed by GC-MS as described below.

Geraniol. Geraniol (**6**) (0.5 mM) predissolved in ethanol, was added to a 0.15 M phosphate solution (pH 5.7) containing 30% v/v ethanol and 40 mM KBr (final pH of the solution, 6.5). Enzymatic reactions containing 23 nM V-BrPO were initiated by addition of 1 or 2 mol equivalents of H₂O₂ (controlled addition via syringe pump, 1 equiv per hour) with respect to the terpene concentration. Product profile analysis was performed by direct injection on a C₁₈ reversed-phase column without prior extraction as described below.

Geranyl acetate. Geranyl acetate (**9**) (0.5 mM) predissolved in ethanol, was added to a 0.15 M phosphate solution (pH 5.7) containing 40% v/v ethanol and 40 mM KBr (final pH of the solution, 6.5). Enzymatic reactions containing 23 nM V-

BrPO were initiated by addition of 1 or 2 mol equivalents of H₂O₂ (controlled addition via syringe pump, 1 equiv per hour) with respect to the terpene concentration. Product profile analysis was performed by GC-MS analysis.

Geranyl acetone. Geranyl acetone (**12**) (0.5 mM) predissolved in ethanol, was added to a 0.15 M phosphate solution (pH 5.7) containing 40% v/v ethanol and 40 mM KBr (final pH of the solution, 6.5). Enzymatic reactions containing 23 nM V-BrPO were initiated by addition of 1 or 2 mol equivalents of H₂O₂ (controlled addition via syringe pump, 1 equiv per hour) with respect to the terpene concentration. Product profile analysis was performed by GC-MS as described below.

All trans (+)-nerolidol. All *trans* (+)-nerolidol (**14**) (0.5 mM) was dissolved in ethanol and added to 0.15 M phosphate solution (pH 5.7) containing 40% v/v ethanol and 40 mM KBr. Enzymatic reactions containing 23 nM V-BrPO, were initiated by addition of 1 or 2 mol equivalents of H₂O₂ (controlled addition via syringe pump, 1 equiv per hour) in relation to **14** concentration. Reactions were extracted with 2 vol hexanes. Alcoholic and ethereal products were fractionated from hydrin products by selective elution on a silica Sep-Pak (Waters Corp.) with 10% ether/pentane. Alcoholic and ethereal portions were resuspended in 100% ethanol, and injected directly for product profile and retention time analysis by reversed-phase HPLC (Analytical C₁₈, ODS-AQ, YMC Inc.).

Cis-5-octene-1-ol. *Cis*-5-octene-1-ol (**19**) (0.5 mM) predissolved in ethanol, was added to a 0.15 M phosphate solution (pH 5.7) containing 30% v/v ethanol and

40 mM KBr (final pH of the solution, 6.5). Enzymatic reactions containing 23 nM V-BrPO were initiated by addition of 1 or 2 mol equivalents of H₂O₂ (controlled addition via syringe pump, 1 equiv per hour) with respect to the terpene concentration. Product profile analysis was performed by GC-MS as described below.

Cis-3-nonene-1-ol. *Cis-5-nonene-1-ol* (**21**) (0.5 mM) predissolved in ethanol, was added to a 0.15 M phosphate solution (pH 5.7) containing 30% v/v ethanol and 40 mM KBr (final pH of the solution, 6.5). Enzymatic reactions containing 23 nM V-BrPO were initiated by addition of 1 or 2 mol equivalents of H₂O₂ (controlled addition via syringe pump, 1 equiv per hour) with respect to the terpene concentration. Product profile analysis was performed by GC-MS as described below.

Product profile analysis. GC-MS and reversed-phase HPLC was used to monitor reaction profiles. Reactions analyzed by GC-MS were quenched by extraction with 2 vol of methylene chloride prior to analysis. One microliter of methylene chloride extract was used for injection.

Reactions analyzed by reversed-phase HPLC (retention time analysis) were injected without prior extraction. A C₁₈ column (analytical 250 x 4.6 mm, ODS-AQ, YMC Inc.) was used on a Waters HPLC system with two 515 pumps. Products were eluted isocratically in 60-80% acetonitrile and water and the UV absorbance was monitored at 214 nm on a dual wavelength detector.

Non-enzymatic reactions with terpene substrates

Reaction of terpene substrates with aqueous bromine was performed using identical reaction conditions as described above for V-BrPO catalyzed reactions. Reactions were initiated by addition of 1 or 2 mol equivalents of aqueous bromine to terpene substrates (nerol (**4**), geraniol (**6**), and all *trans* (+)-nerolidol (**14**)) without addition of V-BrPO or H₂O₂. Aqueous bromine was added in a controlled manner via syringe pump at a rate similar to the bromination rate of MCD by V-BrPO (all reactions were performed in the dark with stirring). TBCO reactions with **6** and **14** were performed under conditions identical to those previously described (Kato et al. 1980; Shieh and Prestwich 1982; Gonzalez and Forsyth 2000). Product profile analysis was the same as was performed for V-BrPO catalyzed reactions.

Larger scale incubations with V-BrPO (structure determinations):

Large-scale reactions were performed and the isolated products characterized. Terpene substrates (nerol (**4**), geraniol (**6**), geranyl acetate (**9**), geranyl acetone (**12**), and (+)-nerolidol (**14**)) (9 mM) predissolved in isopropanol, were added to a 0.15 M phosphate solution (pH 5.7) containing 40% v/v isopropanol and 40 mM KBr (final pH of the solution, 6.5). The final volume of the reaction was 250 ml. Enzymatic reactions containing 23 nM V-BrPO (*C. officinalis*, *Plocamium cartilagineum* or *Laurencia pacifica*), were initiated by controlled addition of H₂O₂ at a rate of 1 mol equivalent per hour with respect to the terpene concentration. Completed reactions were extracted with 3 vol hexanes or methylene chloride, washed with brine, dried with MgSO₄, and reduced to a small volume in vacuo.

Crude extracts were fractionated by flash chromatography. Ultra-purification of ethereal fractions was performed by reversed-phase HPLC. Alcoholic fractions were ultra-purified by reversed-phase or normal-phase HPLC.

Reaction with nerol (4). Flash chromatography of ethereal fractions yielded a novel monobrominated eight-membered cyclic ether **5** as a colorless oil; (5% isolated yield), $^1\text{H NMR } \delta$ 5.23 (br s, 1H), 4.37 (dd, 1H), 4.19 (m, 2H), 3.41-3.32 (m, 1H), 2.28-2.06 (m, 2H) 1.72 (b quartet, 3H, $J = 3.7, 1.2$ Hz), 1.67-1.61 (m, 1H), 1.43 (s, 3H), 1.39 (s, 3H); $^{13}\text{C NMR } \delta$ 132.5 (+), 124.1 (-), 79.7 (+), 63.2 (+), 57.2 (-), 34.5 (+), 30.8 (+), 26.1 (-), 25.9 (-), 22.3 (-); IR (neat) 2972, 2930, 2855, 1446, 1382, 1135, 1107, 1048, 737; HRMS (EI, M^+) calculated for $\text{C}_{10}\text{H}_{17}\text{BrO}$ 232.0462, found 232.0474. Compound **5** is produced as a racemic mixture.

Reaction with geraniol (6). Reversed-phase HPLC of alcoholic fractions collected from flash chromatography yielded two monobrominated cyclic terpenes, **7**, and **8**, respectively (trace amounts). **7**; $^1\text{H NMR } \delta$ 5.38 (d, 1H, $J = 1.1$ Hz), 4.17 (dd, 1H, $J = 9.0, 7.0$ Hz), 3.98 (dd, 1H, $J = 11.5, 3.5$ Hz), 3.86 (dd, 1H, $J = 11.4, 3.6$ Hz), 2.59-2.54 (m, 3H), 1.79 (s, 3H), 1.20 (s, 3H), 1.01 (s, 3H); $^{13}\text{C NMR } \delta$ 134.2 (+), 122.5 (-), 64.4 (-), 61.5 (+), 52.3 (-), 37.97 (+), 34.9 (+), 28.9 (-), 21.8 (-), 17.1 (-); IR (neat) 3410, 2923, 2852, 1455, 1369, 1072, 715; MS (EI) 232, 234 (M^+), 189, 187, 152, 135, 121, 107; HRMS (ESI, $\text{M} + \text{Na}^+$) calculated for $\text{C}_{10}\text{H}_{17}\text{BrONa}$ 255.0360, found 255.0353. Compound **7** is produced as a racemic mixture.

Compound **8**; $^1\text{H NMR } \delta$ 5.04 (s, 1H), 4.79 (s, 1H), 4.15 (dd, 1H, $J = 10.3, 4.2$ Hz), 3.96-3.84 (m, 2H) 2.46-2.42 (m, 1H), 2.31-2.24 (m, 1H), 2.16-2.22 (m, 3H), 1.20 (s,

3H), 0.91 (s, 3H); ^{13}C NMR δ 144.9 (+), 109.7 (+), 65.8 (-), 60.2 (+), 55.4 (-), 40.5 (+), 35.1 (+), 29.7 (+), 28.4 (-), 18.5 (-); IR (neat) 3377, 2924, 2853, 1647, 1460, 1020, 800; MS (EI) 232, 234 (M^+), 189, 187, 152, 135, 121, 107; HRMS (ESI, $\text{M} + \text{Na}^+$) calculated for $\text{C}_{10}\text{H}_{17}\text{BrONa}$ 255.0360, found 255.0363. Compound **8** is produced as a racemic mixture.

Reaction with geranyl acetate (9). Flash chromatography yielded two monobrominated cyclized geranyl acetates **10** and **11** (10% isolated yield). These two products have been previously reported (Wolinsky and Faulkner 1976), and spectroscopic data from the V-BrPO catalyzed reaction is in agreement with reported values. **10**; ^1H NMR δ 5.35 (s, 1H), 4.35 (dd, $J = 3.8, 11.9$ Hz), 4.20 (m, 2H), 2.58 (m, 2H), 2.06 (s, 3H), 1.69 (m, 2H), 1.25 (s, 3H), 1.21 (s, 3H), 0.95 (s, 3H); ^{13}C δ 171.01 (+), 133.76 (+), 122.21 (-), 63.85 (-), 63.68 (+), 48.93 (-), 34.95 (+), 29.71 (+), 28.52 (-), 21.65 (-), 21.17 (-), 16.43 (-). **11**; ^1H NMR δ 4.95 (s, 1H), 4.66 (s, 1H), 4.41-4.31 (m, 2H), 4.13 (add, 1H), 2.40-2.00 (m, 4H), 2.03 (s, 3H), 1.23 (s, 3H), 0.91 (s, 3H); ^{13}C NMR δ 171.14 (+), 143.88 (+), 109.96 (+), 65.94 (-), 62.55 (+), 51.07 (-), 36.13 (+), 35.13 (+), 29.71 (+), 28.24 (-), 21.0 (-), 17.41 (-).

Reaction with geranyl acetone (12). Flash chromatography of ethereal fractions yielded a monobrominated bicyclic vinyl ether **13** as a colorless oil (9% isolated yield). Product **13** has been previously reported (Wolinsky and Faulkner 1976), and spectroscopic data from V-BrPO catalyzed reactions are in agreement with reported values. **13**; ^1H NMR δ 4.47 (m, 1H), 4.01 (dd, $J = 4.0, 12.4$ Hz), 2.23-1.84 (m, 7H), 1.68 (s, 3H), 1.19 (s, 3H), 1.08 (s, 3H), 0.95 (s, 3H); ^{13}C NMR δ 111.1

(+), 94.6 (-), 66.7 (-), 48.3 (-), 40.7 (+), 31.6 (+), 29.7 (-), 29.71 (+), 20.68 (+), 20.26 (-), 19.11 (-), 17.02 (-); HRMS (EI, M + H⁺) calcd for C₁₃H₂₁BrO 272.0776, found 272.0768.

Reaction with all trans (+)-nerolidol (14). Ultra purification by normal-phase HPLC of alcoholic fractions collected from flash chromatography, afforded three monobrominated cyclized alcohols **15**, **16**, and **17** (10% total isolated yield). Products **15** and **16** are the previously characterized marine natural products α - and β -snyderol, respectively (Howard and Fenical 1976). Products **15** and **16** were isolated as a mixture. Spectroscopic data is in agreement with reported values. **15**; ¹H NMR δ 5.84 (dd, $J = 17, 10$ Hz; 1H), 5.1 (d, $J = 17$ Hz; 1H), 5.31 (bs; 1H), 5.01 (d, $J = 10$ Hz; 1H), 4.05 (dd, $J = 9, 7$ Hz; 1H), 1.9-2.4 (m, 7H), 1.66 (s, 3H), 1.29 (s; 3H), 0.91 (s, 3H), 0.83 (s, 3H). **16**; δ 5.88 (dd, $J = 18, 10$ Hz; 1H), 5.14 (d, $J = 18$ Hz; 1H), 4.99 (d, $J = 10$ Hz; 1H), 4.82 (broad singlet, 1H), 4.55 (broad s; 1H), 4.00 (dd, $J = 11, 5$ Hz; 1H), 1.9 – 2.4 (m, 10H), 1.23 (s, 3H), 1.14 (s, 3H), 0.83 (s, 3H). Product **16** is produced as a single diastereomer. Product **17** has also been previously reported, and spectroscopic data from V-BrPO catalyzed reaction is in agreement with reported values (Wolinsky and Faulkner 1976). **17**; ¹H NMR δ 5.85 (dd, $J = 18, 11$ Hz; 1H), 5.16 (d, $J = 18$ Hz; 1H), 5.00 (d, $J = 11$ Hz; 1H), 4.18 (dd, $J = 10, 4$ Hz; 1H), 1.8 – 2.5 (broad m, 8H), 1.60 (s, 3H), 1.29 (s, 3H), 1.19 (s, 3H), 1.16 (s, 3H). Product **17** is produced as a single diastereomer. Reversed-phase HPLC of ethereal fractions collected from flash chromatography yielded a monobrominated bicyclic oxide **18** as a colorless oil (5 % isolated yield). Product **18**

is a previously identified marine natural product from the red alga *Laurencia obtusa* (Faulkner 1976b). Spectroscopic data for the V-BrPO-catalyzed reaction is in agreement with reported values. **18**; $^1\text{H NMR } \delta$ 5.99 (dd, $J = 18, 11$ Hz; 1H), 5.00 (dd, $J = 18, 2$ Hz; 1H), 4.95 (dd, $J = 11, 2$ Hz; 1H), 3.99 (dd, $J = 12, 5$ Hz; 1H), 1.23 – 2.3 (m, H), 1.20 (s, 3H), 1.18 (s, 3H), 1.07 (s, 3H), 0.88 (s, 3H). $[\alpha]_{\text{D}}^{25} = 31.8$ ($c = 1.52$; EtOH). Product **18** is produced as a single diastereomer.

The relative stereochemistry of **7**, **8**, **17** and **18** were determined by one-dimensional nOe analysis. Enantiomeric excesses were established by chiral GC analysis using isotherms of 120 °C for **7**, **8**, 155 °C for **17**, and 165 °C for **18**.

Competitive substrate kinetics:

Competitive kinetics for the bromination of phenol red (50 μM) catalyzed by V-BrPO (5 nM) or aqueous bromine as a function of terpene substrates geraniol **6** and all *trans* (+)-nerolidol **14** concentration, were performed at 25 °C in the presence of 40 mM KBr in 0.1 M phosphate buffer (pH 5.7) containing 40% ethanol. V-BrPO catalyzed experiments were initiated by the addition of 0.5 mM H_2O_2 . Non-enzymatic competition experiments were initiated by the addition of aqueous bromine (stock solution; 5 mM) in 10 μl aliquots at 30 sec intervals. UV absorbance was measured 20 sec after each addition of aqueous bromine. Production of bromophenol blue was monitored at 596 nm.

Results

Bromination of linalool by V-BrPO. When linalool (0.5 mM) (**1**) is allowed to react with V-BrPO (23 nM), bromide (40 mM) and 1 or 2 equivalents of H₂O₂ in the presence of organic co-solvent, the major products of the reaction are bromohydrins (60%) and the cyclized brominated furan **2** and pyran **3** (40%) as identified by GC-MS [Figure 3.1].

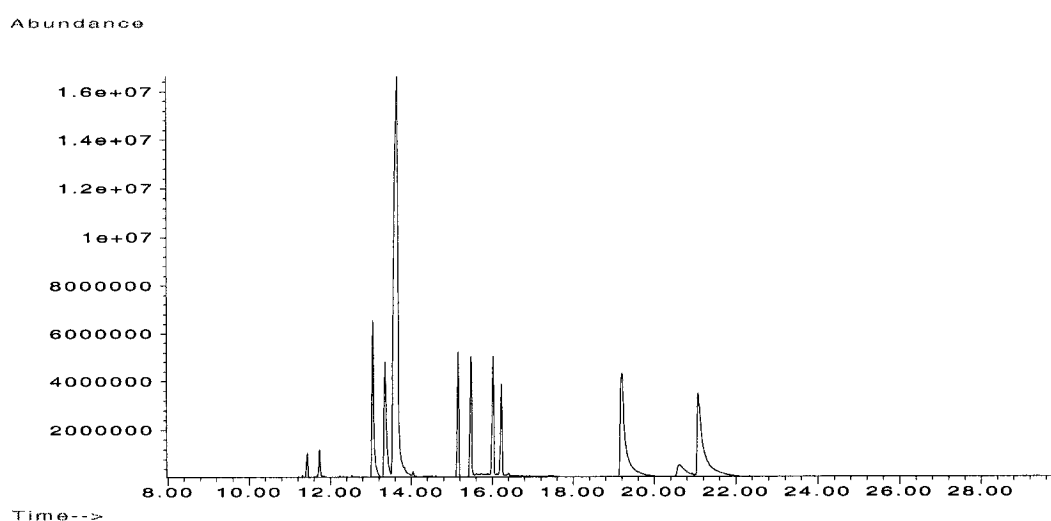


Figure 3.1: GC-MS chromatogram of V-BrPO catalyzed reaction with racemic linalool (**1**). Conditions: 0.5 mM linalool (**1**), 40 mM KBr in 0.15 M phosphate pH 5.7 with 30% ethanol and 23 nM V-BrPO. Reactions were initiated by the addition of H₂O₂ to a final concentration of 1 mM. Reaction time was 1 hour. Reaction was extracted with methylene chloride and one microliter used for injection. Retention times; linalool 13.7 min, 5-membered cyclic bromoethers (**2**) 15.0 – 15.5 min, 6-membered cyclic bromoethers (**3**) 16 – 16.2 min, bromohydrins 19.2 – 21.0 min.

The mass spectra of **2** and **3** indicate that both products are isomeric with one other with molecular ions of m/z of 234, 232 [Figure 3.2, 3.3]. The products at 15.1 and 15.5 minutes were identified as the brominated furans **2** based on

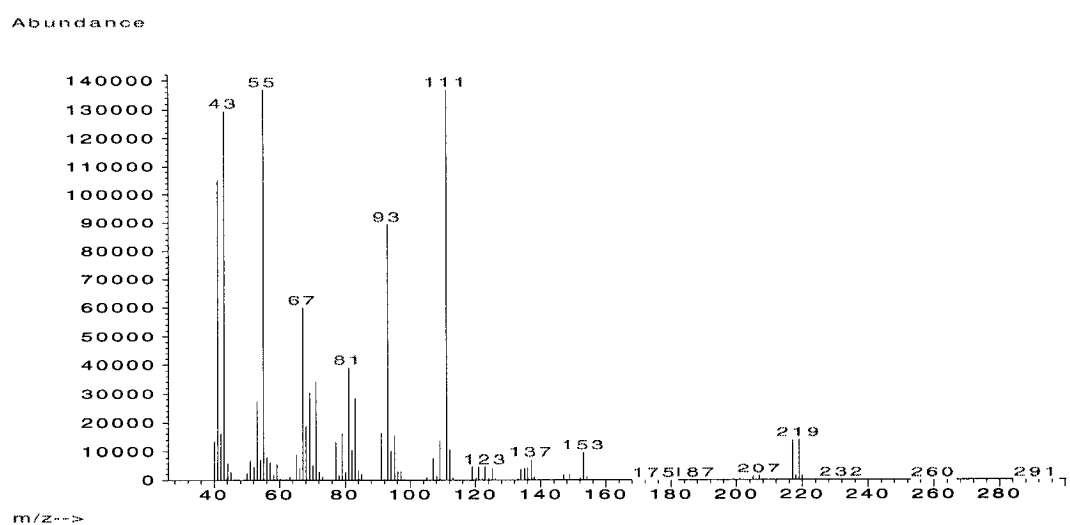


Figure 3.2: EIMS of 5-membered cyclic bromoether product **2**. Retention time on GC-MS chromatogram 15.0 – 15.5 min.

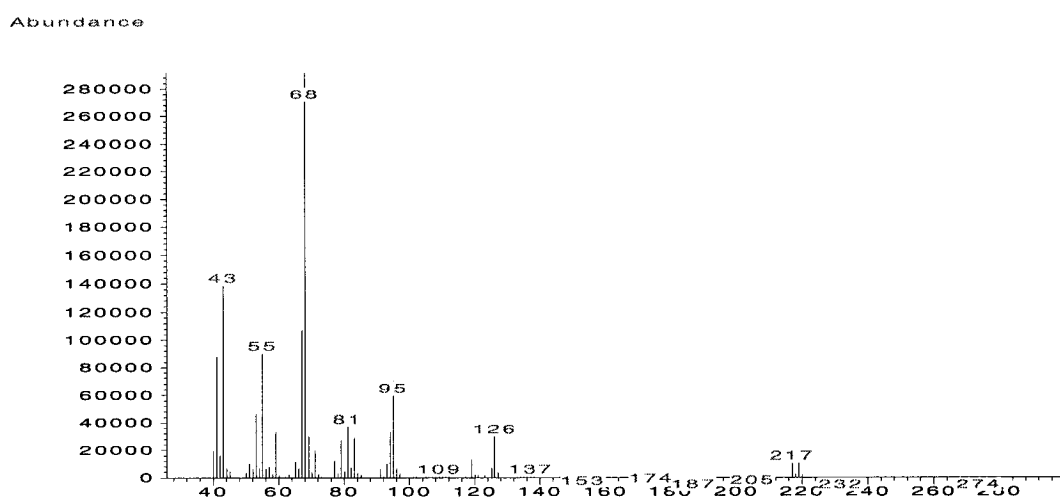


Figure 3.3: EIMS of 6-membered cyclic bromoether product **3**. Retention time on GC-MS chromatogram 16.0 – 16.2 min.

fragmentation analysis as established by Forsyth (Gonzalez and Forsyth 2000), and are proposed to be the 5-exo cyclic products. Likewise, the brominated pyrans **3** at 16.0 and 16.2 minutes were also identified *via* their fragmentation patterns and are designated as the 6-endo cyclic products. The presence of two brominated furans and two brominated pyrans indicate the V-BrPO-catalyzed reaction with racemic linalool (**1**) does not proceed with diastereoselectivity. Proton NMR characterization for a mixture of **2** and **3** was consistent with previously reported values (Gonzalez and Forsyth 2000). Proton NMR analysis of the mixture of **2** and **3** showed the doublet of doublets for the proton alpha to the bromine being split by a nearby diastereotopic methylene group, a useful spectroscopic signal used to identify brominated cyclized terpenes [Figure 3.4].

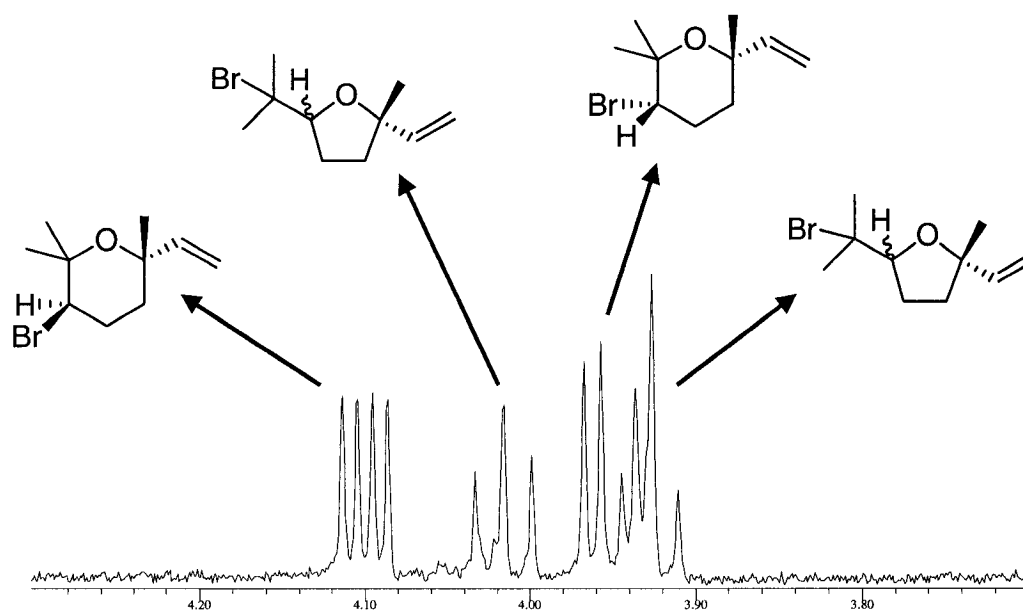
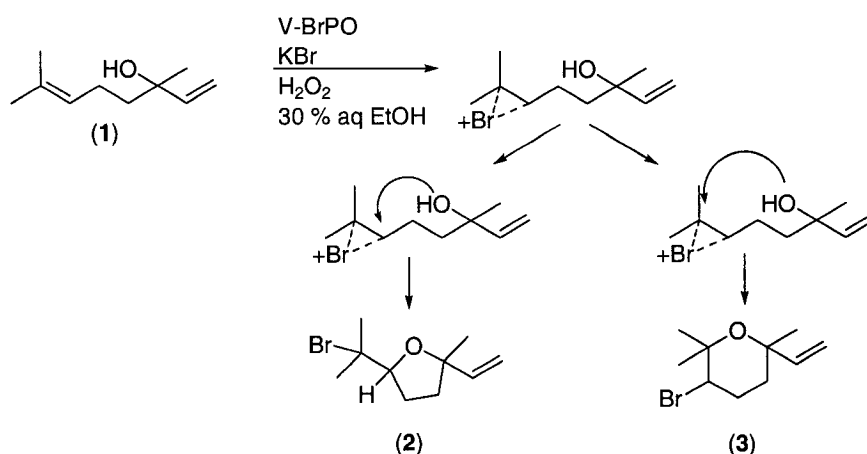


Figure 3.4: ^1H NMR of doublet of doublets for the mixture of bromoethers **2** and **3**.

The brominated furans **2** or pyrans **3** were not observed in the absence of bromide, indicating that in the absence of halide, the peroxo V-BrPO complex could not direct the cyclization of linalool in a terpene cyclase-type reaction. The formation of products **2** and **3** likely occurs from an electrophilic attack of the brominating species on the electron rich C6 – C7 double bond of linalool, yielding a bromonium-linalool intermediate, followed by intra-molecular attack by the tertiary alcohol to yield bromoethers **2** and **3** (Scheme 3.4).



Scheme 3.4: Proposed mechanism for V-BrPO catalyzed cyclization of linalool (**1**) to brominated cyclic ethers **2** and **3**.

Kinetic resolution of linalool using V-BrPO. Kinetic resolution experiments using TBCO, aqueous bromine, or V-BrPO with racemic linalool showed that V-BrPO has a kinetic preference for the *S*-enantiomer of linalool, 2.5:1 as determined

by chiral GC analysis. As expected, a kinetic preference was not observed when TBCO or aqueous bromine was used as the source of the brominating species “Br⁺”. A modest kinetic selectivity factor (k_{rel}) of 4.1 was calculated with a 22% consumption of linalool (Blackmond 2001).

Reaction of linalool with aqueous bromine. Reactions of linalool with aqueous bromine also produced **2** and **3** [Figure 3.5].

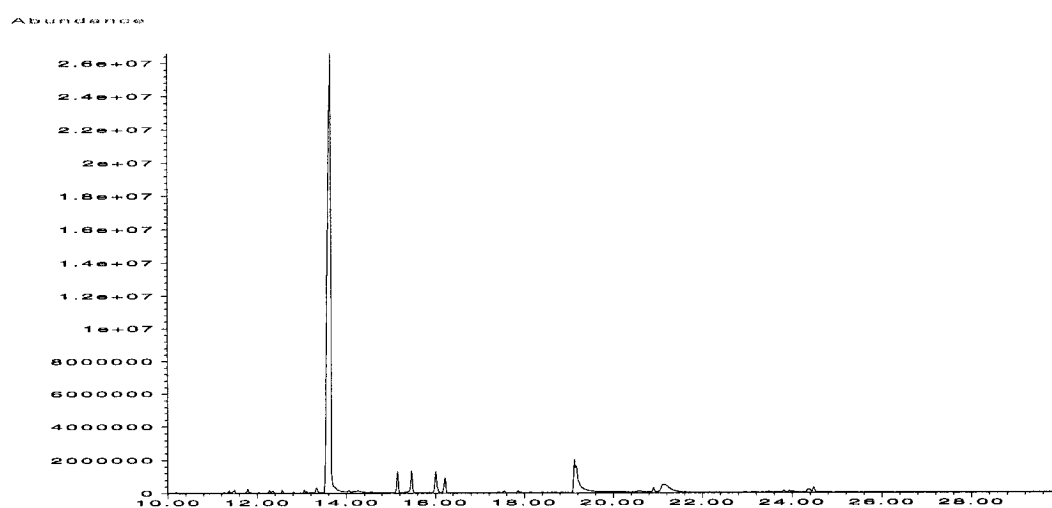


Figure 3.5: GC-MS chromatogram of aqueous bromine reaction with racemic linalool (**1**). Conditions: 0.5 mM linalool (**1**), 40 mM KBr in 0.15 M phosphate (pH 5.7) containing 30% ethanol. The reaction was initiated by the batch addition of aqueous bromine (1 mM). Reaction time was 1 hour. Reaction was extracted with methylene chloride and one microliter used for injection. Retention times: linalool 13.7 min, 5-membered cyclic bromoethers **2** 15.0 – 15.5 min, 6-membered cyclic bromoethers **3** 16 – 16.2 min, bromohydrins 19.2 – 21.0 minutes.

Bromination of nerol (**4**) by V-BrPO. Incubations of nerol (**4**) with V-BrPO, bromide, and hydrogen peroxide produced a mixture of products as identified by GC-MS [Figure 3.6]. The major products of the reaction were the terminal epoxide

(33%) and hydrin species (48 %) at 17.4 minutes and 21.2 – 22.8 minutes, respectively. Hydrin products arise from the nucleophilic quenching of a proposed bromonium-nerol intermediate by a solvent molecule (i.e., water or EtOH) (Scheme 3.5). The epoxide species is formed from the intramolecular attack of the hydroxyl group of the bromohydrin, with SN2 displacement of the bromine. Product profile analysis of the V-BrPO-catalyzed reaction with nerol indicated a potential brominated cyclized product at 18.0 minutes [Figure 3.6].

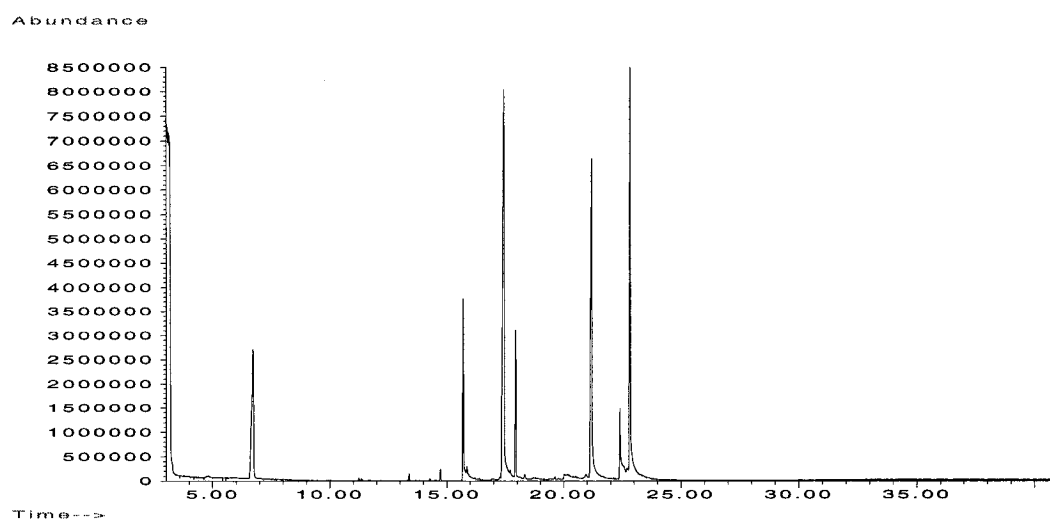
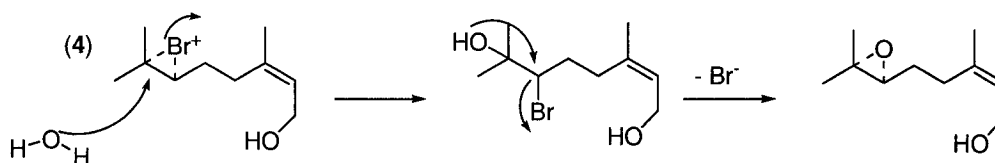


Figure 3.6: GC-MS chromatogram of V-BrPO catalyzed reaction with nerol (**4**). Conditions: 0.5 mM nerol (**4**), 40 mM KBr in 0.15 M phosphate (pH 5.7) containing 30% ethanol. Reactions were initiated by the addition of V-BrPO (23 nM) and H₂O₂ (1 mM final concentration). Reaction time was 1 hour. Reaction was extracted with methylene chloride and one microliter used for injection. Retention times: nerol 15.5 min, epoxide 17.5, eight-membered cyclic bromoether **5** 18 min, bromohydrins 21 - 23 min.



Scheme 3.5: Formation of nerol bromohydrin and epoxide species.

Large scale reactions with nerol (**4**) (1.75 mmol **4** and 1 – 2 eq. H₂O₂) and V-BrPO were carried out in order to determine the structure of the potential brominated cyclized nerol species. Purification of the reaction extract by silica gel chromatography with 10% ether/pentane as solvents yielded a singly brominated eight-membered cyclic ether product **5** (5% yield). Product **5** EIMS spectrum showed molecular ion peaks at m/z 232, 234 in a 1:1 ratio and a fragmentation ion at m/z 152 arising from the loss of a bromine atom [Figure 3.7]. High-resolution mass spectrometry (HRMS) of **5** gave a molecular formula of C₁₀H₁₇BrO, 232.0474. The ¹H NMR spectrum of **5** indicated the presence of two *gem*-dimethyl singlets δ 1.39 ppm and 1.43 ppm, indicating these methyl groups were no longer attached to an olefinic bond. In addition, a doublet of doublets signal at δ 4.37 ppm ($J = 12, 4.8$ Hz) was observed, and assigned to the proton alpha to the bromine on the ring. The cyclic ether functionality was confirmed in the IR absorption spectra of **5** by an absorption band at 1135 cm⁻¹. The IR spectrum also indicated the presence of the

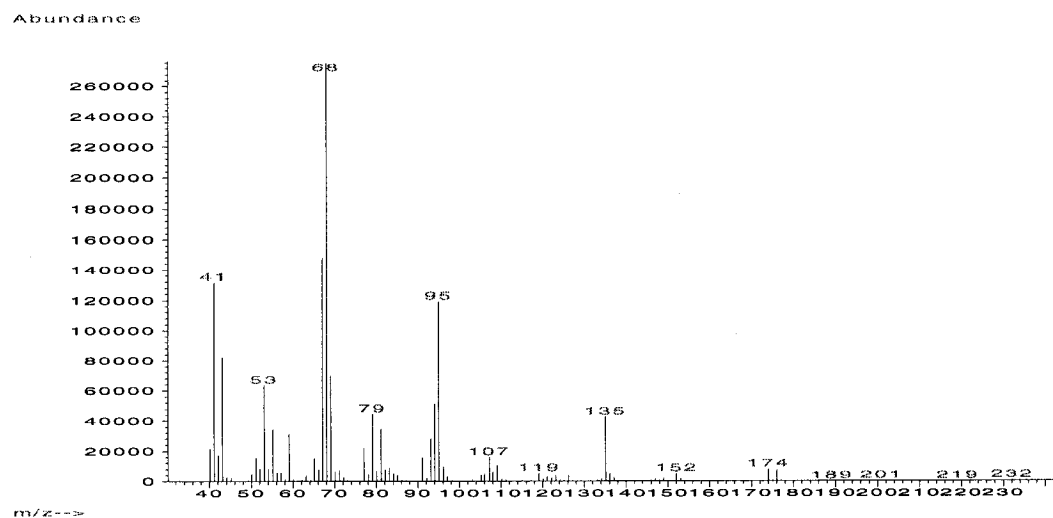
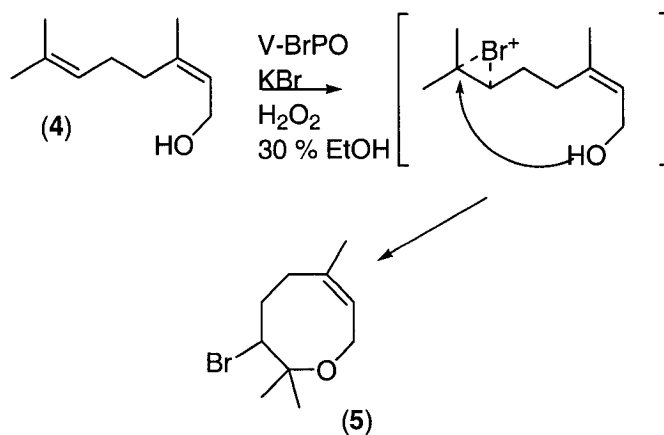


Figure 3.7: EIMS of eight-membered cyclic bromoether product **5**. Retention time on GC-MS chromatogram, 18.0 min.



Scheme 3.6: Proposed mechanism for V-BrPO catalyzed bromination and cyclization of nerol (**4**).

carbon-bromine bond with an absorption band at 737 cm^{-1} . The formation of product **5** is proposed to occur from an electrophilic attack of the brominating species on the electron rich C6 – C7 double bond of nerol, yielding a bromonium-nerol intermediate, followed by nucleophilic trapping of the bromonium intermediate by the pendant alcohol **5** (Scheme 3.6).

Reaction of nerol (**4**) with aqueous bromine and TBCO. Product profile analysis for the bromination of **4** with aqueous bromine was monitored by GC-MS [Figure 3.8]. The GC-MS chromatogram indicated that aqueous bromine produced epoxide and hydrin products, but did not produce the brominated eight-membered cyclic ether product **5**. Reaction of TBCO with nerol in nitromethane did produce **5**.

Bromination of geraniol (**6**) with V-BrPO. Product profile analysis by GC-MS of the reaction of geraniol (**6**), V-BrPO, bromide, and hydrogen peroxide showed the production of 4 compounds [Figure 3.9]. Analogous to the V-BrPO catalyzed reaction with nerol, the major products of the reaction were the epoxide (36%) and hydrin species (60%) at 17.8 minutes and 21.5 – 23.0 minutes, respectively. Hydrin and epoxide species are proposed to form by the same mechanism as was described for nerol. Careful examination of the reaction chromatogram and corresponding mass spectrum indicated the formation of two possible brominated cyclized geraniol species (20.5 – 21.0 minutes). Large scale incubations with geraniol (**6**) (1.75 mmol **6** and 1 – 2 eq. H_2O_2) were performed in order to determine the structures of the possible brominated cyclized species.

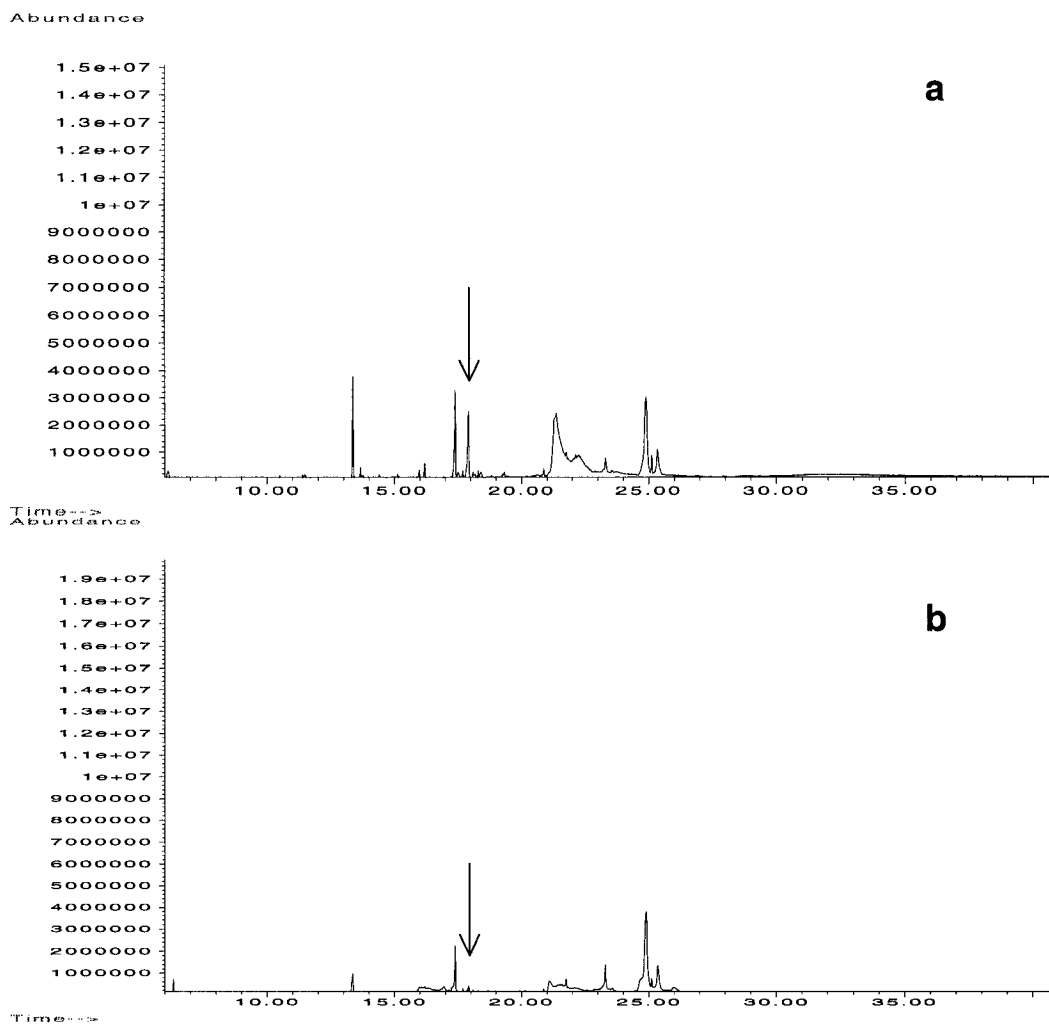


Figure 3.8: GC-MS chromatograms of the bromination of nerol (**4**) by V-BrPO and aqueous bromine. Conditions: 0.5 mM nerol (**4**), 40 mM KBr in 0.15 M phosphate (pH 5.7), with 30% ethanol and either (a) V-BrPO (23 nM) and 1 mM H₂O₂ or (b) 1 mM aqueous bromine. Reaction times were 1 hour. Reactions were extracted with methylene chloride. One microliter of each extract was used for product profile analysis.

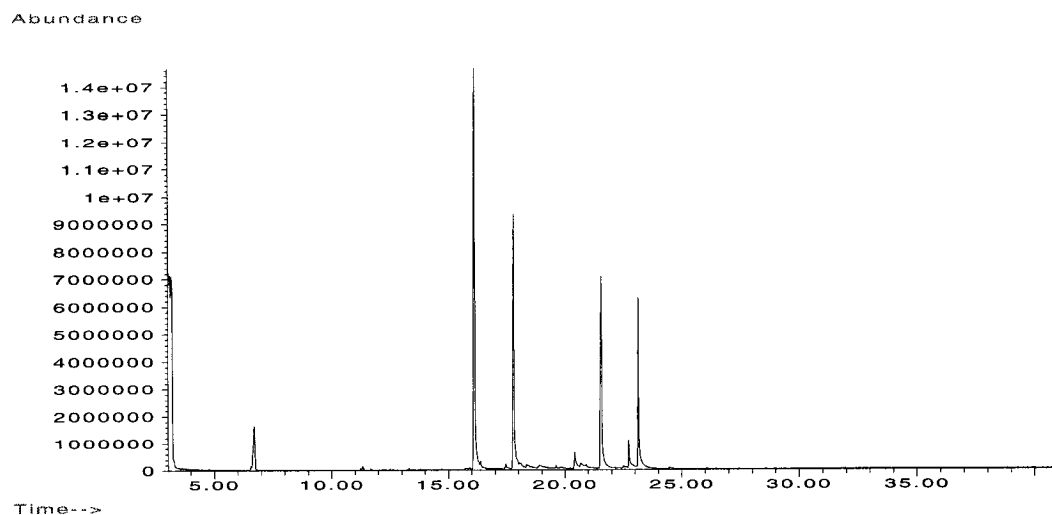


Figure 3.9: GC-MS chromatogram of V-BrPO catalyzed reaction with geraniol (**6**). Conditions: 0.5 mM geraniol (**6**), 40 mM KBr in 0.15 M phosphate (pH 5.7) with 30% ethanol. The reaction was initiated by the addition of V-BrPO (23 nM) and H₂O₂ (1 mM, final concentration). Reaction time was 1 hour. Reaction was extracted with methylene chloride and one microliter used for injection. Retention times; geraniol 16 minutes, epoxide 18.0 minutes, monobrominated cyclized geraniol **7** and **8** 20.5 – 21.0 minutes and bromohydrins 21.5 – 23.5 minutes.

Reaction extracts were purified by silica gel chromatography with 30% ether/pentane yielded bromoalcohol products and bromohydrins. Reversed-phase HPLC with 60% acetonitrile and water of the bromoalcohol fractions yielded two singly brominated cyclized geraniol species **7** and **8** (trace quantities). Products **7** and **8** EIMS spectra showed molecular ion peaks at m/z 232, 234 in a 1:1 ratio and a fragmentation ion at m/z 152 arising from the loss of a bromine atom [Figure 3.10, 3.11]. HRMS of **7** gave a formula of $C_{10}H_{17}BrONa$, 255.0353 for the sodium adduct. Likewise HRMS of **8** indicated a molecular formula of $C_{10}H_{17}BrONa$, 255.0363 for the sodium adduct of **8**. The 1H NMR spectrum of **7** indicated the presence of two *gem*-dimethyl singlets δ 1.01 ppm and 1.20 ppm, a doublet of doublet signal at δ 4.17 ppm ($J = 9, 7$ Hz) for the single proton alpha to the bromine, and an olefinic signal at δ 5.38 ppm. The 1H NMR spectrum of **8** was very similar to **7**, with two *gem*-dimethyl singlets at δ 0.91 ppm and 1.20 ppm, the characteristic doublet of doublets for the proton alpha to the bromine on the cyclohexane ring at δ 4.15 ($J = 10.3, 4$ Hz), and an exocyclic methylene group with signals at δ 4.79 ppm and 5.04 ppm. The IR absorption spectrum for **7** and **8** both contained a large, broad absorption around 3400 cm^{-1} , indicating retention of the primary alcohol of geraniol in products **7** and **8**. The presence of the alcohol moiety suggested that products **7** and **8** were formed by a different reaction mechanism than was proposed for bromoether **5**.

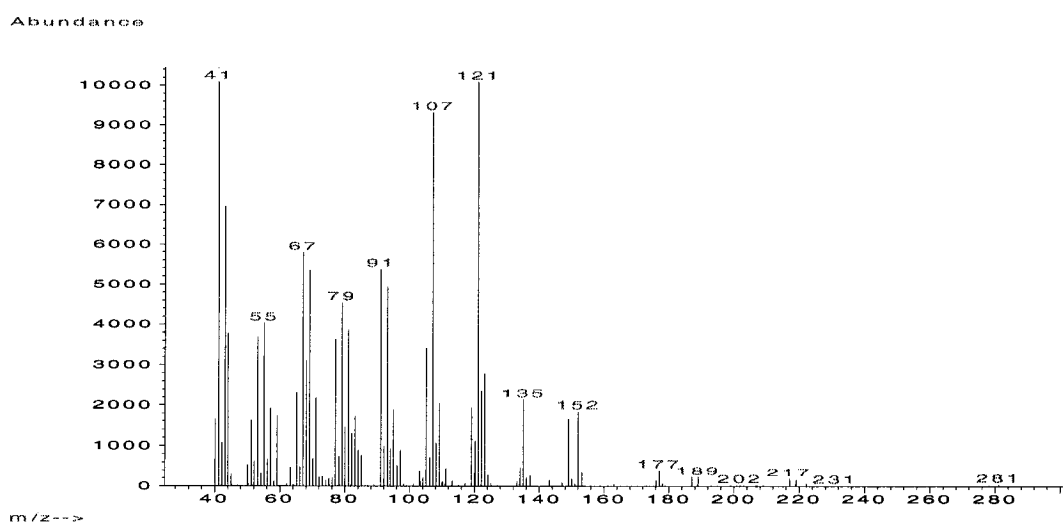


Figure 3.10: EIMS of monobrominated cyclized geraniol product **7**. Retention time on GC-MS chromatogram, 21.0 min.

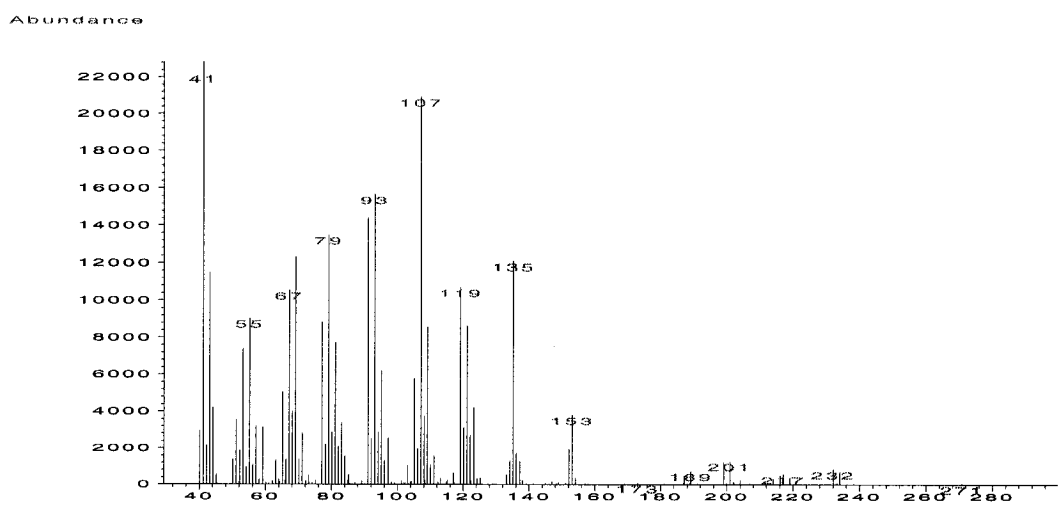
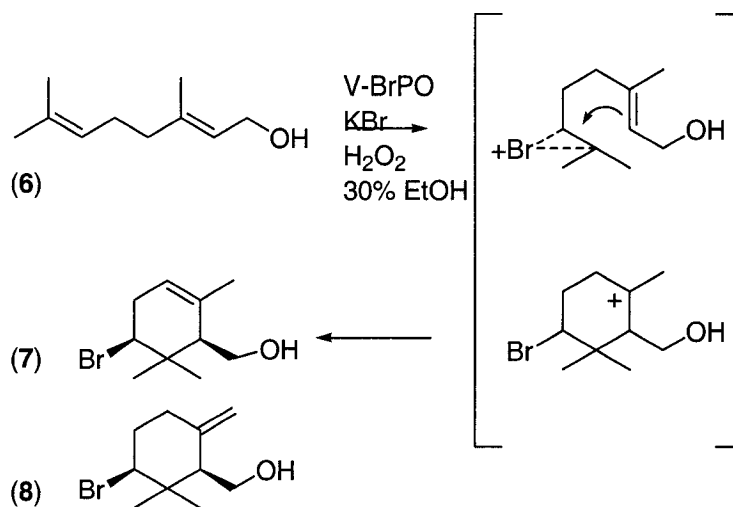


Figure 3.11: EIMS of monobrominated cyclized geraniol product **8**. Retention time on GC-MS chromatogram, 20.5 min.

Products **7** and **8** are proposed to form via attack on the C6 – C7 terminal olefin of geraniol, similar to nerol, to yield a bromonium-geraniol intermediate. The bromonium intermediate is subsequently attacked by the electron-rich internal olefinic bond, followed by elimination reactions leading to products **7** and **8** (Scheme 3.7).



Scheme 3.7: Proposed mechanism for V-BrPO catalyzed bromination and cyclization of geraniol (**6**).

One dimensional nOe analysis confirmed that cyclization of geraniol by V-BrPO occurred diastereoselectively as indicated by a strong nOe signal between the protons at C2 and C6 (geraniol numbering) in the axial positions. nOe analysis and the observed coupling constants for the proton at C6 established the bromine in the equatorial position. Chiral gas chromatography of products **7** and **8** indicated each are produced as single diastereomers without enantioselectivity.

Reaction of geraniol (6) with aqueous bromine and TBCO. Product profile analysis for the bromination of **6** by aqueous bromine was monitored by reversed phase HPLC analysis [Figure 3.12]. At the completion of each reaction, samples were injected directly without prior workup on a C₁₈ reversed-phase analytical column. Products were eluted isocratically using 60% v/v acetonitrile and water. HPLC analysis indicated that aqueous bromine did not produce the brominated monocyclic geraniol products **7** and **8** [Figure 3.12]. Reaction of TBCO with geraniol in nitromethane did produce **7** and **8**.

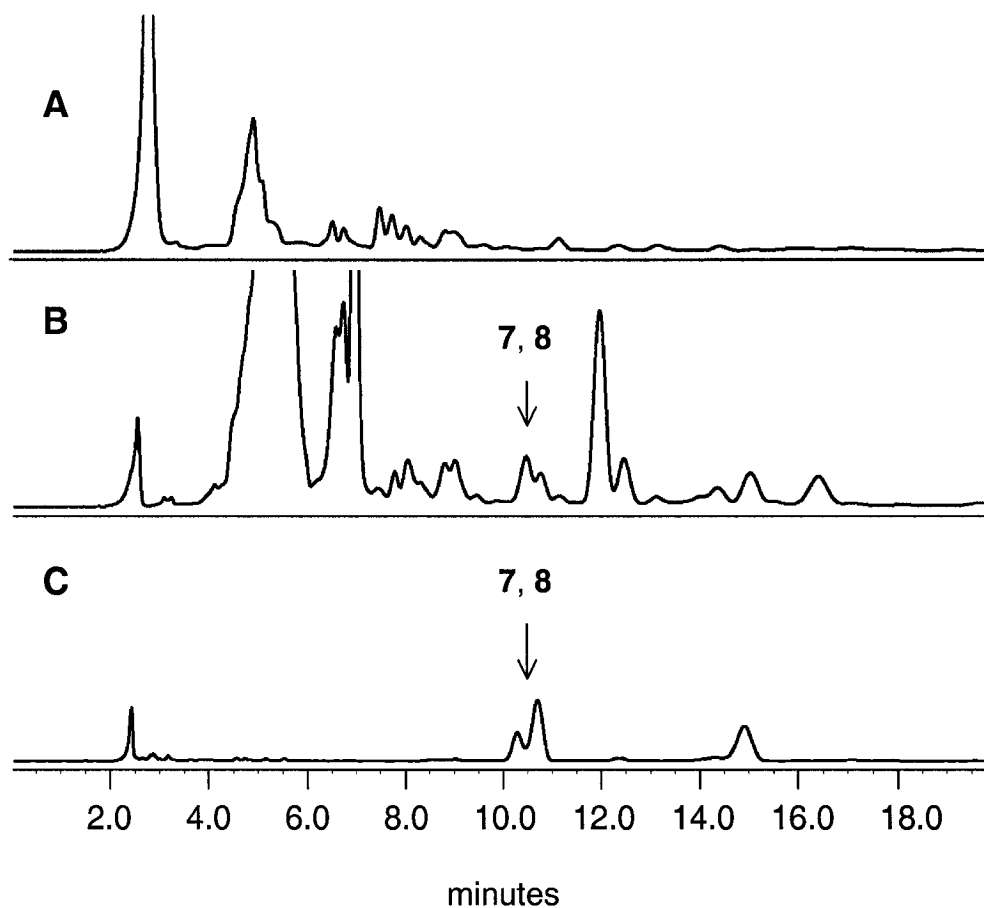


Figure 3.12: HPLC chromatograms of the bromination of geraniol (**6**) by (a) aqueous bromine (1 mM) (b) V-BrPO (23 nM) with H₂O₂ (1 mM) (c) purified standard of products **7** and **8** at 10 – 11 min. Conditions: 0.5 mM geraniol (**6**), 40 mM KBr in 0.15 M phosphate (pH 5.7) with 30% ethanol. Enzymatic reactions were initiated by the addition of V-BrPO and hydrogen peroxide. Reactions with aqueous bromine were the same as above without added hydrogen peroxide or enzyme. Reaction time was 1 hour. Reaction was injected directly (60 μ l) on an analytical YMC-ODS AQ column, and products eluted with acetonitrile and water (60:40) at 1.0 ml/min. Products were detected at 214 nm.

Bromination of geranyl acetate (9) with V-BrPO. GC-MS product profile analysis of the incubation of geranyl acetate (**9**), V-BrPO, bromide, and hydrogen peroxide showed the production of several compounds [Figure 3.13]. The major product of the reaction was bromohydrin (60%) with retention time 23 minutes. Careful examination of the total ion chromatogram and corresponding mass spectrum indicated the formation of two possible brominated cyclized geranyl acetate species at 21.5 – 22.0 minutes. Large-scale incubations (1.75 mmol **9** and 1 – 2 eq. H₂O₂) were performed to determine the structures of the possible brominated cyclized species. Careful chromatography of the crude extract by silica gel with increasing gradients of ether/pentane (10 – 40%) yielded two singly brominated cyclized geranyl acetate products, **10** and **11** (10 – 15% total cyclized products). Products **10** and **11** EIMS spectrum showed a very small molecular ion peaks at *m/z* 292, 290 in a 1:1 ratio and a fragmentation ion at *m/z* 216, 214 arising from the loss of a methylene group and the acetate functionality [Figure 3.14, 3.15]. Both products **10** and **11** have been previously reported (Wolinsky and Faulkner 1976). Spectroscopic data for the V-BrPO-catalyzed formation of **10** and **11** is in agreement with reported values.

Products **10** and **11** are proposed to form via attack on the C8 – C9 terminal olefin of geranyl acetate, similar to geraniol, to yield a bromonium-geranyl acetate intermediate. The bromonium intermediate is subsequently attacked by the internal olefinic bond, followed by elimination reactions to produce **10** and **11** (Scheme 3.8).

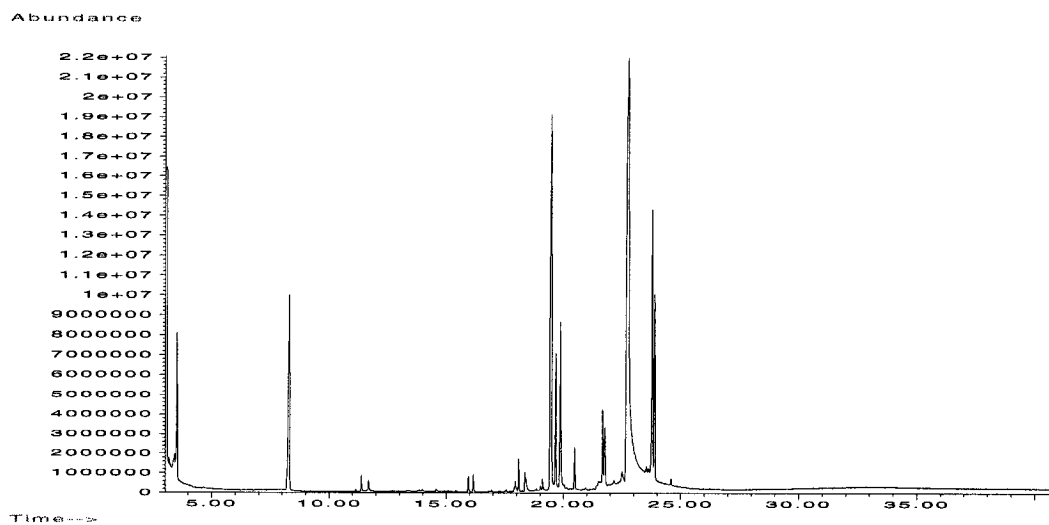


Figure 3.13: GC-MS chromatogram of V-BrPO catalyzed reaction with geranyl acetate (**9**). Conditions: 0.5 mM geranyl acetate (**9**), 40 mM KBr in 0.15 M phosphate (pH 5.7) with 30% ethanol. Reactions were initiated by addition of V-BrPO (23 nM) and H₂O₂ (1 mM, final concentration). Reaction time was 1 hour. Reaction was extracted with methylene chloride and one microliter was used for injection. Retention times: geranyl acetate 18 min, monobrominated cyclized geranyl acetate **10** and **11** 21.7 – 21.8 min, bromohydrins 22.8 min and dibrominated products 23.8 – 24.0 min.

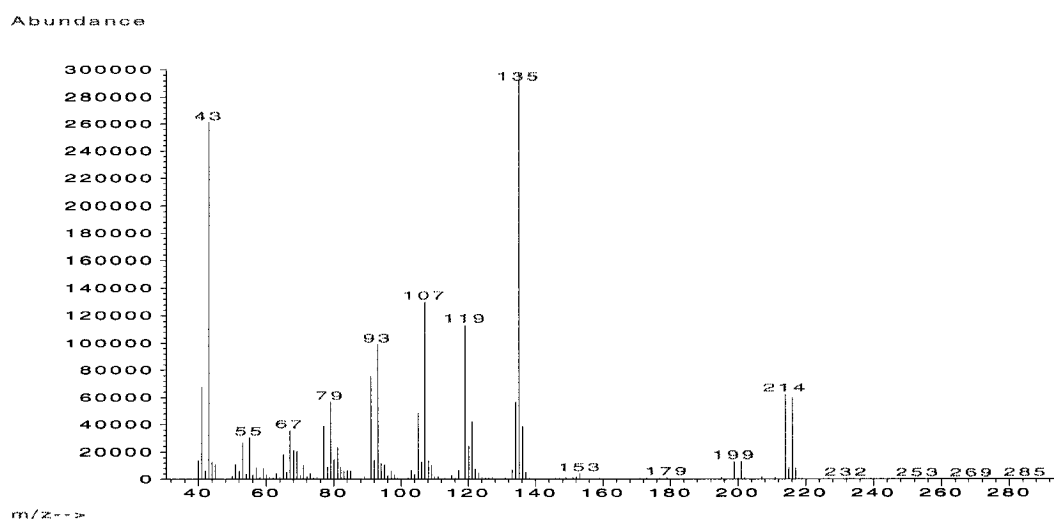


Figure 3.14: EIMS of monobrominated cyclized geranyl acetate product 10. Retention time on GC-MS chromatogram, 21.7 min.

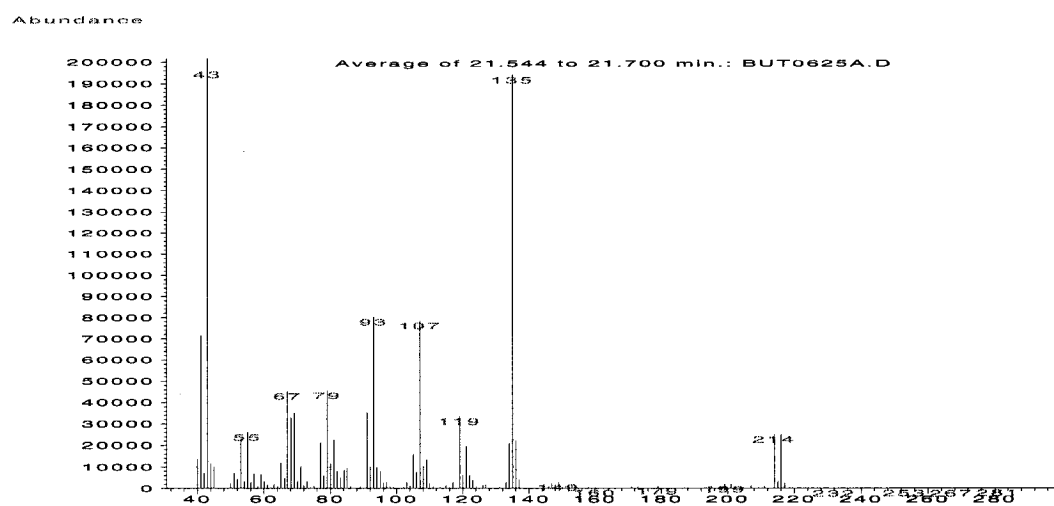
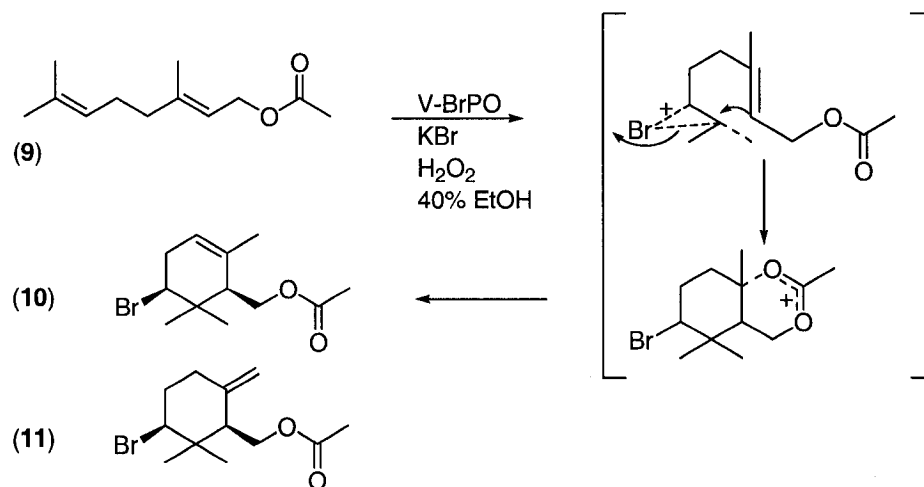


Figure 3.15: EIMS of monobrominated cyclized geranyl acetate product 11. Retention time on GC-MS chromatogram, 21.8 min.

The V-BrPO catalyzed reaction with geranyl acetate (**9**) produced larger quantities of brominated cyclized products when compared to V-BrPO reaction with geraniol (**6**). The different reactivity between geraniol (**6**) and geranyl acetate (**9**) may reflect a role of the acetyl oxygen atom in stabilization of the bromocarbenium ion intermediate prior to elimination reactions to produce **10** and **11**. Stabilization of the carbocation intermediate by delocalization of charges would be absent in reactions with geraniol (**6**).



Scheme 3.8: Proposed mechanism for V-BrPO catalyzed bromination and cyclization of geranyl acetate (**9**) to products **10** and **11**.

Reaction of geranyl acetate (**9**) with aqueous bromine and TBCO. Reaction of geranyl acetate (**9**) and aqueous bromine under identical reaction conditions as V-BrPO reactions produced **10** and **11** in addition to bromohydrins and dibrominated species. Reaction of TBCO with geranyl acetate in nitromethane also produced **10** and **11**.

Bromination of geranyl acetone (12) with V-BrPO. When geranyl acetone (**12**) was incubated with V-BrPO, bromide, and hydrogen peroxide, geranyl acetone (**12**) was converted into a mixture of four products [Figure 3.16]. The major products of the reaction as indicated by their mass spectra were the epoxide (22%) at 20.5 minutes and bromohydrins (71%) at 23.7 and 25 minutes [Figure 3.16]. The product peak observed at 22.0 minutes had a molecular ion m/z of 274, 272, suggesting a single bromination event to geranyl acetone. The structure of the potential cyclized product was determined from large-scale incubations of geranyl acetone (**12**) (1.75 mmol **12** and 1 – 2 eq. H_2O_2) with V-BrPO. The reaction extract was purified by silica gel chromatography using increasing gradients of ether/pentane (10 – 40%). A singly brominated bicyclic vinyl ether product, **13** (10% total products) was obtained. Product **13** EIMS spectrum showed a molecular ion of m/z 274, 272 and a fragmentation ion at m/z 193 arising from the loss of a bromine atom [Figure 3.17]. Product **13** has been previously reported as an intermediate in the biomimetic synthesis of 10-bromo- α -chamigrene marine natural product (Wolinsky and Faulkner 1976). Spectroscopic data for the V-BrPO catalyzed formation of **13** is in agreement with reported values (Wolinsky and Faulkner 1976). Bromination of geranyl acetone by V-BrPO occurs diastereoselectively without enantioselection for bromine-carbon bond formation. Product **13** is proposed to form via attack on the C9 – C10 terminal olefin of geranyl acetone to yield a bromonium-geranyl acetone intermediate. The bromonium intermediate is then subsequently attacked by the electron-rich

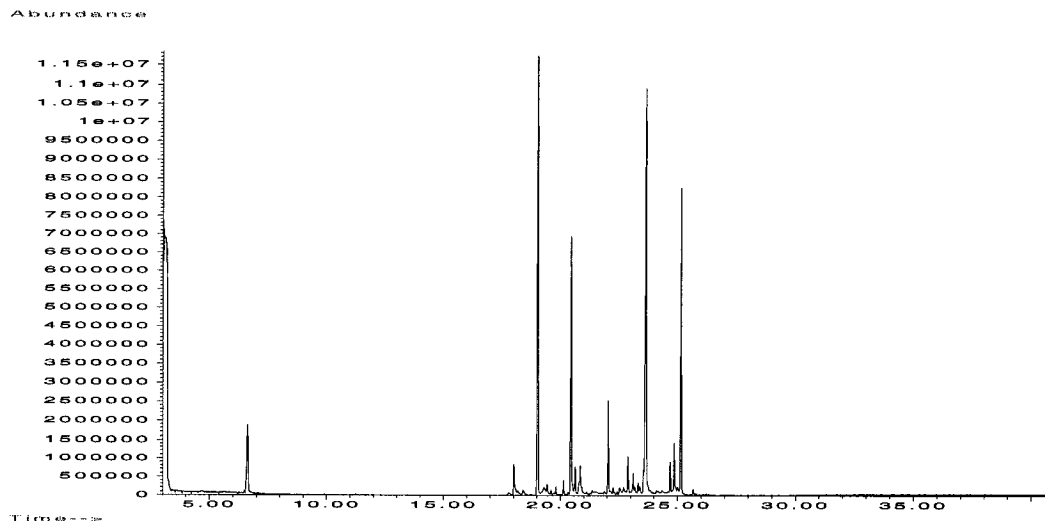


Figure 3.16: GC-MS chromatogram of V-BrPO-catalyzed reaction with geranyl acetone (**12**). Conditions: 0.5 mM geranyl acetone (**12**), 40 mM KBr in 0.15 M phosphate (pH 5.7) with 40% ethanol. Reactions were initiated by the addition of V-BrPO (23 nM) and H₂O₂ (1 mM, final concentration). Reaction time was 1 hour. Reaction was extracted with methylene chloride and one microliter was used for injection. Retention times; geranyl acetone 19 min, epoxide 20.5, brominated bicyclic vinyl ether product **13** 22 min, bromohydrins 23.5 - 25 min.

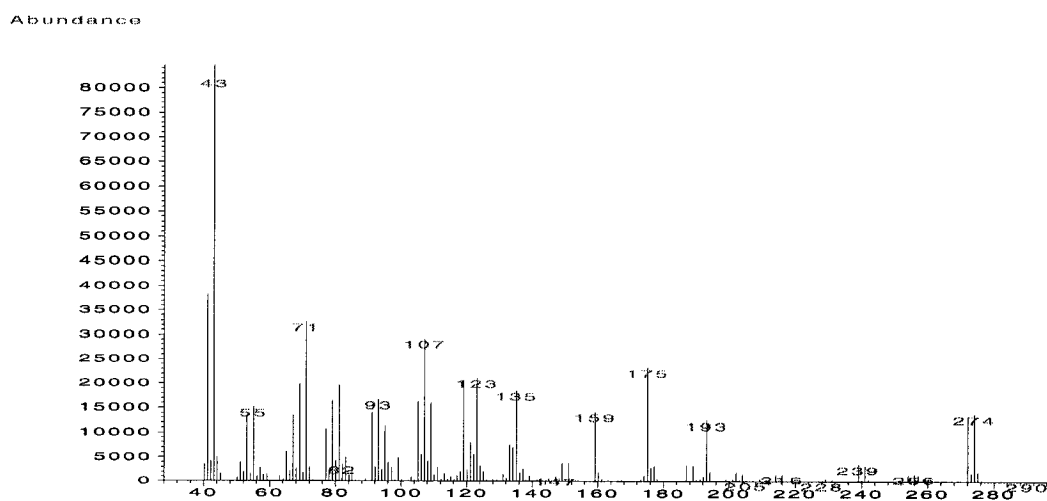
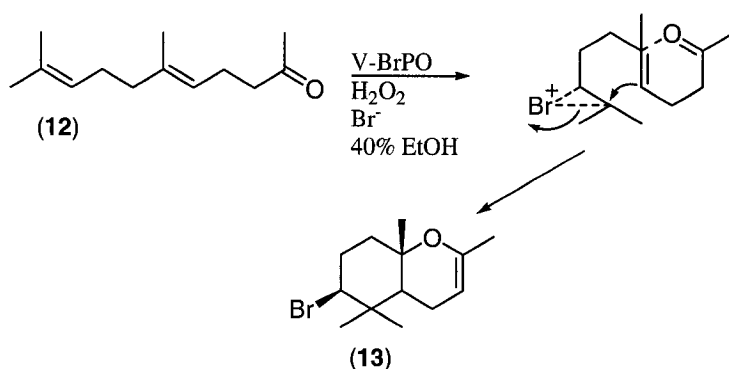


Figure 3.17: EIMS of brominated bicyclic vinyl ether product **13**. Retention time on GC-MS chromatogram, 22 min.

internal olefinic bond, followed by internal nucleophilic quenching of the bromocarbenium ion by the terminal ketone oxygen, leading to product **13** (Scheme 3.9) (Hoye et al. 1981). The V-BrPO catalyzed reaction with geranyl acetone (**12**) produced similar quantities of brominated cyclized product **13** when compared to V-BrPO reaction with geranyl acetate (**9**). The similar reactivity of substrates **9** and **12** to produce brominated cyclized species may reflect a role of oxygen containing functional groups (terminal ketone in **12**) in the stabilization of the bromocarbenium ion intermediates.



Scheme 3.9: Proposed mechanism for V-BrPO catalyzed bromination and cyclization of geranyl acetone (**12**).

Reaction of geranyl acetone (**12**) with aqueous bromine and TBCO.

Reactions with geranyl acetone (**12**) and aqueous bromine under identical reaction

conditions used with V-BrPO produced the bicyclic vinyl ether **13**. Reaction of TBCO with geranyl acetone in nitromethane did not yield **13**.

Bromination of all trans (+)-nerolidol (**14**) with V-BrPO. When all *trans* (+)-nerolidol (1.75 mmol) (**14**) is allowed to react with V-BrPO (23 nM) in aqueous buffer (pH 6.5) containing 40% organic co-solvent (EtOH, *i*PrOH), bromide (40 mM), and 1 – 2 equivalents of hydrogen peroxide, a mixture of ethereal, alcoholic, and hydrin products are obtained. Examination of fractioned ethereal and alcoholic portions revealed the formation of brominated cyclized sesquiterpenes. GC-MS analysis of reaction profiles could not be used effectively due to product peak overlap.

Snyderol products (**15**, **16**, and **17**). Crude extracts of the alcoholic portions collected from flash chromatography were ultra-purified by normal-phase HPLC using isocratic elution of 0.3% v/v isopropanol/hexanes. V-BrPO catalyzed reaction of (+)-nerolidol (**14**) produced three monocyclic brominated alcohols, designated α -, β -, and γ -snyderols (**15**), (**16**), and (**17**) respectively, where **15** and **16** are previously reported natural products from the marine red alga *Laurencia* (Howard and Fenical 1976). Snyderol products (**15** – **17**) were not observed in the absence of V-BrPO or one or more of the reactions substrates (Br^- or H_2O_2), indicating that oxidation of bromide by a peroxo-V-BrPO complex is necessary for the bromination and cyclization of (+)-nerolidol to snyderol products.

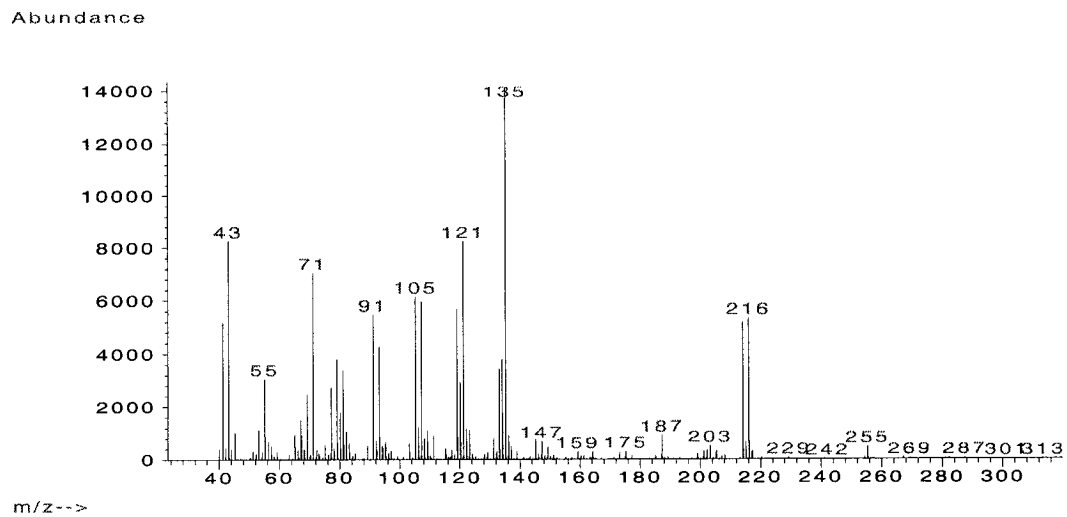


Figure 3.18: EIMS of α -snyderol (**15**).

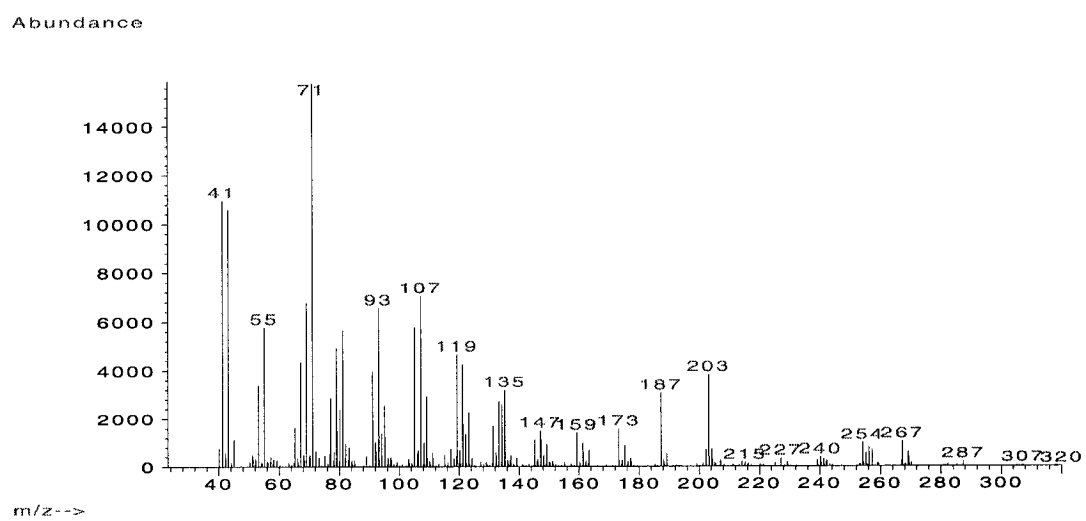


Figure 3.19: EIMS of β -snyderol (**16**).

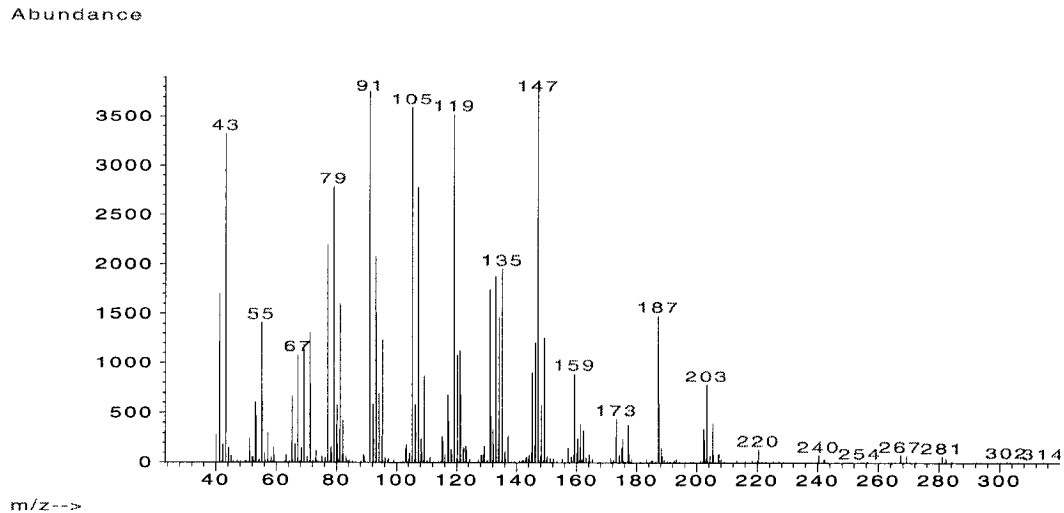


Figure 3.20: EIMS of γ -snyderol (17)

In addition, the presence of organic co-solvent ($\geq 40\%$) was necessary for the formation of snyderols, where the use of isopropanol was preferred to minimize competing nucleophilic reactions by the co-solvent. Products **15**, **16**, and **17**, were produced as 10% of the total isolated products. The remaining 90% of products consisted of epoxide, bromohydrins, and dibrominated species. The EIMS for products **15** and **16** showed molecular ions at m/z 284, 282, indicating a loss of water from the true molecular ion m/z 302, 300, where the mass spectral data is in agreement with reported values [Figure 3.18, 3.19] (Howard and Fenical 1976). Products **15** and **16** were isolated as a mixture and could not be further separated. Product **17** is not a known marine natural product, but has been reported as an intermediate in the biomimetic synthesis of 10-bromo- α -chamigrene (Wolinsky and

Faulkner 1976). The EIMS indicated a molecular ion m/z of 302, 300, consistent with previously reported data [Figure 3.20]. The ^1H NMR spectrum of product **17** showed two *gem*-dimethyl singlets at δ 1.16 ppm and 1.19 ppm confirming these methyl groups were no longer attached to olefinic bonds. Also, the presence of a vinyl methyl singlet at δ 1.60 ppm and no trace of a vinyl proton signal or exocyclic methylene signal confirmed product **17** must contain a tetrasubstituted olefinic bond. The presence of a doublet of doublets signal at δ 4.18 ppm ($J = 10, 4$ Hz) indicated the presence of an equatorial bromine substituent on the cyclohexene ring (Wolinsky and Faulkner 1976). The observed stereochemistry for the suite of snyderols (**15** – **17**) is in agreement with the reported stereochemistry for the isolated marine natural products (Howard and Fenical 1976). The equatorial position of bromine has been observed in many biomimetic cationic cyclization reactions, where the position of the bromine atoms appears to control the conformation of the transition state for the cyclization reaction.

The selectivity of bromine-carbon bond formation for products **15** – **17** by V-BrPO was evaluated by chiral GC-MS. The chiral GC-MS chromatogram indicated V-BrPO catalyzed the asymmetric bromination of the terminal olefin of **14** to yield single diastereomers of **16** and **17**, as indicated by a single peak in the GC chromatogram [Figure 3.21, 3.22]. The retention times for the single diastereomer of **16** and **17** was 75.8 minutes and 91.06 minutes, respectively. Product **15** could not be successfully separated by this method. As was expected, TBCO reactions showed bromination of (+)-nerolidol occurred symmetrically to both sides of the

terminal olefinic bond, as indicated by the presence of the two possible diastereomeric products for each β - and γ -snyderol (**16**) and (**17**), respectively [Figure 3.21, 3.22].

The formation of α -, β -, γ -snyderols in the V-BrPO catalyzed reaction likely results from selective bromination of the C10 - C11 olefinic bond of **14**, yielding a bromonium-nerolidol species (Scheme 3.10). The proposed bromocarbenium ion intermediate is subsequently attacked by the internal olefinic bond, followed by elimination reactions leading to **15**, **16** and **17**. The proposed mechanism of formation for the snyderol products (**15** – **17**) is similar to the proposed route for formation of products **7** and **8**.

(+)-3 β -bromo-8-epicaparrapi oxide (**18**). Examination of the ethereal portions of the V-BrPO catalyzed reaction with **14** yielded the marine natural product (+)-3 β -bromo-8-epicaparrapi oxide (**18**). As was observed with the snyderol products, **18** was produced only when all substrate components of the reaction were present (i.e., V-BrPO, KBr, and H₂O₂). The presence of the (-)-3 β -bromo-8-epicaparrapi oxide was not observed, indicating that epimerization of the tertiary alcohol during the reaction does not occur. Additional 6-membered cyclic bromoether species were also present within the fractioned ethereal portion. The 6-membered cyclic bromoethers have been previously reported and were not further characterized in this study. (+)-3 β -Bromo-8-epicaparrapi oxide (**18**) was isolated in ~5% yield; with remaining cyclic bromoether compounds isolated in 25% yield.

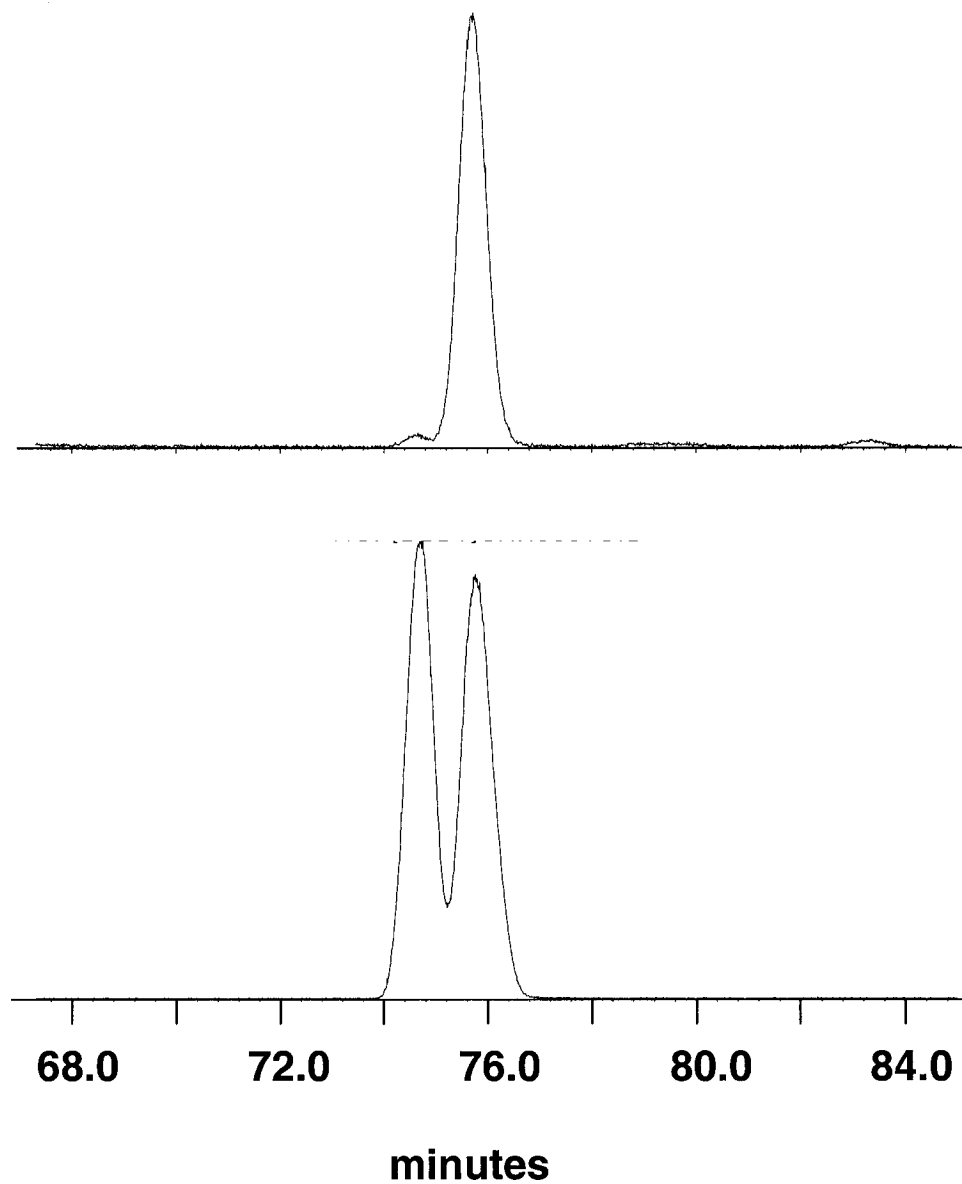


Figure 3.21: Chiral GC-MS total ion chromatogram for β -snyderol (**16**) isolated from (a) V-BrPO catalyzed reactions and (b) TBCO reactions. Gas chromatography was performed using 90 minute, 155 °C isotherm runs.

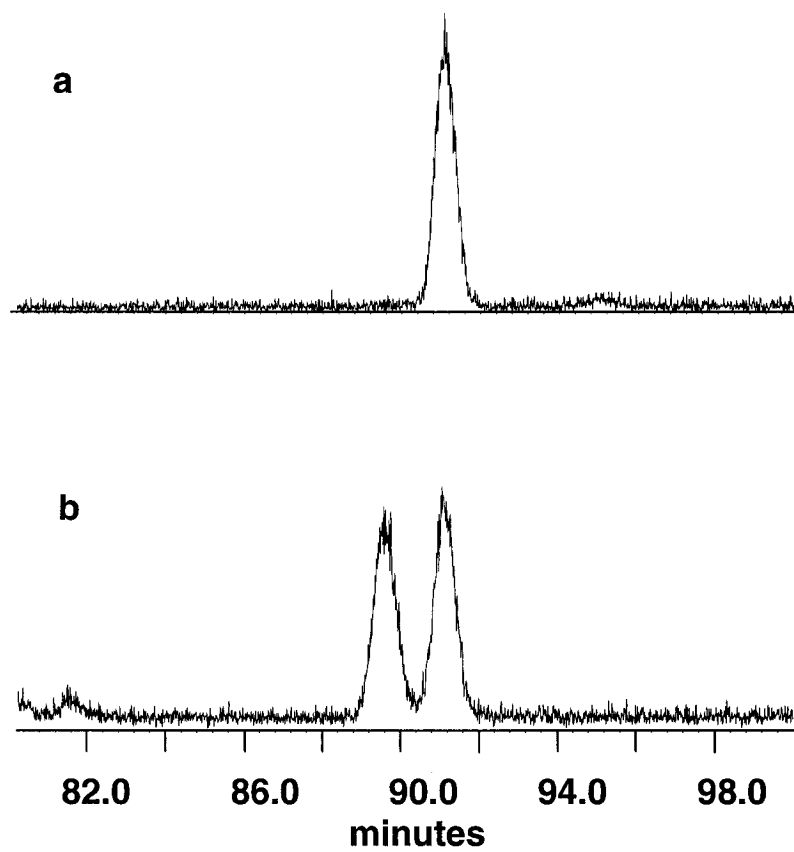
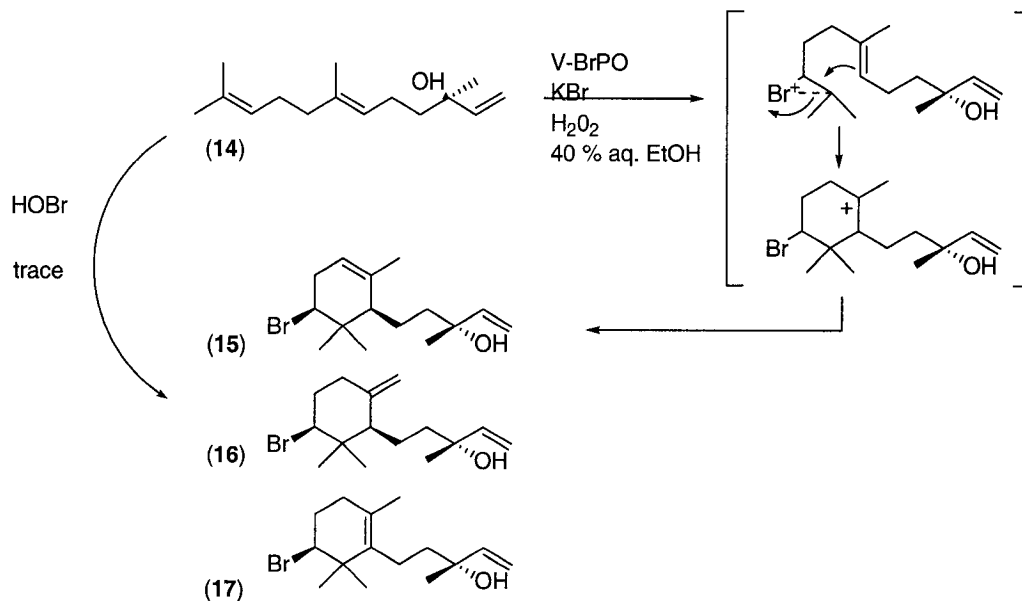


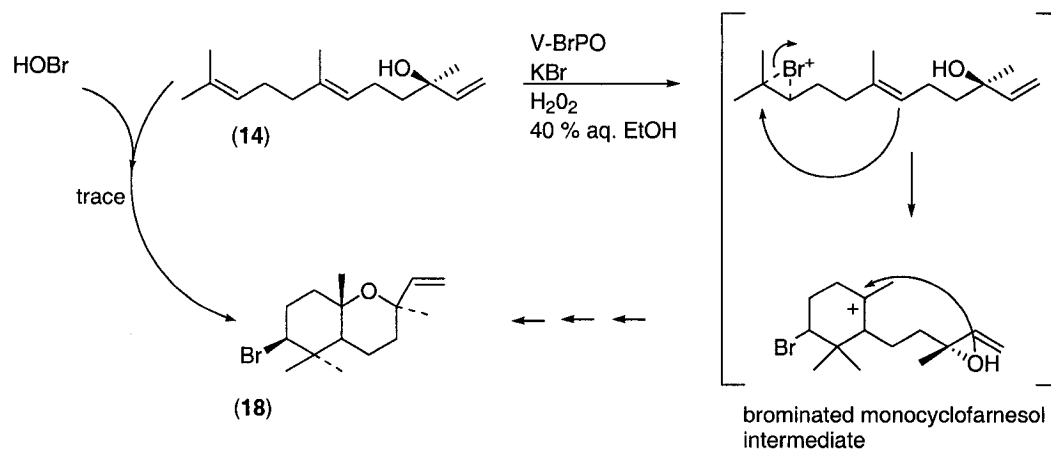
Figure 3.22: Chiral GC-MS total ion chromatogram for γ -snyderol (**17**) isolated from (a) V-BrPO catalyzed reactions and (b) TBCO reactions. Gas chromatography was performed using 90 minute, 155 °C isotherm runs.



Scheme 3.10: Proposed mechanism for V-BrPO catalyzed bromination and cyclization of all *trans* (+)-nerolidol (**14**) to α -snyderol (**15**), β -snyderol (**16**), and γ -snyderol (**17**).

The V-BrPO catalyzed formation of **18** is proposed to occur by a similar mechanism as the snyderol products, through the formation of a proposed monocyclic bromocarbenium ion (Scheme 3.11). Nucleophilic quenching of the bromocarbenium ion by the tertiary alcohol, leading to the bicyclic oxide structure, completes the formation of **18**.

The ¹H NMR spectra of **18** indicated the presence of *gem*-dimethyl singlets at δ 0.88 ppm and 1.07 ppm and two additional (O-C-CH₃) methyl singlets at δ 1.20



Scheme 3.11: Proposed mechanism for V-BrPO catalyzed bromination and cyclization of all *trans* (+)-nerolidol (**14**) to 3β-bromo-8-epicaparrapi oxide (**18**).

ppm and 1.18 ppm. The signal for the proton alpha to the bromine at δ 3.99 ppm ($J = 12, 5$ Hz) is consistent with the position of an equatorial bromine substituent and reported values (Faulkner 1976b; Hoye and Kurth 1979; Kato et al. 1980).

The stereochemistry of **18** was established similarly to the snyderols (**15** – **17**), where the bromine was observed in the equatorial position, and cyclization yielded the *trans*-fused bicyclo[4.4.0] system. The stereochemistry of the bridgehead methyl was deduced by the presence of a strong nOe to the vinylic proton at 6.0 ppm [Figure 3.23]. The stereochemistry for **18** is consistent with previously reported biomimetic cyclization reactions where following bromination

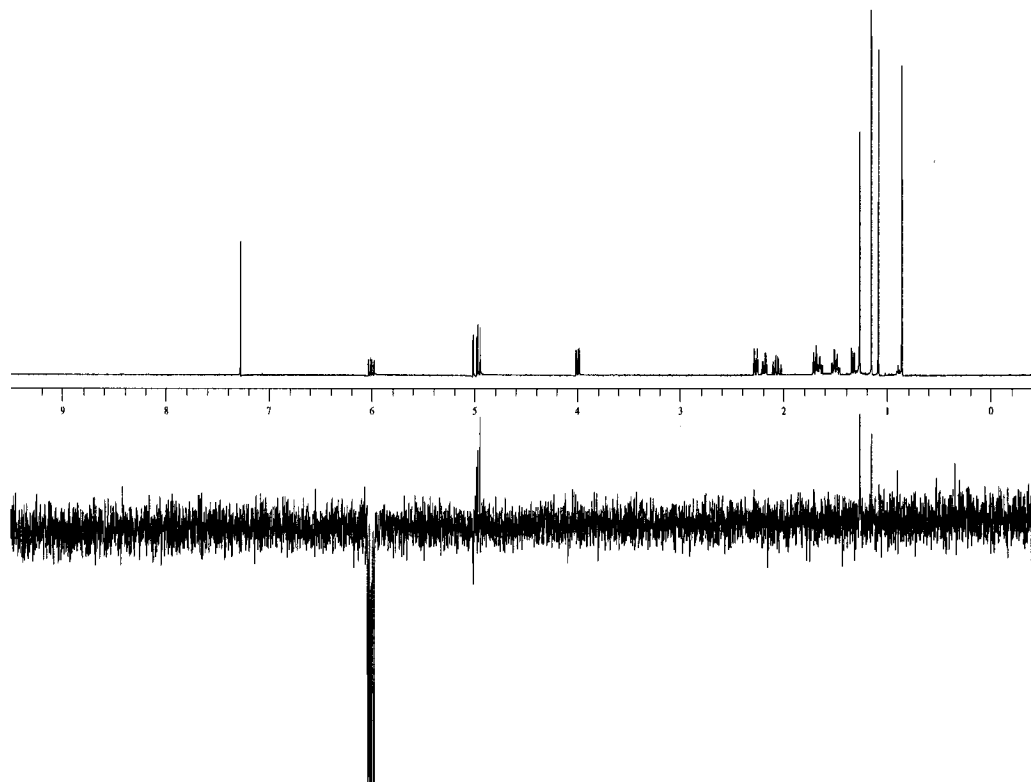


Figure 3.23 : One-dimensional nOe of product **18**, irradiation of 6.00 ppm signal.

the four chiral centers are introduced stereospecifically by cyclization of the terpene alcohol in which the set configuration of the carbon-alcohol bond uniquely determines the remaining three stereocenters (Kato et al. 1976; Kato et al. 1980; Shieh and Prestwich 1982).

The selectivity of bromine-carbon bond formation to yield **18** for V-BrPO and TBCO reactions indicated the formation of a single diastereomer for the V-BrPO catalyzed reaction and equal amounts of two diastereomers of **18** for the TBCO reaction [Figure 3.24].

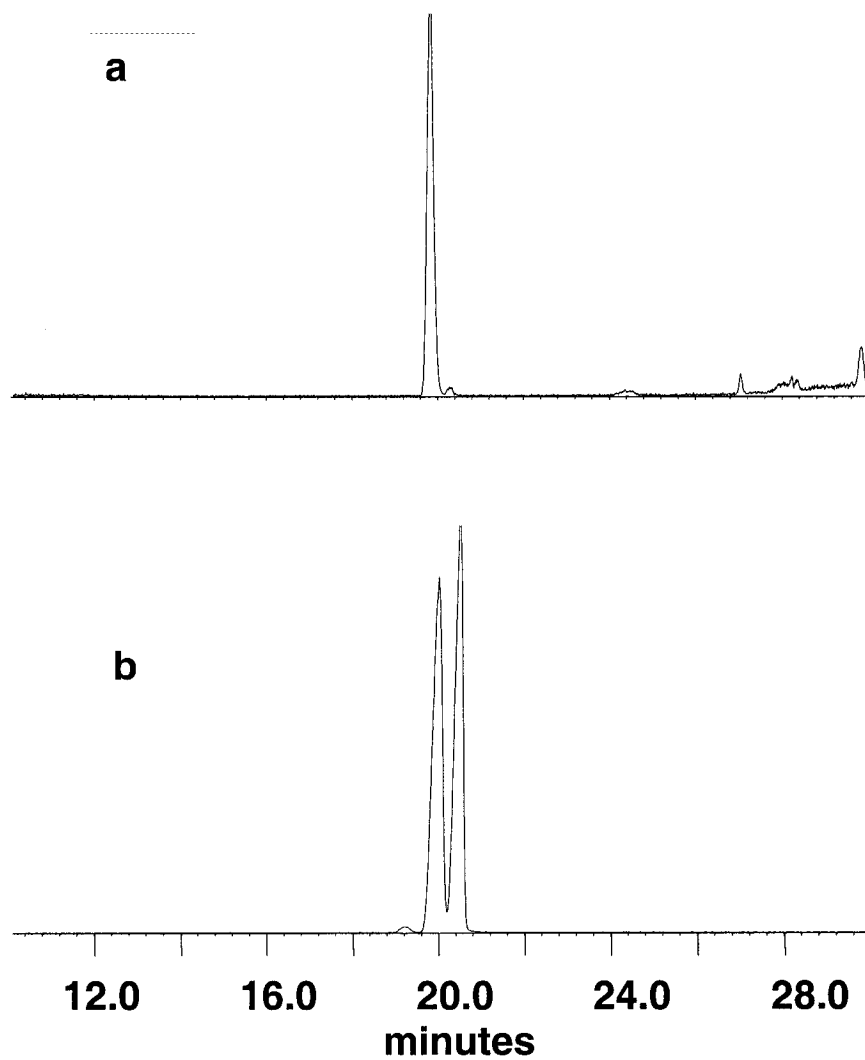


Figure 3.24: Chiral GC-MS total ion chromatogram for 3β-bromo-8-epicaparrapi oxide (**18**) isolated from (a) V-BrPO catalyzed reactions and (b) TBCO reactions. Gas chromatography was performed using 90 minute, 155 °C isotherm runs.

Reaction of all *trans* (+)-nerolidol (**14**) with aqueous bromine and TBCO.

Product profile analysis for the bromination of **14** with aqueous bromine was monitored by reversed-phase HPLC. Reactions with aqueous bromine were compared to V-BrPO catalyzed reactions under identical reaction conditions. Analytical HPLC chromatograms indicated that aqueous bromine reactions produced many of the same products as the V-BrPO catalyzed reaction [Figure 3.25]. The suite of α -, β -, γ -snyderol products (**15**), (**16**), (**17**) and 3 β -bromo-8-epicaparrapi oxide (**18**) were only produced in trace amounts. Reaction of TBCO with all *trans* (+)-nerolidol (**14**) in nitromethane produced **15**, **16**, **17**, and **18** as previously reported (Kato et al. 1980).

Bromination of *cis*-5-octene-1-ol (**19**) by V-BrPO. GC-MS product profile analysis of incubation of *cis*-5-octene-1-ol (**19**) with V-BrPO, bromide, and hydrogen peroxide produced three compounds [Figure 3.26]. Bromohydrins of **19**, at 20.0 and 21.5 minutes were the major products of the reaction. Epoxide products were not detected for this reaction. Careful examination of the reaction chromatogram and corresponding mass spectrum indicated a possible monobrominated cyclized species **20** at 15.7 minutes. The EIMS showed a molecular ion of m/z 208, 206 and a large fragmentation ion at 85, indicative an exocyclic bromine “tail” substituent [Figure 3.27].

The proposed structure for product **20** likely results from bromination of the C5 – C6 *cis* double bond of **19**, forming a bromonium-type intermediate. The

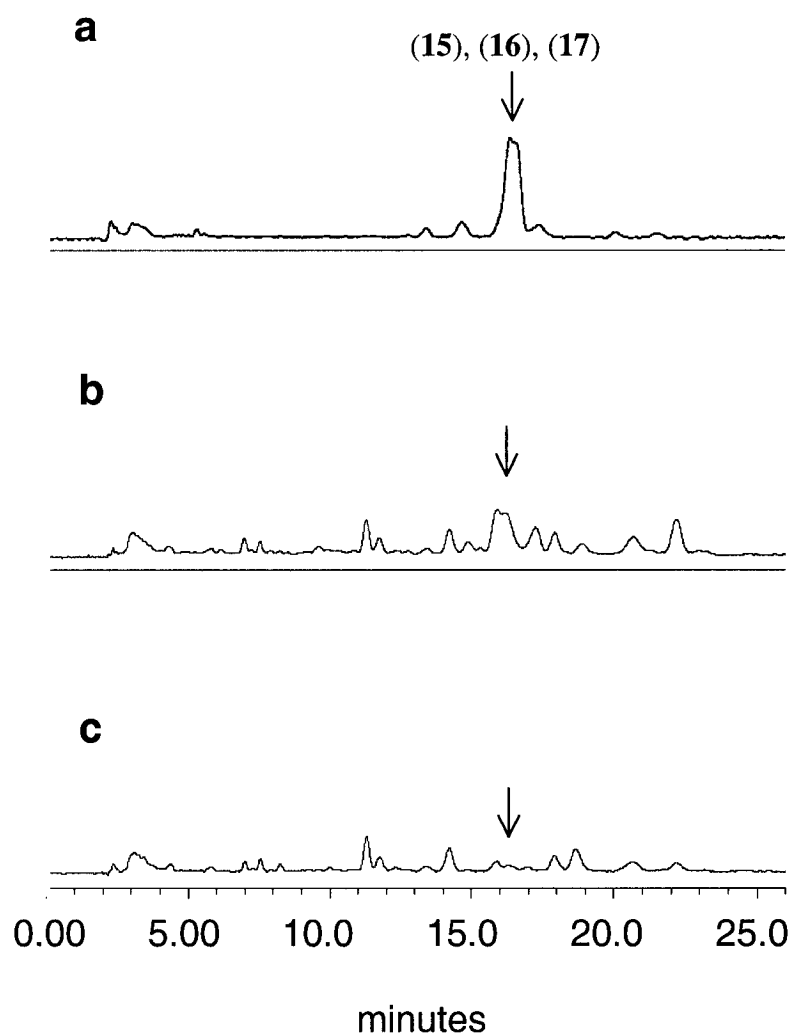


Figure 3.25: Reverse phase HPLC separations of fractionated alcoholic products from the reactions of V-BrPO (23 nM) and aqueous bromine with all-*trans* (+)-nerolidol (**14**). The reaction mixture contained 0.5 mM (+)-nerolidol (**14**), 0.04 M KBr in 0.1 M sodium phosphate (pH 5.7) with 40% v/v ethanol. Enzymatic reactions were initiated by the addition of H₂O₂ (1 mM) and allowed to react at 24 °C for 60 minutes. Aqueous bromine reactions were initiated by addition of NaOBr (1mM) and reacted at 24 °C for 60 minutes. (a) Mixture of α -, β -, γ -snyderol (**15**, **16** and **17**) (i.e. control of the purified brominated alcoholic products); (b) V-BrPO catalyzed reaction; (c) aqueous bromine reaction. Peaks are denoted with numbers corresponding to their structures.

brominated six-membered exocyclic ether **20** is proposed to form via intramolecular attack of the bromonium ion by the primary alcohol moiety (Scheme 3.12), similar to the V-BrPO catalyzed reactions with nerol to yield **5** (Scheme 3.6). Further characterization using this model compound was not performed.

Bromination of *cis*-3-nonen-1-ol (**21**) by V-BrPO. Incubation of *cis*-3-nonen-1-ol (**21**) with V-BrPO, bromide, and hydrogen peroxide resulted in the formation of three compounds [Figure 3.28]. The major products of the reaction were bromohydrins at 21.0 and 22.5 minutes. A small peak was observed at 16.8 minutes had a molecular ion m/z of 222, 220, likely corresponding to a bromoether, product **22**. A large fragmentation ion at m/z 151, 149 suggested the loss of an alkyl tail from the singly brominated species, suggesting that product **22** was a brominated five-membered endocyclic bromoether [Figure 3.29]. An epoxide product was not observed for this reaction, similar to V-BrPO catalyzed reaction with **19**. The proposed mechanism of formation for **22** is similar to the formation of **20**, where the bromonium ion intermediate is quenched by internal nucleophilic trapping by the primary alcohol moiety (Scheme 3.13).

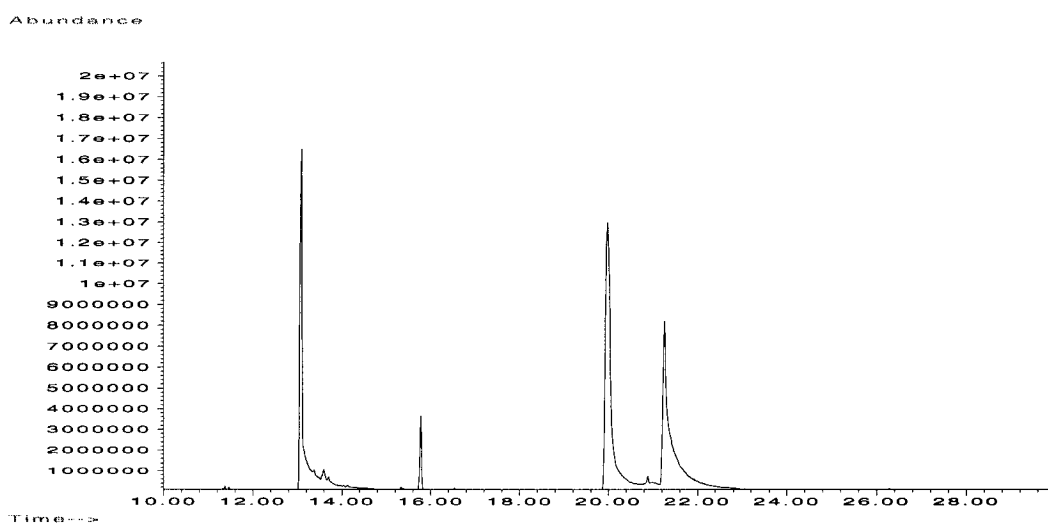


Figure 3.26: GC-MS chromatogram of V-BrPO catalyzed reaction with *cis*-5-octene-1-ol (**19**). Conditions: 0.5 mM **19**, 40 mM KBr in 0.15 M phosphate pH 5.7 with 30% ethanol. Reactions were initiated by the addition of V-BrPO (23 nM) and H₂O₂ (1 mM, final concentration). Reaction time was 1 hour. Reaction was extracted with methylene chloride and one microliter was used for injection. Retention times: *cis*-5-octene-1-ol 14 min, 6-membered cyclic bromoether **20** 15.8 min, bromohydrins 20 and 21.5 min.

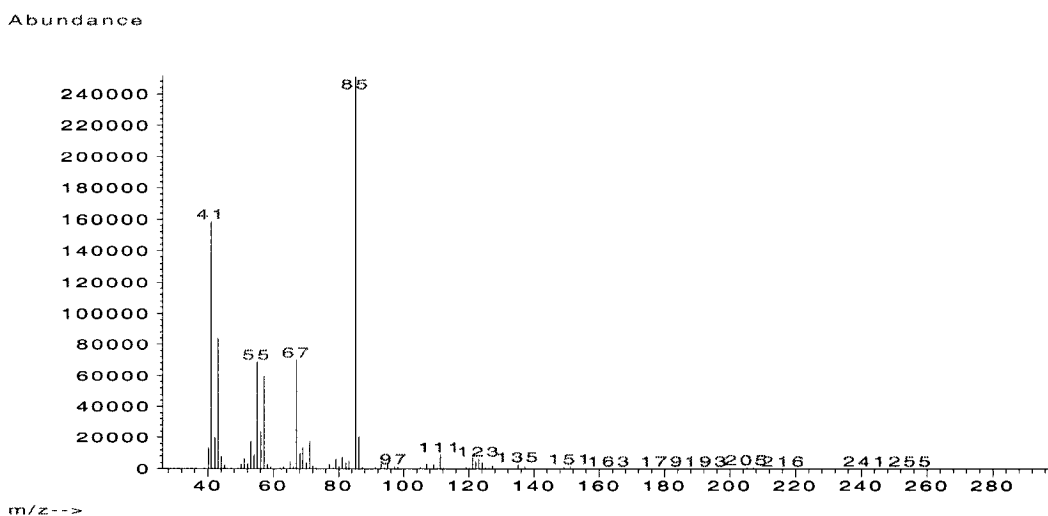
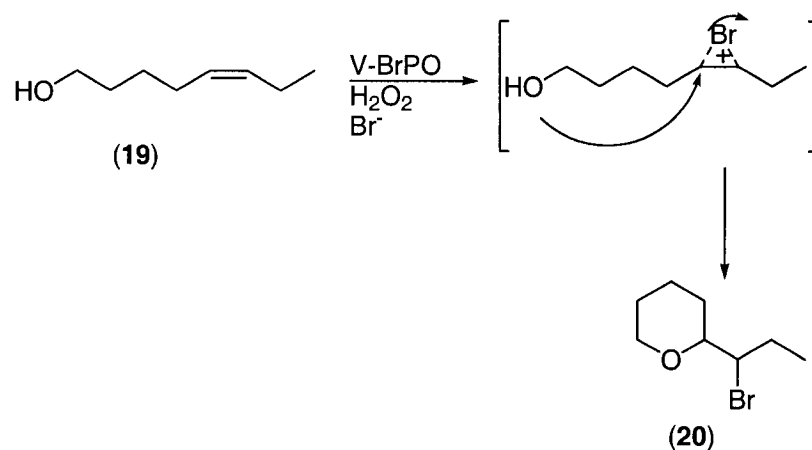


Figure 3.27: EIMS of 6-membered cyclic bromoether product **20** (retention time in GC-MS chromatogram, 15.8 minutes)



Scheme 3.12: V-BrPO catalyzed bromination and cyclization of *cis*-5-octen-1-ol (19) to product 20.

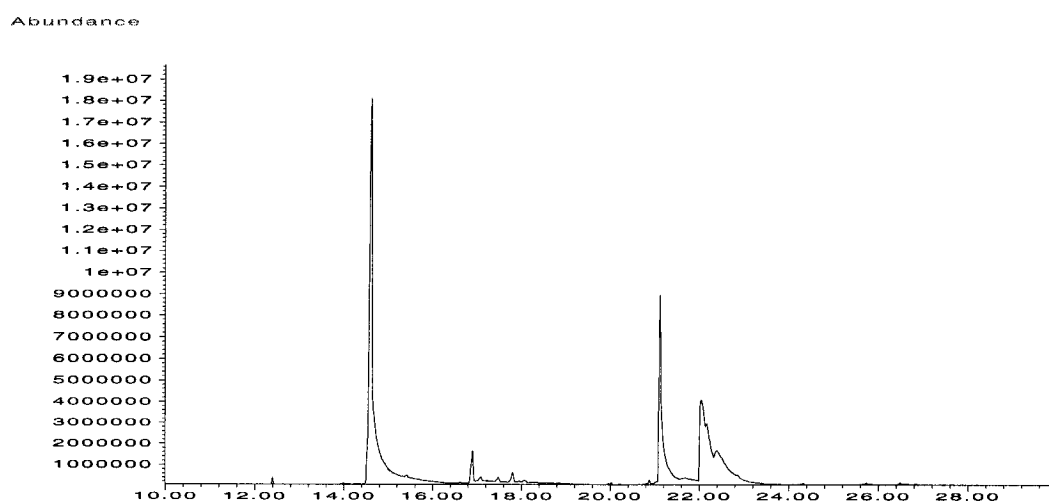
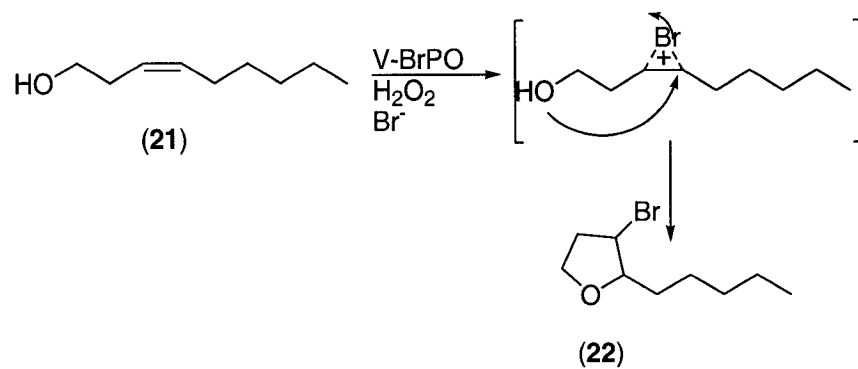


Figure 3.28: GC-MS chromatogram of V-BrPO catalyzed reaction with *cis*-3-nonen-1-ol (21). Conditions: 0.5 mM 21, 40 mM KBr in 0.15 M phosphate (pH 5.7) with 30% ethanol. Reactions were initiated by the addition of V-BrPO (23 nM) and H₂O₂ (1 mM, final concentration). Reaction time was 1 hour. Reaction was extracted with methylene chloride and one microliter used for injection. Retention times: *cis*-3-nonen-1-ol 15 min, 5-membered cyclic bromoether 22 16.8 min, bromohydrins 21 and 22 min.



Scheme 3.13: V-BrPO catalyzed bromination and cyclization of *cis*-3-nonen-1-ol (21) to product 22.

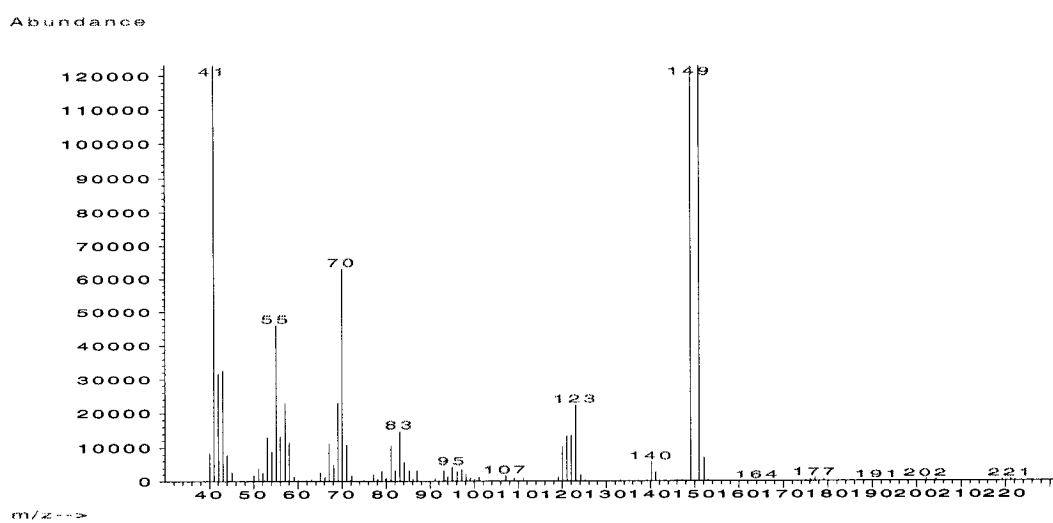


Figure 3.29: EIMS of 5-membered cyclic bromoether product 22 (retention time in GC-MS chromatogram, 16.8 min).

Competitive substrate kinetics:

Comparison of terpene substrate specificity of V-BrPO and aqueous bromine. In a mixture of phenol red (50 μM) and terpene substrates (geraniol (**6**) or nerolidol (**14**)), V-BrPO preferentially catalyzes the bromination of the terpene substrate as indicated by the lag phase in appearance of bromophenol blue at 596 nm [Figure 3.30, 3.31]. The lag phase increases with increasing concentrations of added terpene substrate, and after all terpene substrate has been consumed, the rate of bromination of phenol red proceeds at the same rate as in the absence of added terpene.

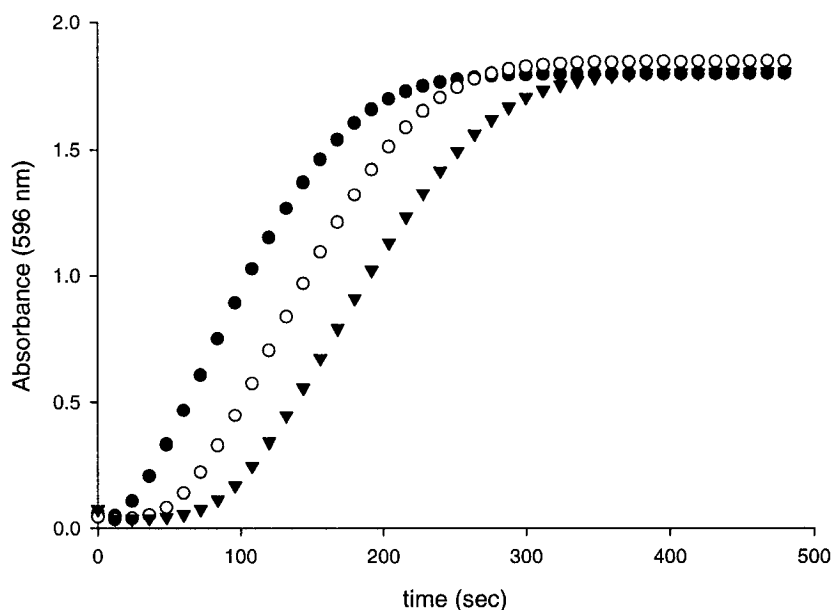


Figure 3.30: Bromination of phenol red (50 μM) by V-BrPO as a function of geraniol (**6**) concentration. ● geraniol concentration 0 μM ; ○ geraniol concentration 50 μM ; ▼ geraniol concentration 100 μM . Reaction conditions: 0.15 M sodium phosphate pH 5.7, 40 mM KBr, 40% ethanol and 50 μM phenol red. V-BrPO reactions were initiated by addition of 0.5 mM H_2O_2 and 5 nM V-BrPO. Production of bromophenol blue was monitored at 596 nm.

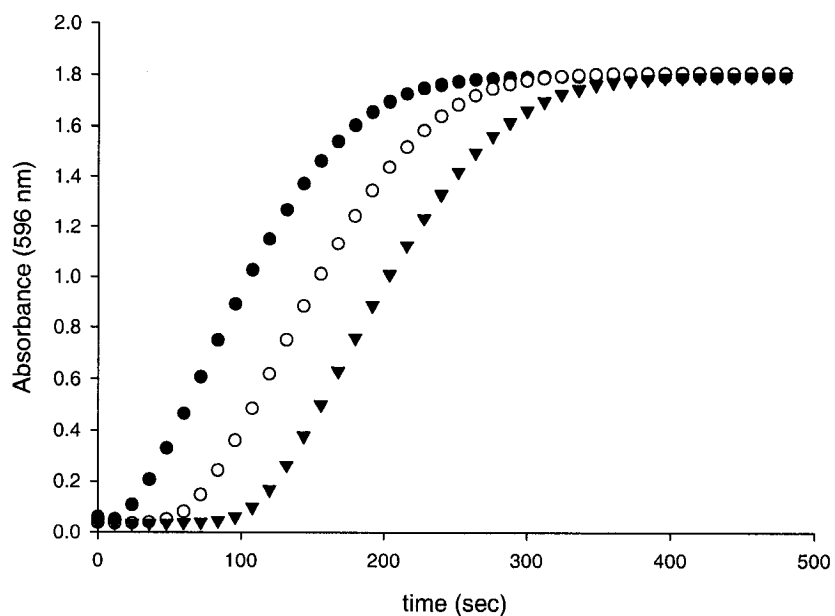


Figure 3.31: Bromination of phenol red ($50 \mu\text{M}$) by V-BrPO as a function of all *trans* (+)-nerolidol concentration (**14**). ● (+)-nerolidol concentration $0 \mu\text{M}$; ○ (+)-nerolidol concentration $50 \mu\text{M}$; ▼ (+)-nerolidol concentration $100 \mu\text{M}$. Reaction conditions: 0.15 M sodium phosphate pH 5.7, 40 mM KBr, 40% ethanol and $50 \mu\text{M}$ phenol red. V-BrPO reactions were initiated by addition of 0.5 mM H_2O_a and 5 nM V-BrPO. Production of bromophenol blue was monitored at 596 nm .

In contrast, the lag-phase observed in V-BrPO catalyzed reactions is absent in the competitive reactions performed with aqueous bromine under identical reaction conditions [Figure 3.32]. If free molecular bromine or hypobromite were the brominating species in the V-BrPO catalyzed reactions then the substrate specificity should be identical with that of the chemical bromination reaction. If, however the terpene substrate binds to the enzyme, then the substrate specificity would be expected to be quite different from that of the chemical bromination reactions. Thus, the differences in reactivity between the V-BrPO/Br⁻/H₂O₂ system and aqueous bromine suggest that the terpene substrate binds to or interacts with V-BrPO, resulting in the observed substrate selectivity.

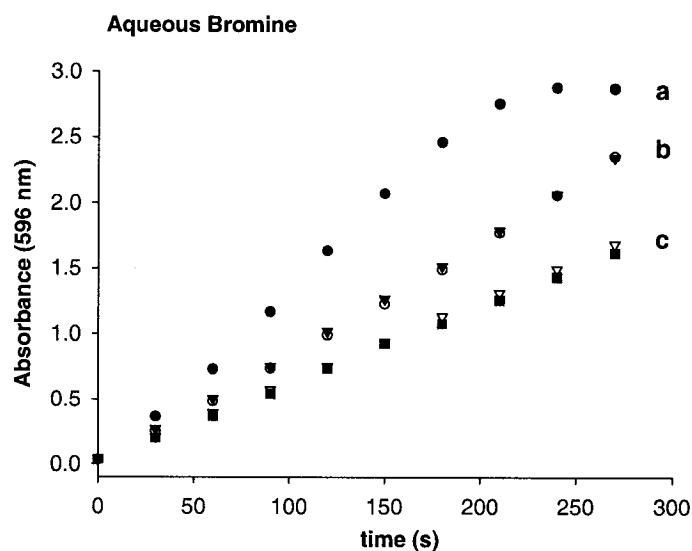


Figure 3.32: Bromination of phenol red (50 μ M) by HOBr as a function of all *trans* (+)-nerolidol concentration (**14**). (a) (+)-nerolidol concentration 0 μ M (b) (+)-nerolidol concentration 50 μ M (c) (+)-nerolidol concentration 100 μ M. Reaction conditions: 0.15 M sodium phosphate pH 5.7, 40 mM KBr, 40% ethanol and 50 μ M phenol red. Aliquots of 10 μ l each of 5 mM aqueous bromine stock solution were added successively at 30-sec intervals to the initial 2 mL reaction, and the absorbance at 596 nm was measured 20 sec after each addition.

Discussion

Vanadium bromoperoxidase was found to react efficiently with terpene substrates, and produced brominated cyclized structures reminiscent of halogenated marine natural products. The products of the reactions are consistent with a mechanism where the electrophilic brominating species (Br^+ , Br_2 , Br_3^- , or Enz-Br) attacks the terminal trisubstituted olefin of the terpene substrate. The fate of the resulting bromonium-terpene intermediate is found to depend on the presence of nearby nucleophilic terminators, and the stability of subsequent intermediates in the reaction pathway (e.g., stabilization of cyclized bromocarbenium ions). In most cases the major products of the reactions with terpenes are the bromohydrin species. Formation of bromohydrins is not surprising, since the most concentrated nucleophiles present to quench the bromonium-terpene intermediate is water. In spite of the large excesses of solvent molecules to terpene substrates, V-BrPO catalyzed the bromination and cyclization of terpenes.

The two major structural features observed in products from V-BrPO catalyzed bromination and cyclization of terpenes is the bromoetherification functionality, and the brominated cyclized polyene functionality. Both of the structures are present in numerous natural products isolated from marine seaweeds (Faulkner 2002). The bromoether functionality is prevalent in the class of non-terpenoid C_{15} acetogenin compounds isolated from the marine alga genus *Laurencia* (Erickson 1983). The cyclic members of this group display the following structural features: (a) various oxane ring sizes, (b) an enyne or allenic side chain, and (c) at

least one bromine atom [Figure 3.33] (Erickson 1983). The lauroxocanes are the largest class of *Laurencia* acetogenins. The lauroxocanes contain the laurencin (**23**) and the laureatin (**24**) structural types [Figure 3.33].

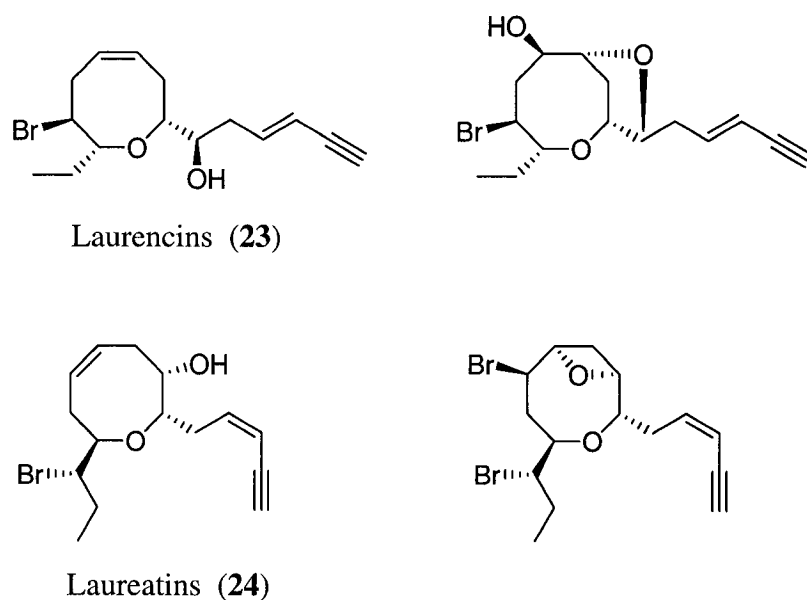
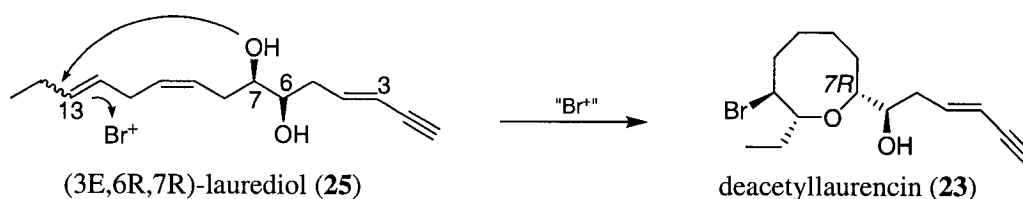


Figure 3.33: Halogenated C₁₅ acetogenins, marine natural products from the red algal genus *Laurencia*.

The V-BrPO catalyzed reaction with the monoterpene nerol (**4**), produced a singly brominated eight-membered cyclic ether **5** structure resembling the laurencin (**23**) class of natural products. For the reaction with nerol, ring closure on the bromonium-nerol intermediate is accomplished *via* attack by the primary alcohol moiety, where internal nucleophilic trapping by the pendant alcohol is competitive with nucleophilic quenching by surrounding water molecules (Scheme 3.6). Ring closure by way of attack by the alcohol moiety is consistent with the mechanism of

formation proposed for the laurencin metabolites, with bromonium attack at C12 – C13 double bond of laurediol (**25**), and ring closure via nucleophilic attack by the C-7 hydroxyl group (Scheme 3.14) (Erickson 1983; Fukuzawa et al. 1992).



Scheme 3.14: Mechanism of bromoetherification for production of laurencin (**23**) marine natural products.

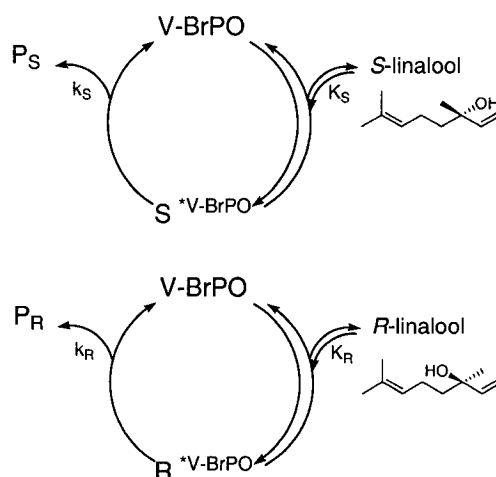
While the 8-*endo* cyclization of nerol is entropically unfavored when compared to smaller ring formation (5 and 6-membered rings), the eight-membered ring product is nevertheless the expected Markovnikov addition product. Bromination and cyclization of nerol by V-BrPO was observed to occur without enantioselectivity, although it is proposed that nerol is not a natural substrate utilized by V-BrPO within algae. Even though the reaction with nerol occurred without selectivity, the bromination and cyclization of nerol was exclusive to V-BrPO. Control reactions with aqueous bromine produced mainly bromohydrin and epoxide products, but did not produce the brominated eight-membered cyclic ether **5**. Formation of **5** by V-BrPO and not by aqueous bromine suggests that bromination and cyclization of nerol occurs at or near the active site of V-BrPO.

The formation of eight-membered bromoethers by V-BrPO is not surprising considering the work by Fukuzawa and coworkers (Fukuzawa et al. 1990a; Fukuzawa et al. 1994). Fukuzawa and coworkers reported the enzymatic bromoetherification of laurediol (**25**) to deacetyl laurencin (**23**) by a crude preparation of a bromoperoxidase isolated from the marine red alga *Laurencia nipponica*. Inhibition studies with azide suggested the bromoperoxidase was an Fe-heme containing haloperoxidase (Fukuzawa et al. 1994). Vanadium bromoperoxidase is also inhibited by low concentrations of sodium azide (See Chapter 5) (Soedjak 1991), and it is likely that the bromoperoxidase in *L. nipponica* is a vanadium-dependent haloperoxidase¹. These insights as well as the bromoetherification of nerol by V-BrPO, suggest a role for V-BrPO in the biosynthetic pathway of laurencin (**23**) and laureatin (**24**) marine natural products.

V-BrPO also catalyzed the bromoetherification of linalool (**1**) to produce two brominated furans **2** and two brominated pyrans **3** (Scheme 3.4). The ability of V-BrPO to catalyze the formation of both 5- and 6-membered heterocyclic structures is not surprising considering that the rate of cyclization for each is fast. Control reactions with aqueous bromine were found to direct the cyclization of racemic linalool to products **2** and **3**. Kinetic resolution experiments using racemic linalool and V-BrPO indicated V-BrPO has a modest preference for (*S*)-linalool, whereas the same experiments performed with aqueous bromine indicated no preference for one

¹ We have recently cloned the active site fragment of V-BrPO from the marine alga *Laurencia pacifica*, further supporting the presence a vanadium-dependent haloperoxidase in this genus of alga.

enantiomer of linalool. The principle of kinetic resolution rests on a difference in the rate of transformation of enantiomers in a racemic mixture (i.e., (*R*)- versus (*S*)-linalool) (Blackmond 2001). Scheme 3.15 depicts the kinetic resolution using V-BrPO (adapted from (Blackmond 2001)). In this model, the simplest form of Michealis-Menten equation is assumed.



Scheme 3.15: Kinetic resolution of racemic linalool by V-BrPO. Adapted from [Blackmond, 2001 #1].

In this model, binding of (*R*)- and (*S*)-linalool to V-BrPO, is followed by an irreversible product formation step. Based on the kinetic resolution experiments with V-BrPO, it is assumed that (*S*)-linalool is the faster reacting substrate. The derived rate expression for the consumption of (*R*)- and (*S*)-linalool, respectively, are described by equations 3.1 and 3.2 (Blackmond 2001).

$$-d[R]/dt = k_R[R^{*V-BrPO}] = k_R K_R [R][V-BrPO] = \frac{k_R K_R [R][V-BrPO]_{total}}{(1 + K_R[R] + K_S[S])} \quad \text{eq. 3.1}$$

$$-d[S]/dt = k_S[S^{*V-BrPO}] = k_S K_S [S][V-BrPO] = \frac{k_S K_S [S][V-BrPO]_{total}}{(1 + K_R[R] + K_S[S])} \quad \text{eq. 3.2}$$

When V-BrPO is added to the reaction mixture, (*R*)-linalool and (*S*)-linalool share the same pool of V-BrPO and the $[V-BrPO]_{total}$ term in both equations describes the different ways in which V-BrPO partitions between reaction with (*R*)- or (*S*)-linalool, equation 3.3 (Blackmond 2001).

$$\begin{aligned} [V-BrPO]_{total} &= [V-BrPO] + [R^{*V-BrPO}] + [S^{*V-BrPO}] \\ &= [V-BrPO](1 + K_R[R] + K_S[S]) \end{aligned} \quad \text{eq. 3.3}$$

When the ratio of consumption of (*R*) and (*S*)-linalool is taken, an expression reminiscent of first-order kinetic resolution remains, equation 3.4 (Blackmond 2001).

$$\frac{d[R]}{d[S]} = \frac{k_R K_R [R]}{k_S K_S [S]} = \frac{k_{rel}[R]}{[S]} \quad \text{eq. 3.4}$$

The selectivity factor k_{rel} describes substrate binding and dissociation as not being perturbed by product formation (Seeman 1983). V-BrPO catalyzed reactions with

racemic linalool produced a discernable consumption ratio of (*R*) to (*S*), 1 to 2.5, with a modest selectivity factor of 4.1. The observed kinetic selection for (*S*)-linalool suggest that V-BrPO binds linalool and directs the bromination and cyclization to products **2** and **3**.

V-BrPO from *Ascophyllum nodosum* mediates the kinetic resolution of racemic five and six-membered cyclic ether sulfides in the direct oxidation to sulfoxides (in the absence of halides) (ten Brink et al. 1999). However, the kinetic resolution described for bromination and cyclization of linalool described here is the first report of its kind. Interestingly, the kinetic preference for (*S*)-linalool by V-BrPO to form the six-membered bromoether structure may suggest a role of the enzyme in the biosynthetic pathway of such marine natural products as thyriferyl 23-acetate (**26**) isolated from a marine red alga *Laurencia* spp., which has the same (*S*)-stereochemistry set in the bromoether moiety of the molecule [Figure 3.34](Gonzalez and Forsyth 2000).

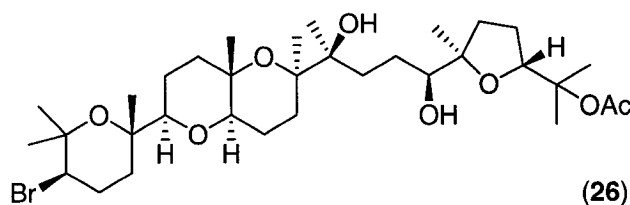


Figure 3.34: Marine natural product thyriferyl 23-acetate (**26**).

V-BrPO also catalyzed the bromoetherification of model compounds *cis*-3-nonen-1-ol and *cis*-5-octen-1-ol to 5- and 6-membered bromoether structures **20** and **22**, respectively. The reported thermal and chemical stability of the enzyme makes V-BrPO potentially useful for synthetic organic chemistry in the production of halogenated cyclic ether structures (Sheffield et al. 1993).

The second type of structural feature present in V-BrPO catalyzed bromination and cyclization of terpenes are the brominated cyclized polyenes. The brominated cyclized sesquiterpenes from marine red algae are one of the most commonly reported class of marine natural products (Faulkner 1976a; Faulkner 2002). Two distinct categories within this class of natural products are the monocyclofarnesanes, and the chamigranes (Martin and Darias 1978). The proposed key step in any biosynthetic scheme the monocyclofarnesanes and chamigranes is a bromonium ion initiated cyclization of an acyclic terpenoid precursor (Faulkner 1976a; Martin and Darias 1978). Marine natural products α - and β -snyderol (**15**) and (**16**), are two examples of isomeric monocyclofarnesane derivatives, and 10-bromo- α -chamigrene (**27**) is considered the most simple skeleton of the chamigrene structural types [Figure 3.35] (Martin and Darias 1978).

Vanadium bromoperoxidase catalyzed the bromination and cyclization of the monoterpene geraniol (**6**), yielding two monobrominated cyclized polyenes **7** and **8** (Scheme 3.7), structures that resembled monocyclofarnesane types of marine natural

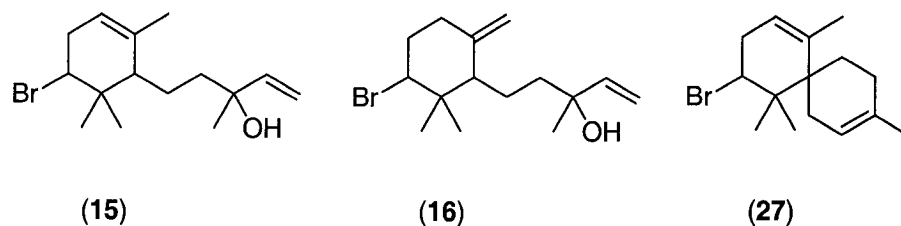
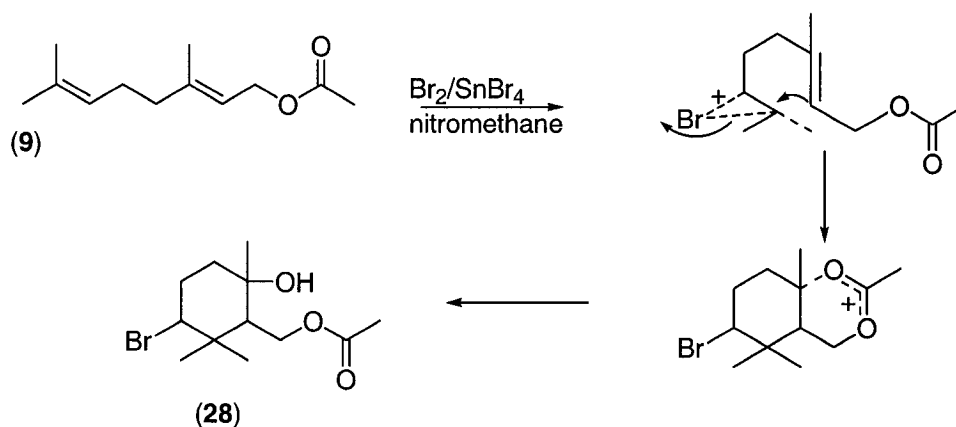


Figure 3.35: Halogenated marine natural products, monocyclofarnesanes (15), (16), and chamigranes (27).

products (Howard and Fenical 1976). Geraniol has an *trans* configuration of its double bonds, whereas isomeric nerol has a single *cis*-double bond at the C2 – C3 position. The *trans* geometry of the C2 – C3 double bond of **6** prohibited the internal nucleophilic trapping by the primary alcohol, leading to the alternative polyene cyclization pathway (Scheme 3.7). The formation of **7** and **8** was exclusive to V-BrPO and was not detected in aqueous bromine reactions. Competitive kinetic measurements using V-BrPO, phenol red and geraniol (**6**) indicated a possible enzyme-substrate interaction, further suggesting that bromination and cyclization of nerol (**4**) and geraniol (**6**) is likely occurring at or near the active site of V-BrPO. It is suggested that the smaller monoterpenes linalool (**1**), nerol (**4**), and geraniol (**6**) and their bromonium-intermediates exhibit many different conformations within the active site of V-BrPO. Binding of the monoterpene along the active site channel could block or trap an oxidized bromine species from escaping to outside the active site, giving rise to the competitive kinetic results, while the possibility of several

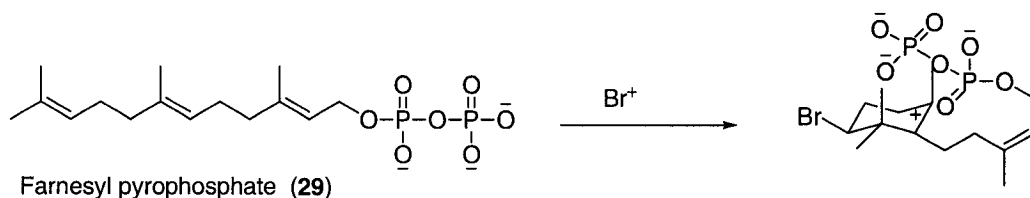
substrate conformations within the active site would contribute to the lack of specificity and decreased yields of cyclized products.

Increasingly longer terpene substrates were tested with V-BrPO, such as geranyl acetate (**9**), geranyl acetone (**12**), and all *trans* (+)-nerolidol (**14**). Experiments with geranyl acetate (**9**) and geranyl acetone (**12**) produced brominated cyclized structures similar to products **7** and **8**, and the monocyclofarnesane class of compounds (Scheme 3.8 and Scheme 3.9). An interesting feature of the V-BrPO-catalyzed reactions with geranyl acetate and geranyl acetone is the proposed stabilization of the bromocarbenium-ion intermediate by a properly positioned internal oxygen containing nucleophile. Nucleophilic trapping or stabilization of carbocations generated in biomimetic cyclizations has been previously reported and used to study the concertedness of overall ring formation process (Garst et al. 1979; Hoye et al. 1981; Gopalan et al. 1992; Snowden et al. 1992). Stabilization of reaction intermediates leads to increased yields of cyclized products. In the case of geranyl acetate (**9**), the bromocarbenium-ion is likely stabilized by resonance delocalization of the positive charge over the oxygen atoms of the acetyl group giving the bicyclic ion (Scheme 3.8). A bicyclic ion intermediate was proposed in the biomimetic cyclization of geranyl acetate using bromine and stannic bromide in nitromethane (Wolinsky and Faulkner 1976), where the major product of the reaction was a cyclized bromoacetate containing a tertiary alcohol **28** on the ring (Scheme 3.16). Product **28** was proposed to form from water hydrolysis of the bicyclic ion during workup.



Scheme 3.16: Biomimetic bromination and cyclization of geranyl acetate (9)

Surprisingly, in the V-BrPO catalyzed reactions in aqueous buffer, the cyclized alcohol **28** was not observed, suggesting that elimination of the bicyclic ion to products **10** and **11** (Scheme 3.8) precluded nucleophilic quenching by solvent molecules. In addition, stabilization of the bromocarbenium-ion by delocalization of the positive charge over oxygen-containing functional groups suggest that terpenyl pyrophosphates would also benefit from a similar stabilization mechanisms leading to cyclic brominated species (Scheme 3.17).



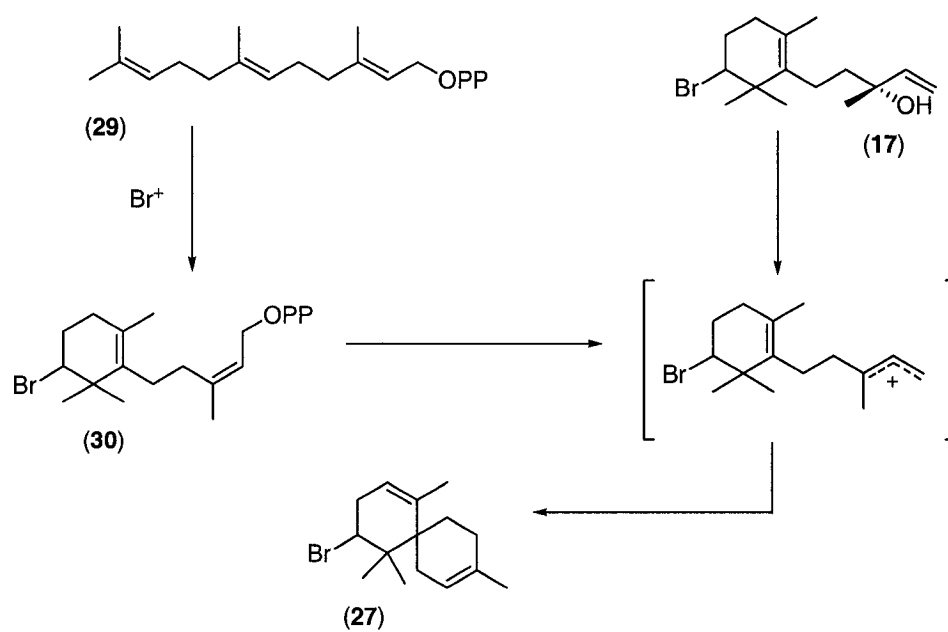
Scheme 3.17: Proposed stabilization of monocyclofarnesyl pyrophosphate cation by internal oxygen containing pyrophosphate moiety.

V-BrPO catalyzed reaction with all *trans* (+)-nerolidol (**14**) produced four brominated monocyclofarnesane structures of interest, most notably α -, β -, γ -snyderols (**15** – **17**; Scheme 3.10), and isomeric (+)-3 β -bromo-8-epicaparrapi oxide (**18**; scheme 3.11). Previously nerolidol was proposed as the biogenetic precursor to the marine natural products α - and β -snyderol (**15**) (**16**) (Kato et al. 1976; Kato et al. 1980). Biomimetic syntheses of products **15**, **16**, and **17** have been successfully performed via bromonium-ion induced carbocyclization mechanisms, but suffered from lack of specificity in bromine-carbon bond formation (Kato et al. 1976; Wolinsky and Faulkner 1976; Martin and Darias 1978).

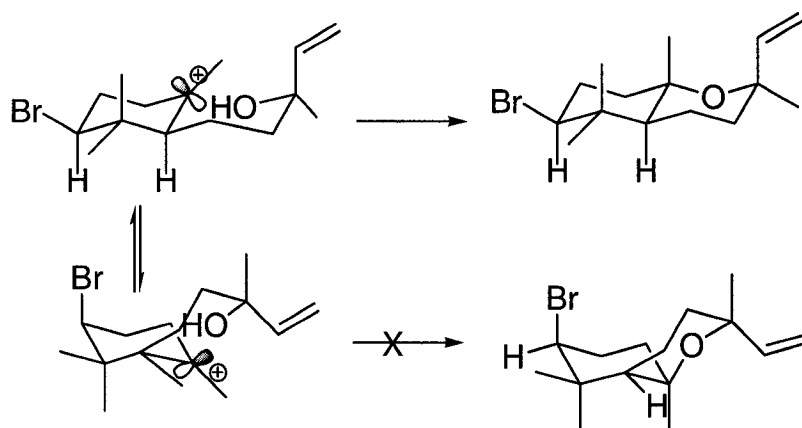
V-BrPO catalyzed the asymmetric bromination of (+)-nerolidol (**14**) to produce single diastereomers **16**, **17** and **18**. Asymmetric bromination by V-BrPO imply that approach of the bromonium-ion to the terminal olefin of (+)-nerolidol (**14**) is a specific event occurring within the active site cavity of V-BrPO. The proposed association of the substrate in the active site is consistent with competitive kinetic results with V-BrPO, phenol red, and (+)-nerolidol. It is proposed that (+)-nerolidol (**14**) is oriented in a favorable conformation within the active site suitable for bromination at a single enantiotopic face of the terminal double bond, likely through some interaction with the allylic alcohol moiety. The ability of V-BrPO to specifically bind and orient substrates has been reported previously and has resulted in the regioselective bromination of indoles as well as the enantiospecific oxidation of sulfides (Andersson et al. 1997; Andersson and Allenmark 1998; ten Brink et al. 1998; Martinez et al. 2001).

The asymmetric formation of γ -snyderol is striking, especially when one considers that this is the first report of an enzymatic bromonium-ion induced cyclization to a tetrasubstituted olefin. The formation of γ -snyderol by V-BrPO supports previous proposals of an enzyme-catalyzed cyclization of farnesyl pyrophosphate (**29**) to 10-bromo- α -chamigrene (**27**) via a tetrasubstituted monobromocyclofarnesyl pyrophosphate intermediate **30** (Scheme 3.18) (Fenical 1975; Faulkner 1976a; Martin et al. 1986). The cyclization of the brominated monocyclofarnesyl pyrophosphate is assumed to proceed through an allylic cation. Previously, Wolinsky et al., in a biomimetic synthesis of 10-bromo- α -chamigrene (**27**), prepared racemic γ -snyderol (**17**) and treated the vinyl alcohol with acid to afford the chamigrene skeleton (Wolinsky and Faulkner 1976).

V-BrPO reaction with **14** also produced the [4.4.0] bicyclic ring system of (+)-3 β -bromo-8-epicaparrapi oxide (**18**), which is similar to the ring system of product **13**. The biosynthesis of the *trans*-fused ring system of **18** by exclusion of the *cis*-fused ring system can be rationalized by assuming the planar bromocarbenium-ion intermediate being quenched by internal nucleophilic trapping on the empty *p*-orbital by the allylic alcohol group in an equatorial position (Scheme 3.19). Formation of the *cis*-fused ring system is hindered by unfavorable isomerization of the equatorial bromine to the axial position causing 1,3-diaxial interactions (Hoye and Kurth 1978).



Scheme 3.18: Proposed biosynthetic pathway to chamigrene skeleton (**27**) via tetrasubstituted monocyclofarnesane intermediate (**30**)



Scheme 3.19: Cyclization mechanism for (+)-nerolidol (**14**) leading to the observed stereochemistry of 3β-bromo-8-epicaparrapi oxide (**18**).

The difference in reactivity between the V-BrPO/H₂O₂/Br⁻ system and aqueous bromine with terpene substrates nerol (**4**), geraniol (**6**), and (+)-nerolidol (**14**) suggest an enzyme-trapped or enzyme-bound brominating species, and not a freely diffusible brominating species. These results are consistent with previously reported indole substrates interacting with V-BrPO (Tschirret-Guth and Butler 1994; Martinez et al. 2001).

The asymmetric recognition of the terminal olefin by V-BrPO to generate the bromonium-nerolidol species controls the stereoselectivity for the successive cyclization to **18**. The asymmetric bromination and cyclization of **14** by V-BrPO is to enzymes such as terpene cyclases, which also control the cyclization of isoprenoids by the asymmetric protonation of the terminal olefin with successive cyclization by stabilization of carbocation intermediates and substrate conformations within enzyme cavities made of aromatic residues (Dougherty 1996). The enantioselective bromination of **14** by V-BrPO leading to products **15**, **16**, **17** and **18** is consistent with all *trans* (+)-nerolidol (**14**) orienting within the active site channel of V-BrPO affording preferential bromination of **14** rather than release of a freely diffusible brominating species. The high specificity of bromine-carbon bond formation to yield single diastereomers of **16** – **18** imply that (+)-nerolidol (**14**) specifically binds to V-BrPO and is not randomly docking within the active-site cavity. In the case of random substrate docking, one might expect symmetric bromination on both faces of the terminal olefinic bond leading to equal distribution of diastereomeric products. Recently, X-ray crystallographic studies of V-BrPO

from *C. officinalis* show that the vanadium-binding site resides at the bottom of a 20 Å deep substrate channel (Isupov et al. 2000). Hydrophobic patches of residues dominate the substrate channel leading to the vanadium site, where there are three hydrophilic residues (Glu124, Arg395, Asp292) within 7.5 Å of the vanadate O⁴ oxygen atom except those involved in coordination or hydrogen bond contacts to the vanadate ion. The hydrophobic surface of the substrate cavity in addition to subtly placed charged residues likely provides an ideal binding surface necessary for (+)-nerolidol docking and bromination. Similarly, the enantioselective oxidations of bicyclic sulfides in the absence of halides by V-BrPO (*C. officinalis*) likely results from a specific substrate docking event within the active site channel (Andersson et al. 1997; Andersson and Allenmark 1998).

The presence of additional products (i.e., hydrins, epoxide, bromoethers, and dibrominated species) seems to implicate the cyclization of the bromonium-terpene species rather than a bromination event as being responsible for the modest yield of cyclized products in V-BrPO catalyzed reactions. Additional experiments are being pursued to further understand the interactions between sesquiterpenes and V-BrPO that drive the cyclization process, as well as reaction conditions which mimic those found within algae, to further increase the yields of cyclized products.

Vanadium bromoperoxidase catalyzes the asymmetric bromination and cyclization of sesquiterpenes towards the production of chiral brominated sesquiterpene marine natural products **15**, **16**, and **18**. V-BrPO catalyzed production of marine natural products suggests a role of V-BrPO in the biogenesis of

halogenated metabolites in marine organisms, where further application of V-BrPO chemistry in the biosynthetic pathway towards other halogenated marine metabolites should be explored.

References

- Andersson, M. and S. Allenmark (1998). "Asymmetric Sulfoxidation Catalyzed by a Vanadium Bromoperoxidase: Substrate Requirements of the Catalyst." *Tetrahedron* **54**: 15293-15304.
- Andersson, M., A. Willetts and S. Allenmark (1997). "Asymmetric Sulfoxidation Catalyzed by a Vanadium-Containing Bromoperoxidase." *J. Org. Chem* **62**: 8455-8458.
- Blackmond, D. G. (2001). "Kinetic Resolution Using Enantioimpure Catalysts: Mechanistic Considerations of Complex Rate Laws." *J. Am. Chem. Soc.* **123**: 545-553.
- Brindley, A. A., A. R. Dalby, M. N. Isupov and J. A. Littlechild (1998). "Preliminary X-ray Analysis of a New Crystal Form of the Vanadium-Dependent Bromoperoxidase from *Corallina officinalis*." *Acta Crystallogr., Sect. D* **54**: 454-457.
- Butler, A., J. N. Carter and M. T. Simpson (2001). Vanadium in Proteins and Enzymes. Handbook on Metalloproteins. I. Bertini, A. Sigel and H. Sigel. New York, Marcel Dekker, Inc.: 153-179.
- Butler, A. and J. V. Walker (1993). "Marine Haloperoxidases." *Chem. Rev.* **93**: 1937-1944.
- Carter, J. N., K. E. Beatty, M. T. Simpson and A. Butler (2002). "Reactivity of Recombinant and Mutant Vanadium Bromoperoxidase from the Red Alga *Corallina officinalis*." *J. Inorg. Biochem.* **91**: 59-69.
- de Boer, E. and R. Wever (1988). "The Reaction-Mechanism of the Novel Vanadium-Bromoperoxidase - a Steady-State Kinetic-Analysis." *J. Biol. Chem.* **263**: 12326-12332.
- Dougherty, D. A. (1996). "Cation-pi Interactions in Chemistry and Biology: A New View of Benzene, Phe, Tyr, and Trp." *Science* **271**: 163-168.
- Erickson, K. L. (1983). Constituents of *Laurencia*. Marine Natural Products. P. J. Scheuer., Academic Press Inc. **V**: 131-257.
- Everett, R. R., H. S. Soedjak and A. Butler (1990). "Mechanism of Dioxygen Formation Catalyzed By Vanadium Bromoperoxidase - Steady State Kinetic Analysis and Comparison to the Mechanism of Bromination." *J. Biol. Chem.* **265**: 15671-15679.

- Faulkner, D. J. (1976a). "Biomimetic Synthesis Of Marine Natural Products." *Pure & Appl. Chem.* **48**: 28-28.
- Faulkner, D. J. (1976b). "3B-Bromo-8-Epicaparrapi Oxide, The Major Metabolite of *Laurencia obtusa*." *Phytochemistry* **15**: 1993-1994.
- Faulkner, D. J. (2002). "Marine Natural Products." *Nat. Prod. Rep.* **19**: 1-48.
- Fenical, W. (1975). "Halogenation in the Rhodophyta, A Review." *J. Phycol.* **11**: 245-259.
- Fukuzawa, A., M. Aye, M. Nakamura, M. Tamura and A. Murai (1990a). "Biosynthetic Formation of Cyclic Bromo-Ethers Initiated by Lactoperoxidase." *Chem. Lett.*: 1287-1290.
- Fukuzawa, A., M. Aye, Y. Takasugi, M. Nakamura, M. Tamura and A. Murai (1994). "Enzymatic Bromo-Ether Cyclization of Laurediols with Bromoperoxidase." *Chem. Lett.* 2307-2310.
- Fukuzawa, A., Y. Takasugi, A. Murai, M. Nakamura and M. Tamura (1992). "Enzymatic Single-step Formation of laureatin and Its Key Intermediate. Prelaureatin from (3Z, 6S, 7S)-Laurediol." *Tetrahedron Lett* **33**: 2017-2018.
- Fusetani, N. (2000). *Drugs from the Sea*. Basel, Switzerland, Karger Press.
- Garst, M., C. Y. and W. Johnson (1979). "Biomimetic Polyene Cyclizations. Trapping of the Resultant Carbocation by an Internal Nucleophile." *J. Am. Chem. Soc.* **101**: 4404-4406.
- Gonzalez, I. C. and C. J. Forsyth (2000). "Total Synthesis of Thyrsiferyl 23-Acetate, a Specific Inhibitor of Protein Phosphatase 2A and an Anti-Leukemic Inducer of Apoptosis." *J. Am. Chem. Soc.* **122**: 9099-9108.
- Gopalan, A., R. Prieto, B. Mueller and D. Peters (1992). "Polyene Cyclizations Using Mercury (II) Triflate-N,N-Dimethylaniline Complex- Participation by Internal Nucleophiles." *Tetrahedron Lett.* **33**: 1679-1682.
- Hager, L. P., D. R. Morris, F. S. Brown and H. Eberwein (1966). "Chloroperoxidase .2. Utilization of Halogen Anions." *J. Biol. Chem.* **241**: 1769.
- Hemrika, W., R. Renirie, H. Dekker and R. Wever (1998). *ACS Symp. Ser* **711**: 216-227.

- Howard, B. M. and W. Fenical (1976). "Alpha and beta Snyderol; New Bromo-Monocyclic Sesquiterpenes from the Seaweed *Laurencia*." *Tetrahedron Lett.* **1**: 41-44.
- Hoye, T. R., A. J. Caruso and M. J. Kurth (1981). "Internal Nucleophilic Termination in Mercuric Ion Initiated Diene Cyclizations." *J. Org. Chem.* **46**: 3550-3552.
- Hoye, T. R. and M. J. Kurth (1978). "Brominative Cyclization of Geranyl Derivatives." *J. Org. Chem.* **43**: 3693-3697.
- Hoye, T. R. and M. J. Kurth (1979). "Mercuric Trifluoroacetate Mediated Brominative Cyclizations of Dienes. Total Synthesis of dl-3B-Bromo-8-epicaparappi Oxide." *J. Org. Chem.* **44**: 3461-3467.
- Isupov, M. N., A. R. Dalby, A. A. Brindley, Y. Izumi, T. Tanabe, G. N. Murshudov and J. A. Littlechild (2000). "Crystal structure of dodecameric vanadium-dependent bromoperoxidase from the red algae *Corallina officinalis*." *J. Mol. Biol.* **299**: 1035-1049.
- Itoh, N., A. Hasan, Y. Izumi and H. Yamada (1988). "Substrate-Specificity, Regiospecificity and Stereospecificity of Halogenation Reactions Catalyzed by Non-Heme-Type Bromoperoxidase of *Corallina pilulifera*." *Eur. J. Biochem.* **172**: 477-484.
- Itoh, N., Y. Izumi and H. Yamada (1987). "Characterization of Nonheme Iron and Reaction-Mechanism of Bromoperoxidase in *Corallina pilulifera*." *J. Biol. Chem.* **262**: 11982-11987.
- Kato, T., I. Ichinose, A. Kamoshida and Y. Kitahara (1976). "Cyclization of Polyenes. Biogenetic-Type Synthesis of Snyderols." *J.C.S. Chem. Comm.*: 518-519.
- Kato, T., K. Ishii, I. Ichinose, Y. Nakai and T. Kumagai (1980). "Brominative Cyclization of Nerolidol and Geranyl-Linalool." *J.C.S. Chem. Comm.*: 1106-1108.
- Krenn, B. E., Y. Izumi, H. Yamada and R. Wever (1989). "A Comparison of Different (Vanadium) Bromoperoxidases - the Bromoperoxidase from *Corallina pilulifera* Is Also a Vanadium Enzyme." *Biochem. et Biophys. Acta* **998**: 63-68.
- Martin, J. D. and J. Darias (1978). Algal Sesquiterpenoids. Marine Natural Products: Chemical and Biological Perspectives, Academic Press. **1**: 125-174.
- Martin, J. D., J. M. Palazon, C. Perez and J. L. Ravelo (1986). "Syntheses of Marine Molecules." *Pure & Appl. Chem.* **58**: 395-406.

- Martinez, J. S., G. L. Carroll, R. A. Tschirret-Guth, G. Altenhoff, R. D. Little and A. Butler (2001). "On the Regiospecificity of Vanadium Bromoperoxidase." *J. Am. Chem. Soc.* **123**: 3289-3294.
- Seeman, J. I. (1983). "Effect of Conformational Change on Reactivity in Organic-Chemistry - Evaluations, Applications, and Extensions of Curtin-Hammett Winstein-Holness Kinetics." *Chemical Reviews* **83**: 83-134.
- Sheffield, D. J., T. Harry, A. J. Smith and L. J. Rogers (1993). "Purification and Characterization of the Vanadium Bromoperoxidase from the Macroalga *Corallina officinalis*." *Phytochemistry* **32**: 21-26.
- Shieh, H. and G. D. Prestwich (1982). "Chiral, Biomimetic Total Synthesis of (-)-Aplysistatin." *Tetrahedron Lett.* **23**: 4643-4646.
- Snowden, R., J. Eichenberger, S. Linder, P. Sonnay, C. vial and K. Schulte-Elte (1992). "Internal Nucleophilic Termination in Biomimetic Acid Mediated Polyene Cyclizations: Stereochemical and Mechanistic Implications. Synthesis of (+/-)-Ambrox and Its Diastereoisomers." *J. Org. Chem.* **57**: 955-960.
- Soedjak, H. (1991). Investigation of Vanadium Bromoperoxidase: Kinetics and Mechanism. Ph.D. Thesis, University of California, Santa Barbara.
- Soedjak, H. S., J. V. Walker and A. Butler (1995). "Inhibition and Inactivation of Vanadium Bromoperoxidase by the Substrate Hydrogen-Peroxide and Further Mechanistic Studies." *Biochemistry* **34**: 12689-12696.
- ten Brink, H. B., H. L. Holland, H. E. Schoemaker, H. van Lingen and R. Wever (1999). "Probing the Scope of the Sulfoxidation Activity of Vanadium Bromoperoxidase from *Ascophyllum nodosum*." *Tetrahedron: Asymmetry* **10**: 4563-4572.
- ten Brink, H. B., A. Tuynman, H. Dekker, W. Hemrika, Y. Izumi, T. Oshiro, H. E. Schoemaker and R. Wever (1998). "Enantioselective Sulfoxidation Catalyzed by Vanadium Haloperoxidases." *Inorg. Chem.* **37**: 6780-6784.
- Tschirret-Guth, R. A. and A. Butler (1994). "Evidence for Organic Substrate Binding to Vanadium Bromoperoxidase." *J. Am. Chem. Soc.* **116**: 411-412.
- Weyand, M., H. J. Hecht, M. Kiess, M. F. Liaud, H. Vilter and D. Schomburg (1999). "X-ray Structure Determination of a Vanadium-Dependent Haloperoxidase from *Ascophyllum nodosum* at 2.0 Angstrom Resolution." *J. Mol. Biol.* **293**: 595-611.

Wolinsky, L. E. and D. J. Faulkner (1976). "A Biomimetic Approach to the Synthesis of *Laurencia* metabolites. Synthesis of 10-Bromo-Alpha-Chamigrene." J. Org. Chem. **41**: 597-600.

Ziderman, I. (1972). Isr. J. Chem **11**: 7-20.

Chapter Four

Chemical Defense of the Marine Red Alga *Delisea pulchra*

Introduction

Seawater, unlike air, is a microbe-rich environment. Seawater typically contains 10^7 viruses, 10^6 bacteria, 10^3 fungi, and 10^3 microalgae per milliliter of seawater (Reinheimer 1992). Given that marine organisms, which include marine animals, plants, and microbes, are continuously exposed to a wide array of microorganisms, it is not surprising that communities of microbes form biofilms that colonize the surfaces of marine organisms. In fact, the estimated biomass of bacteria on marine eukaryotes, determined from scanning electron microscopy, is 2 – 20 μg of biomass per cm^2 , which roughly translates to 10^6 – 10^7 cells/ cm^2 (Wahl 1995; Maximilien et al. 1998). Surface fouling by microbes on marine organisms can have deleterious effects such as mortality (Littler and Littler 1995), degradation of host tissue (Correa and Sanchez 1996), competition for nutrients, inhibition of gaseous exchange (Lewandowski 1994) and, for marine plants, decreased photosynthesis by blocking incident light (Sand-Jensen 1977). In order for marine organisms to survive in what would appear to be a hostile environment, marine organisms have evolved defense strategies to control biofilm formation or the overall density of microbes at their surfaces.

Secondary metabolites produced by marine organisms are one such strategy used to mediate defense against microbial fouling (Engel et al. 2002). Many recent publications report inhibition of biofouling by secondary metabolites and have

shown that many secondary metabolites exert their effects by targeting phenotypes that control biofilm formation in bacteria (Engel et al. 2002). One such phenotype affected by some marine secondary metabolites is cell-to-cell communication by bacteria, otherwise termed quorum sensing. Quorum sensing in gram-negative bacteria is accomplished *via* small polar signaling molecules, such as acyl homoserine lactones (AHLs) [Figure 4.1]. AHLs diffuse in, out, and between bacterial cells. When bacterial populations increase the concentration of AHL increases. In turn, the AHLs signals dock to specific receptor proteins within the bacteria leading to the enhanced transcription of genes for expression of a particular phenotype, such as surface colonization and biofilm formation (Whitehead et al. 2001).

One of the most in depth studies of chemical defense by marine organisms via secondary metabolites is with the red alga *Delisea pulchra*. *D. pulchra* has varied amounts of microbial colonization on its surface, with little biofouling at the alga's apical tips (Steinberg et al. 2001), which correlates with the localization of halogenated furanone secondary metabolites (Dworjanyn et al. 1999). The halogenated furanones in *D. pulchra* are concentrated in gland cells present at the surface of the alga (Dworjanyn et al. 1999). The structural similarity of the halogenated furanones to AHLs has prompted bioassays to determine their effect on bacterial quorum sensing [Figure 4.1]. Recent studies show that the halogenated furanones inhibit several AHL-dependent quorum-sensing traits such as swarming in *Serratia liquefaciens* (Rasmussen et al. 2000),

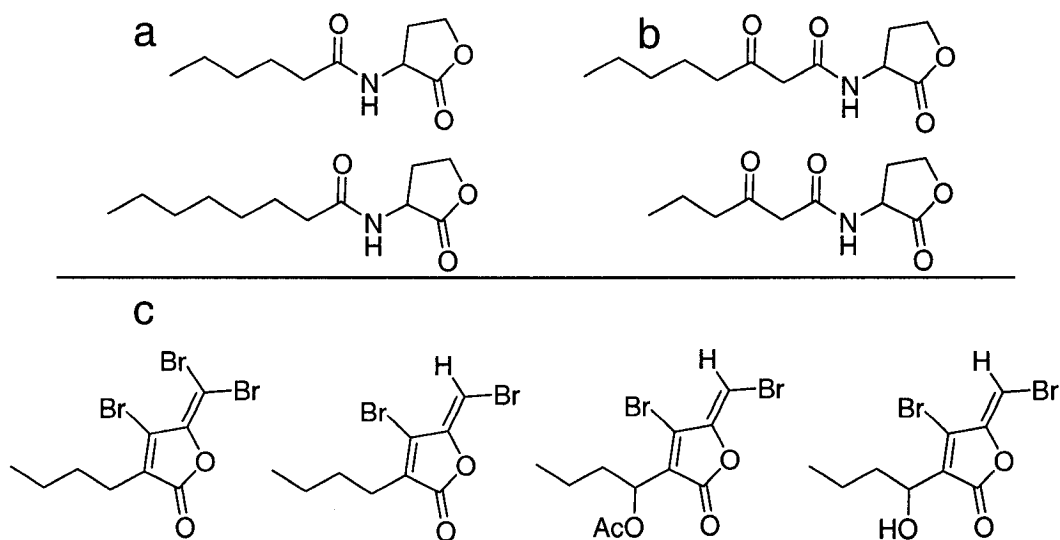


Figure 4.1: Chemical structures of (a) representative N-acyl homoserine lactones, (b) representative 3-oxo-acyl homoserine lactones and (c) halogenated furanones.

antibiotic and exoenzyme production in *Erwinia carotovora* (Manefield et al. 2001), and biofilm formation by *Pseudomonas aeruginosa* (Hentzer et al. 2002). Also, additional studies show that the halogenated furanones inhibit quorum sensing by modulating the LuxR-type protein activity by inducing the accelerated turnover of Lux-R (Manefield et al. 2002).

In addition to secondary metabolites that ward off predators of marine organisms, another mechanism is the “oxidative burst response”. The oxidative burst response is generated by degradation of the marine plant cell wall (usually by bacterial metabolism) thereby producing oligosaccharides (Kupper et al. 2001).

Oligosaccharides induce the production of reactive oxygen species (ROS), such as superoxide and hydrogen peroxide, at concentrations high enough to kill the invading microbes and/or signal the upregulation of additional defense genes.

Additional defense strategies against microbial fouling likely exist in the marine environment, but bioassays relevant to natural systems are limited. Taking clues from terrestrial microorganisms has provided additional ideas on strategies used by organisms to defend against microbial fouling. For example, several enzymes produced by gram-positive soil bacteria have been identified that target the AHL components of bacterial quorum sensing systems. Enzymes such as lactonases and acylases act directly on AHLs, curbing the activity of the signaling molecules (Dong et al. 2000; Leadbetter and Greenberg 2000). Lactonases and acylases have not yet been identified as defense strategies used by marine organisms. However, other enzyme systems present at the surfaces of marine organism may confer protection against microbial fouling.

Described in this chapter is the identification of a vanadium bromoperoxidase at the surface of the marine red alga *D. pulchra*. The ability of V-BrPO to inactivate AHL signaling molecules and disrupt quorum sensing in the reporter strain *Agrobacterium tumefaciens* NTL4 was tested as a proposed enzymatic defense strategy used by marine seaweeds. Biomimetic syntheses of synthetic analogues of halogenated furanones utilizing V-BrPO from *D. pulchra* are also described.

Methods and Materials

General methods

Professor Bill Baker at the University Southern Florida collected the temperate marine alga *Delisea pulchra* on an expedition to Anartica in December 2001. The alga was shipped on dry ice and upon receipt was immediately placed at $-80\text{ }^{\circ}\text{C}$ for long-term storage. Partial purification of V-BrPO from the alga was performed as previously described for other V-BrPOs isolated from marine red algae (see also Chapter 2) (Carter et al. 2002).

^1H NMR spectra were recorded on a Varian 500 instrument using deuteriochloroform as the solvent (CHCl_3 , standard, $\delta = 7.27$ ppm). Multiplicities are indicated by s (singlet), d (doublet), t (triplet), q (quartet), m (multiplet), a (apparent), or br (broadened). Coupling constants, J , are reported in hertz. Consumption and formation of reaction substrates and products were monitored using thin layer chromatography on Whatman SiO_2 pre-coated plates (60 F₂₅₄, 250 μm thick) with mixtures of hexanes/ethyl acetate as mobile phases. Flash column chromatography was performed using 230 - 400 mesh silica gel (EM Science) with mixtures of ethyl acetate and hexanes as eluent. Atmospheric pressure chemical ionization (APCI) mass spectrometry was performed using a VG-Fisons Platform II (Micromass) quadropole mass spectrometer. The APCI probe was operated at 500 $^{\circ}\text{C}$ and the ion source temperature was maintained at 150 $^{\circ}\text{C}$. The cone voltage was

set at 50V. UV-visible spectra were acquired on a Varian Cary 3E or 300-Bio UV-vis spectrometer at 25 °C.

Reagents 4-pentynoic acid, and 3-oxo-hexanoylhomoserine lactone were purchased from Sigma-Aldrich and used as received. Quorum sensing reporter strains, *Agrobacterium tumefaciens* NTL4 and *A. tumefaciens* KYC6 were kindly provided by Professor Clay Fuqua, University of Indiana. Bacterial strains were maintained as reported in the literature (Zhu et al. 1998).

General bromoperoxidase activities of whole algal samples or partially purified enzymes were detected by bromination of phenol red to bromophenol blue. Assays consisted of 100 µM phenol red, 100 mM KBr in 0.15 M sodium phosphate buffer (pH 6.0) and 1 – 2 mg of washed *D. pulchra* or 40 nM partially purified V-BrPO in 1 – 2 mL. Reactions were initiated with 1 – 2 mM H₂O₂ (final concentration). Production of bromophenol blue was monitored at 596 nm or by visible detection.

Reaction of acyl-homoserine lactones with the marine macroalga *Delisea pulchra*:

Reaction conditions with whole algal samples. Small pieces (approx. 2.5 mm x 2 mm) of *D. pulchra* were repeatedly washed with doubly deionized water. Cleaned algal pieces (1 – 2 mg) were placed in 1 mL of either 0.15 M phosphate (pH 6.0), 100 mM KBr or natural seawater (NSW), 100 mM KBr containing 50 µM 3-oxo-hexanoylhomoserine lactone (**1**) in a sterile Petri dish. Reactions were initiated by the addition of hydrogen peroxide over ten minutes to a final concentration of 2

mM. Reactions were gently agitated for 1 hour on a shaking platform at 25 rpm at ambient room temperatures (22 – 27 °C). At the completion of an hour the algal pieces were removed using ethanol-sterilized tweezers and the aqueous mixture extracted with 3 vol methylene chloride. The organic phases were combined and dried under a gentle stream of argon. The colorless crude residue was resolubilized in 20 µL of acetonitrile, and injected directly for APCI mass spectrometry (Michels et al. 2000).

Reaction of partially purified V-BrPO (*D. pulchra*) with acyl-homoserine lactones. 3-Oxo-hexanoyl homoserine lactone (**1**) (50 µM) predissolved in ethanol was added to 0.15 M phosphate (pH 6.0), 40 mM KBr, or NSW containing 40 mM KBr. Vanadium bromoperoxidase (40 nM) was added, and the reaction initiated by the bulk addition of H₂O₂ to a final concentration of 1 mM. The final reaction volume was 1 mL. The reaction progress was monitored on a Varian Cary spectrophotometer between 190 – 350 nm. Background and baseline correction modes were used. Scans were completed every 30 seconds for 10 minutes. Non-enzymatic control reactions were performed as described above without added V-BrPO.

Quorum sensing of *Agrobacterium tumefaciens* NTL4 with products from reactions of 3-oxo-hexanoyl homoserine lactone with *D. pulchra* and purified V-BrPO:

A. tumefaciens NTL4 (pCF218)(pCF372) is an acyl homoserine lactone (HSL) reporter strain. The strain is Ti plasmidless, and the *traR* plasmid (218) and *traI-lacZ* plasmid (372) provide sensitive detection of acyl HSLs, Tc^R, and Sp^R. The

NTL4 strain is identical to the published A136 strain, but is more stable for maintenance of the plasmid (Zhu et al. 1998).

Products from the reaction between partially purified V-BrPO from *D. pulchra* with 3-oxo-hexanoyl homoserine lactone (**1**) were tested for their ability to elicit a quorum sensing response in *A. tumefaciens* NTL4. Single colonies of *A. tumefaciens* NTL4 were streaked on six L.B. agar plates containing 4.5 µg/mL tetracycline and 2% X-gal. Plates were labeled 1 – 6 (Table 4.1). For each plate 20 µL of the corresponding reaction mixture was placed in 2 µL aliquots around the bacterial streak (Stickler et al. 1998; Borchardt et al. 2001).

Plate number	Sample
1	pH 6.0, V-BrPO reaction without added 3-oxo-hexanoylhomoserine lactone
2	pH 6.0, Positive control reaction with 3-oxo-hexanoylhomoserine lactone without added V-BrPO
3	pH 6.0, V-BrPO reaction with 3-oxo-hexanoylhomoserine lactone
4	NSW, V-BrPO reaction without added 3-oxo-hexanoylhomoserine lactone
5	NSW, Positive control reaction with 3-oxo-hexanoylhomoserine lactone without added V-BrPO
6	NSW, V-BrPO reaction with 3-oxo-hexanoylhomoserine lactone

Table 4.1: *Delisea pulchra*/V-BrPO reactions used in the bioactivity quorum sensing reporter assay with *A. tumefaciens* NTL4.

L.B. agar plates were dried face up for 30 minute at room temperature, followed by incubation at 30 °C for 48 hours. An quorum sensing response by *A. tumefaciens* NTL4 was detected by the appearance of blue color in the bacteria due to the conversion of X-gal by β -galactosidase.

Biomimetic synthesis of halogenated lactones by *D. pulchra*/V-BrPO:

4-Pentynoic acid (**2**) (10 mM) was predissolved in a small volume of ethanol and added to 0.15 M sodium phosphate buffer (pH 6.0), 100 mM KBr,. Enzymatic reactions containing 40 nM partially purified V-BrPO from *D. pulchra* were initiated by addition of 1 - 4 mol equivalents of H₂O₂ in relation to 4-pentynoic acid (**2**) concentration via syringe pump (1 equivalent per hour). All reactions were performed in the dark.

At the completion of the reaction the aqueous mixture was extracted with 2 vol methylene chloride. All products were carefully purified by flash chromatography using increasing gradient mixtures of ethyl acetate in hexanes. A single major product **3** was detected in addition to remaining substrate; **3** ~25% isolated yield, ¹H NMR δ 6.00 (t, 1H, $J = 2$ Hz), 2.7 – 3.0 (m, 4H). Product **3** has been previously reported (Krafft and Katzenellenbogen 1981). Enzymatic synthesis of **3** was in agreement with reported values.

Results

Detection of haloperoxidase activity in whole algal samples of *Delisea pulchra*:

The occurrence of novel biologically active halogenated metabolites at the surface of *D. pulchra* prompted research for a putative haloperoxidase at or near the surface of the alga. Using conditions for the standard phenol red assay adapted for use in a Petri dish, brominating activity was detected at the surface of small pieces of *D. pulchra* [Figure 4.2]. Halogenating activity with chloride as the halide was not detected, suggesting the haloperoxidase at the surface is a bromoperoxidase. In addition to the bromination of phenol red, small bubbles could be seen forming at the surface of the algal pieces. The bubbles formed at the alga-buffer interface were likely due to the halide-assisted disproportionation of hydrogen peroxide to form singlet oxygen (Everett and Butler 1989; Everett et al. 1990a).

The bromoperoxidase in *D. pulchra* could be stripped from the surface by gentle agitation in natural seawater or with 0.1 M Tris-HCl buffer pH 8.0. The type of bromoperoxidase in *D. pulchra* was evaluated by RT-PCR experiments (see Chapter 2). *D. pulchra* was found to possess two isoforms of the vanadium-dependent bromoperoxidase. Each of these isoforms (*rDpDV*-BrPO and *rDpEV*-BrPO) showed greater than 89% amino acid sequence identity to the V-BrPOs isolated from Coralline algae (see Chapter 2, Figure 2.5). Interestingly, the isoform *rDpEV*-BrPO was virtually identical with *rDpDV*-BrPO with the exception of three amino acid changes. An important amino acid change occurred in the third conserved

a



b

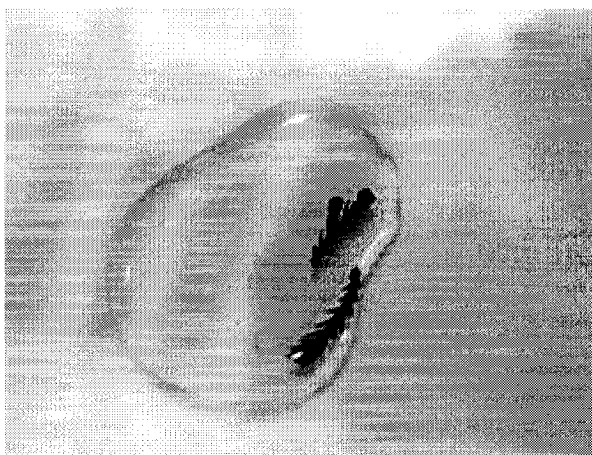


Figure 4.2: Bromination of phenol red to bromophenol blue by whole algal pieces of *D. pulchra*. (a) 1 minute after addition of hydrogen peroxide, (b) 3 minutes after addition of hydrogen peroxide. Reaction conditions: 1 – 2 mg of *D. pulchra* in 0.15 M sodium phosphate buffer (pH 6.0), 100 mM KBr, 100 μ M phenol red, and 1 – 2 mM H_2O_2 .

D. pulchra-D	1	MGIPADNLQNRKASFDTRVSAEELALARGVVPSFANGEELPYRDPDPEN
D. pulchra-E	1	MGIPADNLQNRKASFDTRVSAEELALARGVVPSFANGEELPYRDPDPEN
D. pulchra-D	51	GDPSFIASF ^T TKGLPHDDNGAIIDPDDFLAFVRAINS ^G DEKEIADLT ^L LGPA
D. pulchra-E	51	GDPSFIASF ^T TKGLPHDDNGAIIDPDDFLAFVRAINS ^G DEKEIADLT ^L LGPA
D. pulchra-D	101	RDPDTGLPIWRSDLANSLELEVRGWANSSAGLTFDLEGPDAQSIAMP ^P AP
D. pulchra-E	101	RDPDTGLPIWRSDLANSLELEVRGWANSSAGLTFDLEGPDAQSIAMP ^P AP
D. pulchra-D	151	VLTSPELIAEIAELYLMALGREIEFSEFDS ^P KNAEYIQFAIDQLNGLEW ^F
D. pulchra-E	151	VLTSPELIAEIAELYLMALGREIEFSEFDS ^P KNAEYIQFAIDQLNGLEW ^F
D. pulchra-D	201	NTPAMLGDP ^P AEIRRRRGEVTVGNLFRGILPGSEVGPYLSQYIIVGSKQI
D. pulchra-E	201	NTPAMLGDP ^P AEIRRRRGEVTVGNLFRGILPGSEVGPYLSQYIIVGSKQI
D. pulchra-D	251	GSATVGSKTLVSPNAAEFDGEIAYGSITISQ ^R VR ^I ATPGRDFMTDLK ^V F
D. pulchra-E	251	GSATVGSKTLVSPNAAEFDGEIAYGSITISQ ^R VR ^I ATPGRDFMTDLK ^V F
D. pulchra-D	301	LDVQDAADFRGFESYEPGARLIR ^T IRDLATWVHFDALYEAYLNACLILLA
D. pulchra-E	301	LDVQDAADFRGFESYEPGARLIR ^T IRDLATWVHFDALYEAYLNACLILLA
D. pulchra-D	351	NRVPFDPNIPFQQEDKLDNQDVFVNF ^G DAHVLSLVTEVATRALKAVRYQK
D. pulchra-E	351	NRVPFDPNIPFQQEDKLDNQDVFVNF ^G DAHVLSLVTEVATRALKAVRYQK
D. pulchra-D	401	FNIHRRLRPEATGGLISV ^N KIAAEKGESV ^F PEVDLAVEELGDILEKAEIS
D. pulchra-E	401	FNIHRRLRPEATGGLISV ^N KIAAEKGESV ^F PEVDLAVEELGDILEKAEIS
D. pulchra-D	451	NRKQNIADGDPDPDP ^S FLLPQAF ^A E ^G SPFHP ^S Y ^G SGH ^A V ^A GACV ^T ILKA
D. pulchra-E	451	NRKQNIADGDPDPDP ^S FLLPQAF ^A E ^G SPFHP ^S Y ^G SGH ^A V ^A GACV ^T ILKA
D. pulchra-D	501	FFDSNFQIDQVFEVDKDEDKLVKSSFKG ^T TLVAGELNKLADNIA ^T GRNMA
D. pulchra-E	501	FFDSNFQIDQVFEVDKDEDKLVKSSFKG ^T TLVAGELNKLADNIA ^T GRNMA
D. pulchra-D	551	EVRY ^F SDQFESILLGEQVAIGILEEQSLTYGENFFNLPKFDG ^T TIQI*
D. pulchra-E	551	EVRY ^F SDQFESILLGEQVAIGILEEQSLTYGENFFNLPKFDG ^T TIQI*

Figure 4.3: Alignment of deduced amino acid sequences for recombinant isoforms of V-BrPO from (*D. pulchra*-D vs. *D. pulchra*-E) the red alga *D. pulchra*. H553R mutation in clone *D. pulchra*-E designated by circle around the residue.

active-site domain [Figure 4.3]. The amino acid substitution in clone *D. pulchra*-E of histidine 553 to an arginine, occurs at the conserved histidine that directly coordinates the vanadium cofactor. Multiple clones from RT-PCR experiments were sequenced to confirm that the H553R mutation was not a sequencing error.

Although one could argue that the mutated isoform could result from errors in the RT-PCR, a very high-fidelity reverse-transcriptase and polymerase were used in all experiments. The function of the mutated isoform of V-BrPO in *D. pulchra* is not clear at this time.

Reaction of 3-oxo-hexanoylhomoserine lactone with whole algal pieces of *D. pulchra* and partially purified V-BrPO:

The preceding experiment demonstrated bromoperoxidase activity (i.e., Figure 4.2) on the surface of the alga. Additional experiments examined the ability of V-BrPO localized on the surface to react with AHL signaling molecules, thereby potentially altering bacterial cell-to-cell communication. Algal pieces added to sodium phosphate buffer (pH 6.0) containing 3-oxo-hexanoylhomoserine lactone (**1**) brominated **1** in the presence of added bromide and hydrogen peroxide. APCI mass spectrometry of the reaction extract showed the formation a dibrominated-3-oxo-hexanoylhomoserine lactone **4** species [Figure 4.4]. The molecular ions m/z at 396, 394, 392 indicated the formation of a sodium adduct of product **4**. The 1:2:1 ratio for the molecular ion also confirmed the presence of a dibrominated species. The ion at m/z 102 for the lactone head group in the APCI spectrum suggested that bromination occurred at the α -carbon of **1**, and that the lactone part of the molecule

was not brominated. Reaction between the partially purified V-BrPO from *D. pulchra* and 3-oxo-hexanoylhomoserine lactone (**1**) at pH 6.0 produced a similar APCI spectrum as observed with whole algal pieces (see Appendix for spectrum). The similar APCI mass spectrum produced using partially purified V-BrPO suggest this is the same enzyme working at the surface of the alga. V-BrPO bromination kinetics of **1** was monitored by UV-visible spectroscopy at pH 6.0 and in NSW (~pH 8.0). The UV-vis spectrum showed an increase in the spectrum as a function of time, in addition to a slight spectral red shift of the brominated product at both pHs tested [Figure 4.5]. The bathochromic and hyperchromic effect observed in the UV spectrum of the brominated species is expected for the $n \rightarrow \pi^*$ transition of carbonyl compounds (Lambert et al. 1998). The UV-vis data support dibromination of the α -carbon and not on the lactone ring. Bromination of the α -carbon of **1** is in agreement with previous experiments performed with stabilized hypobromite solution and **1** at pH 6.0 (Michels et al. 2000).

In addition to the reactivity of whole alga pieces with **1** at pH 6.0, NSW was tested to mimic the aqueous conditions found in the ocean (~pH 8.0). In the presence of added bromide and hydrogen peroxide, V-BrPO present at the surface of *D. pulchra* reacted with **1** forming a dibrominated species. The APCI mass spectrum of the NSW reaction was different than the spectrum for the reaction at pH 6.0. The molecular ion observed in the mass spectrum was m/z 319, 317, 315 [Figure

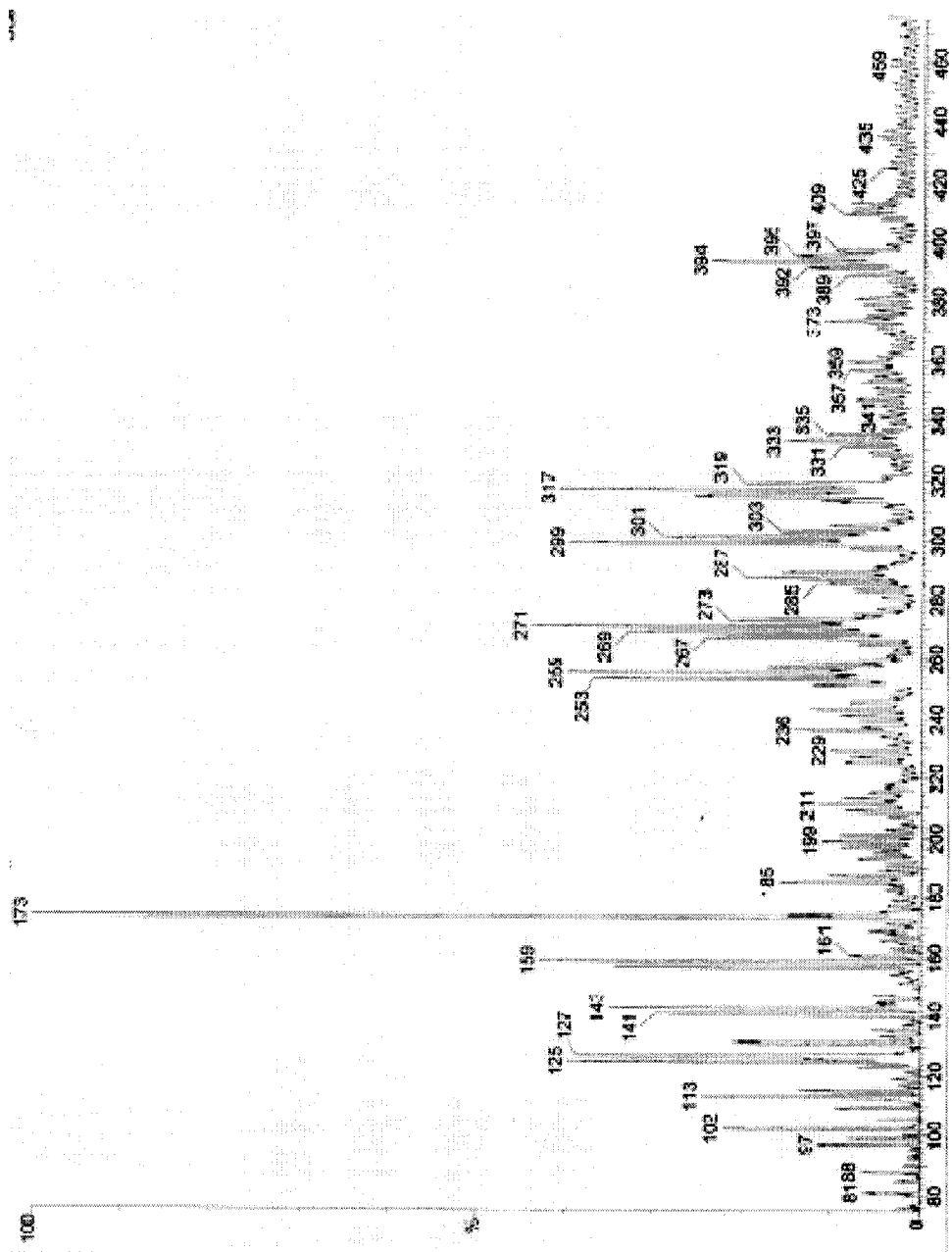


Figure 4.4: APCI mass spectrum of the sodium adduct of α,α -dibrominated-3-oxo-hexanoylhomoserine lactone (**4**). Product **4** was generated by the bromination of 3-oxo-hexanoylhomoserine lactone ($50\ \mu\text{M}$) by whole algal pieces of *D. pulchra* upon addition of $100\ \text{mM}$ KBr in 0.15 sodium phosphate buffer ($\text{pH } 6.0$), and $1 - 2\ \text{mM}$ H_2O_2 .

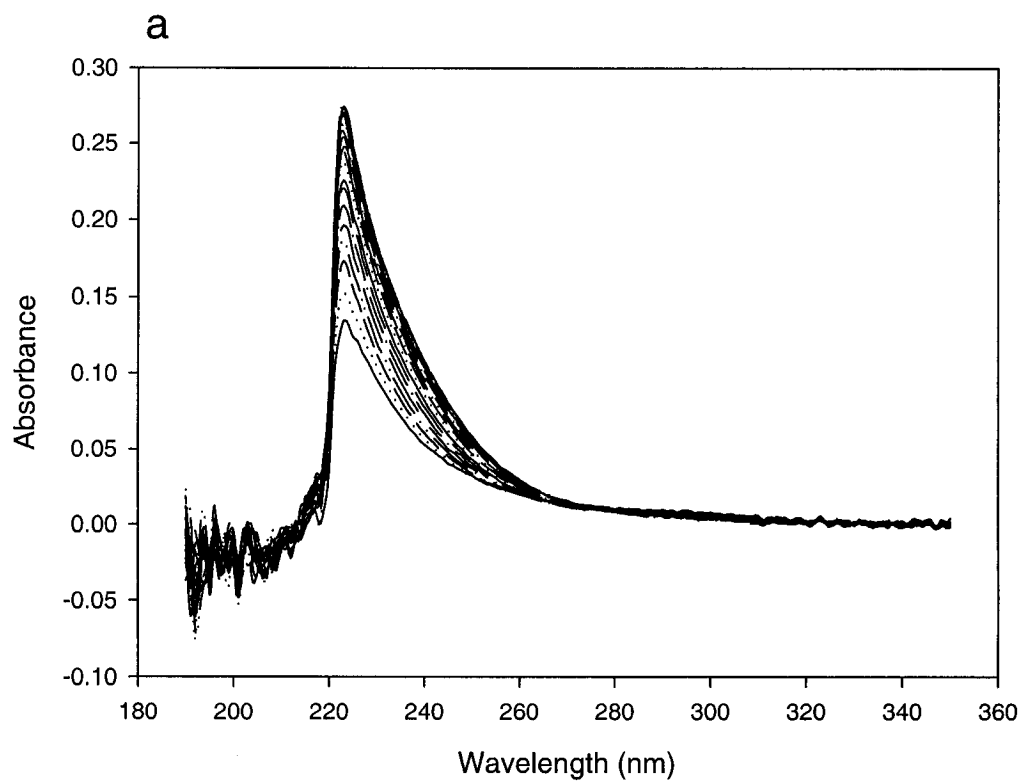


Figure 4.5 continued: (a) UV-visible spectrum of the time dependent bromination of 3-oxo-hexanoylhomoserine lactone (**1**). Spectra were collected at 30 sec intervals for 10 minutes. Reaction condition were, 0.15 M sodium phosphate buffer (pH 6.0), 40 mM KBr, 40 nM partially purified V-BrPO from *D. pulchra*, 50 μ M **1**. Reaction was initiated by the addition of 1 mM H₂O₂.

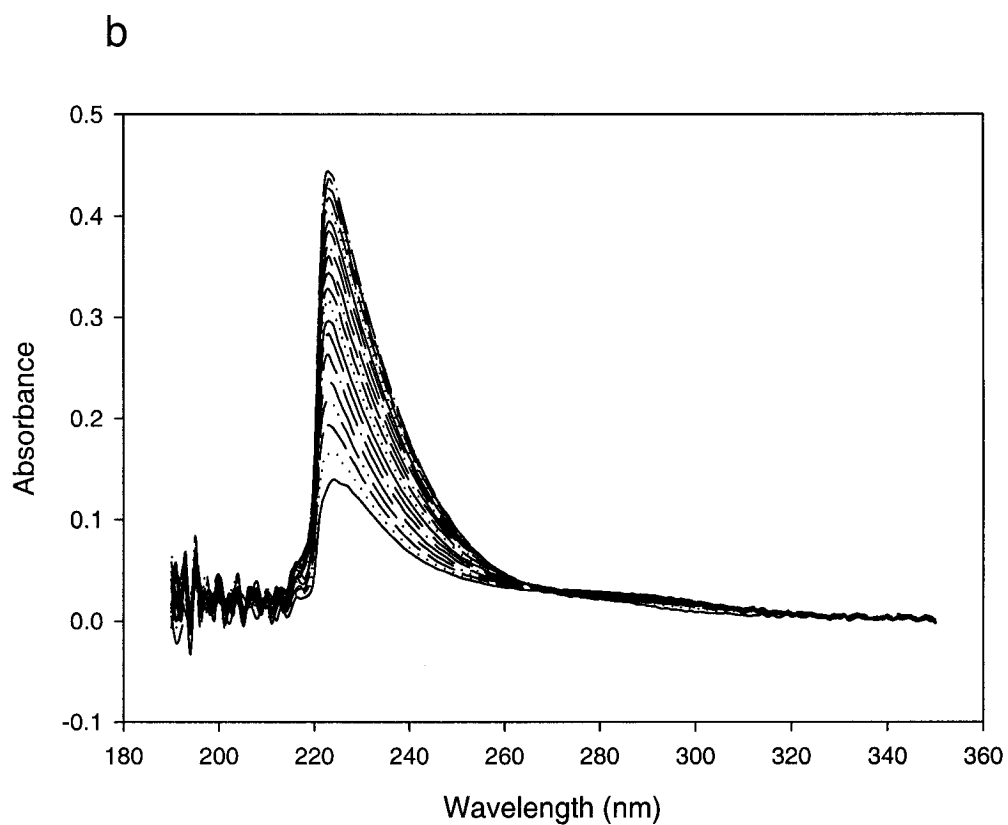


Figure 4.5 continued: (b) UV-visible spectrum of the time dependent bromination of 3-oxo-hexanoylhomoserine lactone (**1**). Spectra were collected at 30 sec intervals for 10 minutes. Reaction condition were, natural seawater ~ pH 8.0, 40 mM KBr, 40 nM partially purified V-BrPO from *D. pulchra*, 50 μ M **1**. Reaction was initiated by the addition of 1 mM H_2O_2 .

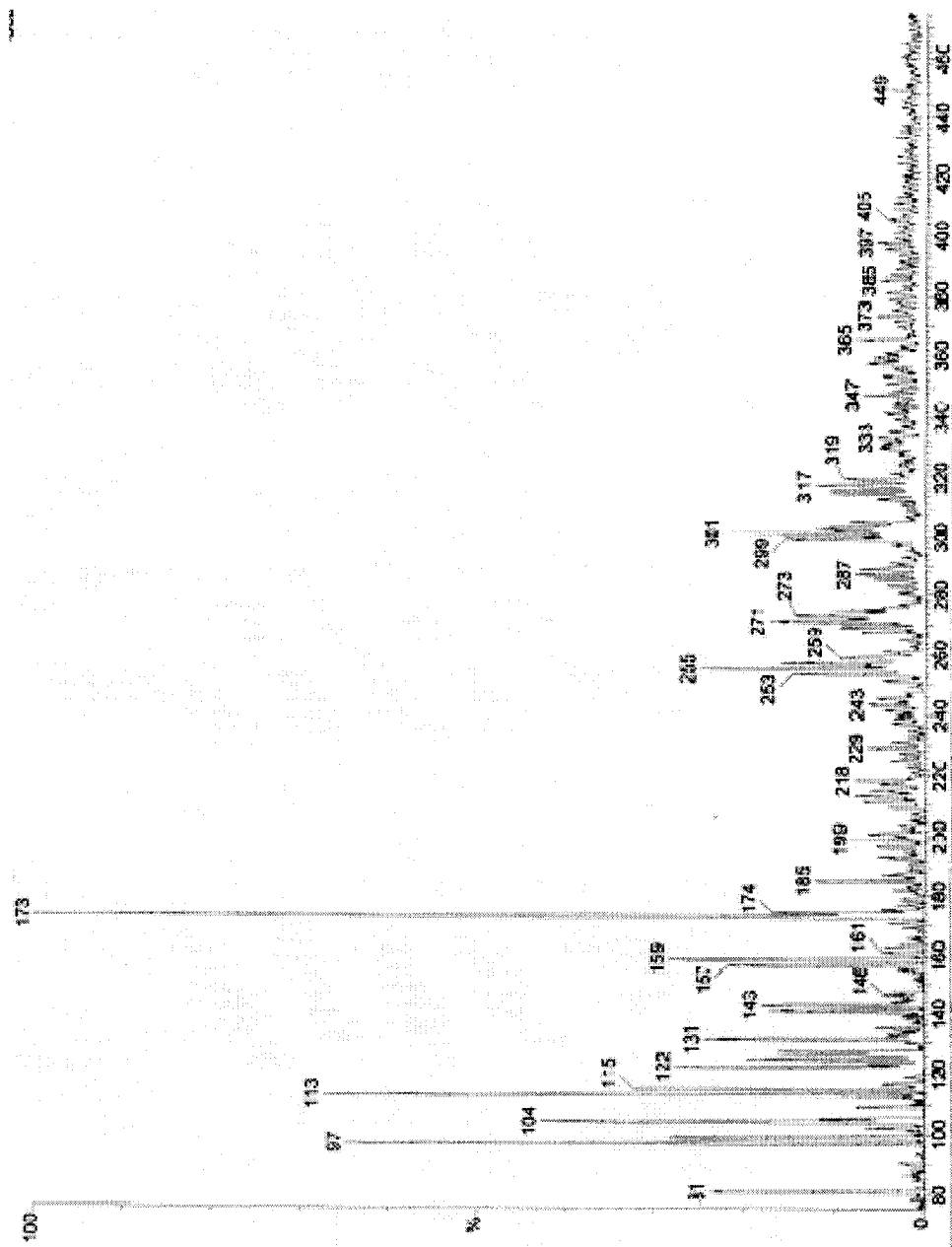
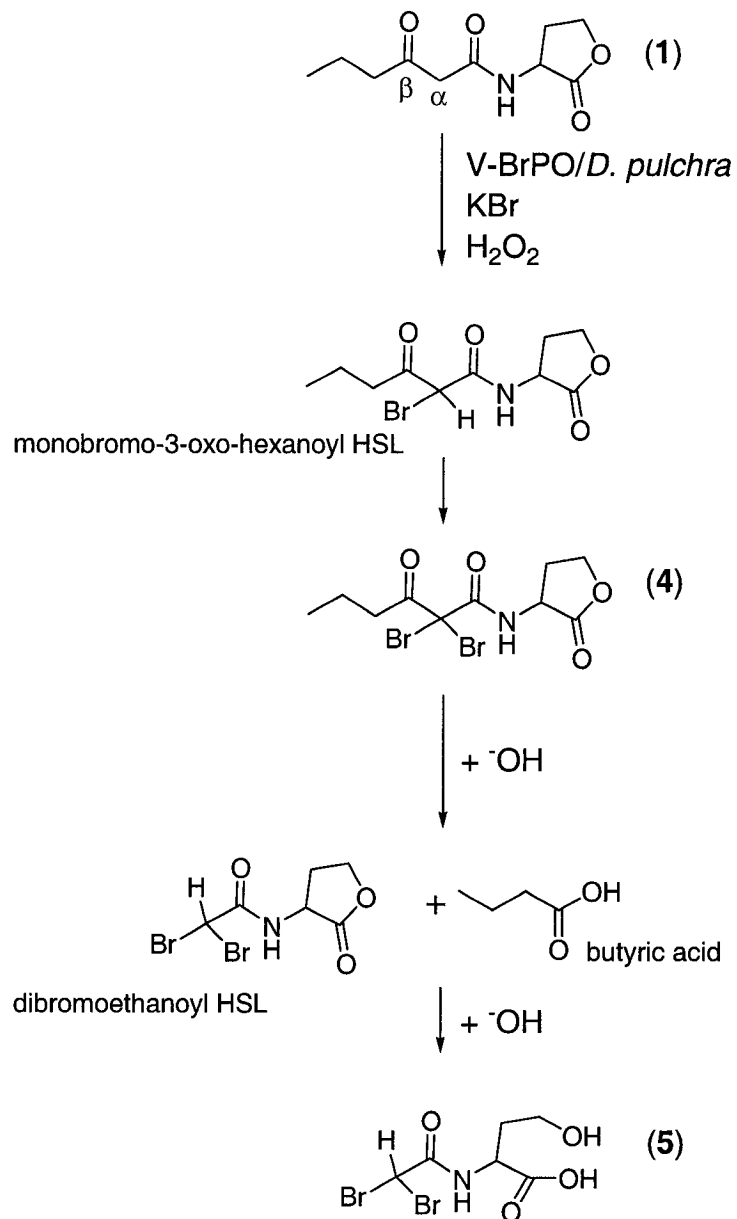


Figure 4.6: APCI mass spectrum of the sodium adduct of α,α -dibromoethanoly-2-(4-hydroxy)butanoic acid (**5**). Product **5** was generated by the bromination of 3-oxo-hexanoylhomoserine lactone ($50\ \mu\text{M}$) by whole algal pieces of *D. pulchra* upon addition of $100\ \text{mM}$ KBr in NSW ($\sim\text{pH } 8.0$), and $1 - 2\ \text{mM}$ H_2O_2 .

4.6]. The APCI spectrum confirmed dibromination of **1** occurred, as indicated by the 1:2:1 ratio of the molecular ion. The spectrum for the dihalogenated product is likely of α,α -dibromoethanoyl-2-(4-hydroxy)butanoic acid (**5**). Product **5** is proposed to form after dibromination of the α -carbon of **1**, followed by α - β hydrolysis and opening of the lactone ring moiety (Scheme 4.1). Scission of the α - β bond of α,α -dibrominated hexanoyl homoserine lactone (**4**) appears to occur at higher pH (Borchardt et al. 2001). These results are consistent with the halogenation of **1** using HOCl and stabilized hypobromite in industrial cooling water at pH 8.0, producing α,α -dibromoethanoyl-2-(4-hydroxy)butanoic acid (**5**) as the major product (Michels et al. 2000).

It is clear from these results that V-BrPO at the surface of *D. pulchra* can brominate β -keto-amide homoserine lactone molecules, where different products result at different pHs. The rate of bromination of β -diketone compounds, such as monochlorodimedone (MCD), by highly purified V-BrPO is well documented (Hager et al. 1966; Itoh et al. 1987; de Boer and Wever 1988; Everett et al. 1990b; Van Schijndel et al. 1994). Determination of bromination rates of compounds presented at the surface of the alga will serve to give a clearer understanding of the chemistry occurring at the interface between the alga and the surrounding aqueous environment. The nature of the oxidized halogen species being produced by V-BrPO at the surface of *D. pulchra* is still unclear. Additional kinetic experiments with whole algal pieces will be needed to determine whether the brominating species is freely-diffusible or if enzyme-substrate interaction occurs during bromination.



Scheme 4.1: Proposed bromination pathway of 3-oxo-hexanoylhomoserine lactone (1) by V-BrPO/*D. pulchra* (adapted from Michels 2000).

Bromination of 3-oxo-hexanoylhomo-serine lactone; effects on quorum sensing sensing activity:

As described above, V-BrPO at the surface of *D. pulchra* is able to brominate 3-oxo-hexanoylhomo-serine lactone (**1**) at the α -carbon to generate doubly brominated homo-serine lactone species. Bioassays using the reporter strain *A. tumefaciens* NTL4 were performed to determine how the ability of **1** to induce a quorum sensing response was affected by bromination. Reaction products from experiments with partially purified V-BrPO were used in these experiments. Using the *A. tumefaciens* NTL4 bioassay, the dibrominated homo-serine lactone **4** produced at pH 6.0, was not able to elicit a quorum sensing response as indicated by the lack of conversion of X-gal by β -galactosidase (Table 4.2, plate 3) [Figure 4.7]. Control reactions performed in the absence of V-BrPO (Table 4.2, plate 2) showed the strong ability of **1** to elicit a quorum sensing response as indicated by the blue-green pigment within the bacteria (conversion of X-gal by β -galactosidase) [Figure 4.7]. Table 4.2 summarizes the results of the quorum sensing bioassays with 3-oxo-hexanoylhomo-serine lactone and V-BrPO. The *A. tumefaciens* NTL4 bioassay with V-BrPO and **1** support another study where whole fronds (30 grams each) of the brown alga *Laminaria digitata* were able to brominate **1** and eliminate the ability of the signaling molecule to function in cell-to-cell communication (Borchardt et al. 2001).

Plate number	Quorum Sensing Response (+ / -)
1	pH 6.0, Effect of V-BrPO reaction without added 3-oxo-hexanoylhomoserine lactone (-)
2	pH 6.0, Effect of 3-oxo-hexanoylhomoserine lactone without added V-BrPO (+)
3	pH 6.0, Effect of V-BrPO reaction with 3-oxo-hexanoylhomoserine lactone (-)
4	NSW, Effect of V-BrPO reaction without added 3-oxo-hexanoylhomoserine lactone (-)
5	NSW, Effect of 3-oxo-hexanoylhomoserine lactone without added V-BrPO (+)
6	NSW, Effect of V-BrPO reaction with 3-oxo-hexanoylhomoserine lactone (-)

Table 4.2: Results from *A. tumefaciens* bioassay with 3-oxo-hexanoylhomoserine lactone reacted with V-BrPO (*D. pulchra*). (+) indicate a quorum sensing response (production of blue pigment), (-) indicate a loss of quorum sensing activity (lack of blue pigment).

In addition, the slow degradation of 3-oxo-hexanoylhomoserine lactone (1) occurs at alkaline pH due to hydrolysis of the lactone ring (Michels et al. 2000). The visual inspection of the bacteria for plate 5 showed a fainter blue pigment (qualitative assessment) than for plate 2, suggesting a weaker quorum sensing response, likely due to some hydrolysis of the homoserine lactone molecule in the NSW control reactions.

a

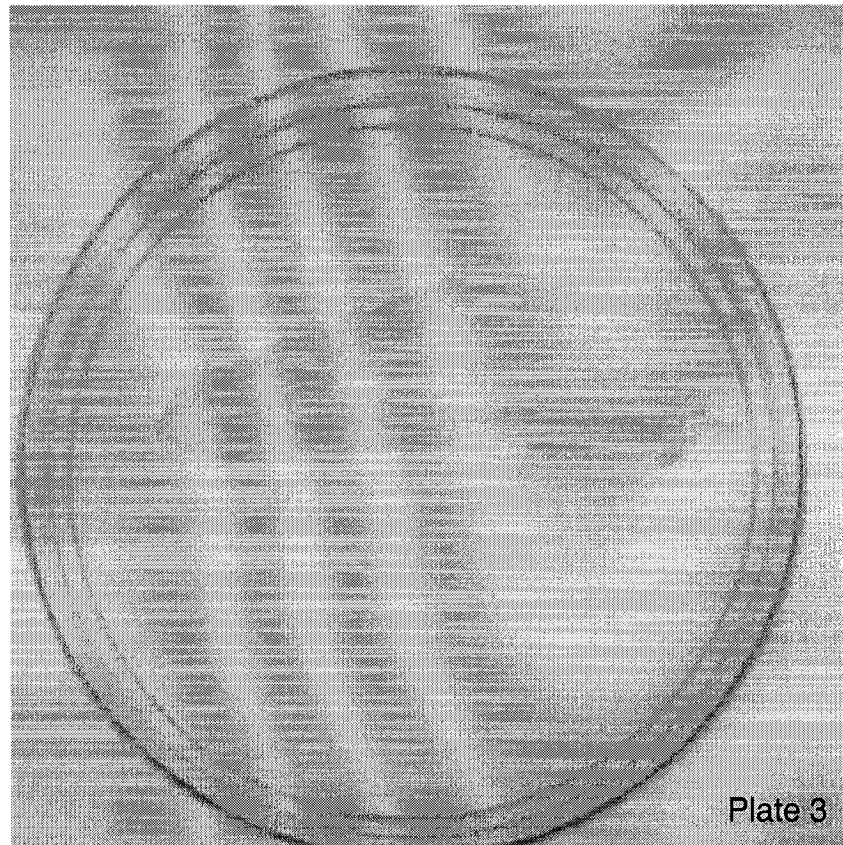


Figure 4.7: (a) Effect of V-BrPO bromination of 3-oxo-hexanoylhomoserine lactone on bioactivity with quorum sensing reporter strain *A. tumefaciens* NTL4 (plate 3). Evidence for quorum-sensing response to AHL is indicated by the expression of β -galactosidase activity (blue-green coloration) in the reporter strain. Lack of β -galactosidase activity indicates disruption of quorum sensing or lack of activity of added AHL (no blue-green coloration) in the reporter strain.

b

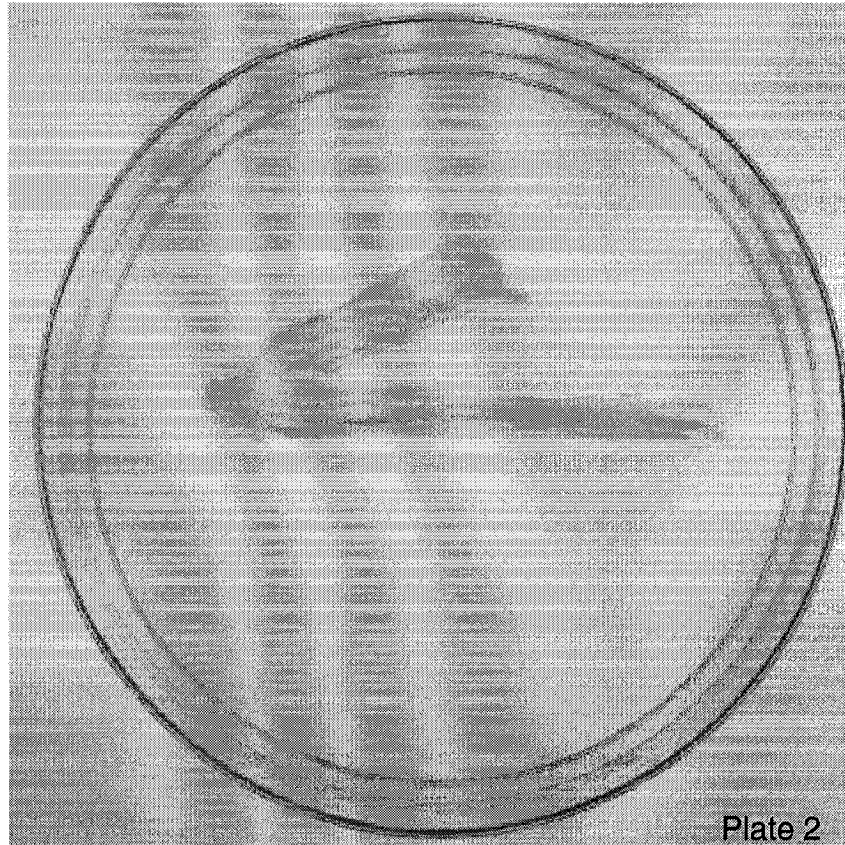


Figure 4.7 continued: (b) Control reaction of H_2O_2 , KBr and 3-oxo-hexanoyhomoserine lactone, but without added V-BrPO (plate 2). Evidence for quorum-sensing response to AHL is indicated by the expression of β -galactosidase activity (blue-green coloration) in the reporter strain (*A. tumefaciens*). Lack of β -galactosidase activity indicates disruption of quorum sensing or lack of activity of added AHL (no blue-green coloration) in the reporter strain.

Biomimetic synthesis of halogenated furanones by V-BrPO (*D. pulchra*):

Halolactonization reactions have been used for decades in the organic synthesis of halolactones and haloethers as precursors or intermediates of target molecules. V-BrPO isolated from *D. pulchra* was used to direct the bromolactonization of 4-pentynoic acid (**2**) to 5*E*-bromomethylidenetetrahydro-2-furanone (**3**). Product **3** was successfully purified from the starting acid on base-neutralized SiO₂ (1% triethylamine) using 25% ethyl acetate and hexanes. The yield of product **3** (~25%) could only be estimated due to hydrolysis of the lactone during column purifications (Krafft and Katzenellenbogen 1981; Borchardt et al. 2001). In addition, remaining starting material was detected after addition of four equivalents of hydrogen peroxide, indicating that partitioning of the oxidized halide intermediate favored the bromide-assisted disproportionation of H₂O₂ over bromination of **2**. The ¹H NMR spectrum of product **3** was identical to reported values [Figure 4.8]. V-BrPO-catalyzed halolactonization is the first report of its kind. The structure of product **3** is interesting because of its similarity to natural halogenated furanones isolated from *D. pulchra* and to synthetic halogenated furanone analogues [Figure 4.9] that disrupt cell-to-cell communications in gram-negative bacteria.

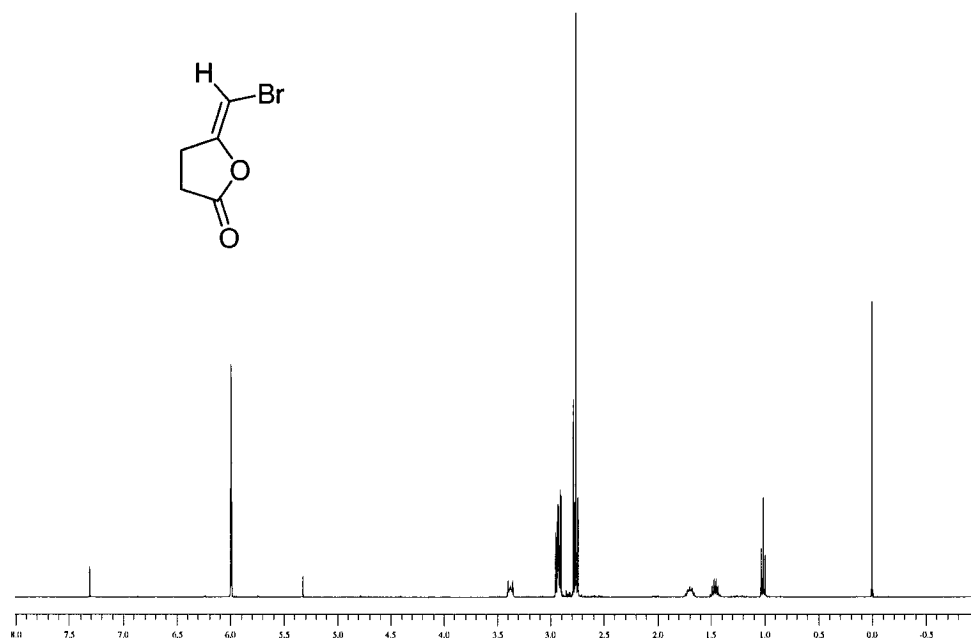


Figure 4.8: ^1H NMR of 5*E*-bromomethylenetetrahydro-2-furanone (**3**).

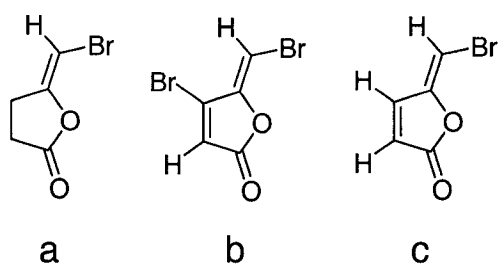


Figure 4.9: Structural comparison of (a) product **3**, and (b) & (c) synthetic halogenated furanone analogues (Manefield 2002).

Discussion

Chemical defense mediated by vanadium bromoperoxidase:

The lack of microbial fouling on the surface of the red alga *D. pulchra* has prompted research into how this alga naturally discourages biofilm formation. The discovery of halogenated furanones at the surface of *D. pulchra* which act as competitive inhibitors to AHL signal receptor proteins provided clues to the chemical means by which marine eukaryotes defend themselves against microbes. In addition to secondary metabolites acting as chemical deterrents, enzyme systems can also participate in the defense against microbial attack. Isolation of an AHL lactonase in *Bacillus* 240B1 was the first AHL-inactivating enzyme identified (Dong et al. 2000). AHL-lactonase hydrolyzes the homoserine lactone ring of AHLs, thereby decreasing AHL activity by a factor of 1000. Another enzymatic system that mediates AHL inactivation is an AHL-acylase reported in soil bacteria (Leadbetter and Greenberg 2000). AHL-acylases work to inactivate AHL signals by hydrolyzing the amide linkage between the acyl chain and the homoserine lactone headgroup.

In this study vanadium bromoperoxidase localized at the surface of *D. pulchra* was tested as an AHL-inactivating enzyme system. Oxidized halogens such as HOCl or HOBr have long been used as antimicrobial agents in natural and industrial settings. Primarily hypohalous acids have a biocidal effect against bacteria, but these compounds are also reactive with biofilm components thereby inducing biofilm dispersal (LeChevallier et al. 1990; van der Wende 1991). Recent publications demonstrated the efficiency with which oxidized halogens (HOCl and

stabilized hypobromite) reacted with 3-oxo-acyl homoserine lactone signaling molecules, resulting in the disruption of cell-to-cell communication in quorum sensing reporter strains and dispersal of *P. aeruginosa* biofilm components (Michels et al. 2000; Borchardt et al. 2001). Peroxidase enzyme systems such as myeloperoxidase and eosinophil peroxidase in human leukocytes release oxidized chloride and bromide species having bactericidal activity towards microorganisms and inactivating invading viruses (Thomas et al. 1995) (Wiess et al. 1986; Gaut et al. 2001).

In this study whole algal pieces of *D. pulchra* were shown to have very strong bromoperoxidase activity in response to added hydrogen peroxide in buffered solution (pH 6.0) and in natural NSW. V-BrPO was identified as an enzyme at the surface of the alga. V-BrPO was found to effectively inactivate 3-oxo-hexanoyl HSL (**1**) signaling molecule by dibrominating the α -carbon of the 3-oxo moiety to produce a dihalogenated acyl homoserine lactone (Scheme 4.1) (Michels et al. 2000). Acyl homoserine lactones lacking the 3-oxo moiety are not affected by oxidized halogens (Michels et al. 2000; Borchardt et al. 2001). Bromination of **1** by the V-BrPO/*D. pulchra* enzyme system effectively disrupted the bioactivity of **1** in quorum sensing reporter assays. The disruption of bioactivity by bromination of **1** is consistent with certain AHL analogs exhibiting antagonistic effects on wild-type *A. tumefaciens* TraR-AHL responsive transcriptional regulator (Zhu et al. 1998). Recently, the X-ray crystal structure of TraR bound to 3-oxo-octanoyl AHL and its target DNA was solved (Vannini et al. 2002). The AHL binding site is a narrow

cleft lined predominately with hydrophobic residues that make contacts with the AHL acyl chain. It is proposed that bromination and hydrolysis of **1** would likely disrupt necessary ligand contacts within the buried AHL-binding cleft.

Bromination of **1** has also been demonstrated using naturally produced HOBr from the marine brown alga *Laminaria digitata*, producing similar results. However, the *Laminaria* system required 15×10^3 more algal mass to brominate and inactivate **1** compared to the amount needed of *D. pulchra*. The small amounts of *D. pulchra* required to brominate **1** suggest that the bromoperoxidase response in *D. pulchra* is a more effective AHL-inactivating enzyme system.

The prerequisite for an efficient defense system against microbial fouling is the quick recognition and response of the attacked organism. Pathogen attack and defensive response by the marine brown alga *L. digitata* and the marine red alga *Gracilaria conferta* are macroalgal models that have been well studied (Weinberger et al. 1999; Kupper et al. 2001). Using these model algae, it was demonstrated that biotic or abiotic attack on the algae elicited the formation of reactive oxygen species (ROS) such as hydrogen peroxide and superoxide that contest the attacker and/or recruit additional defense systems. The production of ROS or an oxidative burst in response to pathogen attack is an evolutionary conserved defense system in plants and mammals (Bolwell 1999). Based on the macroalgal models of *Laminaria* and *Gracilaria*, a plausible mechanism utilized by *D. pulchra* is the recruitment of V-BrPO enzyme system following the release of ROS such as H_2O_2 . V-BrPO could utilize the released H_2O_2 and halides from surrounding seawater to produce oxidized

halogen antimicrobials at the surface of *D. pulchra*. The oxidized halogen species could act as an antimicrobial on the attacking bacteria, or as demonstrated in vitro, act to destroy bacterial cell-to-cell communications by bromination of AHL molecules. The efficiency of such a system would likely be dependent on the strength or rate of bromoperoxidase activity in response to the localization and concentration of released ROS. It is possible that in the absence of an oxidative burst response the V-BrPO system at the surface of the alga could also utilize hydrogen peroxide generated during photosynthesis to oxidize surrounding halides.

V-BrPO biomimetic production of halogenated-furanone type metabolites:

The biosynthetic route by which the halogenated furanones are made in *D. pulchra* is still unknown. However, it is known that these secondary metabolites are released from gland cells at the surface of the alga at biologically relevant concentrations (Dworjanyn et al. 1999). In recent studies synthetic analogues of the halogenated furanones were shown to block cell signaling and biofilm formation in *Pseudomonas aeruginosa* (Hentzer et al. 2002). Partially purified V-BrPO from *D. pulchra* was used in the biomimetic synthesis of a halogenated furanone analogue **3**. Brominated furanone **3** was the only major product detected, although the purification scheme used to obtain **3** has not been optimized and additional minor products may also be produced. It is not clear from these experiments if V-BrPO is involved in the biosynthetic route towards production of the halogenated furanones in *D. pulchra*. However, the ability of V-BrPO to direct the halolactonization of precursor molecules in the synthesis of halogenated furanone-type compounds may

expand the arsenal of chemical analogs known to act as antagonists of bacterial quorum sensing and biofilm formation (Zhu et al. 1998; Hentzer et al. 2002; Fast 2003). The ability of product **3** to mimic the halogenated furanone activity has not yet been tested.

References

- Bolwell, G. P. (1999). "Role of Active Oxygen Species and NO in Plant Defense Response." *Curr. Opin. Plant Biol.* **2**: 287-294.
- Borchardt, S. A., E. J. Allain, J. J. Michels, G. W. Stearns, R. F. Kelly and W. F. McCoy (2001). "Reaction of Acylated Homoserine Lactone Bacterial Signaling Molecules with Oxidized Halogen Antimicrobials." *Appl. Environ. Microbiol.* **67**: 3174-3179.
- Carter, J. N., K. E. Beatty, M. T. Simpson and A. Butler (2002). "Reactivity of Recombinant and Mutant Vanadium Bromoperoxidase from the Red Alga *Corallina officinalis*." *J. Inorg. Biochem.* **91**: 59-69.
- Correa, J. A. and P. A. Sanchez (1996). "Ecological Aspects of Algal Infectious Diseases." *Hydrobiologia* **326/327**: 89-96.
- de Boer, E. and R. Wever (1988). "The Reaction Mechanism of a Novel Vanadium-Bromoperoxidase. A Steady-State Kinetic Analysis." *J. Biol. Chem.* **236**: 12326-12332.
- Dong, Y. H., J. L. Xu, X. Z. Li and L. H. Zhang (2000). "AiiA, an Enzyme that Inactivates Acylhomoserine Lactone Quorum-Sensing Signal and Attenuates the Virulence of *Erwinia carotovora*." *Proc. Natl. Acad. Sci. USA* **97**: 3526-3531.
- Dworjanyn, S. A., R. De Nys and P. D. Steinberg (1999). "Localisation and Surface Quantification of Secondary Metabolites in the Red Alga *Delisea pulchra*." *Mar. Biol.* **133**: 727-736.
- Engel, S., P. R. Jensen and W. Fenical (2002). "Chemical Ecology of Marine Microbial Defense." *J. Chem. Ecol.* **28**: 1971-1985.
- Everett, R. and A. Butler (1989). "Bromide-Assisted Hydrogen Peroxide Disproportionation Catalyzed by Vanadium Bromoperoxidase: Absence of Direct Catalase Activity and Implications for the Catalytic Mechanism." *Inorg. Chem.* **28**: 393-395.
- Everett, R. R., J. R. Kanofsky and A. Butler (1990b). "Mechanistic Investigations of the Novel Non-Heme Vanadium Bromoperoxidases - Evidence For Singlet Oxygen Production." *J. Biol. Chem.* **265**: 4908-4914.
- Everett, R. R., H. S. Soedjak and A. Butler (1990a). "Mechanism of Dioxygen Formation Catalyzed By Vanadium Bromoperoxidase - Steady State Kinetic

Analysis and Comparison to the Mechanism of Bromination." J. Biol. Chem. **265**: 15671-15679.

Fast, W. (2003). "Molecular Radio Jamming: Autoinducer Analogs." Chemistry and Biology **10**: 1-3.

Gaut, J. P., G. C. Yeh, T. H. D., J. Byun, J. P. Henderson, G. M. Richter, M. L. Brennan, A. J. Lysis, A. Belaaouaj, R. S. Hotchkiss and J. W. Heinecke (2001). "Neutrophils Employ the Myeloperoxidase System to Generate Antimicrobial Brominating and Chlorinating Oxidants During Sepsis." Proc. Natl. Acad. Sci. USA **98**: 11961-11966.

Hager, L. P., D. R. Morris, F. S. Brown and H. Eberwein (1966). "Chloroperoxidase: Utilization of Halogen Anions." J. Biol. Chem. **241**: 1769-1777.

Hentzer, M., K. Riedel, T. B. Rasmussen, A. Heydorn, J. B. Andersen, M. R. Parsek, S. A. Rice, L. Eberl, S. Molin, N. Hoiby, S. Kjelleberg and M. Givskov (2002). "Inhibition of Quorum Sensing in *Pseudomonas aeruginosa* Biofilm by a Halogenated Furanone Compound." Microbiology-SGM **148**: 87-102.

Itoh, N., Y. Izumi and H. Yamada (1987). "Characterization of Nonheme Iron and Reaction-Mechanism of Bromoperoxidase in *Corallina pilulifera*." J. Biol. Chem. **262**: 11982-11987.

Krafft, G. A. and J. A. Katzenellenbogen (1981). "Synthesis of Halo Enol Lactones. Mechanism-Based Inactivators of Serine Proteases." J. Am. Chem. Soc. **103**: 5459-5466.

Kupper, F. C., B. Kloareg, J. Guern and P. Potin (2001). "Oligoguluronates Elicit an Oxidative Burst in Brown Algal Kelp, *Laminaria Digitata*." Plant Physiol. **125**: 278-291.

Lambert, J. B., H. F. Shurvell, D. A. Lightner and R. G. Cooks (1998). Organic Structural Spectroscopy. Upper Saddle River, New Jersey, Prentice Hall.

Leadbetter, J. R. and E. P. Greenberg (2000). "Metabolism of Acyl-Homoserine Lactone Quorum-Sensing Signals by *Variovorax paradoxus*." J. Bacteriol. **182**: 6921-6926.

LeChevallier, M. W., C. D. Lowry and R. G. Lee (1990). "Disinfecting Biofilm in a Model Distribution System." J. Am. Water Works Assoc. **82**: 87-99.

Lewandowski, Z. (1994). Dissolved Oxygen Gradients Near Microbially Colonized Surfaces. Biofouling and Biocorrosion in Industrial Water Systems. G. G. Geesey, Lewandowski, Z. and Flemming, H. C. Boca Raton, Lewis Publishers.

Littler, M. M. and D. S. Littler (1995). "Impact of CLOD Pathogen on Pacific Coral Reefs." *Science* **267**: 1356-1360.

Manefield, M., T. B. Rasmussen, M. Henzter, J. B. Andersen, P. D. Steinberg, S. Kjelleberg and M. Givskov (2002). "Halogenated Furanones Inhibit Quorum Sensing Through Accelerated LuxR Turnover." *Microbiology* **148**: 1119-1127.

Manefield, M., M. Welch, M. Givskov, G. P. Salmond and S. Kjelleberg (2001). "Halogenated Furanones from the Red Alga *Delisea pulchra*, Inhibit Carbapenem Antibiotic Synthesis and Exoenzyme Virulence Factor Production in the Phytopathogen *Erwinia carotovora*." *FEMS Microbiol. Lett.* **205**: 131-138.

Maximilien, R., R. De Nys, R. Holmstrom, C. Gram, S. Kjelleberg and P. D. Steinberg (1998). "Bacterial Fouling is Regulated by Secondary Metabolites from the Red Alga *Delisea pulchra*." *Aquat. Microb. Ecol.* **15**: 233-246.

Michels, J. J., E. J. Allain, S. A. Borchardt, P. Hu and W. F. McCoy (2000). "Degradation Pathway of Homoserine Lactone Bacterial Signal Molecules by Halogen Antimicrobials Identified by Liquid Chromatography with Photodiode Array Mass Spectrometric Detection." *J. Chromatogr.* **898**: 153-165.

Rasmussen, T. B., M. Manefield, J. B. Andersen, L. Eberl, U. Anthoni, C. Christophersen, P. D. Steinberg, S. Kjelleberg and M. Givskov (2000). "How *Delisea pulchra* Furanones Affect Quorum Sensing and Swarming Motility in *Serratia liquefaciens*." *Microbiology* **146**: 3237-3244.

Reinheimer, G. (1992). Aquatic Microbiology, 4th ed. New York, Wiley.

Sand-Jensen, K. (1977). "Effects of Epiphytes on Eelgrass Photosynthesis." *Aquatic Botany* **3**: 55-63.

Steinberg, P. D., R. Schneider and S. Kjelleberg (2001). "Chemical Defense of Seaweeds Against Microbial Colonization." *Biodegradation* **8**: 211-220.

Stickler, D. J., N. S. Morris, R. J. McLean and C. Fuqua (1998). "Biofilms on Indwelling Urethral Catheters Produce Quorum-Sensing Signal Molecules In Situ and In Vitro." *Appl. Environ. Microbiol.* **64**: 3486-3490.

- Thomas, E. L., P. M. Bozeman, M. M. Jefferson and C. C. King (1995). "Oxidation of Bromide by Human Leukocyte Enzymes Myeloperoxidase and Eosinophil Peroxidase: Formation of Bromamines." *J. Biol. Chem.* **270**: 2906-2913.
- van der Wende, E. (1991). Biocide Action of Chlorine on *Pseudomonas aeruginosa* Biofilm. Bozeman, Montana State University.
- Van Schijndel, J., P. Barnett, J. Roelse, E. Vollenbroek and R. Wever (1994). "The Stability and Steady-State Kinetics of Vanadium Chloroperoxidase from the Fungus *Curvularia inaequalis*." *Eur. J. Biochem.* **225**: 151-157.
- Vannini, A., C. Volpari, C. Gargioli, E. Muraglia, R. Cortese, R. De Francesco, P. Neddermann and S. Di Marco (2002). "The Crystal Structure of the Quorum Sensing Protein TraR Bound to its Autoinducer and Target DNA." *EMBO J.* **21**: 4393-4401.
- Wahl, M. (1995). "Bacterial Epibiosis on Bahamian and Pacific Ascidiarians." *J. Exp. Mar. Biol. Ecol.* **191**: 239-255.
- Weinberger, F., M. Friedlander and H. G. Hoppe (1999). "Oligoagars Elicit a Physiological Response in *Gracilaria conferta* (Rhodophyta)." *J. Phycol.* **35**: 747-755.
- Whitehead, N. A., A. M. Barnard, H. Slater, N. J. Simpson and G. P. Salmond (2001). "Quorum-Sensing in Gram-Negative Bacteria." *FEMS Microbiol. Rev.* **25**: 365-404.
- Wiess, S. J., S. T. Test, C. M. Eckmann, D. Roos and S. Regiani (1986). "Brominating Oxidants Generated by Human Eosinophils." *Science* **234**: 200-203.
- Zhu, J., J. W. Beaver, M. I. More, C. Fuqua, A. Eberhard and S. C. Winans (1998). "Analogues of the Autoinducer 3-Oxooctanoyl-Homoserine Lactone Strongly Inhibit Activity of the TraR Protein of *Agrobacterium tumefaciens*."

Chapter Five

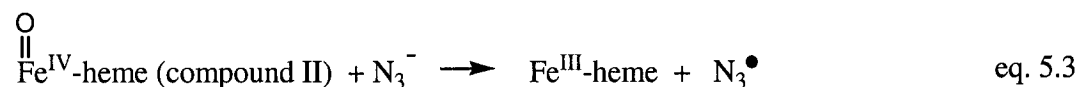
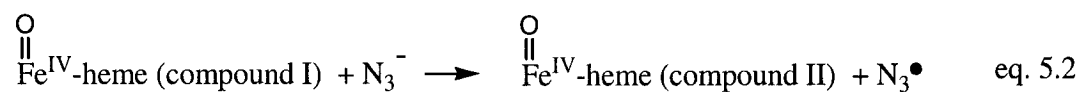
Azide Inhibition of Vanadium Bromoperoxidase from the

Red Alga *Corallina officinalis*

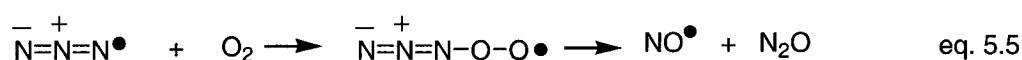
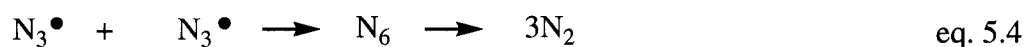
Introduction

Azide inhibition of iron heme peroxidases has been studied for many decades. Much of the understanding of how azide inhibits metalloproteins has been learned from heme peroxidases. Heme peroxidases such as chloroperoxidase from *Caldariomyces fugmago* (Samokyszyn and Ortiz de Montellano 1991), horseradish peroxidase from the root of horseradish plant (Ortiz de Montellano et al. 1988), myeloperoxidase from blood leukocytes (Kalyanaraman et al. 1985), *Coprinus macrorhizus* peroxidases (DePillis and Ortiz de Montellano 1989), lignin peroxidase from the white rot fungus *Phanerochaete chrysosporium* (DePillis et al. 1990), and yeast cytochrome c peroxidase from *Saccharomyces cerevisiae* (DePillis et al. 1991) are all irreversibly inactivated by azide.

Horseradish peroxidase, chloroperoxidase, lactoperoxidase, and myeloperoxidase in the presence of azide and hydrogen peroxide all catalyze the one electron oxidation of the azide anion by compounds I and II to form the azidyl free radical, as determined by ESR spin trapping experiments (equations 5.1 – 5.3) (Kalyanaraman et al. 1985).



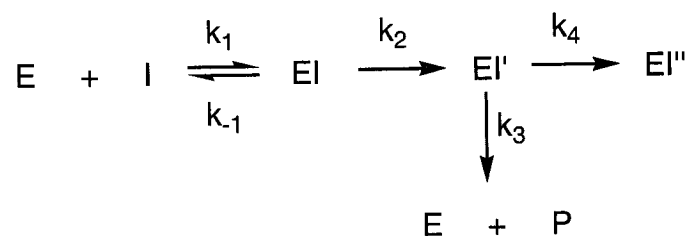
In these experiments oxygen uptake during oxidation of azide and the production of gaseous nitrogenous products (N_2 , NO , N_2O) were detected (Kalyanaraman et al. 1985). Molecular nitrogen is proposed to form via the rapid dimerization of azidyl radicals ($2k = 9 \times 10^9 \text{ M}^{-1} \text{ s}^{-1}$) (equation 5.4) (Hayon and Simic 1970), whereas formation of NO and N_2O are proposed to form by reaction of the azidyl radical with molecular oxygen (equation 5.5) (Theorell and Ehrenberg 1952; Keilin and Hartree 1954; Keilin and Nicholls 1958). Reactions between the azidyl radical and molecular oxygen to form nitrogenous products are reported to be relatively slow (i.e., $\leq 10^6 \text{ M}^{-1} \text{ s}^{-1}$) compared to dimerization of the azidyl radical, however the formation of NO and N_2O catalyzed by Fe-heme peroxidases is best explained by reaction between azide and oxygen (Hayon and Simic 1970; Eriksen et al. 1981). It has been postulated that compound I may mediate formation of an oxygen-azide intermediate that dissociates from the enzyme to form NO and N_2 (Tatarko and



Bumpus 1997).

Subsequent biochemical studies of azide inactivation of horseradish peroxidases showed the catalytically generated azidyl radical covalently modified the δ -meso edge of the heme moiety, thus inactivating the enzyme (Ortiz de Montellano et al. 1988). Similar heteroatom additions to the prosthetic heme group were obtained using the peroxidases from *Coprinus macrorhizus* using phenylhydrazine or azide and with lignin peroxidase using azide (DePillis and Ortiz de Montellano 1989; DePillis et al. 1990).

Early reports of the marine derived vanadium-dependent bromoperoxidases (V-BrPO) were not clear regarding V-BrPO inhibition by azide (Vilter 1983). V-BrPO from the brown alga *Ascophyllum nodosum* (AnV-BrPO) was reported not to be affected by 1 mM azide, although the reaction conditions were not described (Wever et al. 1985). In contrast, V-BrPO isolated from the red alga *Corallina pilulifera* was reported to be reversibly inactivated by 1 mM azide as well as 1 mM phenylhydrazine (Itoh et al. 1986). Richard R. Everett (Everett 1990) and Helena S. Soedjak (Soedjak 1991) established that AnV-BrPO was irreversibly inactivated by azide under catalytic conditions. Azide was determined to fulfill the requirements of a mechanism-based inactivator of AnV-BrPO (Silverman 1988; Soedjak 1991). Mechanism-based enzyme inactivation results from a relatively inert compound, similar in structure to a substrate or product, being activated by an enzymatic process to a species that binds to the enzyme and inactivates it (Silverman 1988). Mechanism-based inactivation is generally characterized by;



AnV-BrPO was inactivated by azide in a time-dependent manner and was protected against inactivation by substrates bromide and chloride (Soedjak 1991). The binding constant of azide (K_I) to *AnV*-BrPO was 24 mM with a rate of inactivation (k_{inact}) of 1.2 min^{-1} . Initial experiments suggested that the vanadium-dependent peroxidases catalyze the oxidation of azide to an activated azide intermediate, which then reacts with the protein matrix (Soedjak 1991). The nature of the azide oxidation, and the identity of the activated azide intermediate (an azidyl radical in the case of horseradish peroxidases) have not been determined.

Described in this chapter is the azide inactivation of *V*-BrPO from the red alga *Corallina officinalis* (*CoV*-BrPO). The study examined the differences in the ranges of azide concentrations required to inactivate *CoV*-BrPO compared to *AnV*-BrPO, saturation kinetics, bromide protection against inactivation, and the indirect detection of gaseous nitrogenous products during azide inactivation.

Methods and Materials

General methods:

Vanadium bromoperoxidase from the marine algae *Corallina officinalis* (CoV-BrPO) was isolated as described previously (Carter et al. 2002). Enzyme stock solutions were stored in 50 mM Tris-HCl, pH 8.0 or 50 mM HEPES, pH 7.0 at 4 °C. Concentrations of H₂O₂ (30% aqueous solutions) were determined spectrophotometrically by the formation of triiodide (I₃⁻) (Bjorksten 1968). Protein concentrations were determined by the bicinchoninic acid assay (BCA) (Pierce Chemical Co.). Monochlorodimedone (MCD) was purchased from Sigma, and used as received. All other materials were reagent grade.

Bromoperoxidase activity measurements:

Bromoperoxidase activity was measured spectrophotometrically by the bromination of MCD: $\Delta\epsilon = 19,900 \text{ M}^{-1} \text{ cm}^{-1}$ at 290 nm (Hewson and Hager 1980). The standard assay conditions consisted 50 μM MCD, 0.1 M KBr in 0.1 M phosphate/0.2 M Na₂SO₄ pH 6.5. Reactions were initiated by the addition of H₂O₂ to a final concentration of 2 mM. Specific activity is expressed in units per milligram, which is defined as the micromoles of MCD brominated per minute per milligram of bromoperoxidase. Specific activity of CoV-BrPO isolated from *C. officinalis* was ca. 150 – 200 U/mg.

Kinetics of inactivation of V-BrPO by sodium azide:

Saturation kinetics for the inactivation of CoV-BrPO by azide was performed at 4 °C in order to use a wide range of azide concentrations. Reactions for

inactivation with azide were prepared in 1.5 mL Eppendorf tubes with 0.1 M HEPES buffer (pH 6.0), various concentrations of azide (0.025 mM – 5 mM) and CoV-BrPO (132 nM) (total reaction volume, 250 μ L) at 4 °C. Reactions were allowed to equilibrate at the above temperature for 15 minutes prior to initiation of the reaction with H₂O₂ (1 mM, final concentration). Aliquots (20 μ L) were removed at 30 sec intervals for 8 minutes. Aliquots were diluted into 980 μ L of standard MCD buffer (0.1 M phosphate/ 0.2 M Na₂SO₄ buffer pH 6.5, containing 0.1 M KBr and 50 μ M MCD) equilibrated at 4 °C in Eppendorf tubes. Remaining CoV-BrPO activity was measured by transferring 990 μ L of each solution to a cuvette and the reaction was initiated by the addition of 10 μ L of 0.2 M H₂O₂ for a final concentration of 2 mM.

The rate of inactivation by azide (k_{obs}) at each azide concentration was calculated using a linear regression program on the data points of the log of the percent (%) remaining activity *versus* time. The saturation kinetic curve was obtained by plotting the rates of inactivation (k_{obs}) by azide *versus* [azide] concentration. The binding constant of azide to CoV-BrPO (K_I) could be calculated from the double reciprocal plot of the inactivation rates as a function of azide concentration.

Partition ratio titration:

CoV-BrPO (20 nM) was incubated at 4 °C for 3 hours in 50 mM HEPES buffer pH 6.0 and various concentrations of azide (0 – 1 mM) and H₂O₂ (1 mM).

The remaining enzyme activity of each solution was measured by diluting 20 μL aliquots into MCD buffer and assayed as described above.

Protection against azide inactivation by bromide:

CoV-BrPO was incubated with H_2O_2 (2 mM) and various concentrations of azide (from 0.200 mM to 5 mM), and bromide (from 0.250 mM to 2.5mM) in 50 mM HEPES (pH 6.0) at 4 $^\circ\text{C}$. The remaining enzyme activity as a function of time for each solution was measured by diluting 20 μL aliquots into MCD buffer and assaying as described above.

The rates of inactivation by azide in the presence of bromide (k_{obs}) at each specific azide concentration were calculated by a linear regression program on the data points of the log of the percent (%) remaining activity *versus* time.

Production of $\text{NO}\cdot$ during azide inactivation of *CoV*-BrPO:

Experiments to determine if low concentrations of nitric oxide are produced during azide inactivation of *CoV*-BrPO were performed using the fluorescent substrate 4-amino-5-methylamino-2',7'-difluorescein (DAF-FM). DAF-FM was purchased from Molecular Probes and suspended in 350 μL of anhydrous DMSO upon receipt. DAF-FM was stored covered in foil at $-20\text{ }^\circ\text{C}$. DAF-FM alone has a very weak quantum yield (~ 0.005), but its quantum yield increases (~ 0.81) after reaction with nitric oxide (Kojima et al. 1999) [Figure 5.1]. The azide inactivation of *V*-BrPO was performed in a microtiter plate assay in the presence of DAF-FM in order to test for production of nitric oxide. The reaction medium consisted of 2 mM

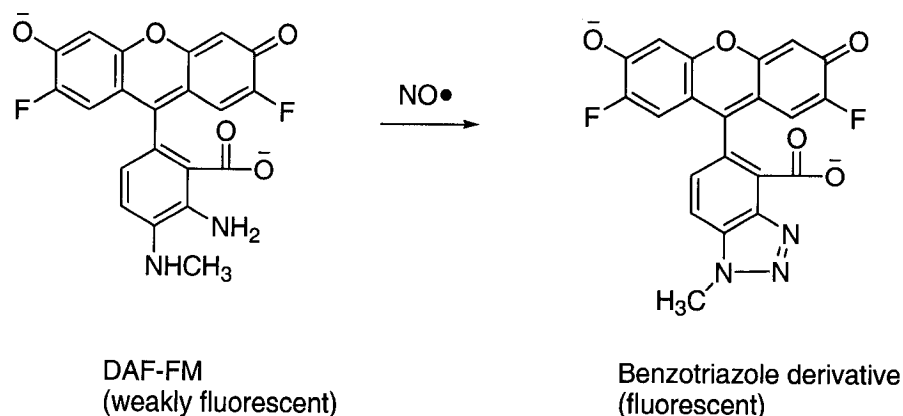


Figure 5.1: Reaction scheme for the detection of nitric oxide (NO) using DAF-FM.

azide, 8.75 μM DAF-FM, 132 nM CoV-BrPO in 0.1 M HEPES (pH 6.0) in a final volume of 250 μL . The reaction was initiated by the addition of H_2O_2 to a final concentration of 2 mM. Spectra were recorded on a Varian Cary Eclipse Fluorimeter with a 96-well microtiter plate platform. The reaction was excited at 490 nm and emission was monitored between 500 – 600 nm. Spectra were recorded every minute for 10 minutes. Control reactions were performed in the absence of added H_2O_2 . Substrate protection by bromide was performed with 20 mM KBr added to the above reaction medium.

Results

Time dependent inactivation of *CoV*-BrPO by sodium azide:

Incubation of *CoV*-BrPO with fixed concentrations of hydrogen peroxide and varied concentrations of azide resulted in the time-dependent, first order inactivation of *CoV*-BrPO by azide, consistent with a model for mechanism-based inactivation [Figure 5.2]. Mechanism based inactivation can be described by equations 5.6 and 5.7 (Kitz and Wilson 1962; Silverman 1988).

$$\frac{\delta \ln [E]}{\delta t} = k_{\text{obs}} \quad \text{eq. 5.6}$$

$$k_{\text{obs}} = \frac{k_{\text{inact}} [I]}{K_I + [I]} \quad \text{eq. 5.7}$$

Where [E] is the concentration of *CoV*-BrPO, [I] is the concentration of azide and K_I is the concentration of azide that produces half of the maximal rate of inactivation. The rate constant k_{inact} is a complex mixture of rates k_2 , k_3 , k_4 , etc. When initial experiments were performed at 25 °C saturation kinetics, for enzyme inactivation were not observed. Lowering the reaction temperature to 4 °C produced enzyme saturation for *CoV*-BrPO inactivation. The slopes of the lines of log % remaining activity (k_{obs}) were found to be dependent on azide concentrations.

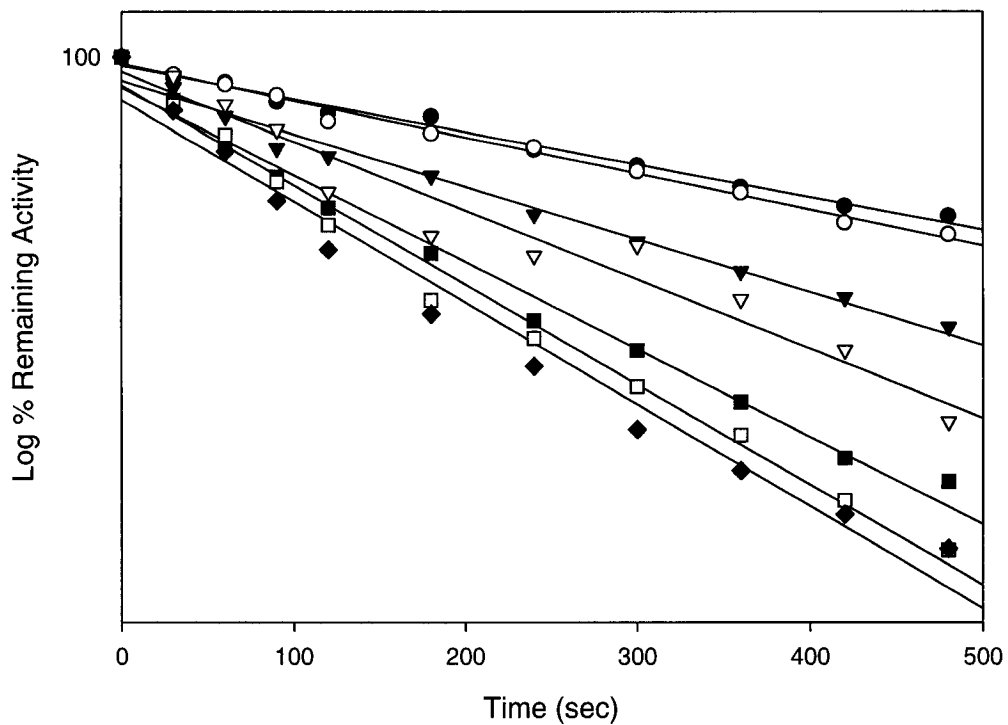


Figure 5.2: Plots of log% remaining activity vs. time ● 50 μM azide, ○ 75 μM azide, ▼ 100 μM azide, ▽ 125 μM azide, ■ 175 μM azide, □, 250 μM azide, ◆ 400 μM azide. CoV-BrPO (132 nM) was incubated with 1 mM H_2O_2 and various azide concentrations in 50 mM HEPES pH 6.0 at 4 °C.

Plots of k_{obs} for each azide concentration showed saturation kinetic behavior [Figure 5.3]. At low concentrations of azide the rate of inactivation was proportional to azide concentration, whereas at high concentrations of azide inactivation was saturating. Saturation kinetics of azide inactivation of CoV-BrPO occurred in the concentration range of 25 – 400 μM azide.

The plot of enzyme half-life ($t_{1/2}$) at each azide concentration *versus* the reciprocal azide concentration produced a straight line, indicating at infinite azide concentration there is a finite half-life for enzyme inactivation (intercept of ordinate is greater than zero) [Figure 5.4]. The equation for the half-life of CoV-BrPO against azide inactivation can be derived from equation 5.8 (Silverman 1988).

$$t_{1/2} = \frac{0.69}{k_{\text{inact}}} + \frac{0.69 K_1}{k_{\text{inact}}[\text{I}]} \quad \text{eq. 5.8}$$

The value for the half-life of CoV-BrPO ($t_{1/2}$) against azide inactivation was determined from Figure 5.2, where $t_{1/2}$ is equal to the incubation time at which 50% of initial bromoperoxidase activity remained. From the plot of half-life *versus* reciprocal azide the y-axis intercept corresponds to the rate constant of inactivation at saturation, and the x-axis intercept gives the $1/K_1$ value. The K_1 value at saturation for sodium azide is 400 μM , and indicates that sodium azide binds reversibly to CoV-BrPO prior to conversion to the reactive intermediate. In addition, the rate constant at saturation ($k_{\text{inact}} = 0.693/t_{1/2}$) is 0.364 min^{-1} , and shows that the value of

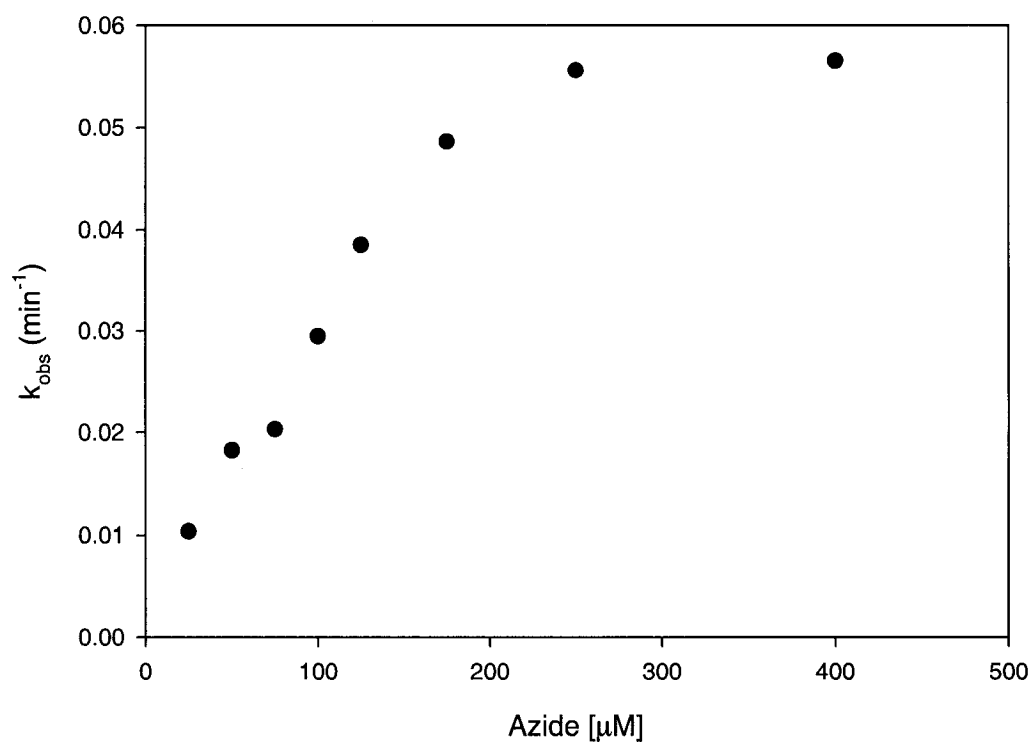


Figure 5.3: Saturation kinetic plot of k_{obs} vs. azide concentration. Reaction conditions: CoV-BrPO (132 nM) was incubated with 1 mM H_2O_2 and various azide concentrations in 50 mM HEPES pH 6.0 at 4 °C. K_{obs} were determined from slopes of the line of log% remaining activity *versus* time [Figure 5.2].

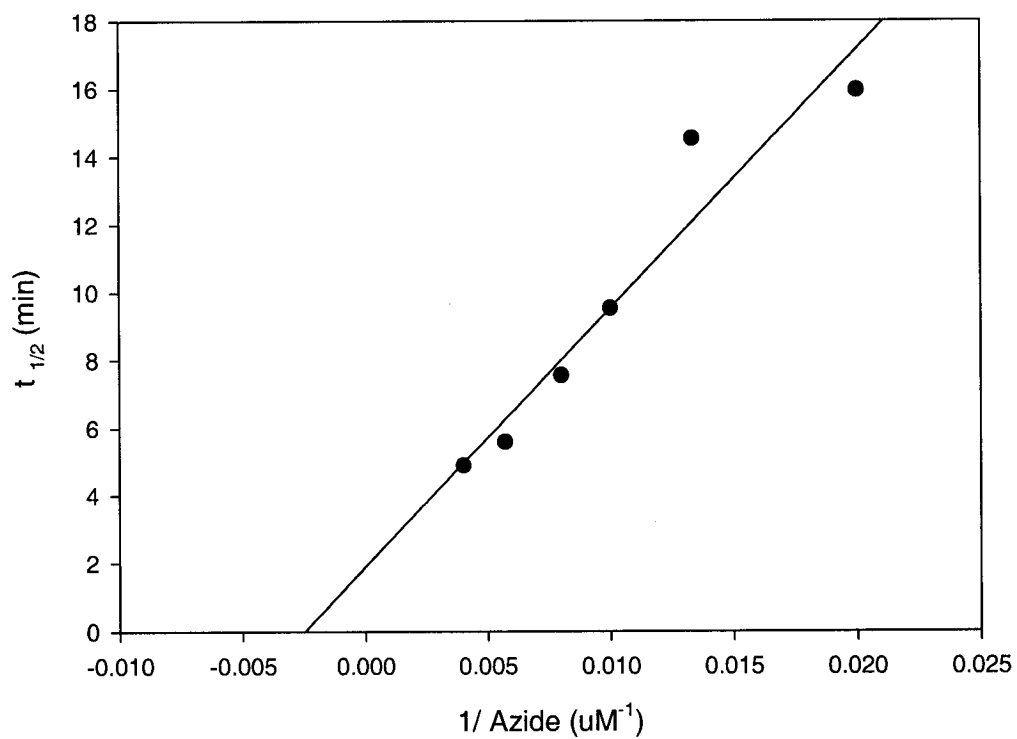


Figure 5.4: Plot of half-life of *CoV-BrPO* vs. reciprocal azide concentration. Reaction conditions: *CoV-BrPO* (132 nM) was incubated with 1 mM H_2O_2 and various azide concentrations in 50 mM HEPES (pH 6.0) at 4 °C.

k_{inact} is low and enzyme inactivation does not occur very quickly under these conditions. The inactivation of V-BrPO by sodium azide was found to occur irreversibly. Bromoperoxidase activity could not be restored when the incubation mixtures were buffer-exchanged by gel-filtration or dialysis to remove azide and peroxide.

Stoichiometry of azide binding to CoV-BrPO:

The number of azide binding sites to CoV-BrPO was evaluated using the Hill equation (equation 5.9) (Segel 1975)

$$\frac{v}{V_{\text{max}}} = \frac{[S]^n}{K' + [S]^n} \quad \text{eq. 5.9}$$

The number of azide binding sites per molecule of CoV-BrPO is designated by (n). In addition, K' is a constant describing interaction factors a , b , c , as well as the intrinsic dissociation constant K_s (Segel 1975). The Hill equation can be rewritten in the useful linear form of equation 5.10.

$$\log \frac{v}{V_{\text{max}} - v} = n \log [S] - \log K' \quad \text{eq. 5.10}$$

A plot of $\log[v / (V_{\text{max}} - v)]$ versus $\log [S]$ should results in a straight line with a slope of n. For azide binding to CoV-BrPO, v is described by k_{obs} , determined from

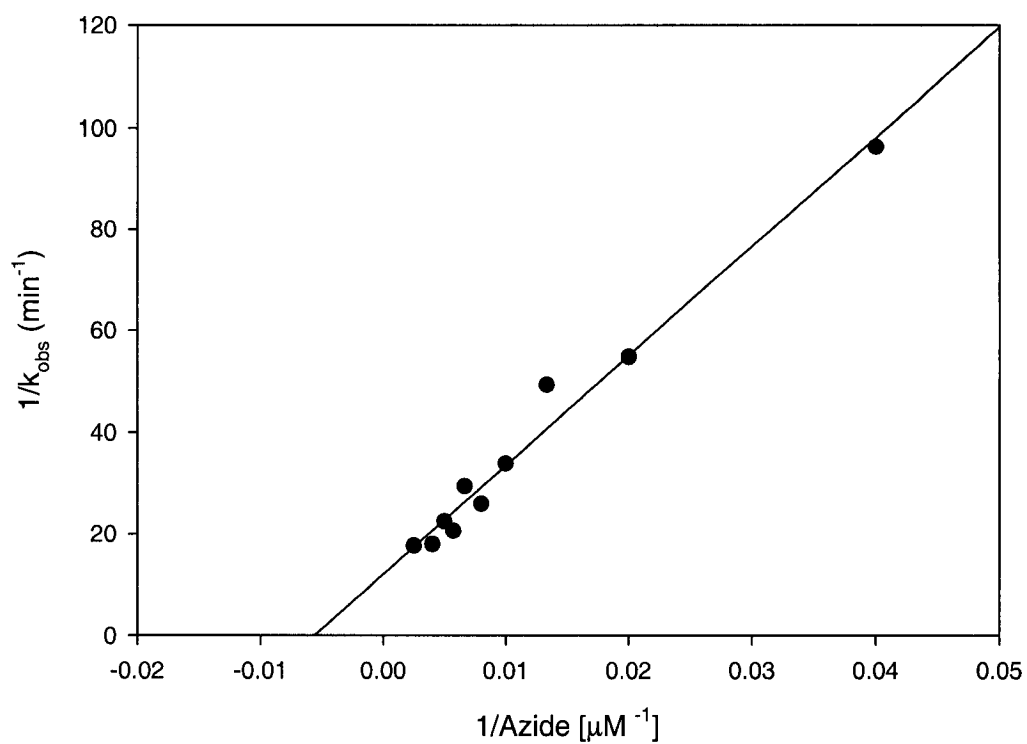


Figure 5.5: Double reciprocal plot of k_{obs} vs. azide concentration. Reaction conditions: CoV-BrPO (132 nM) was incubated with 1 mM H_2O_2 and various azide concentrations in 50 mM HEPES pH 6.0 at 4 °C. K_{obs} were determined from slopes of the line of log% remaining activity versus time [Figure 5.2].

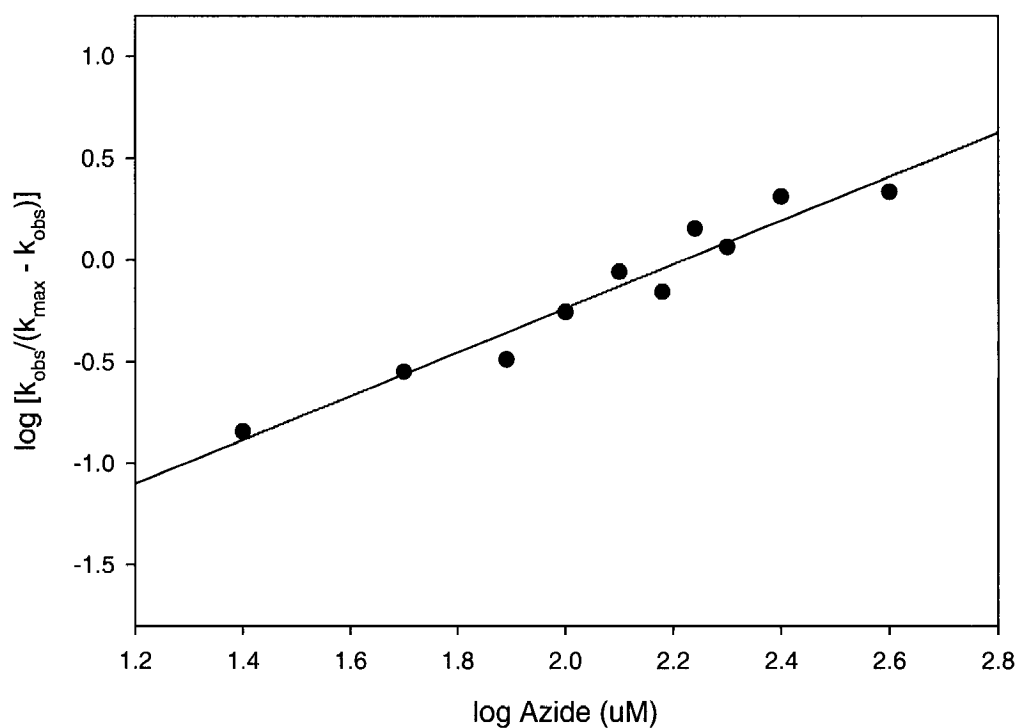


Figure 5.6: Stoichiometry of azide binding to CoV-BrPO. Plot of $\log (k_{\text{obs}} / (k_{\text{max}} - k_{\text{obs}}))$ vs. $\log [\text{azide}]$ (Hill Plot). The number of azide binding sites (n) was obtained from the slope of the line. The slope of the line is 1.07.

the time-dependent inactivation of CoV-BrPO (Figure 5.2). V_{\max} in equation 5.10 is described by the maximal value of k_{obs} (k_{max}). k_{max} was calculated from the reciprocal of the intercept at the y-axis of the double reciprocal plot of k_{obs} versus azide concentration [Figure 5.5]. The number of binding sites (n) was obtained from the slope of the line of $\log [k_{\text{obs}} / (k_{\text{max}} - k_{\text{obs}})]$ versus $\log [\text{azide}]$ [Figure 5.6]. The slope of line in Figure 5.6 is 1.07.

Partition ratio for the inactivation of CoV-BrPO:

The dependence between the extent of CoV-BrPO inactivation by azide was determined in incubations where increasing amounts of azide were added to a constant concentration of CoV-BrPO. Reactions were initiated with a constant concentration of hydrogen peroxide (2 mM). The plot of the percent remaining activity versus the ratio of the concentrations of azide to CoV-BrPO is linear at lower ratios of azide to CoV-BrPO, and non-linear at higher ratios [Figure 5.7]. A non-linear loss of enzyme activity at higher ratios is common, possibly due to a product inhibition or product protection of the enzyme toward further inactivation (Silverman 1988). The maximal amount of azide inactivation achieved was 80%. Figure 5.8 shows a plot of *vulnerable* activity that remains versus $[\text{azide}]/[\text{CoV-BrPO}]$. The *vulnerable* activity was obtained by subtracting the observed 20% residual activity from all the other rate constants and assumes that 100% activity corresponds to the corrected value in the absence of azide. Extrapolation of the linear portion of the curve gives a partition ratio of approximately 1200 molecules of azide per CoV-BrPO molecule needed for complete inactivation at 4 °C.

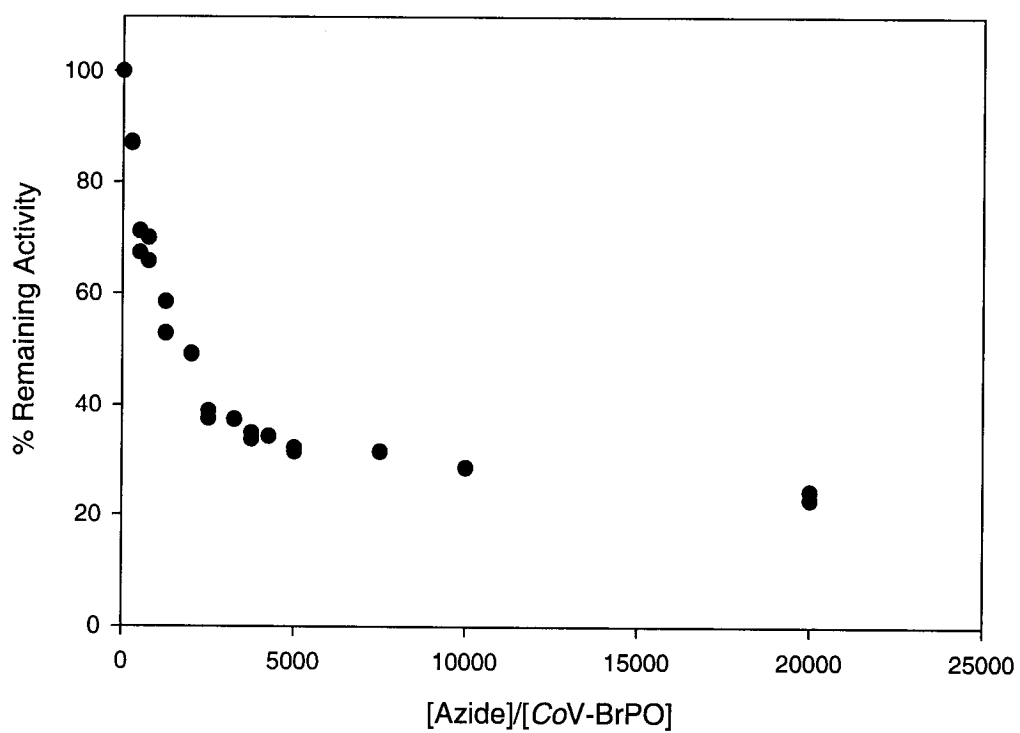


Figure 5.7: Plot of percent remaining *CoV-BrPO* MCD activity vs. $[\text{azide}]/[\text{CoV-BrPO}]$. The reaction conditions are described in Materials and Methods.

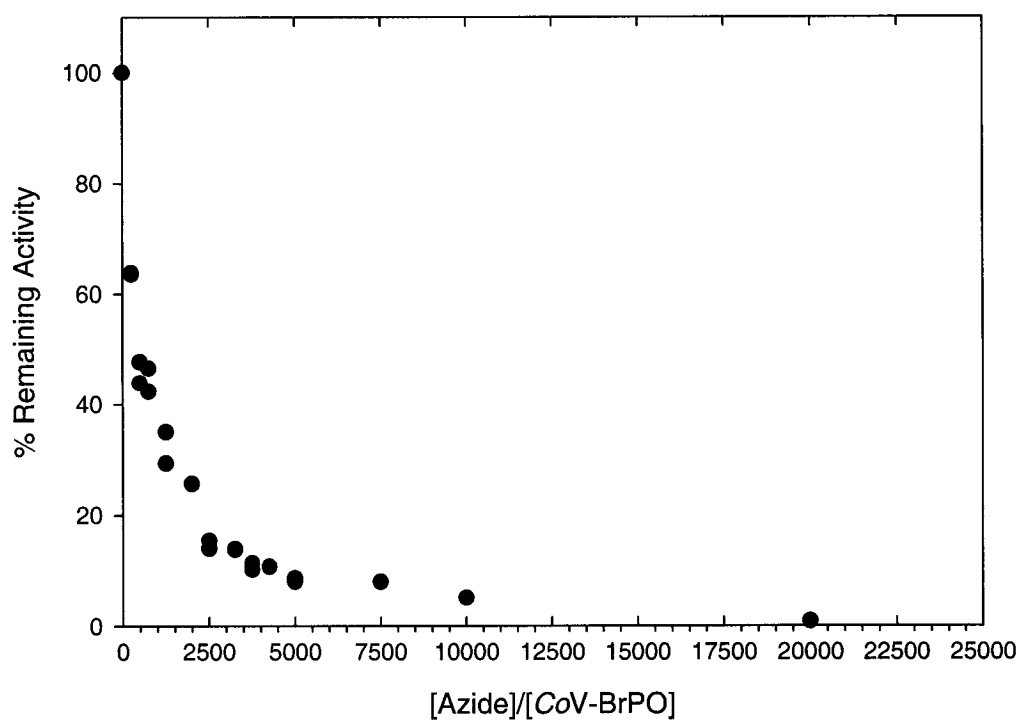


Figure 5.8: Plot of percent remaining *vulnerable* CoV-BrPO MCD activity vs. [azide]/[CoV-BrPO]. Reaction conditions: CoV-BrPO (20 nM) was incubated for 3 hours with 1 mM H₂O₂ and various azide concentrations in 50 mM HEPES (pH 6.0) at 4 °C.

Protection of CoV-BrPO against azide inactivation by bromide:

One of the requirements of a mechanism-based inhibitor is the protection against inactivation by natural substrates. For CoV-BrPO, it is expected that the rate of azide inactivation would decrease in the presence of increasing concentrations of bromide or chloride. The plots of the percent remaining activity of CoV-BrPO as a function of time at varying concentrations of bromide (0.25 mM - 2.5 mM) and azide (0.200 mM - 5 mM) at pH 6.0 show some protection against azide inactivation with increasing concentrations of bromide in the reaction mixtures [Figures 5.9 – 5.11]. The slopes of the plots (k_{obs}) were calculated from the linear portion of the data (Table 5.1). Data presented in Table 5.1 indicate that CoV-BrPO is not sufficiently protected against azide inactivation at low concentrations of bromide (i.e., 0.25 mM and 0.50 mM bromide), where comparison of the k_{obs} at 200 μM azide in the presence of 0.250 mM bromide ($k_{\text{obs}} = 8.08 \times 10^{-4} \text{ sec}^{-1}$) is approximately the same as the k_{obs} for 250 μM azide in the absence of bromide ($k_{\text{obs}} = 9.26 \times 10^{-4} \text{ sec}^{-1}$). Protection against azide inactivation was observed in incubation mixtures containing higher concentrations of bromide (i.e., 2.5 mM bromide). At 2.5 mM bromide the k_{obs} in the presence 1 mM azide ($k_{\text{obs}} = 5.8 \times 10^{-4} \text{ sec}^{-1}$) is similar to reactions without added bromide in the presence of 150 μM azide ($k_{\text{obs}} = 5.6 \times 10^{-4} \text{ sec}^{-1}$), indicating CoV-BrPO is protected against azide inactivation at 2.5 mM bromide.

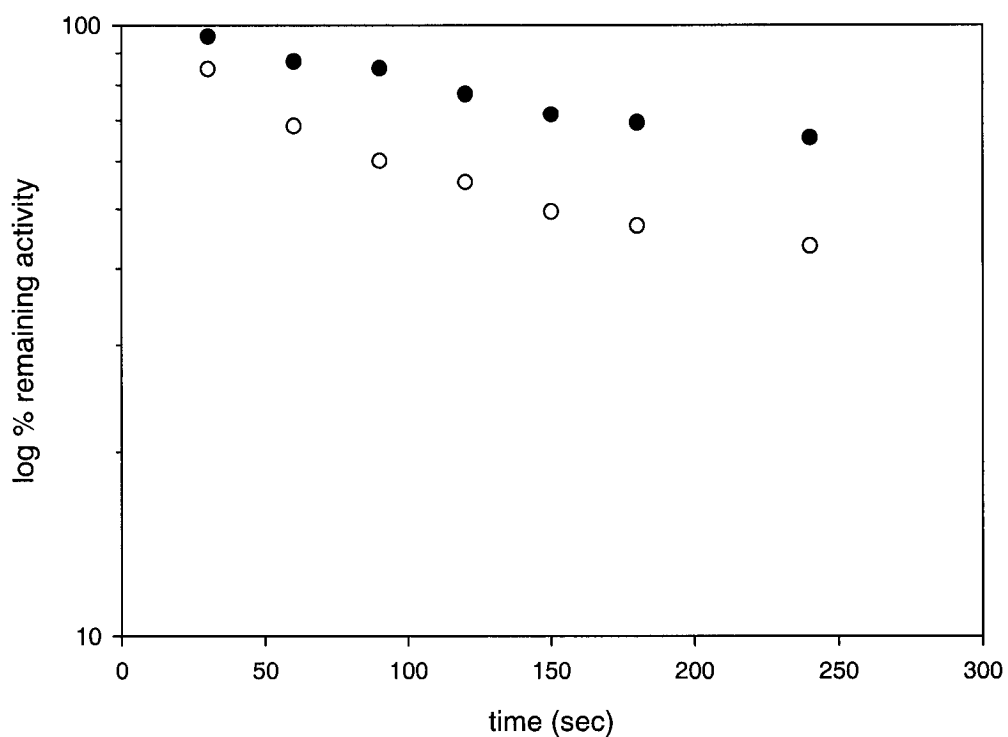


Figure 5.9: Plot of percent remaining *CoV-BrPO* activity vs. time in the presence of 0.25 mM bromide and different azide concentrations. ● 200 μM azide, ○ 1 mM azide. Reaction conditions: *CoV-BrPO* (132 nM) was incubated with 1 mM H₂O₂, bromide (0.25 mM) and various concentrations of azide in 50 mM HEPES (pH 6.0) at 4 °C.

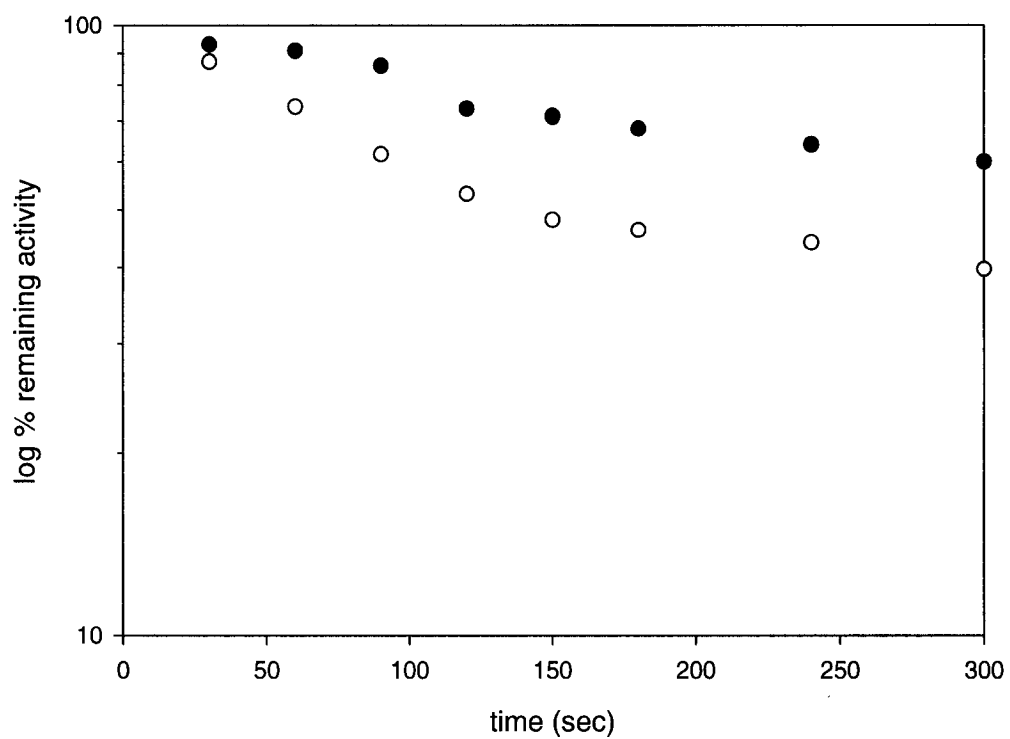


Figure 5.10: Plot of percent remaining *CoV-BrPO* activity vs. time in the presence of 0.50 mM bromide and different azide concentrations. ● 200 μM azide, ○ 1 mM azide. Reaction conditions: *CoV-BrPO* (132 nM) was incubated with 1 mM H_2O_2 , bromide (0.50 mM) and various concentrations of azide in 50 mM HEPES (pH 6.0) at 4 $^\circ\text{C}$.

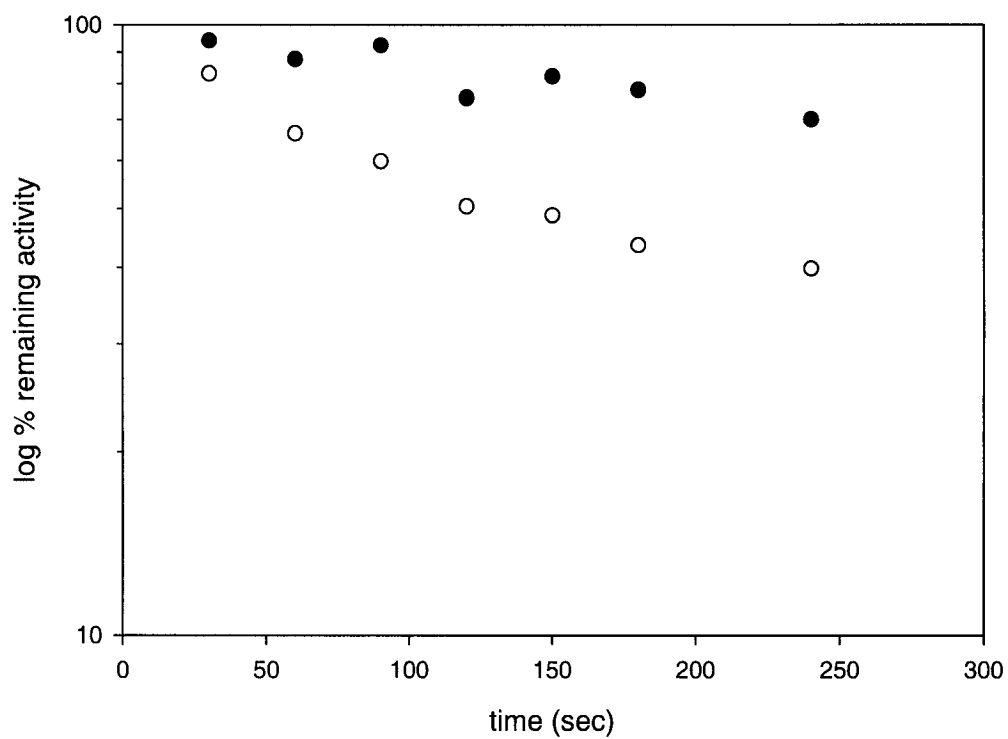


Figure 5.11: Plot of percent remaining *CoV-BrPO* activity vs. time in the presence of 0.50 mM bromide and different azide concentrations. ● 1 mM azide, ○ 5 mM azide. Reaction conditions: *CoV-BrPO* (132 nM) was incubated with 1 mM H_2O_2 , bromide (2.5 mM) and various concentrations of azide in 50 mM HEPES (pH 6.0) at 4 °C.

Azide (mM)	$k_{\text{obs}} \times 10^{-3} \text{ (sec}^{-1}\text{)}$	$k_{\text{obs}} \times 10^{-3} \text{ (sec}^{-1}\text{)}$	$k_{\text{obs}} \times 10^{-3} \text{ (sec}^{-1}\text{)}$	$k_{\text{obs}} \times 10^{-3} \text{ (sec}^{-1}\text{)}$
	No added Br ⁻	0.250 mM Br ⁻	0.500 mM Br ⁻	2.5 mM Br ⁻
0.150	0.565	--	--	--
0.200	--	0.808	0.801	--
0.250	0.926	--	--	--
0.400	0.942	--	--	--
1.0	--	2.04	2.20	0.58
5.0	--	--	--	1.94

Table 5.1: Bromide protection of CoV-BrPO against azide inactivation. k_{obs} calculated from the linear part of the plots from Figures 5.2 and 5.9 – 5.11.

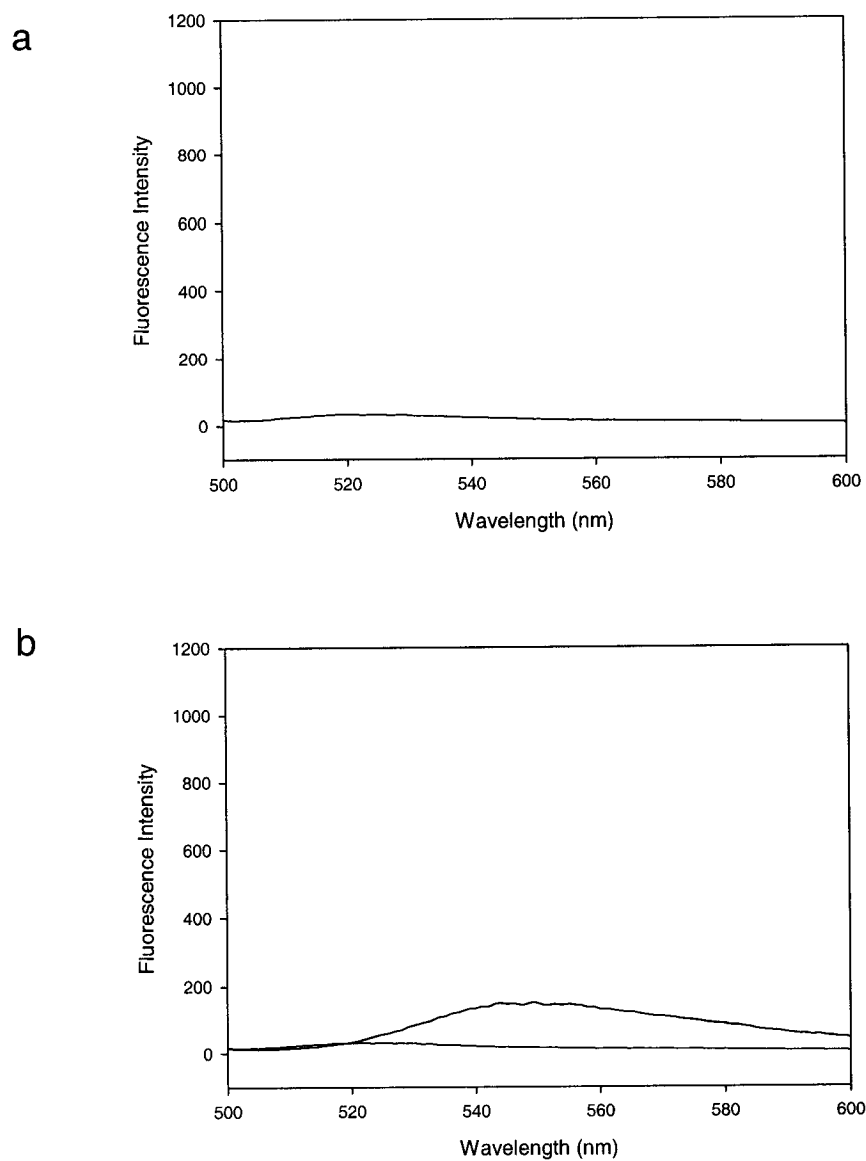


Figure 5.12: (a) Fluorescence emission spectra of DAF-FM ($8.75 \mu\text{M}$) in solution with *CoV*-BrPO (132 nM) and 2 mM azide in 0.1 M HEPES buffer ($\text{pH } 6.0$) at room temperature. H_2O_2 was not added to the reaction. (b) Fluorescence emission spectra of DAF-FM ($8.75 \mu\text{M}$) in solution with *CoV*-BrPO (132 nM), 2 mM azide, and 20 mM KBr in 0.1 M HEPES buffer ($\text{pH } 6.0$) at room temperature. Reaction was initiated by addition of 2 mM H_2O_2 .

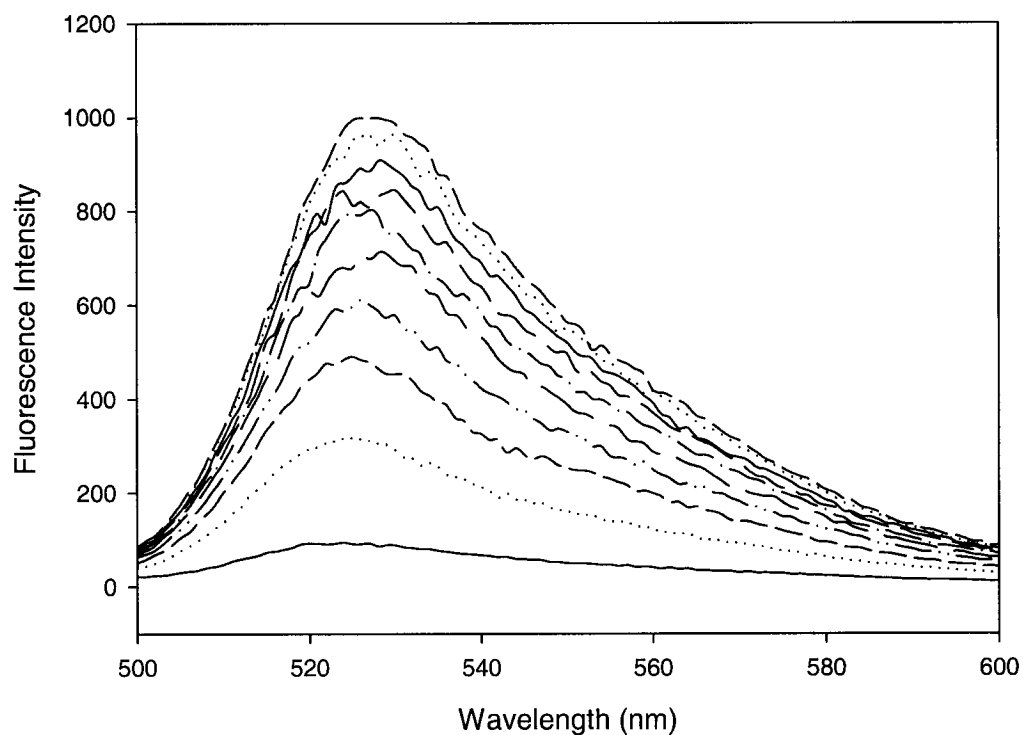
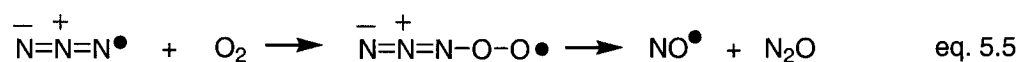


Figure 5.13: Fluorescence emission spectra of DAF-FM-NO species in solution containing 132 nM *CoV*-BrPO, 2 mM Azide, and 8.75 μ M DAF-FM in 0.1 M HEPES buffer (pH 6.0) at room temperature. Reactions were initiated by the addition of 2 mM H_2O_2 . Excitation wavelength was 490 nm. Emission was monitored between 500 – 600 nm. Spectra were recorded every minute for 10 minutes.

Production of NO• during azide inactivation of CoV-BrPO:

Previously V-BrPO from the brown alga *A. nodosum* was shown to consume oxygen during azide inactivation (Soedjak 1991). The presence of 5,5-dimethyl-1-pyrroline-N-oxide (DMPO) inhibited O₂-uptake by the AnV-BrPO/azide/H₂O₂ system. DMPO can act as a radical scavenger and is commonly used to trap transient radicals to give a stable DMPO-radical adduct. In reactions with V-BrPO and azide, it is proposed that an azidyl radical is formed, similar to formation of an azidyl radical by the heme peroxidases (Kalyanaraman et al. 1985; DePillis and Ortiz de Montellano 1989; DePillis et al. 1991; Harris et al. 1991). The proposed formation of an azidyl radical in addition to oxygen consumption data suggest that the azidyl radical reacts with oxygen to form NO and N₂O species by the following reaction (Kalyanaraman et al. 1985).



The formation of nitric oxide during azide inactivation of CoV-BrPO was indirectly detected using DAF-FM, a NO-reactive fluorescent indicator. A DAF-FM-NO species was not detected in V-BrPO reactions without added hydrogen peroxide, indicating CoV-BrPO does not catalyze the oxidation of azide in the absence of hydrogen peroxide [Figure 5.12, a]. A time dependent increase in the DAF-FM-NO species UV spectrum was observed following addition of hydrogen peroxide [Figure 5.13]. Also, the DAF-FM-NO species was not detected when azide inactivation of

CoV-BrPO was performed in the presence of excess bromide, supporting enzyme protection by native halide substrates [Figure 5.12, b] (Silverman 1988).

Discussion

Incubation of *CoV*-BrPO with azide and hydrogen peroxide resulted in the inactivation of *CoV*-BrPO. Inhibition by azide required the addition of hydrogen peroxide, thus inactivation of *CoV*-BrPO was observed only under catalytic conditions. Inactivation of *CoV*-BrPO by azide is a first-order, irreversible process with a $K_I = 400 \mu\text{M}$ and $k_{\text{inact}} = 0.364 \text{ min}^{-1}$. The rate of inactivation, as required by a mechanism-based inactivator, was dependent on the concentration of azide (Silverman 1988). Under the conditions used saturation kinetics for inhibition were observed (4 °C) for azide inactivation of *CoV*-BrPO. The results are similar to azide inactivation of *AnV*-BrPO. Azide inactivation of *AnV*-BrPO resulted in a K_I of 24 mM and $k_{\text{inact}} = 1.2 \text{ min}^{-1}$ (Soedjak 1991). The K_I for azide determined for *CoV*-BrPO suggest that reversible azide binding to *CoV*-BrPO occurs with much greater affinity than to *AnV*-BrPO prior to conversion to the reactive intermediate. However, the rate of inactivation of *CoV*-BrPO occurs much more slowly than for *AnV*-BrPO.

Partition ratio titration for azide and *CoV*-BrPO indicate ~1200 molecules of azide are required to inactivate a single enzyme molecule at 4 °C. The non-linear deviations observed at the higher [azide]/[*CoV*-BrPO] ratios are likely due to product inhibition or product protection of the enzyme towards further inactivation (Silverman 1988). The greater number of azide molecules needed to inactivate *CoV*-BrPO compared to the number of azide molecules needed to inactivate *AnV*-BrPO (~150 molecules) (Soedjak 1991) and the incomplete inactivation of *CoV*-BrPO

suggest that the activated azide species reacts slightly differently at the active sites of these two vanadium bromoperoxidases. It is proposed that an azide-derived intermediate reacts with *CoV*-BrPO in such a way to protect the enzyme from complete inactivation. Incomplete azide inactivation of heme peroxidases has also been observed, however the protecting species has not been characterized (Ortiz de Montellano et al. 1988; DePillis et al. 1991; Tuisel et al. 1991; Tatarko and Bumpus 1997). Additional experiments are required to determine whether the 20% remaining activity can be further inactivated following dialysis or gel filtration chromatography to remove any “protecting species”. Hill plot analysis of activated azide binding to *CoV*-BrPO indicated a stoichiometry of 1 to 1.

The rate of azide inactivation of *CoV*-BrPO was diminished in the presence of bromide (concentrations $> K_m^{\text{Br}^-} = 1 \text{ mM}$). Protection by bromide suggests that activation of azide and inactivation of *CoV*-BrPO occur at the active site. It has been previously demonstrated that bromide and chloride are competitive inhibitors of azide with *AnV*-BrPO (Soedjak 1991).

The means by which azide inactivates *V*-BrPO is not known. It has been proposed that *V*-BrPO oxidizes azide in one electron process to an azidyl radical, which reacts irreversibly with the protein to render it inactive (Everett 1990; Soedjak 1991). The detection of a DAF-FM-NO species by fluorescence spectroscopy suggests the formation of NO during azide inactivation of *CoV*-BrPO. Reaction of an azidyl radical with oxygen is relatively slow, compared to diffusion limited azidyl radical dimerization, as determined from pulse radiolysis experiments (Eriksen et al.

1981). All the same, the oxygen uptake data determined for *AnV*-BrPO and the detection of DAF-FM-NO adduct in *CoV*-BrPO catalyzed reactions suggest reaction of an azidyl radical or azidyl radical derived species with molecular oxygen in the V-BrPO catalyzed reaction.

Previous studies on azide inactivation of *AnV*-BrPO showed that inactivation of *AnV*-BrPO does not involve the removal of vanadium from the active site nor does it reduce vanadium (V) to vanadium (IV) (Soedjak 1991). Azidyl radicals react rapidly with the free amino acids cysteine, tyrosine and especially tryptophan (Land and Prutz 1979; Alfassi and Schuler 1985). Assuming that an azidyl radical or azidyl radical derived species is generated at the active site of *CoV*-BrPO during inactivation, it is likely that the azidyl radical species reacts with an active site amino acid. Site-directed mutagenesis of amino acids coordinating the vanadate cofactor for V-BrPO and V-ClPO have resulted in the irreversible loss of halide oxidation due to disruption of native hydrogen bond contacts to the vanadate cofactor (Hemrika et al. 1999; Macedo-Ribeiro et al. 1999; Carter et al. 2002). In addition, mutation of the extra-histidine residue in proximity to the vanadium cofactor in *CoV*-BrPO to an alanine resulted in ~96% loss of bromide oxidation and diminished iodide oxidation (Carter et al. 2002). Similarly, the irreversible loss of bromide oxidation by azide inactivated *CoV*-BrPO suggests that the activated azide species reacts with an active site amino acid involved in maintaining the intricate hydrogen bond network to the vanadate cofactor. Modification of the surrounding protein matrix by an activated azide species is further supported by the observation that reconstitution of the apo-

inactivated enzyme with fresh vanadate does not restore bromide oxidation. It has yet to be determined whether azide inactivated *CoV*-BrPO or *AnV*-BrPO can oxidize iodide, or pseudohalide derivatives such as thiocyanate and cyanide, or perform the halide-independent oxidation of sulfides to sulfoxides. These will likely be subjects of further investigation.

References

- Alfassi, Z. B. and R. H. Schuler (1985). "Reaction of Azide Radicals with Aromatic Compounds. Azide as a Selective Oxidant." *J. Phys. Chem.* **89**: 3359-3363.
- Bjorksten, F. (1968). "A Kinetic Study of the Horseradish Peroxidase-Catalyzed Oxidation of Iodide." *Eur. J. Biochem.* **5**: 133-142.
- Carter, J. N., K. E. Beatty, M. T. Simpson and A. Butler (2002). "Reactivity of Recombinant and Mutant Vanadium Bromoperoxidase from the Red Alga *Corallina officinalis*." *J. Inorg. Biochem.* **91**: 59-69.
- DePillis, G. D. and P. R. Ortiz de Montellano (1989). "Substrate Oxidation by the Heme Edge of Fungal Peroxidases. Reaction of *Coprinus macrorhizus* Peroxidase with Hydrazines and Sodium Azide." *Biochemistry* **28**: 7947-7952.
- DePillis, G. D., B. P. Sishta, A. G. Mauk and P. R. Ortiz de Montellano (1991). "Small Substrates and Cytochrome c are Oxidized at Different Sites of Cytochrome c Peroxidase." *J. Biol. Chem.* **266**: 19334-19341.
- DePillis, G. D., H. Wariishi, M. H. Gold and P. R. Ortiz de Montellano (1990). "Inactivation of Lignin Peroxidase by Phenylhydrazine and Sodium Azide." *Arch. Biochem. Biophys.* **280**: 217-223.
- Eriksen, T. E., J. Lind and G. Merenyi (1981). "The Reactivity of the Azide Radical (N_3^-) Toward Dioxygen Species." *Radiochem. Radioanal. Lett.* **48**: 405-410.
- Everett, R. R. (1990). A Novel Vanadium Bromoperoxidase: Investigation of Enzyme Kinetics and Reaction Mechanisms. Ph.D. Thesis, University of California, Santa Barbara.
- Harris, R. Z., H. Wariishi, M. H. Gold and P. R. Ortiz de Montellano (1991). "The Catalytic Site of Manganese Peroxidase. Regiospecific Addition of Sodium Azide and Alkylhydrazines to the Heme Group." *J. Biol. Chem.* **266**: 8751-8758.
- Hayon, E. and M. Simic (1970). "Absorption Spectra and Kinetics of Intermediate Produced from Decay of Azide Radicals." *J. Am. Chem. Soc.* **92**: 7486-7487.
- Hemrika, W., R. Renirie, S. Macedo-Ribeiro, A. Messerschmidt and R. Wever (1999). "Heterologous Expression of the Vanadium-Containing Chloroperoxidase from *Curvularia inaequalis* in *Saccharomyces cerevisiae* and Site-Directed Mutagenesis of the Active Site Residues His496, Lys353, Arg360, and Arg490." *J. Biol. Chem.* **274**: 23820-23827.

Hewson, W. D. and L. P. Hager (1980). "Bromoperoxidase and Halogenated Lipids in Marine Algae." *J. Phycol.* **16**: 340-345.

Itoh, H., Y. Izumi and H. Yamada (1986). "Characterization of Nonheme Type Bromoperoxidase in *Corallina pilulifera*." *J. Biol. Chem.* **261**: 5194-5200.

Kalyanaraman, B., E. G. Janzen and R. P. Mason (1985). "Spin Trapping of the Azidyl Radical in Azide/Catalase/H₂O₂ and Various Azide/Peroxidase/H₂O₂ Peroxidizing Systems." *J. Biol. Chem.* **260**: 4003-4006.

Keilin, D. and E. F. Hartree (1954). "Reactions of Methaemoglobin and Catalase with Peroxides and Hydrogen Donors." *Nature* **173**: 720-723.

Keilin, D. and P. Nicholls (1958). "Reactions of Catalase with Hydrogen Peroxide and Hydrogen Donors." *Biochim. Biophys. Acta* **29**: 302-307.

Kitz, R. J. and I. B. Wilson (1962). "Esters of Methanesulfonic Acid as Irreversible Inhibitors of Acetylcholinesterase." *J. Biol. Chem.* **237**: 3245-3249.

Kojima, H., Y. Urano, K. Kikuchi, T. Higuchi, Y. Hirata and T. Nagano (1999). "Fluorescent Indicators for Imaging Nitric Oxide Production." *Angew. Chem. Int. Ed.* **21**: 3209-3212.

Land, E. J. and W. A. Prutz (1979). "Charge-Transfer in Peptides: Pulse-Radiolysis Investigation of One-Electron Reactions in Dipeptides of Tryptophan and Tyrosine." *Int. J. Radiat. Biol.* **36**: 75-83.

Macedo-Ribeiro, S., W. Hemrika, R. Renirie, R. Wever and A. Messerschmidt (1999). "X-ray Crystal Structures of Active Site Mutants of the Vanadium-Containing Haloperoxidase for the Fungus *Curvularia inaequalis*." *J. Biol. Inorg. Chem.* **4**: 209-219.

Ortiz de Montellano, P. R., S. K. David, M. A. Ator and D. Tew (1988). "Mechanism-Based Inactivation of Horseradish Peroxidase by Sodium Azide. Formation of *Meso*-Azidoporphyrin IX." *Biochemistry* **27**: 5470-5476.

Samokyszyn, V. M. and P. R. Ortiz de Montellano (1991). "Topology of the Chloroperoxidase Active Site: Regiospecificity of Heme Modification by Phenylhydrazine and Sodium Azide." *Biochemistry* **30**: 11646-11653.

Segel, I. H. (1975). Enzyme Kinetics: Behavior and Analysis of Rapid Equilibrium and Steady-State Enzyme Systems, John Wiley and Sons, Inc.

Silverman, R. B. (1988). Mechanism-Based Enzyme Inactivation: Chemistry and Enzymology. Boca Raton, Florida, CRC Press, Inc.

Soedjak, H. S. (1991). Investigation of Vanadium Bromoperoxidase: Kinetics and Mechanism. Ph.D. Thesis, University of California, Santa Barbara.

Tatarko, M. and J. A. Bumpus (1997). "Further Studies on the Inactivation by Sodium Azide of Lignin Peroxidase from *Phanerochaete chrysosporium*." Arch. Biochem. Biophys. **339**: 200-209.

Theorell, H. and A. Ehrenberg (1952). "Magnetic Properties of Some Peroxide Compounds of Myoglobin, Peroxidase and Catalase." Arch. Biochem. Biophys. **41**: 442-461.

Tuisel, H., T. A. Grover, J. R. Lancaster, J. A. Bumpus and S. D. Aust (1991). "Inhibition of Lignin Peroxidase H₂ by Sodium Azide." Arch. Biochem. Biophys. **288**: 456-462.

Vilter, H. (1983). "Peroxidases From Phaeophyceae 3.: Catalysis of Halogenation by Peroxidases from *Ascophyllum nodosum*." Bot. Mar. **26**: 429-435.

Wever, R., H. Plat and E. de Boer (1985). "Isolation Procedure and Some Properties of the Bromoperoxidase from the Seaweed *Ascophyllum nodosum*." Biochim. Biophys. Acta **830**: 181-186.

Chapter Six

Structure and Amphiphilic Properties of a Suite of Siderophores

Isolated from a Marine Bacterium

Introduction

The relative scarcity of iron in the oceanic environment, where the diffusion of siderophores may be of concern, raises questions about the types of siderophores β -hydroxy-aspartic acid residue. The N-terminus contains an appendage of one of a series of fatty acid tails, ranging from C-12 to C-16. The aquachelins, produced by *Halomonas aquamarina*, possess a seven amino acid peptidic headgroup with N-terminal appendages ranging from C-12 to C-14 fatty acids. The suite of fatty acids found in marinobactins and aquachelins contain both saturated and unsaturated alkyl chains containing one double bond in the *cis* configuration. The marinobactins are now known to partition into semisynthetic vesicles (Xu et al. 2002), indicating that these amphiphilic peptides could potentially associate with bacterial membranes as a means to prevent siderophore diffusion. However, under our growth and isolation conditions both the marinobactins and aquachelins are primarily observed in the growth medium.

Amphiphilic siderophores produced by terrestrial bacteria include the ornibactins, produced by *Burkholderia (Pseudomonas) cepacia*, corrugatin, produced by *Pseudomonas corrugata*, acinetoferrin, produced by *Acinetobacter*

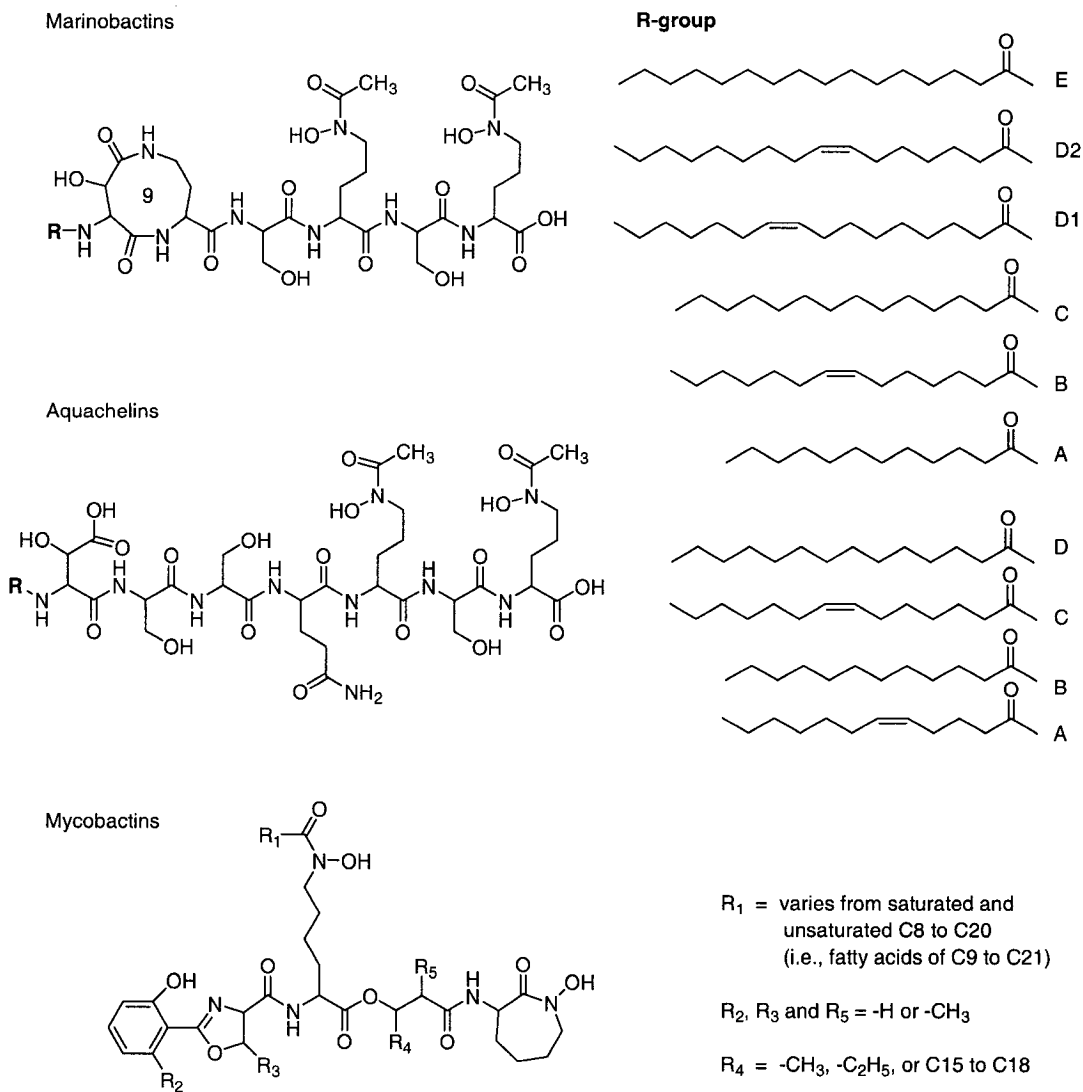


Figure 6.1: Structures of the amphiphilic marinobactins and aquachelins produced by *Marinobacter* sp. strain DS40M6 and *H. aquamarina* strain DS40M3, respectively, and the lipophilic mycobactins produced by Mycobacteria.

haemolyticus, rhizobactin 1021, produced by *Sinorhizobium meliloti*, and the carboxymycobactins, produced by *Mycobacteria*, all of which are produced and secreted into the growth that marine bacteria produce. Two suites of amphiphilic peptidic siderophores, the marinobactins and aquachelins, which are produced by distinct genera of marine bacteria have been isolated and characterized [Figure 6.1] (Martinez et al. 2000). The marinobactins, produced by *Marinobacter* sp. strain DS40M6, possess a six amino acid peptide headgroup that coordinates iron through two hydroxamate groups and a medium [Figure 6.2]. With the exception of the ornibactins and carboxymycobactins, these are all single siderophores as opposed to a suite of siderophores that vary in the nature of the fatty acid tail (Ratledge 1984; Stephan et al. 1993; Okujo et al. 1994; Gobin and Horwitz 1996; Lynch et al. 2001). *Mycobacteria*, as well as other high G + C Gram-positive bacteria, produce a family of siderophores that are found only associated with the bacterial membrane, and are not secreted into the growth medium. The mycobactins [Figure 6.1] produced by *Mycobacteria* are a suite of siderophores that differ in fatty acid chain length (C-9 to C-21) or minor modifications in the head group (Ratledge 1984; Gobin and Horwitz 1996). Mycobactins coordinate iron (III) through both oxygen atoms of the hydroxamate groups and the nitrogen and oxygen of the 2-hydroxyphenyloxazoline moiety.

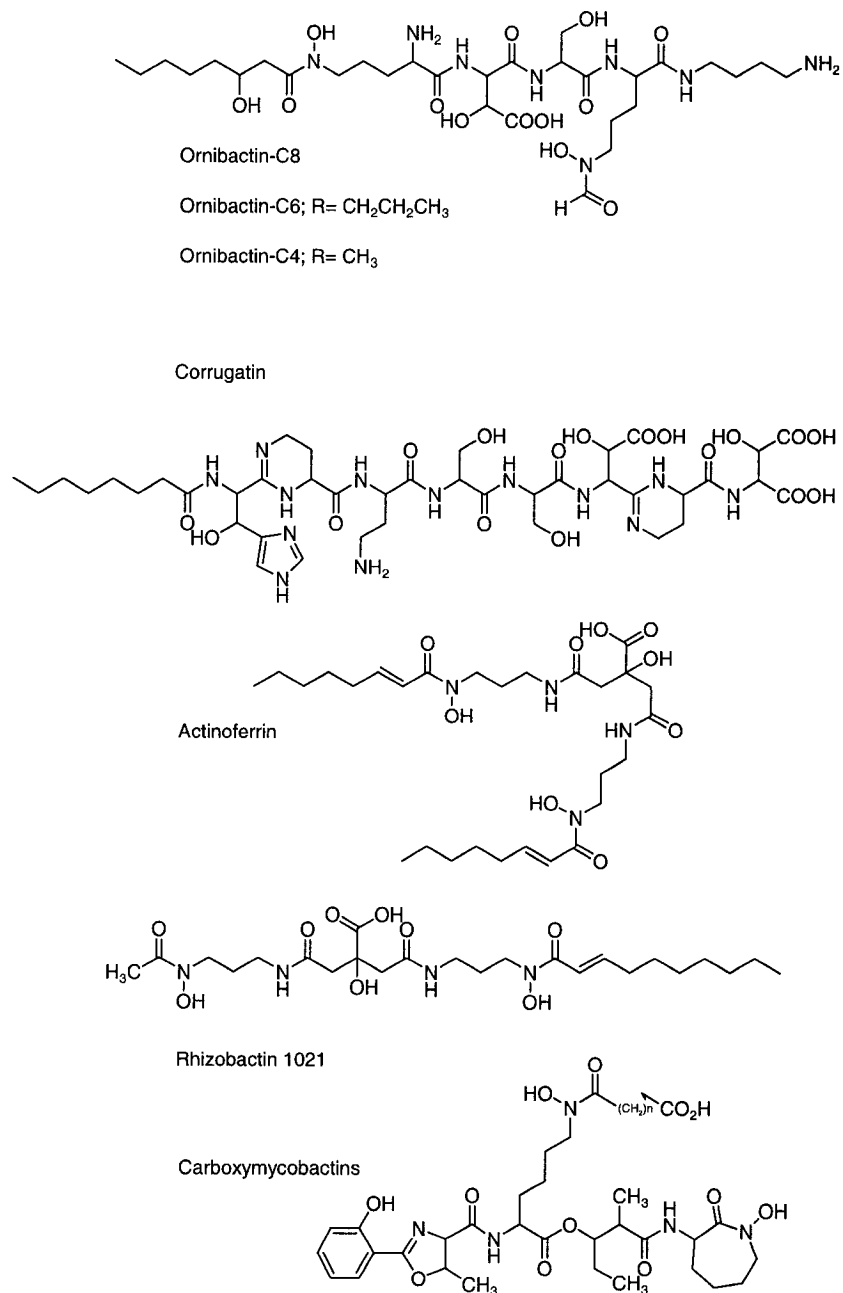
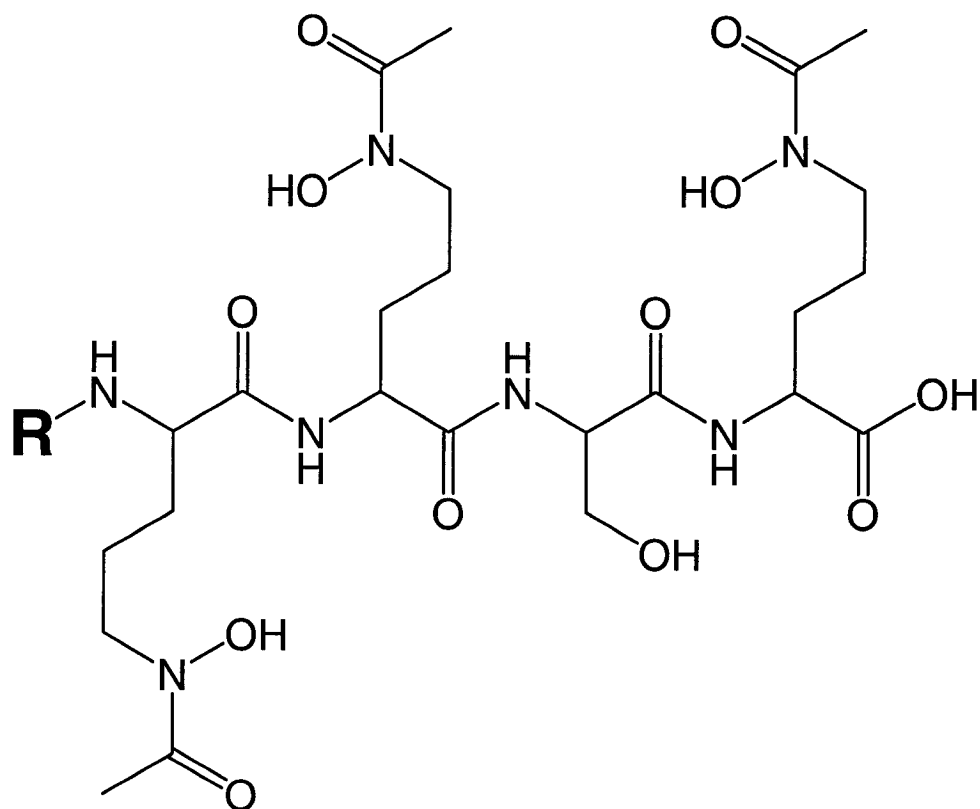


Figure 6.2: Structures of terrestrial amphiphilic siderophores; ornibactins produced by *Burkholderia (Pseudomonas) cepacia*, corrugatin produced by *Pseudomonas corrugata*, acinetoferin produced by *Acinetobacter haemolyticus*, rhizobactin 1021 produced by *Sinorhizobium melioli*, and carboxymycobactins produced by *Mycobacteria*.

Described herein are the completed structures of a new suite of amphiphilic siderophores produced by a marine Gram-negative bacterium (*Vibrio* sp. R-10), the amphibactins. Jennifer S. Martinez, Ph.D, described the partial structure determination for the peptidic head group for the suite siderophores (10 total) [Figure 6.3]. The peptidic headgroup of each amphibactin contains the same amino acids (one L-serine, two D-ornithines, and one L-ornithine). The connectivity and derivitization of the amino acids were established by tandem mass spectrometry. The ornithine residues of the amphibactins are N-hydroxylated and acetylated, forming the hydroxamate group that coordinates iron (III). It was proposed from the partial structure determination that the suite of amphibactins possessed a fatty acid moiety attached to the N-terminus of the peptide. Mass spectrometry and tandem MS analysis predicted the fatty acid tail appendages ranged from C-14 to C-18 [Figure 6.3].

The completed structures of 8 amphibactins include the peptidic head group and one of a series of fatty acid tails attached to the N-terminus of the peptide. In addition to the completed structures, the amphiphilic properties of the physiological mixture of the amphibactins are described.



Roatan-10 siderophores (M + H) ⁺	R-group
902	CH ₃ CH(OH)(CH ₂) ₆ CH=CH(CH ₂) ₇ CO
886	CH ₃ (CH ₂) ₁₇ CO
876	CH ₃ (CH ₂) ₇ CH=CH(CH ₂) ₇ CO
874	CH ₃ CH(OH)(CH ₂) ₁₃ CO
860	CH ₃ CH(OH)(CH ₂) ₆ CH=CH(CH ₂) ₅ CO
	CH ₃ (CH ₂) ₁₅ CO
858	CH ₃ CH(OH)(CH ₂) ₆ CH=CH(CH ₂) ₄ CO
	CH ₃ (CH ₂) ₁₄ CO
856	CH ₃ (CH ₂) ₇ CH=CH(CH ₂) ₅ CO
848	CH ₃ (CH ₂) ₇ (CH=CH) ₂ (CH ₂) ₃ CO
832	CH ₃ CH(OH)(CH ₂) ₁₁ CO
816	CH ₃ (CH ₂) ₁₂ CO
	CH ₃ (CH ₂) ₇ CH=CH(CH ₂) ₂ CO

Figure 6.3: Proposed structure of the siderophores produced by the *Vibrio* sp. R-10 (adapted from Jennifer S. Martinez, Ph.D thesis).

Methods and Materials

General methods:

The production of siderophores was assayed using the chromazurol S (CAS) shuttle-solution assay containing CAS/Fe(III)/HDTMA (hexadecyl-triethylammonium bromide) and sulfosalicylic acid (Schwyn and Neilands 1987). The assay was positive (blue to pink color change) using equal volumes of broth culture and CAS-shuttle solution during growth or one part eluent to two parts CAS during siderophores purification of siderophores.

Stock solutions of R-10 bacterial isolates were made in Difco Marine Broth 2216/glycerol and stored at $-80\text{ }^{\circ}\text{C}$. One bacterial colony was grown in 5 mL Difco Marine Broth 2216 and allowed to come to mid-log phase growth (approximately 12 hours). Bacterial stocks were made following addition of 40% bacterial suspension to 60% sterile dilute-glycerol (20% in media, final concentration) and stored at $-80\text{ }^{\circ}\text{C}$. Bench cultures of Roatan-10 were maintained by replating once every two weeks onto a maintenance medium. The maintenance medium consisted of 15 g/L Bacto-agar, 5 g/L Bacto-peptone, and 0.5 g/L yeast extract in natural seawater. Natural seawater was obtained from the Biology II pipeline, UCSB. The seawater was pumped through an 18-inch diameter polyvinyl chloride pipe located off the coast of UCSB. Seawater was stored in 20 L HDPE (high-density polyethylene) or polycarbonate carboys and aged for 1 – 5 months at $4\text{ }^{\circ}\text{C}$ in the dark prior to use.

Isolation of siderophores:

Vibrio sp. R-10 was obtained from nearshore seawater at Roatan, Honduras by M. Haygood (Scripps Institution of Oceanography) in June 1990 and isolated on SWC agar plates (Haygood et al. 1993). For siderophore isolation, R-10 was grown in natural seawater medium (NSW) (Martinez et al. 2001) for 20 hours on a rotary shaker (150 rpm) at ambient temperature. The cells were harvested by centrifugation (10,800 g) and the supernatant and pellet were tested for siderophore production with the CAS-shuttle solution assay (Schwyn and Neilands 1987). The bacterial pellet, from each 150 mL culture, was washed with doubly deionized water (ddH₂O, Nanopure®), transferred to 50 mL conical tubes, and shaken with 45 mL ethanol for 24 hours at 4 °C. The ethanol extract was filtered through Whatman filter paper, concentrated *in vacuo* to roughly 20% of the original volume, and purified by HPLC as described below. When the cultures were in late stationary phase, the same set of siderophores normally associated with the cell pellets could be, on rare occasions, found in the supernatant as well. These secreted siderophores were isolated from the supernatant by batch adsorption onto Amberlite XAD-2 resin and elution with methanol as previously described (Martinez et al. 2001). Siderophore-containing fractions, corresponding to elution with 100% methanol, were pooled, dried *in vacuo*, and applied to a C4 reversed-phase HPLC column (Vydac). The siderophores were purified using a gradient of 100/0 (% A/B) to 0/100 (% A/B) over 37 minutes, the program was held an additional 10 minutes at 0/100 (% A/B), after which the gradient was reversed, returning to 100/0 (% A/B) over 10 minutes [A =

99.95% ddH₂O (Nanopure®) and 0.05% trifluoroacetic acid (TFA); B = 19.95% ddH₂O, 0.05% TFA, and 80% methanol]. The absorbance of the eluent was monitored at 215 nm.

Structure determination:

The masses and amino acid connectivity of the amphibactins were determined previously by Jennifer S. Martinez, Ph.D (Martinez 2002). Briefly, the masses and amino acid connectivity were determined by electrospray MS and tandem MS with instrumentation similar to that described previously (Martinez et al. 2000; Martinez et al. 2001). The amino acid composition of the amphibactins, including the enantiomeric configuration, was determined with Marfey's reagent [1-fluoro-2,4-dinitrophenyl-5-L-alanine amide] (Marfey 1984). The position of the D- and L-Orn residues could not be determined by partial peptide fragmentation and subsequent amino acid analysis, because none of the peptide fragments would have a unique D- or L-Orn composition. The UV-visible absorption spectra of the ferric-bound amphibactins were compared to spectra from other tris-hydroxamates (Winkelmann 1991).

Structural determination of fatty acid appendages. Purified amphibactins (~1 mg each) were individually treated with methanolic-HCl (3 M, Supelco) in glass vials with Teflon-laminated screw caps. The vials were tightly capped and placed in an oven at 110 °C for 3 hours to generate the methyl esters of the fatty acid appendages. Following methanol evaporation under a gentle stream of nitrogen, the resulting fatty acid methyl esters (FAMES) were extracted with 1 mL of hexane.

Gas chromatography-mass spectrometry of the FAMES was performed to identify the fatty acid appendages. Gas chromatography-mass spectrometry was performed on a Hewlett-Packard model HP-5890 instrument with a DV5MS column. The injector and detector temperatures were 250 °C and 280 °C respectively. The temperature of the column was 80 °C for the initial 2 minutes and was programmed to increase from 80 °C to 300 °C at a rate of 7 °C/minute and held at 300 °C for 10 minutes. The fatty acid methyl esters were identified by their mass spectra and confirmed by co-injection with bacterial fatty acid standards (Supelco). The position of the double bond in the unsaturated fatty acids was determined by co-injection with FAME standards or reductive work-up of ozonolysis products (Zhang 1999).

Partition experiments with amphibactins:

The partition coefficients for the suite of amphibactins between membrane and aqueous phases were measured by HPLC. Unilamellar vesicles were prepared by extrusion of L- α -dimyristoylphosphatidylcholine (DMPC) thin films through polycarbonate filters (200 nm average pore size) in 10 mM Tris-HCl, 0.1 M KCl, pH 8.0 (Xu et al. 2002). DMPC vesicles (concentration range of 0 – 15 mM) were incubated with 70 μ M amphibactin mixture in acid-washed centrifuge tubes in the dark at 27 °C with gentle shaking (60 rpm rotary shaker). Following 2.5 hours of equilibration, the siderophore/vesicle mixture was centrifuged for 3 hours at 200,000 g. The supernatant, containing non-partitioned siderophore, was removed and assayed by HPLC for siderophore concentration using an analytical C4 reversed-phase column (Vydac) with a linear gradient of 0-100% B over 37 minutes [A =

99.9% ddH₂O and 0.1% TFA; B = 19.9% ddH₂O, 0.1% TFA, and 80% methanol].

The absorbance of the eluent was monitored at 215 nm. The concentration of amphibactin siderophores remaining in the supernatant (water phase) was determined by comparing the area of the chromatographic peak to a standard curve for the physiological mixture of amphibactins. Controls were completed to monitor and correct for any adsorption of the siderophore onto the centrifuge tubes.

Comparison of membrane partition coefficients between the amphibactins and marinobactins (Xu et al. 2002) was completed.

Results

Amphibactin structure determination:

The *Vibrio* sp. R-10 produces a suite of at least ten siderophores, named the amphibactins, ranging in mass from 816 to 902 (M+H)⁺. The amphibactin siderophores were isolated from the cellular pellet of R-10 by extraction with ethanol, making this one of the few bacteria shown to produce cell-associated siderophores [Figure 6.4].

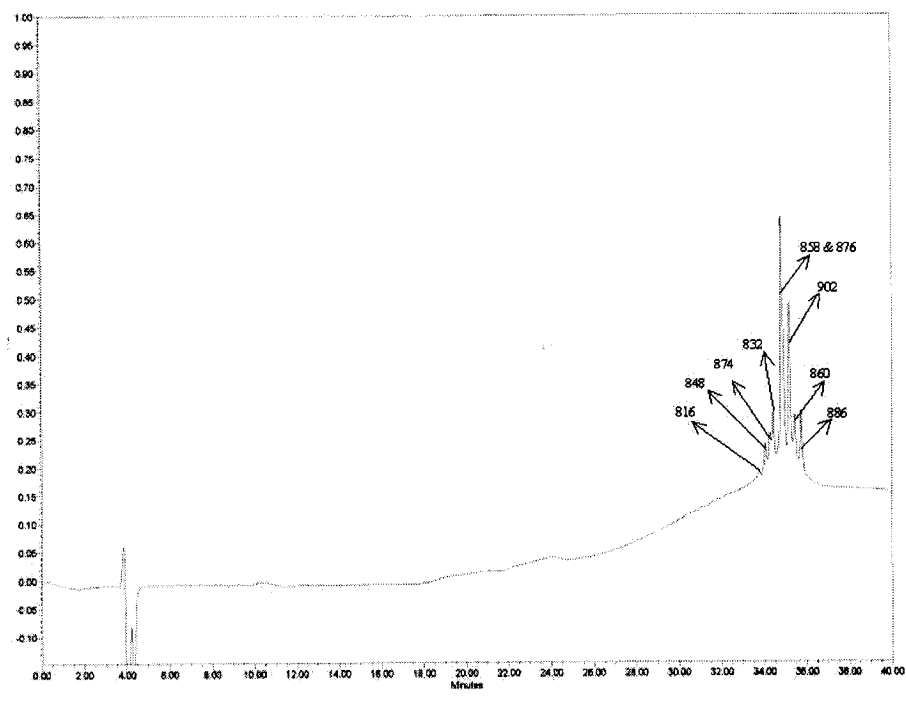


Figure 6.4: HPLC chromatogram of ethanol extractable siderophores from the membrane of bacterial strain Roatan-10. A C₄ reversed-phase HPLC column (Vydac, 4 mm ID x 250 mm L) was used with a gradient of 100/0 (% A/B) to 0/100 over 37 minutes [A = 99.95% ddH₂O and 0.05% TFA; B = 19.95% ddH₂O, 0.05% TFA, and 80% methanol]. The absorbance of the eluent was monitored at 215 nm. The labeled peaks correspond to the masses (M + H) of the eluting siderophores.

The structure of the amphibactin peptidic head group was determined previously by Jennifer S. Martinez, Ph.D., using a combination of amino acid analysis and mass spectrometry. The peptide headgroup of each amphibactin contained the same amino acids (one L-serine, two D-ornithines, and one L-ornithine). Similar to other marine siderophores (Martinez et al. 2000), the ornithine residues of the amphibactins are N-hydroxylated and acetylated, forming the hydroxamate group that coordinates iron (III). According to previous tandem MS and amino acid analysis data it was suggested that the difference in the masses of the isolated amphibactins was a result of different fatty acid (R)-group [Figure 6.3].

Characterization of the fatty acid appendages in the amphibactins. The fatty acid moieties were structurally characterized by acid hydrolysis of the fatty acid tail from the peptidic headgroup followed by methylation using methanolic acid. The resulting methyl esters were extracted in hexane and analyzed by GC-MS. Figure 6.5 (a – d) show the GC chromatograms of the FAMES extracted from the physiological mixture of amphibactins prepared by mixing amphibactin fractions from the HPLC column purifications. The GC chromatograms were compared to methyl esters prepared from ultra-purified samples of individual amphibactins and FAME GC standards (Supelco, Inc.).

The mass spectra of eight peaks identified as fatty acid appendages originating from the amphibactins are shown in Figure 6.6 (a – h). The fatty acid

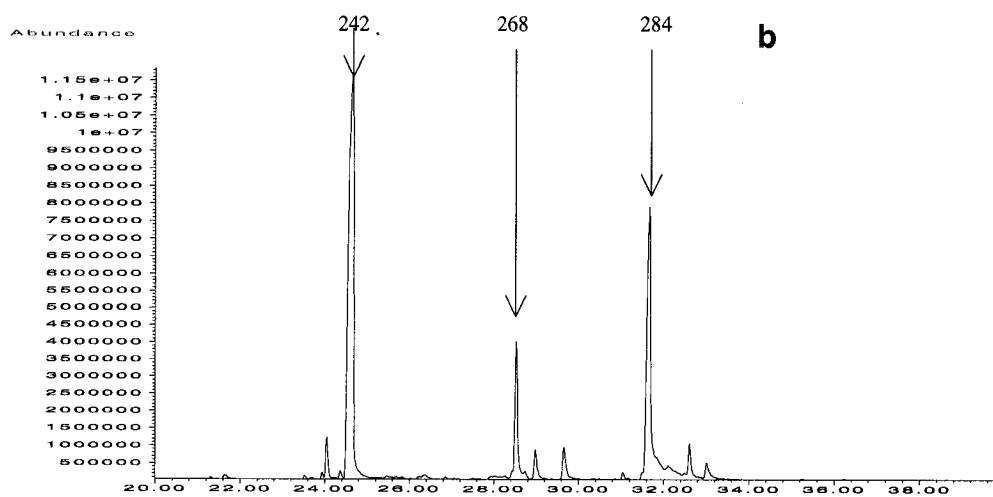
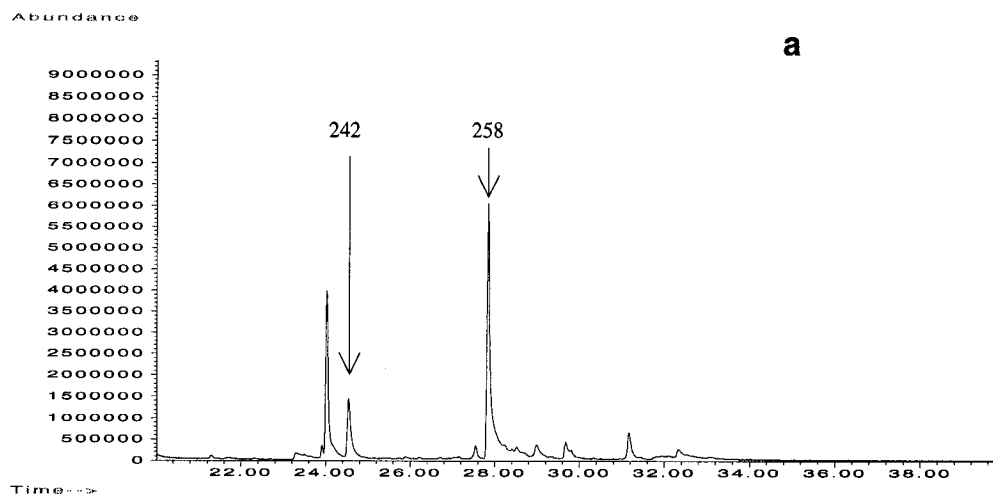


Figure 6.5 (a – d): GC chromatograms of methyl esters extracted from the physiological mixture of amphibactins after methylation using methanolic HCl. The numbers above the arrows represent the mass (m/z) of the methylated fatty acid for the specified peak. See materials and methods for GC-MS parameters.

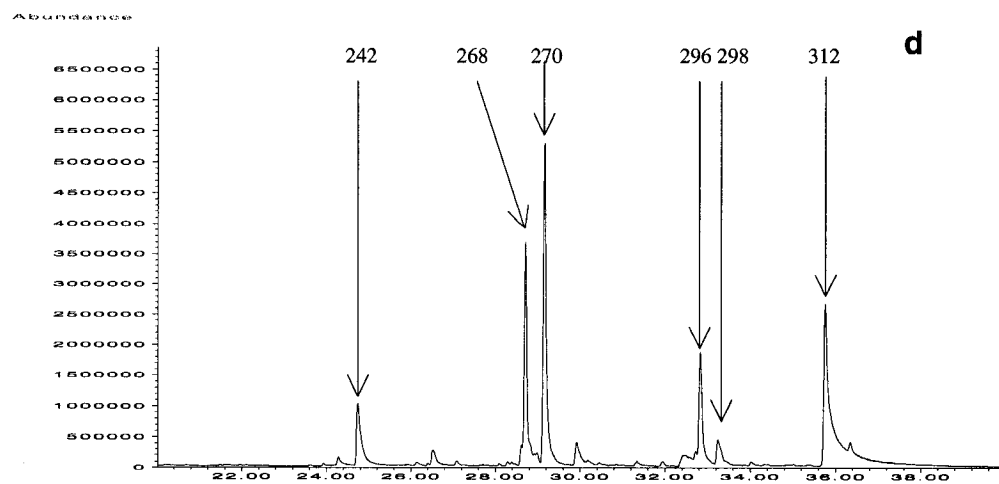
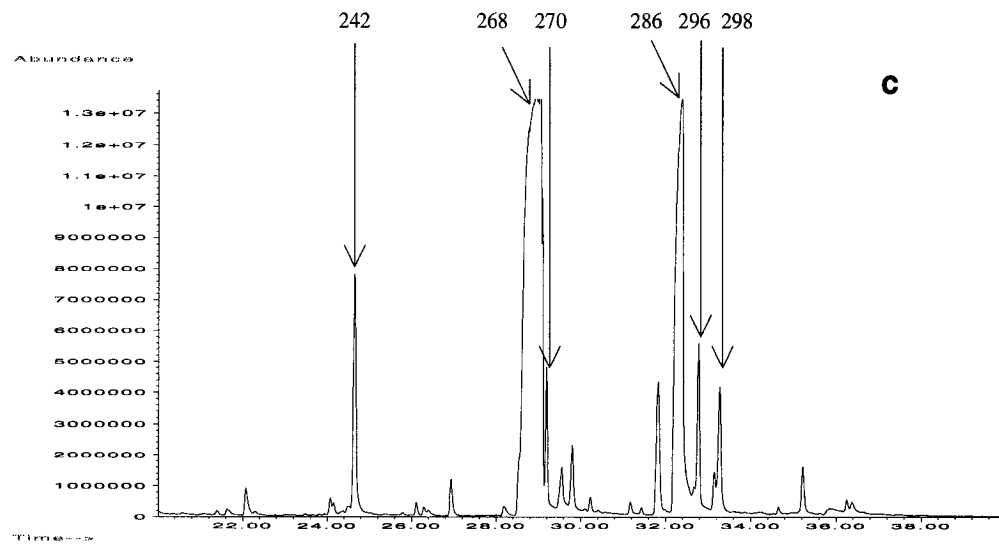


Figure 6.5 (continued): GC-MS chromatogram of methyl esters extracted from the physiological mixture of amphibactins.

moieties were structurally characterized by comparison of the mass fragmentation of amphibactin methyl esters to those of FAME standards. The mass units for the FAME originating from amphibactin-902, -886, -876, -874, -858, -856, -848, and -832 are 312, 296, 286, 284, 268, 270, 258, and 242, respectively. The FAME masses minus the methyl ester functional group ($\text{CH}_3\text{CO}-$), correspond to the predicted masses of the proposed fatty acid appendage for each of the individual amphibactin siderophores [Figure 6.3]. By comparison of the mass spectra with literature data (Murphy 1993) and FAME standards, the fatty acid tails of amphibactins-902, -886, -876, -874, -860, -858, -848, and -832 were determined to be: methyl 3-hydroxy-*cis*-9-octadecenoate (3-OH, 18:1 ω 9c), methyl *cis*-9-octadecenoate (18:1 ω 9c), methyl 3-hydroxyhexadecanoate (3-OH, 16:0), methyl 3-hydroxy-*cis*-9-hexadecenoate (3-OH, 16:1 ω 7c), methyl hexadecanoate (16:0), methyl *cis*-9-hexadecenoate (C16:1 ω 7c), methyl 3-hydroxytetradecanoate (3-OH, C14:0) and methyl tetradecanoate (C14:0), respectively [Figure 6.7]. The double bond position and configuration of amphibactins-902, -886, -874, -858, and 848 were further confirmed by co-injection with standards or ozonolysis of the isolated FAME (performed for amphibactin-902).

Ozonolysis was used to locate the double bound position in the fatty acid chain of amphibactin-902 (FAME-312). Ozonolysis of FAME-312, followed by reductive workup resulted in two aldehyde fragments, which were extracted into hexanes. The MS spectra of the two fragments confirm the double bond position as ω -9. The free alkyl aldehyde was identified as nonanal, and was confirmed by

comparison to a nonanal standard [Figure 6.8]. The *cis*-configuration of the double bond was deduced from comparison of nonanal standard generated from methyl-*cis*-octadecenoate. The standard of nonanal and nonanal generated from ozonolysis of FAME-312 had identical mass spectrums. The methyl ester alkyl aldehyde was also observed, and its mass spectra confirmed the position of the 3-hydroxy group with an observed molecular ion m/z of 103 [Figure 6.9].

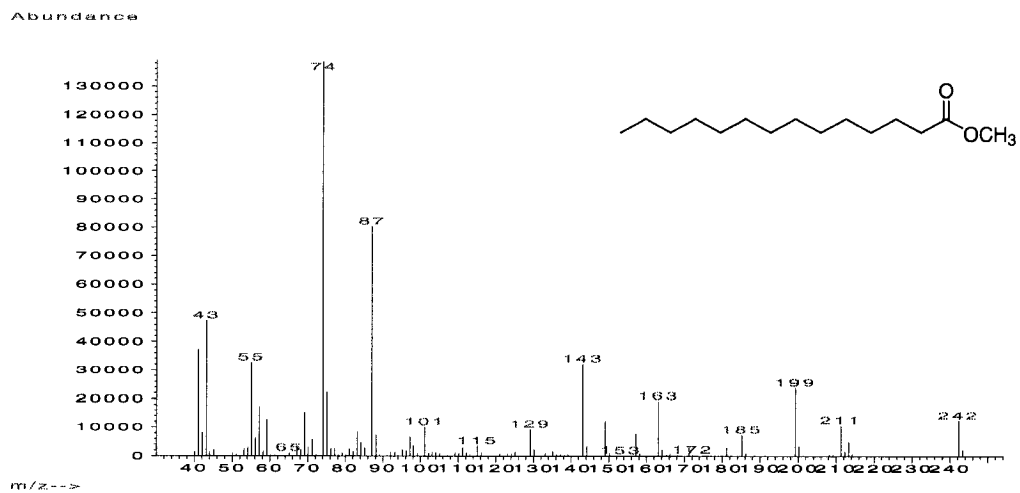


Figure 6.6a: Mass spectrum of GC peak labeled 242 in Figure 6.5. The fatty acid tail is proposed to be attached to amphibactin-832.

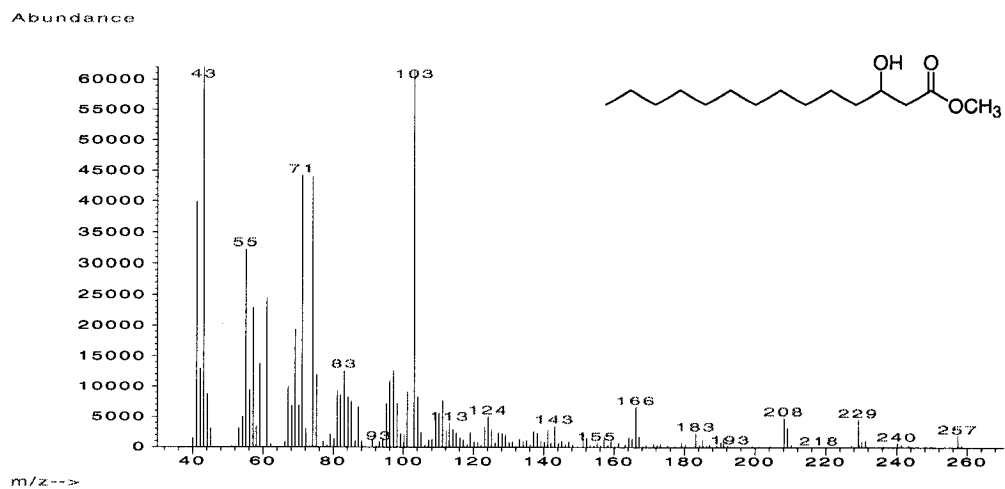


Figure 6.6b: Mass spectrum of GC peak labeled 258 in Figure 6.5. The fatty acid tail is proposed to be attached to amphibactin-848.

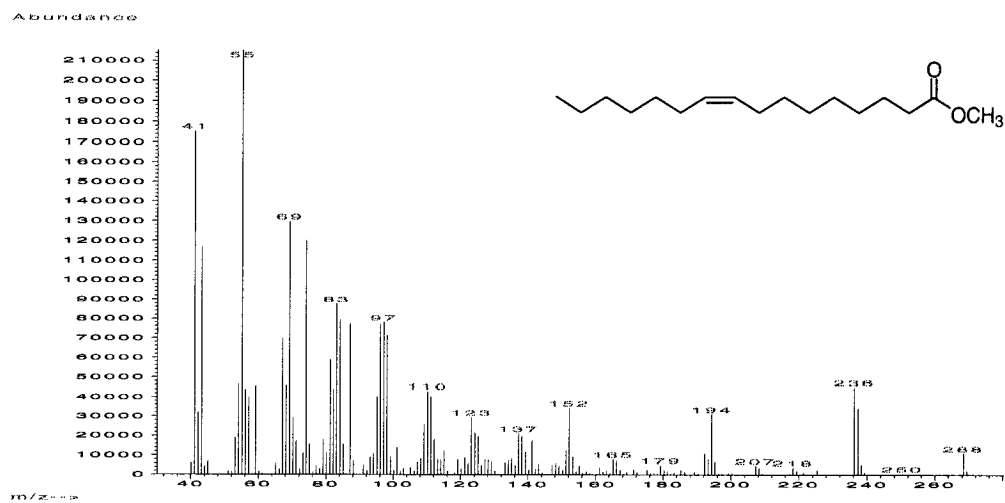


Figure 6.6c: Mass spectrum of GC peak labeled 268 in Figure 6.5. The fatty acid tail is proposed to be attached to amphibactin-858.

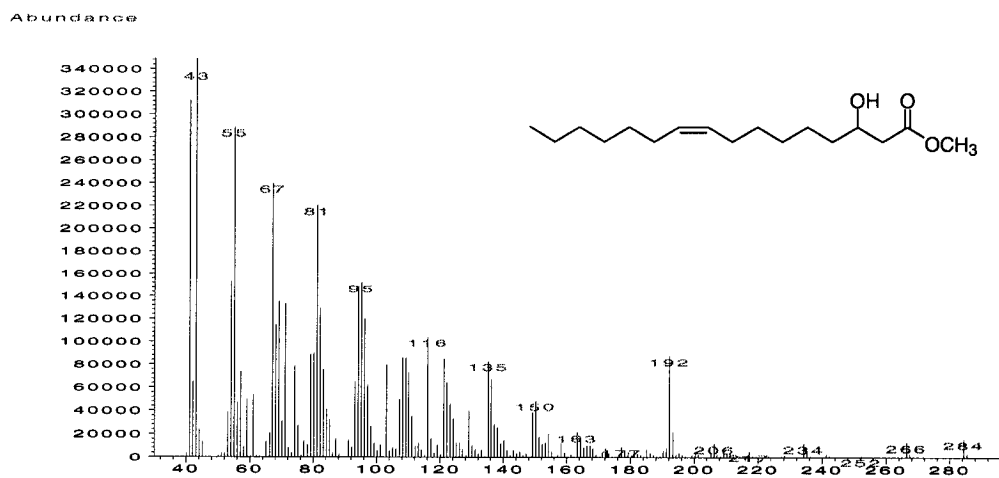


Figure 6.6d: Mass spectrum of GC peak labeled 284 in Figure 6.5. The fatty acid tail is proposed to be attached to amphibactin-874.

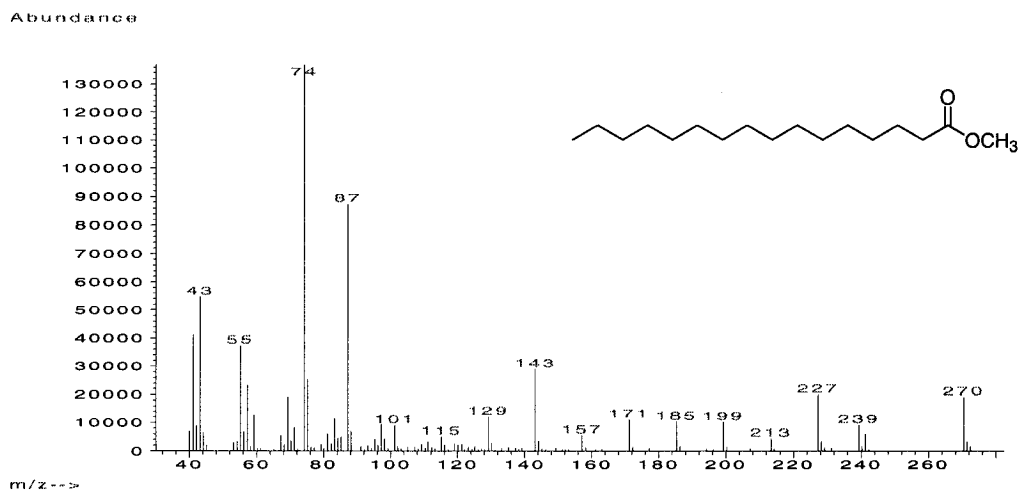


Figure 6.6e: Mass spectrum of GC peak labeled 270 in Figure 6.5. The fatty acid tail is proposed to be attached to amphibactin-860.

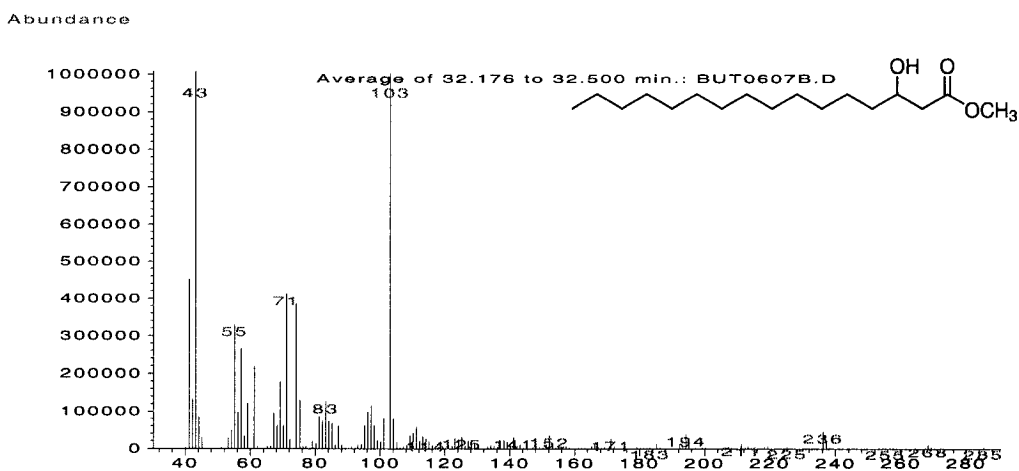


Figure 6.6f: Mass spectrum of GC peak labeled 286 in Figure 6.5. The fatty acid tail is proposed to be attached to amphibactin-876.

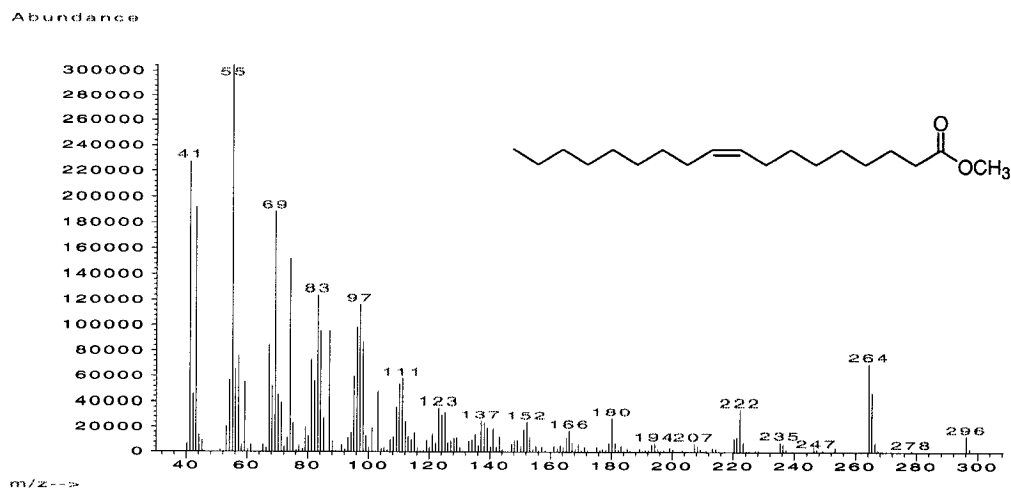


Figure 6.6g: Mass spectra of GC peak labeled 296 in Figure 6.5. The fatty acid tail is proposed to be attached to amphibactin-886.

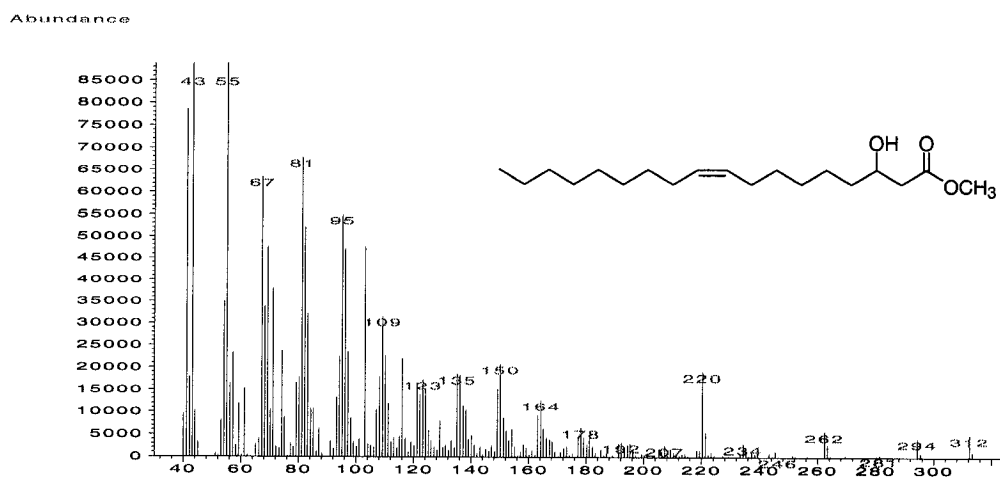
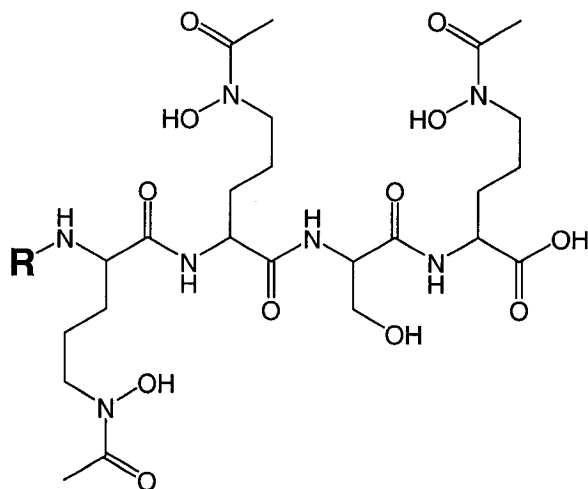


Figure 6.6h: Mass spectra of GC peak labeled 312 in Figure 6.5. The fatty acid tail is proposed to be attached to amphibactin-902.



Amphibactin siderophores (M + H) ⁺	R-group
902	
886	
876	
874	
860	
858	
848	
832	

Figure 6.7: Proposed structures of amphibactin siderophores and their fatty acid appendages.

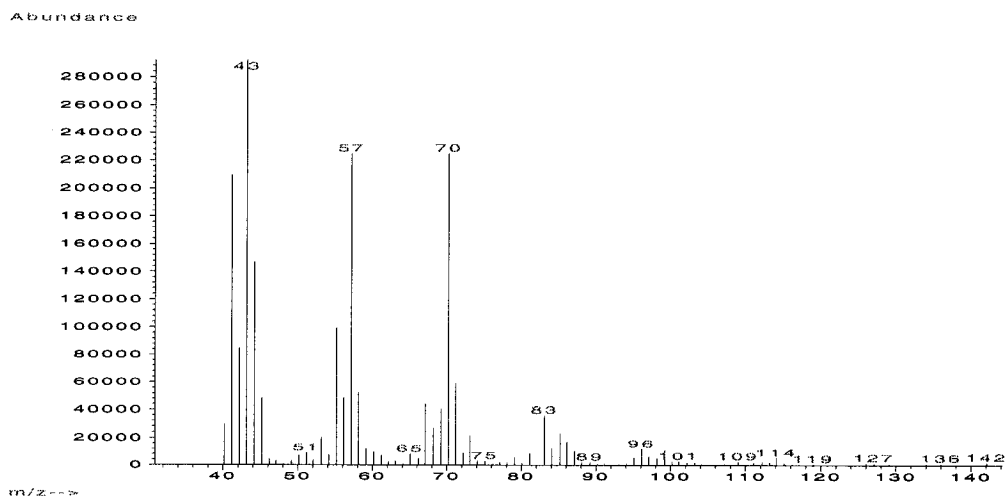


Figure 6.8: Mass spectrum of nonanal product produced by ozonolysis of amphibactin-902. Product was identified by comparison with nonanal standard.

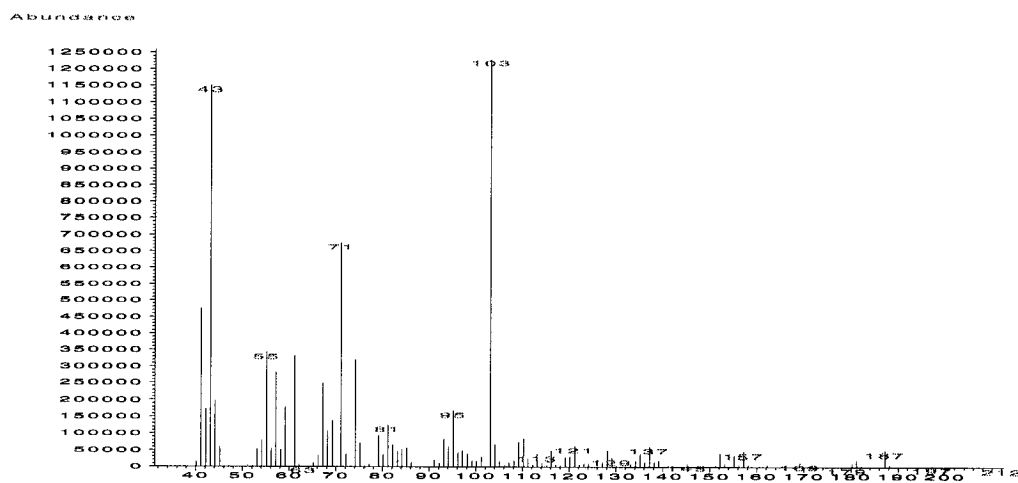


Figure 6.9: Mass spectrum of methyl ester alkyl aldehyde species produced by ozonolysis of amphibactin-902.

Partition experiments with the physiological mixture of amphibactins:

A distinctive feature of the amphibactins is their fatty acid appendage. Variations in the nature of the hydrophilic head group and the hydrophobic fatty acid tail will likely affect the partitioning of these amphiphilic siderophores into the cell membranes. To compare the partition tendency of the amphibactins to other amphiphilic siderophores (i.e., marinobactins) the partitioning of the amphibactins into dimyristoylphosphatidyl choline (DMPC) vesicles was measured. Oceanic heterotrophic bacteria are believed to be within the size range of 0.1 to 0.6 microns *in situ* (Azam and Hodson 1977; Campbell et al. 1994), suggesting that DMPC vesicles on the order of 200 nm diameter are appropriate models to study amphibactin-semi-synthetic membrane interactions.

The HPLC chromatogram of the physiological mixture of amphibactin siderophores before and after incubation with 1 mM DMPC vesicles clearly indicate that all of the amphibactins partition substantially into DMPC vesicles [Figure 6.10].

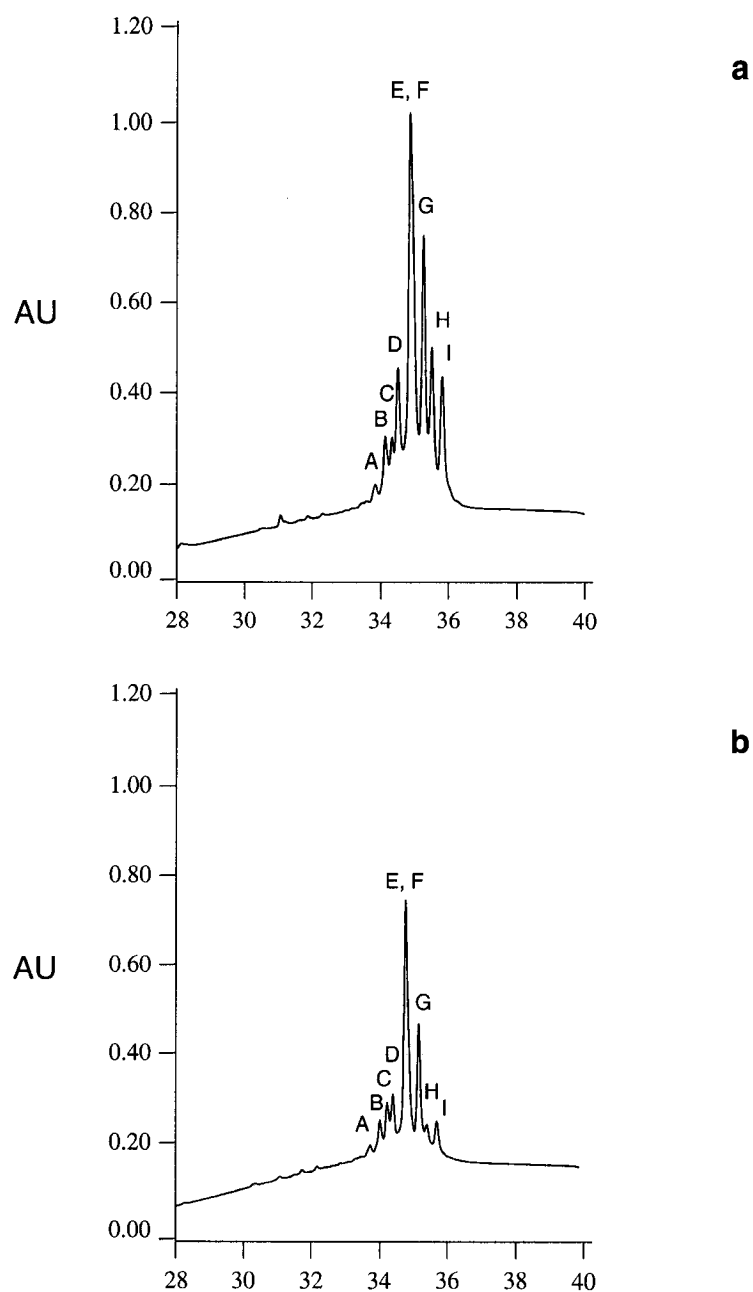


Figure 6.10: HPLC chromatograms of the physiological mixture of the amphibactins equilibrated with DMPC model membranes. (a) The amphibactin physiological mixture (70 μM) before equilibration with 1 mM DMPC. (b) The remaining mixture of amphibactins in the water phase after equilibration with 1 mM DMPC. The lettering above each peak identifies the amphibactin species. Only the nine most predominant amphibactins are shown. A = amphibactin-816, B = -848, C = -874, D = -832, E = -858, F = -876, G = -902, H = -860, I = -886.

When a fixed concentration of a physiological mixture of amphibactins was incubated with varying concentrations of DMPC vesicles, the ratio of siderophores remaining in solution (D_w) to the initial siderophore concentration (D_T) was inversely proportional to the concentration of DMPC [Figure 6.11](Xu et al. 2002). The data was fit to the function

$$D_w/D_T = 1 / [K(L) + 1] ; D_T = D_w + D_L \quad \text{eq. 6.1}$$

Where D_L is the amount of siderophores in the DMPC phase. The partition coefficient (K) for each siderophores was expressed as

$$K = D_L / [L] [D_w] \quad \text{eq. 6.2}$$

The partition coefficients for apo-amphibactin-902, -886, -856, -848, and -832, are 833 ± 108 , 1018 ± 194 , 3784 ± 225 , 1338 ± 161 , and 1915 ± 140 , respectively [Figures 6.12 (a – e)]. Table 6.1 summarizes the partition coefficients for each of the predominant amphibactin siderophores as compared with the previously determined partition coefficients for the physiological mixture of marinobactins (apo- M_{A-E}) (Xu et al. 2002).

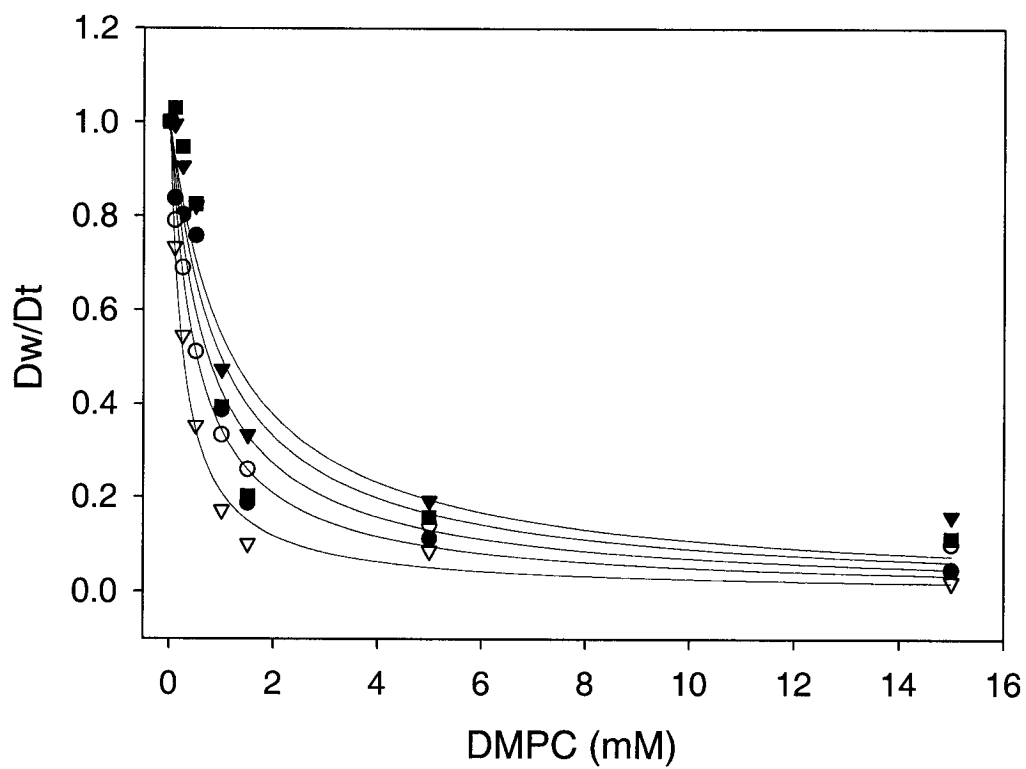


Figure 6.11: Partitioning of apo-amphibactins physiological mixture into large unilamellar DMPC vesicles. 70 μM apo-amphibactins were mixed with varying concentrations of DMPC. Following incubation, the mixture was ultracentrifuged and the supernatant was assayed for siderophore concentration by HPLC. The ratio of siderophores remaining in the water phase to the initial concentration (D_w/D_T) is plotted *versus* the lipid concentration. The solid lines are fits to the experimental data according to equation 6.1.

R10-832

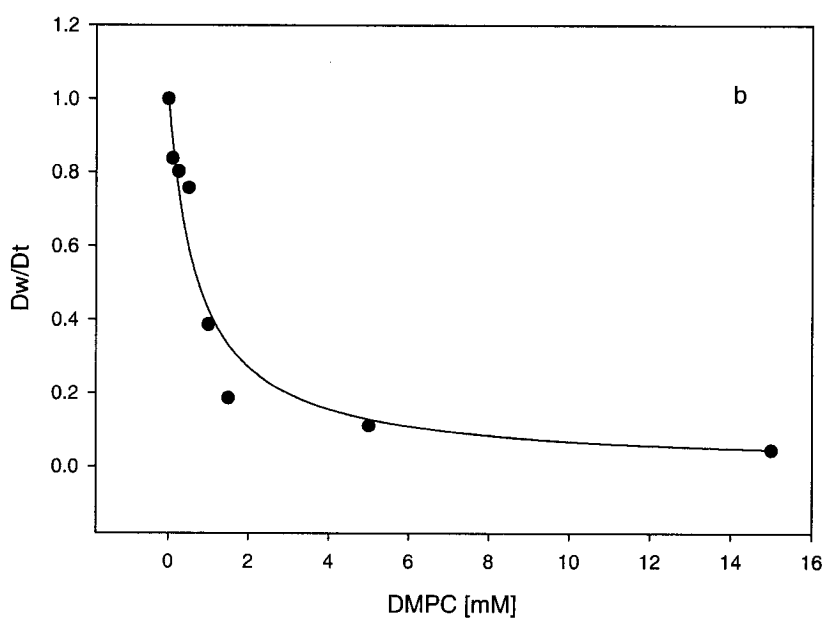
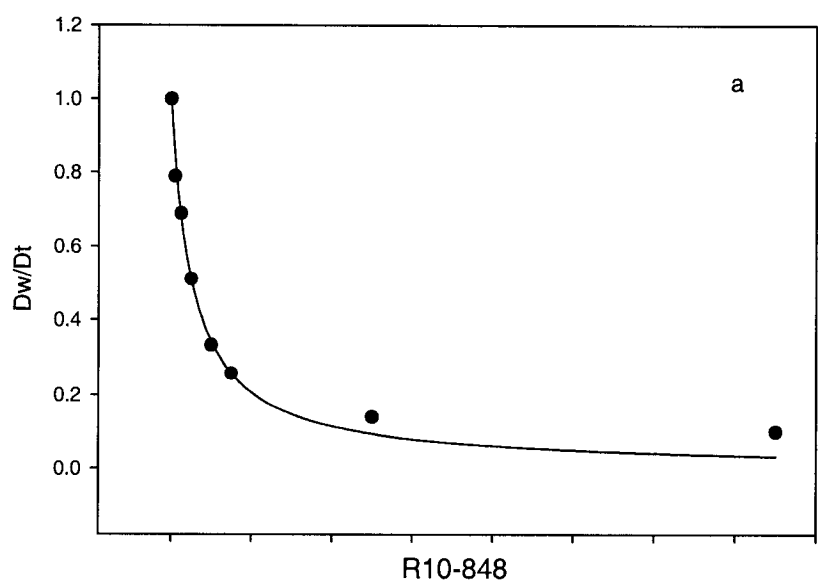
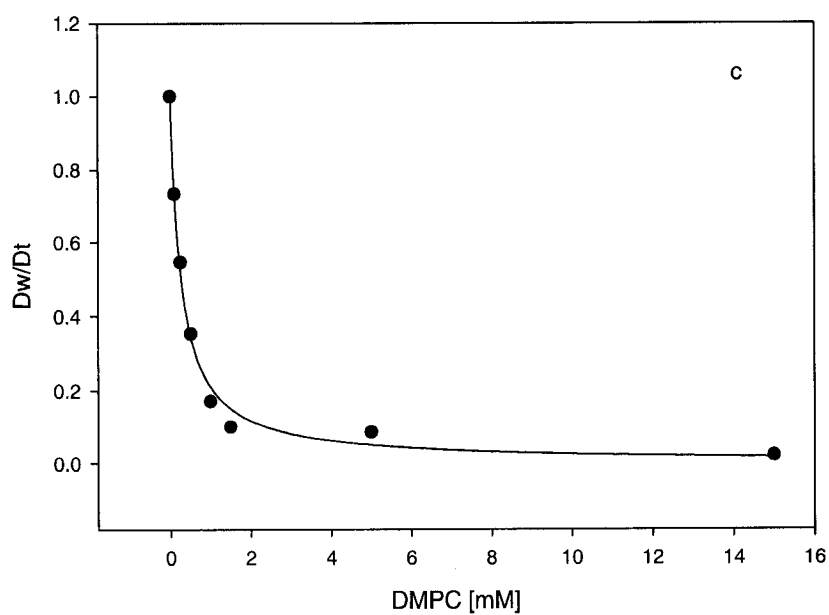


Figure 6.12 (a – e): Individual partitioning curves for amphibactins-832, and –848, from figure 6.11. The solid lines are fits to the experimental data according to equation 6.1.

R10-860



R10-886

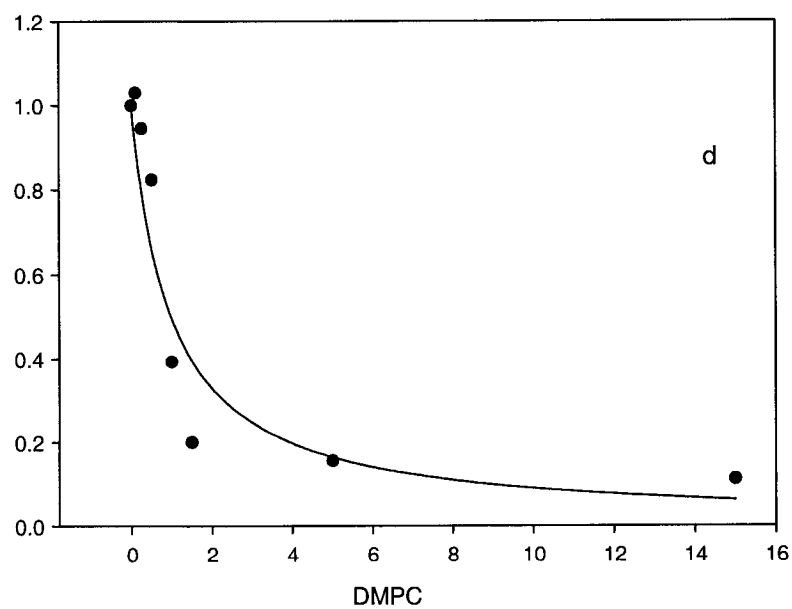


Figure 6.12 (continued): Individual partitioning curves for amphibactins-860, and -886, from Figure 6.11. The solid lines are fits to the experimental data according to equation 6.1.

R10-902

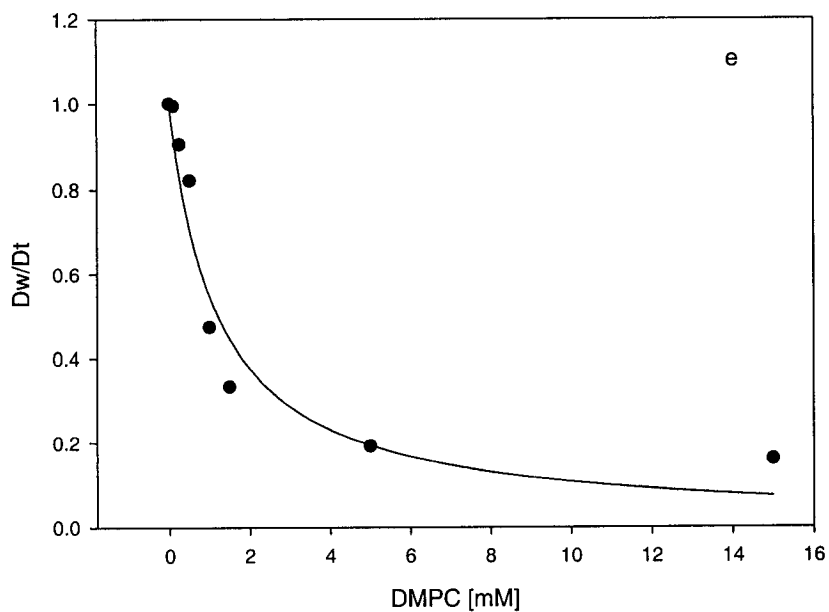


Figure 6.12 (continued): Individual partitioning curve for amphibactin-902 from Figure 6.11. The solid lines are fits to the experimental data according to equation 6.1.

	Siderophore	Fatty Acid Tail Moieity	Partition Coefficient (M^{-1})
Amphibactins	Apo-R10 ₉₀₂	C18:1; 3-OH	833 ± 108
	Apo-R10 ₈₈₆	C18:1	1018 ± 194
	Apo-R10 ₈₄₈	C14:0;3-OH	1338 ± 161
	Apo-R10 ₈₃₂	C14:0	1915 ± 140
	Apo-R10 ₈₆₀	C16:0	3784 ± 225
Marinobactins	Apo-M _A	C12:0	36 ± 7
	Apo-M _B	C14:1	25 ± 4
	Apo-M _C	C14:0	195 ± 21
	Apo-M _D	C16:1	209 ± 28
	Apo-M _E	C16:0	5818 ± 694

Table 6.1: Partition coefficients for the physiological mixtures of amphibactins and marinobactin siderophores in DMPC vesicles.

Discussion

It is intriguing that nearly half of the known marine siderophore structures are amphiphilic, a far higher percentage than for known terrestrial siderophores. Characterized marine bacteria such as *Halomonas aquamarina*, and *Marinobacter* sp. DS40M6 (which produce the suites of aquachelin and marinobactin siderophores) are diverse bacteria spanning the varied subgroups of Gram-negative bacteria [Figure 6.13] (Martinez et al. 2003). Phylogenetic tree analysis of *Vibrio* sp. R-10 was performed in collaboration with Dr. Elizabeth Mann and Professor Margo Haygood at Scripps Institute of Oceanography. The discovery of the amphibactins from the marine *Vibrio* sp. R-10 extends the number of relatively rare amphiphilic siderophores to the *Vibrionaceae* family of the gamma *Proteobacteria*. Furthermore, the amphibactins are the first fully characterized class of cellular bound siderophores outside of the high G + C Gram-positive bacterial species.

The peptidic headgroup of the amphibactins bears structural similarity to the peptide scaffolds of other siderophores isolated from marine bacteria (i.e., marinobactins and aquachelins) that coordinate iron through hydroxymate functional groups. The peptide headgroup of the amphibactins is considerably shorter (4 amino acids) than those of the marinobactins and aquachelins (6 and 7 amino acids, respectively). The fatty acid appendages of the amphibactins range in length from C-14 to C-18 and differ by both the degree of unsaturation and hydroxylation. Microorganisms are known to make a variety of saturated and unsaturated

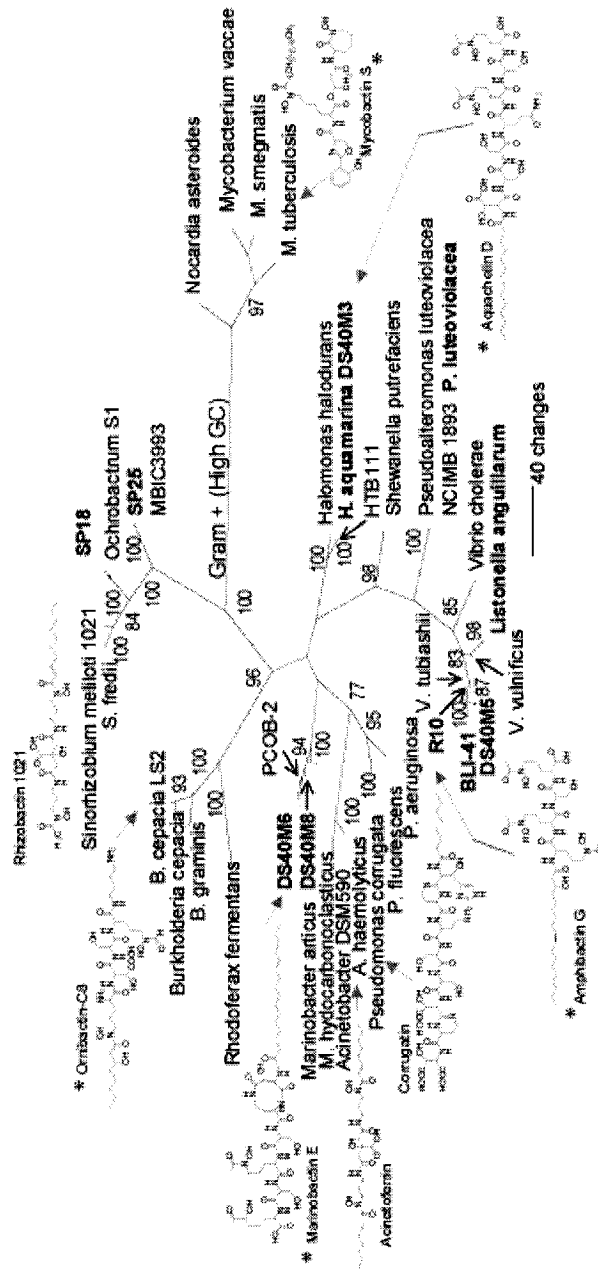


Figure 6.13: Phylogenetic tree of siderophore producing bacteria based on maximum parsimony analysis of SSU rRNA DNA sequences (Martinez, 2003). The α , β , and γ *Proteobacteria* as well as the high G + C Gram-positive bacteria are marked. This latter clade, containing *Mycobacterium* and *Nocardia*, was used as the out group. Marine isolates are in bold type. The tree shown here is one of two equally parsimonious trees, which differ only in a minor rearrangement within the *Vibrio* group. Bootstrap values greater than 75% are shown. For clarity, the bootstrap value (87) between the γ *Proteobacteria* DS40M6, 8 and PCOB-2 has been omitted. Amphibactin G, marinobactin E, and aquachelin D (Martinez, 2000) are amphiphilic siderophores produced by marine bacteria. Also included are most of the terrestrially produced amphiphilic siderophores, corrugatin, ornibactin (Stephan, 1993), rhizobactin 1021 (Lynch, 2001), acinetoferrin (Okujo, 1994) and mycobactin S (Ratledge, 1984). Some siderophores, designated with a star (*) next to their name, make suites of siderophores like the amphibactins.

oxyfunctionalized fatty acids (Ratledge and Wilkinson 1988). The amphibactins fatty acid tails are also generally longer than those of the marinobactins and aquachelins. Interestingly, the amphibactin siderophores tails are similar in length to the fatty acid chains of the mycobactins produced by *Mycobacteria* (Ratledge 1984; Gobin and Horwitz 1996). The amphibactins, like the suite of mycobactins, are found within the bacterial cellular membranes.

The high percentage of marine bacteria producing suites of amphiphilic siderophores suggest that marine bacteria (and possibly freshwater bacteria) have evolved a unique strategy to sequester iron in an environment where diffusion of the siderophores is likely a serious problem. Modification of the peptide backbone by appending a fatty acid tail extends the Fe(III) scavenging capabilities of marine bacteria when compared to traditional freely diffusible siderophores (i.e., alterobactins, (Reid and Butler 1991)). One can imagine that the ability of amphiphilic siderophores to associate with the bacterial membranes in aquatic environments may act to counter diffusion of the siderophores beyond the reach of the bacterium. Suites of siderophores with large variations in membrane partitioning such as the marinobactins and the aquachelins, could assemble gradients of siderophores with differing hydrophobicities extending away from the cell (Table 6.1) (Xu et al. 2002).

The partitioning experiments for the physiological mixture of amphibactins showed larger partition coefficients overall than the physiological mixture of marinobactins. Whereas the partition coefficients of the marinobactins dropped by

an order of magnitude upon introduction of one double bond (Apo-M_E, 5818 M⁻¹ vs. Apo-M_D, 209 M⁻¹) in the fatty acid or upon chain shortening by two methylene carbons (Apo-M_C, 195 M⁻¹ vs. Apo-M_A 36 M⁻¹), the difference in partition coefficients is less significant for similar changes in the amphibactins (Table 6.1) (Xu et al. 2002). For the amphibactins the partition coefficients of Apo-R10₈₆₀ and Apo-R10₈₃₂ are the same order of magnitude even with chain shortening by two methylene carbons from C16:0 to C14:0. The membrane partition coefficients of the amphibactins in general span a smaller range than the marinobactins and may reflect variations in how these bacteria use their siderophores to acquire iron as well as counter diffusion in the aquatic environment. The smaller range in partition coefficients for the amphibactins compared to the suite of marinobactins may reflect a role of the peptidic headgroup in partitioning. For the amphibactins, the smaller peptidic headgroup (4 amino acids) may aid siderophore insertion into the lipid membrane more than the larger peptidic headgroup (6 amino acids) of the marinobactins. Physiologically the *Vibrio* sp. R-10 likely counters diffusion of siderophores in aquatic environments by tethering of the siderophores to the cell surface and might provide a more efficient iron scavenging mechanism than production of freely diffusible siderophores. Whereas the marinobactin siderophores may acquire iron and limit diffusion by establishing a concentration gradient of siderophores (reflected in the wider range of partition coefficients for the physiological mixture of marinobactins) extending out from the bacterial cell surface. These results are further supported by isolation experiments, where the

suite of amphibactin siderophores are found predominately associated with the bacterial cell membrane, whereas the marinobactins are predominately secreted into the culture media.

References

- Azam, F. and R. E. Hodson (1977). "Size Distribution and Activity of Marine Microheterotrophs." *Limnol. Oceanogr.* **22**: 492-501.
- Campbell, L., H. A. Nolla and D. Vaultot (1994). "The Importance of *Prochlorococcus* to Community Structure in the Central North Pacific Ocean." *Limnol. Oceanogr.* **39**: 954-961.
- Gobin, J. and M. A. Horwitz (1996). "Exochelins of *Mycobacterium tuberculosis* Remove Iron from Human Iron-Binding Proteins and Donate Iron to Mycobactins in the *M. tuberculosis* Cell Wall." *Journal of Experimental Medicine* **183**(4): 1527-1532.
- Haygood, M. G., P. D. Holt and A. Butler (1993). "Aerobactin Production by a Planktonic Marine *Vibrio* sp." *Limnol. Oceanogr.* **38**(5): 1091 - 1097.
- Lynch, D., J. O'Brien, T. Welch, P. Clarke, P. Ó. Cuív, J. H. Crosa and M. O'Connell (2001). "Genetic Organization of the Region Encoding Regulation, Biosynthesis, and Transport of Rhizobactin 1021, a Siderophore Produced by *Sinorhizobium meliloti*." *J. Bacteriol.* **183**: 2576 - 2585.
- Marfey, P. (1984). "Determination of D-amino acids. II. Use of a Bifunctional Reagent, 1,5-Difluoro-2,4-Dinitrobenzene." *Carlsberg Research Communications* **49**: 591-596.
- Martinez, J. S. (2002). Mechanisms of Siderophore Mediated Sequestration by Marine Bacteria. Ph.D. Thesis, University of California, Santa Barbara.
- Martinez, J. S., J. N. Carter-Franklin, E. L. Mann, J. D. Martin, M. G. Haygood and A. Butler (2003). "Structure and Membrane Affinity of a Suite of Amphiphilic Siderophores Produced by a Marine Bacterium." *Proc. Natl. Acad. Sci. USA* **100**: 3754 - 3759.
- Martinez, J. S., M. G. Haygood and A. Butler (2001). "Identification of a Natural Desferrioxamine Siderophore Produced by a Marine Bacterium." *Limnol. Oceanogr.* **46**: 420-424.
- Martinez, J. S., G. P. Zhang, P. D. Holt, H. Jung, C. J. Carrano, M. G. Haygood and A. Butler (2000). "Self-Assembling Amphiphilic Siderophores from Marine Bacteria." *Science* **287**: 1245-1247.
- Murphy, R. C. (1993). Mass Spectrometry of Lipids, Plenum Press.

Okujo, N., Y. Sakakibara, T. Yoshida and S. Yamamoto (1994). "Structure of Acinetoferrin, a New Citrate-Based Dihydroxamate Siderophore from *Acinetobacter haemolyticus*." *BioMetals* **7**: 170-176.

Ratledge, C. (1984). Metabolism of Iron and Other Metals by Mycobacteria. The Mycobacteria, a Sourcebook. G. P. W. Kubica, L. G., Dekker, New York: 603-627.

Ratledge, C. and S. G. Wilkinson (1988). Fatty Acids, Related and Derived Lipids. Microbial Lipids. C. W. Ratledge, S. G. London, Academic Press Limited. **1**.

Reid, R. T. and A. Butler (1991). "Investigation of the Mechanism of Iron Acquisition by the Marine Bacterium *Alteromonas luteoviolaceus*: Characterization of Siderophore Production." *Limnol. Oceanogr.* **36**: 1783-1792.

Schwyn, B. and J. B. Neilands (1987). "Universal Chemical Assay for the Detection and Determination of Siderophores." *Anal. Biochem.* **160**: 47 - 56.

Stephan, H., S. Freund, W. Beck, G. Jung, J. M. Meyer and G. Winkelmann (1993). "Ornibactins- A New Family of Siderophores from *Pseudomonas*." *BioMetals* **6**: 93-100.

Winkelmann, G. (1991). Handbook of Microbial Iron Chelates, CRC, Boca Raton, FL.

Xu, G., J. S. Martinez, J. T. Groves and A. Butler (2002). "Membrane Affinity of the Amphiphilic Marinobactin Siderophores." *J. Am. Chem. Soc.* **124**: 13408 - 13415.

Zhang, G. P. (1999). Marinobactins and Petrobactins: Two New Sets of Siderophores From Marine Bacteria. Ph.D. Thesis, University of California, Santa Barbara.

APPENDIX

¹H NMR of brominated cyclized nerol product (5).

APT spectrum of brominated cyclized nerol product (5).

IR spectrum of brominated cyclized nerol product (5).

¹H NMR of brominated cyclized geraniol product (7).

APT spectrum of brominated cyclized geraniol product (7).

One-dimensional nOe of brominated cyclized geraniol product (7). Irradiation at 4.17 ppm signal.

IR spectrum of brominated cyclized geraniol product (7).

¹H NMR of brominated cyclized geraniol product (8).

APT spectrum of brominated cyclized geraniol product (8).

One-dimensional nOe of brominated cyclized geraniol product (8). Irradiation at 4.15 ppm signal.

IR spectrum of brominated cyclized geraniol product (8).

¹H NMR of brominated cyclized geranyl acetate product (10).

APT spectrum of brominated cyclized geranyl acetate product (10).

IR spectrum of brominated cyclized geranyl acetate product (10).

¹H NMR of brominated cyclized geranyl acetate product (11).

IR spectrum of brominated cyclized geranyl acetate product (11).

¹H NMR of brominated bicyclic geranyl acetone product (13).

APT spectrum of brominated bicyclic geranyl acetone product (13).

¹H NMR of α/β -snyderol (15), (16) mixture.

¹H NMR of γ -snyderol product (**17**).

One-dimensional nOe of γ -snyderol (**17**). Irradiation at 4.18 ppm signal.

¹H NMR of (+)-3 β -bromo-8-epicaparrapi oxide product (**18**).

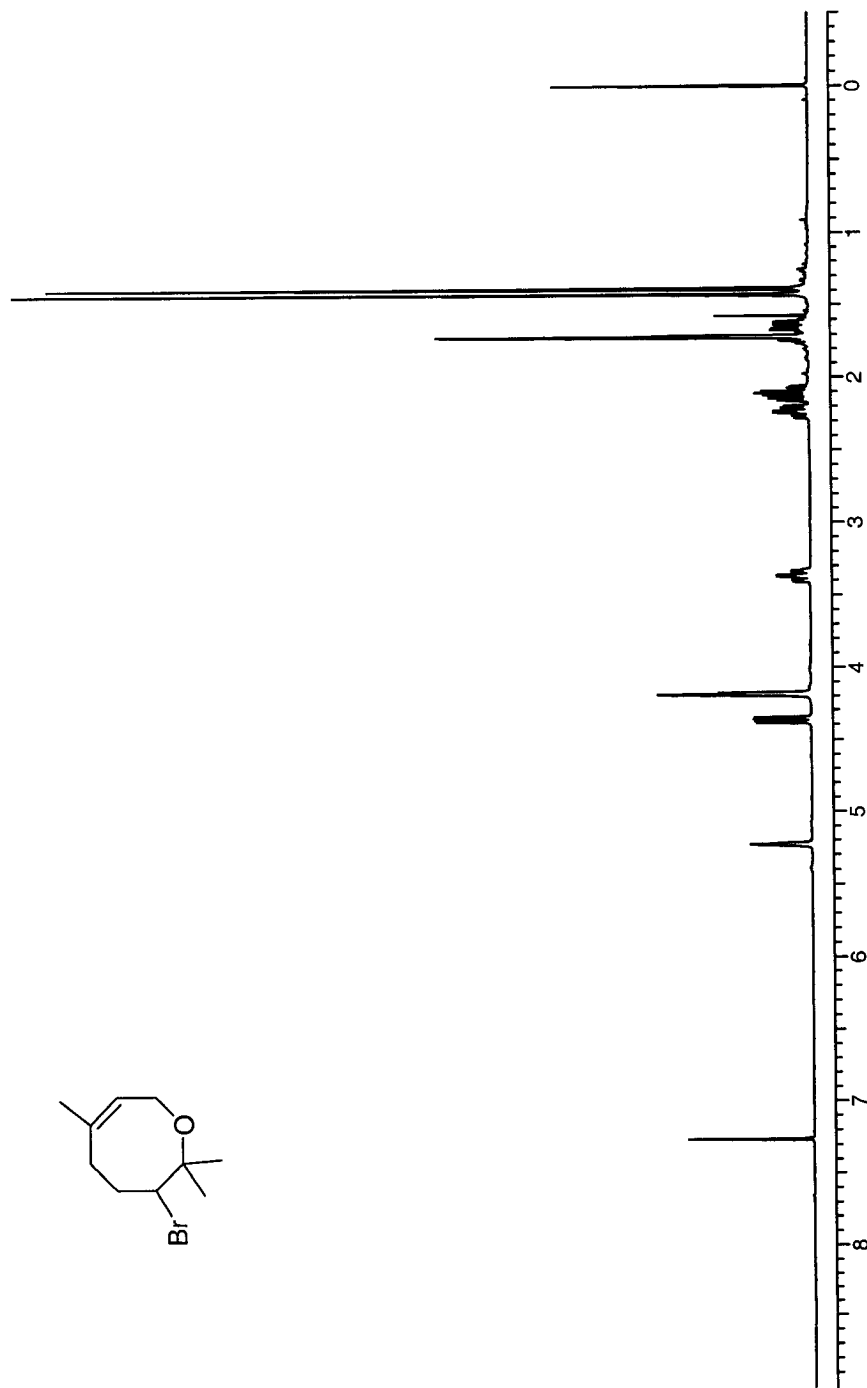
One-dimensional nOe of (+)-3 β -bromo-8-epicaparrapi oxide product (**18**).
Irradiation at 4.00 ppm signal.

One-dimensional nOe of (+)-3 β -bromo-8-epicaparrapi oxide product (**18**).
Irradiation at 6.00 ppm signal.

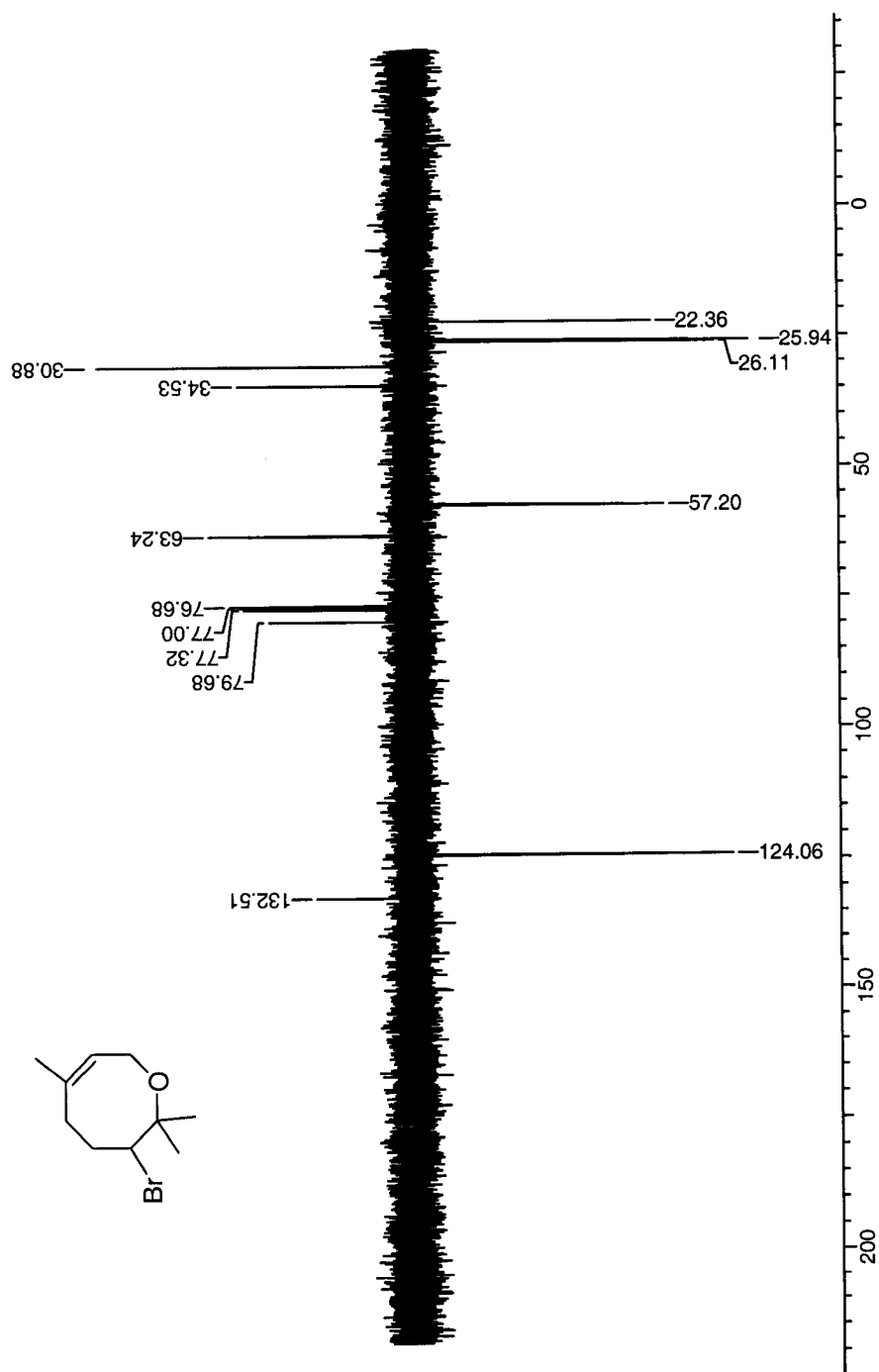
¹H NMR of (-)-3 β -bromo-8-epicaparrapi oxide.

APCI mass spectrum of the α,α -dibrominated-3-oxo-hexanoylhomoserine lactone.

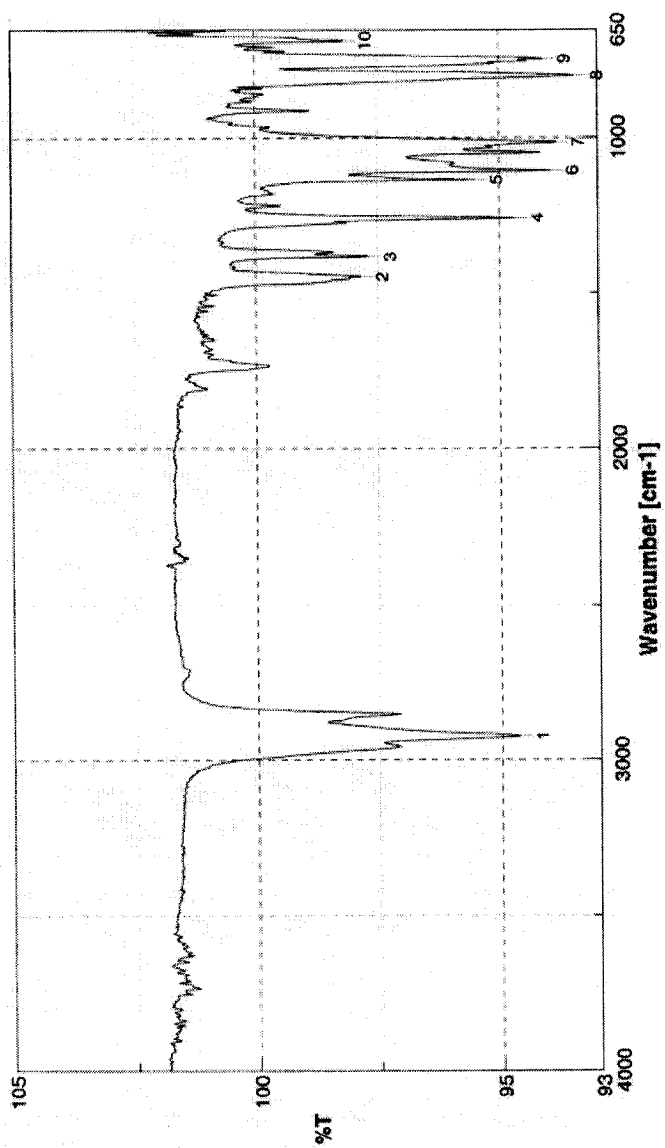
^1H NMR of brominated cyclized nerol, product (5).



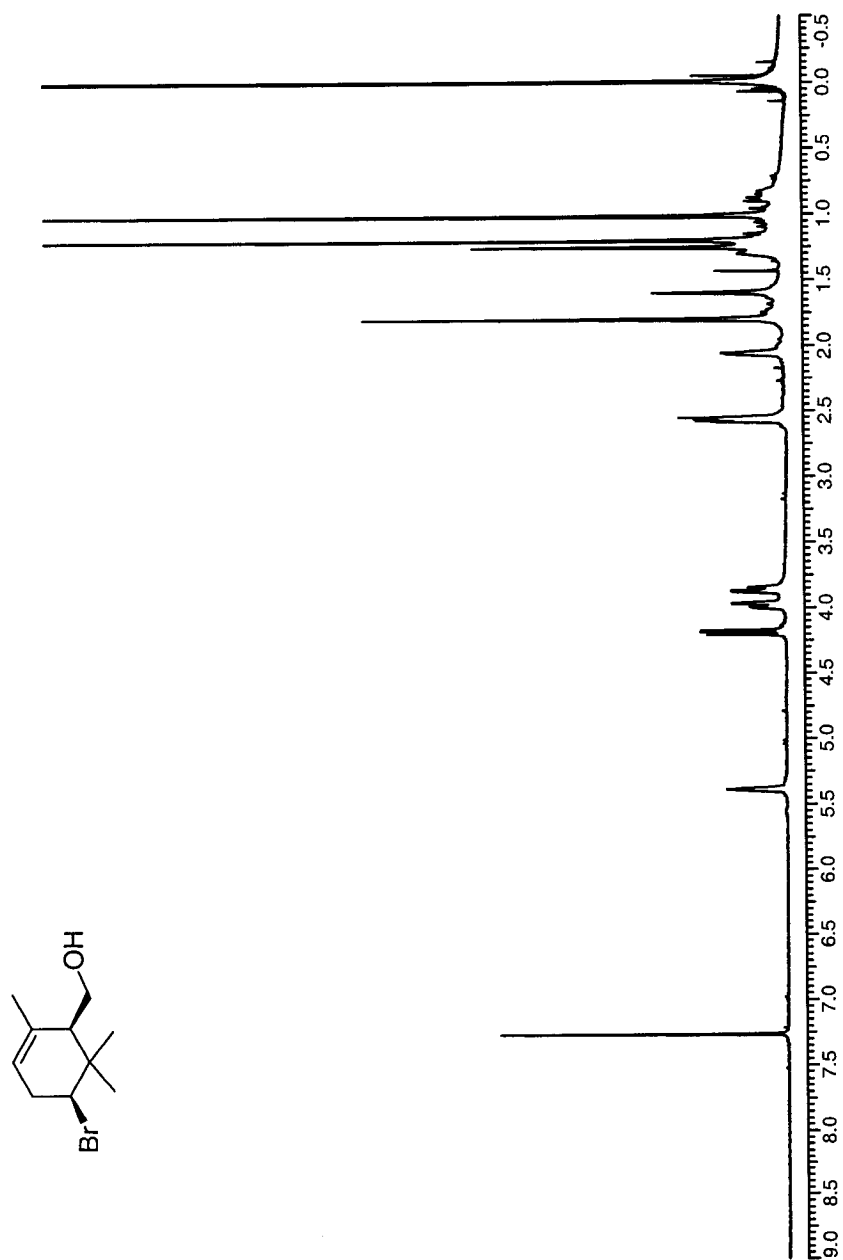
APT spectrum of brominated cyclized nerol, product (5).



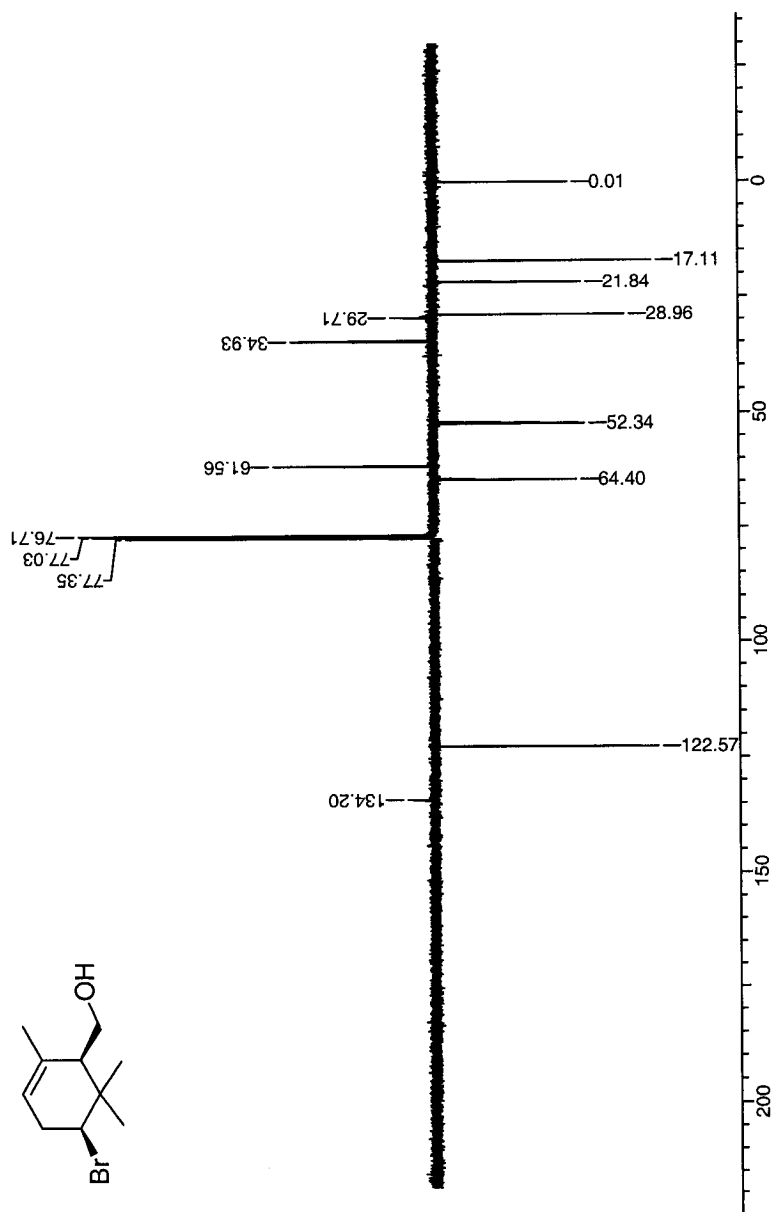
IR spectrum of brominated nerol, product (5).



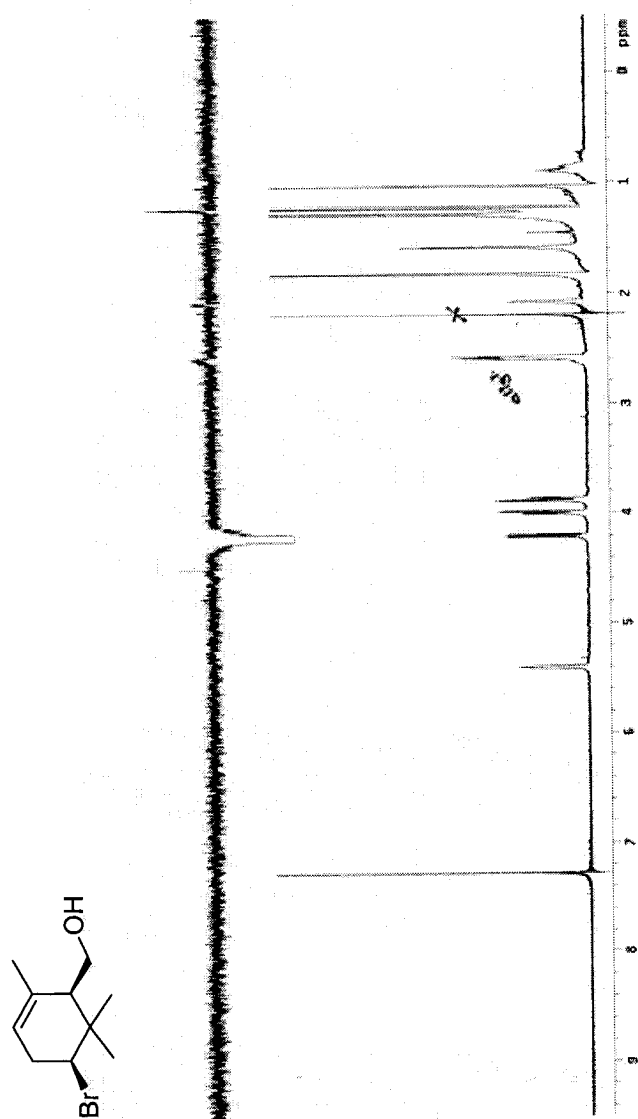
^1H NMR of brominated cyclized geraniol product (7).



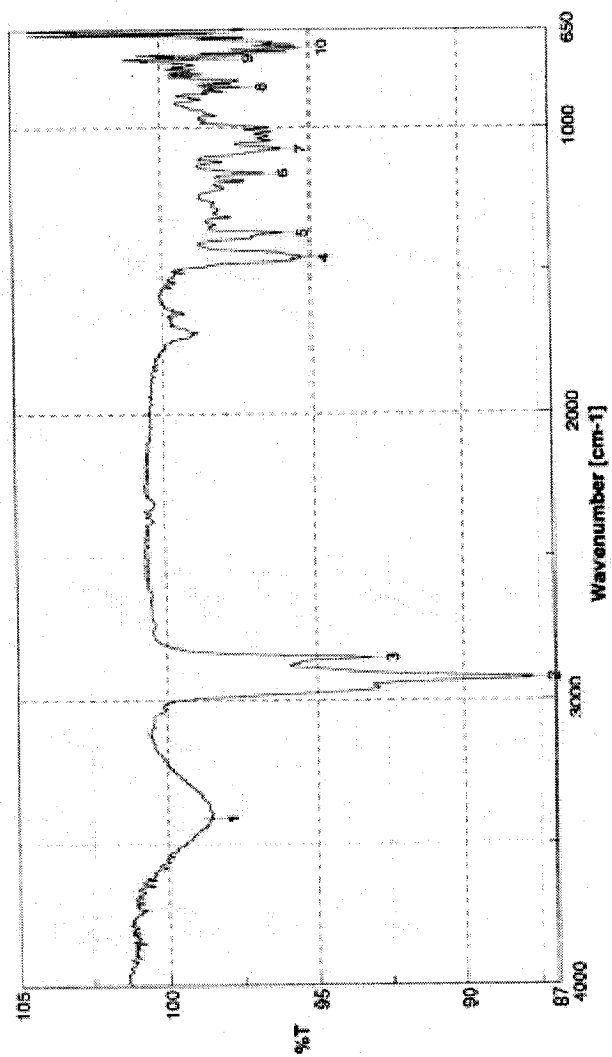
APT spectrum of brominated cyclized geraniol product (7).



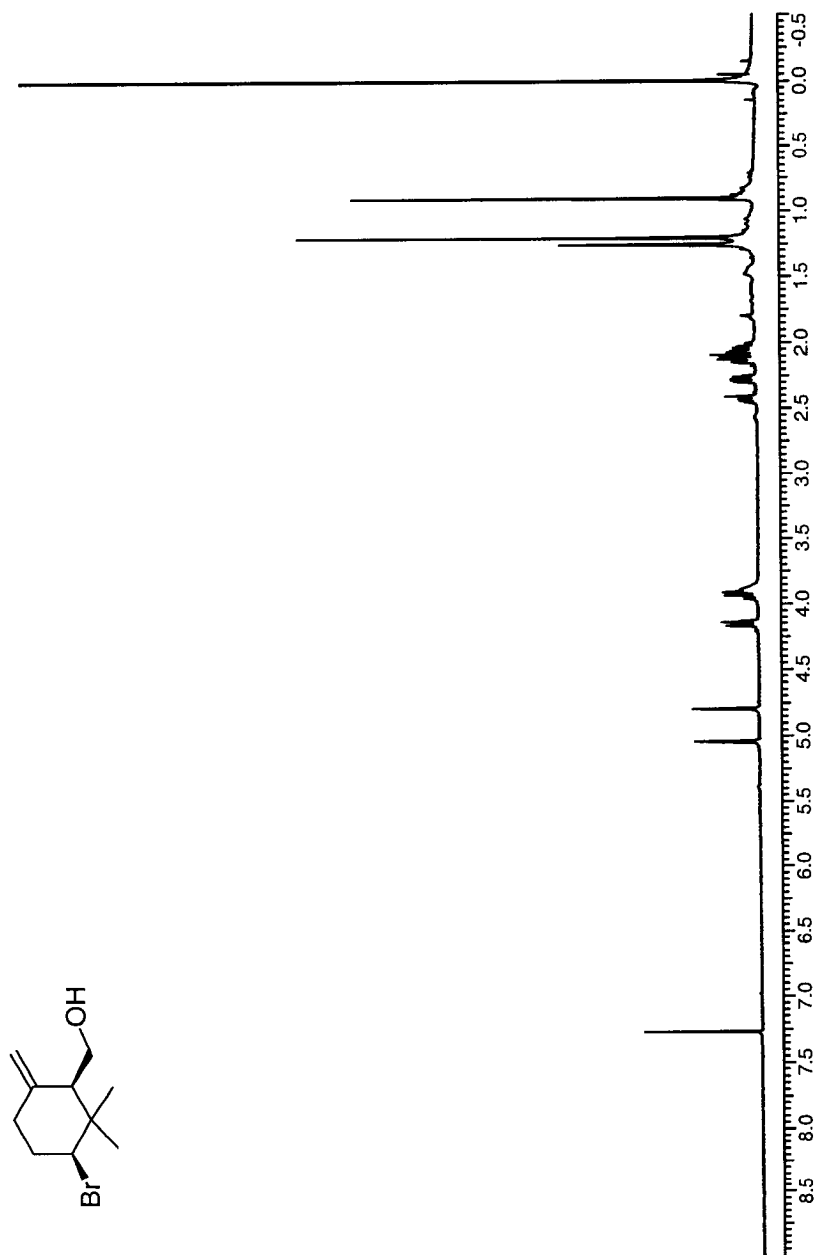
One-dimensional nOe of brominated cyclized geraniol product (7). Irradiation at 4.17 ppm signal.



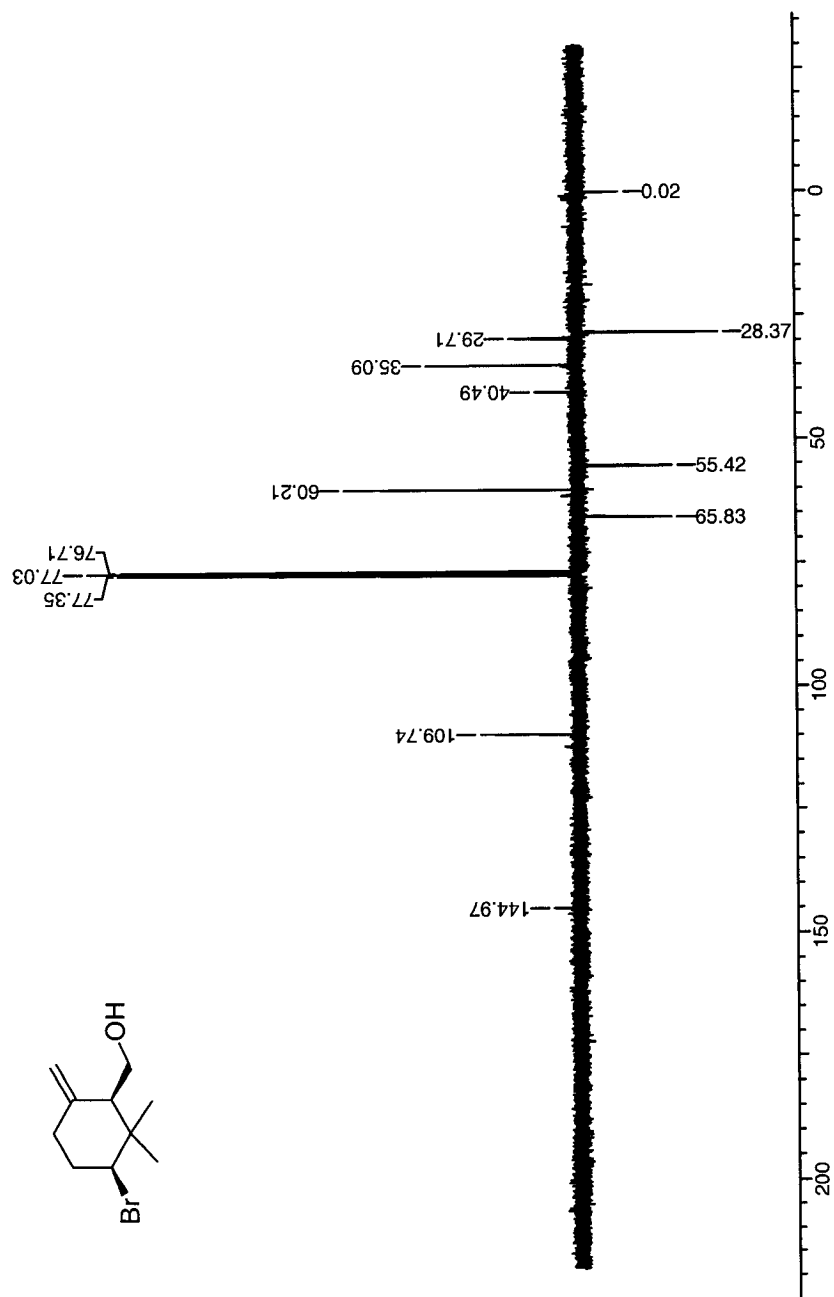
IR spectrum of brominated cyclized geraniol product (7).



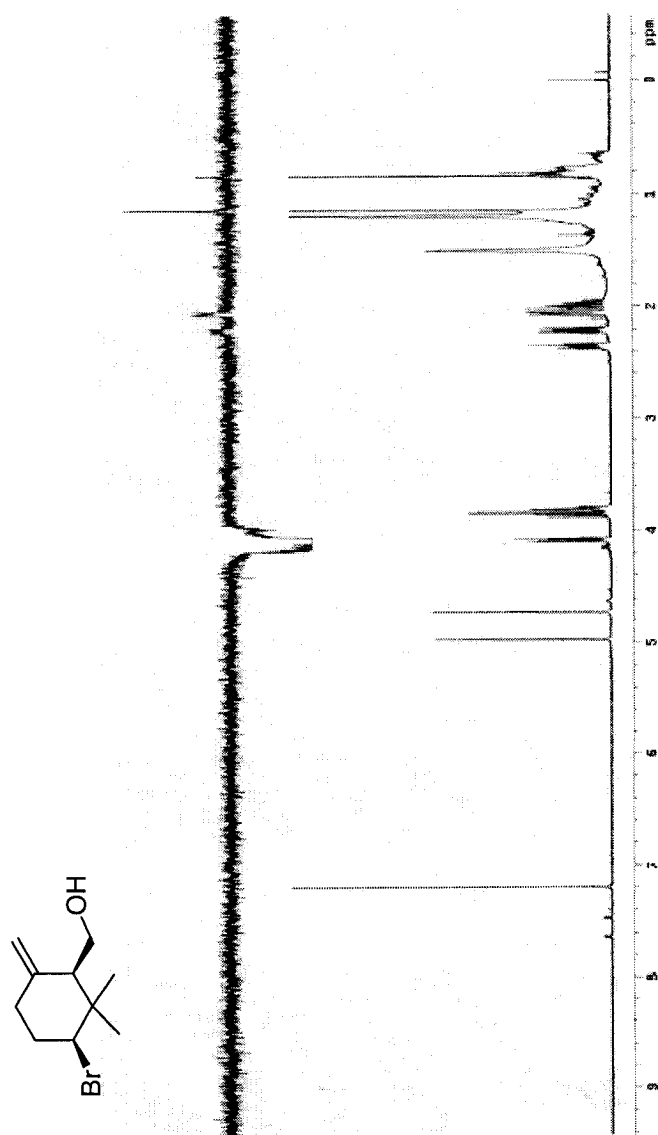
^1H NMR of brominated cyclized geraniol product (**8**).



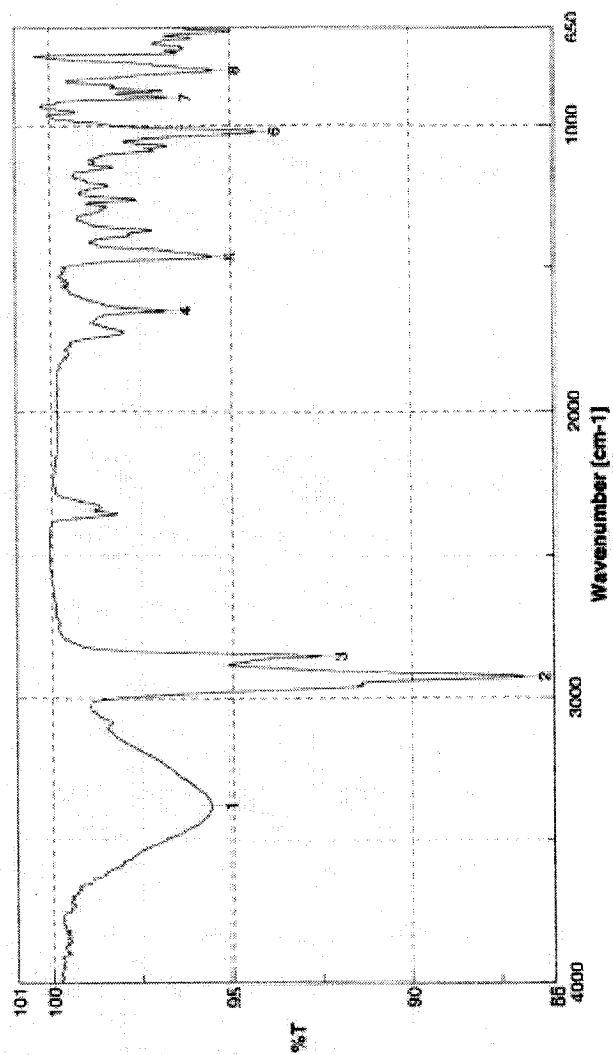
APT spectrum of brominated cyclized geraniol product (8).



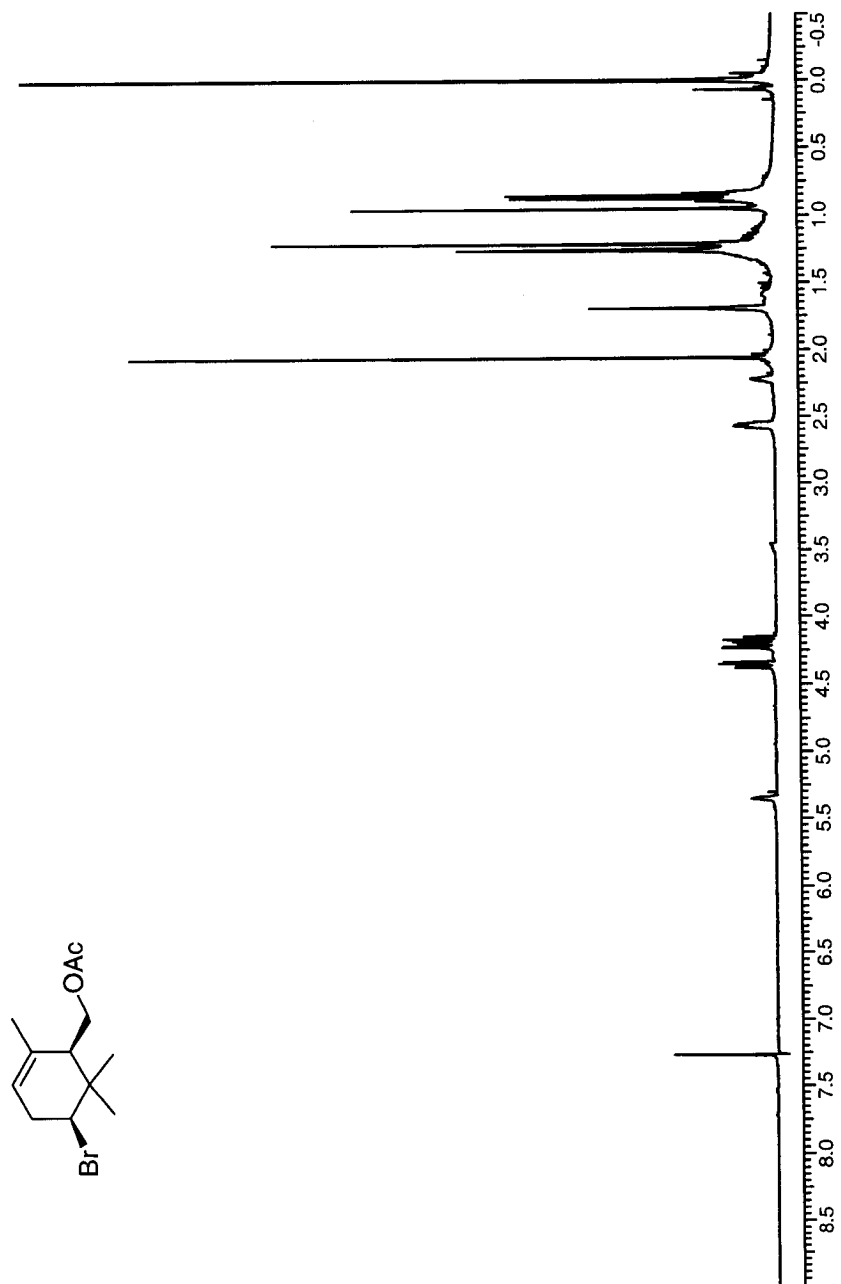
One-dimensional nOe of brominated cyclized geraniol product (8). Irradiation at 4.17 ppm signal.



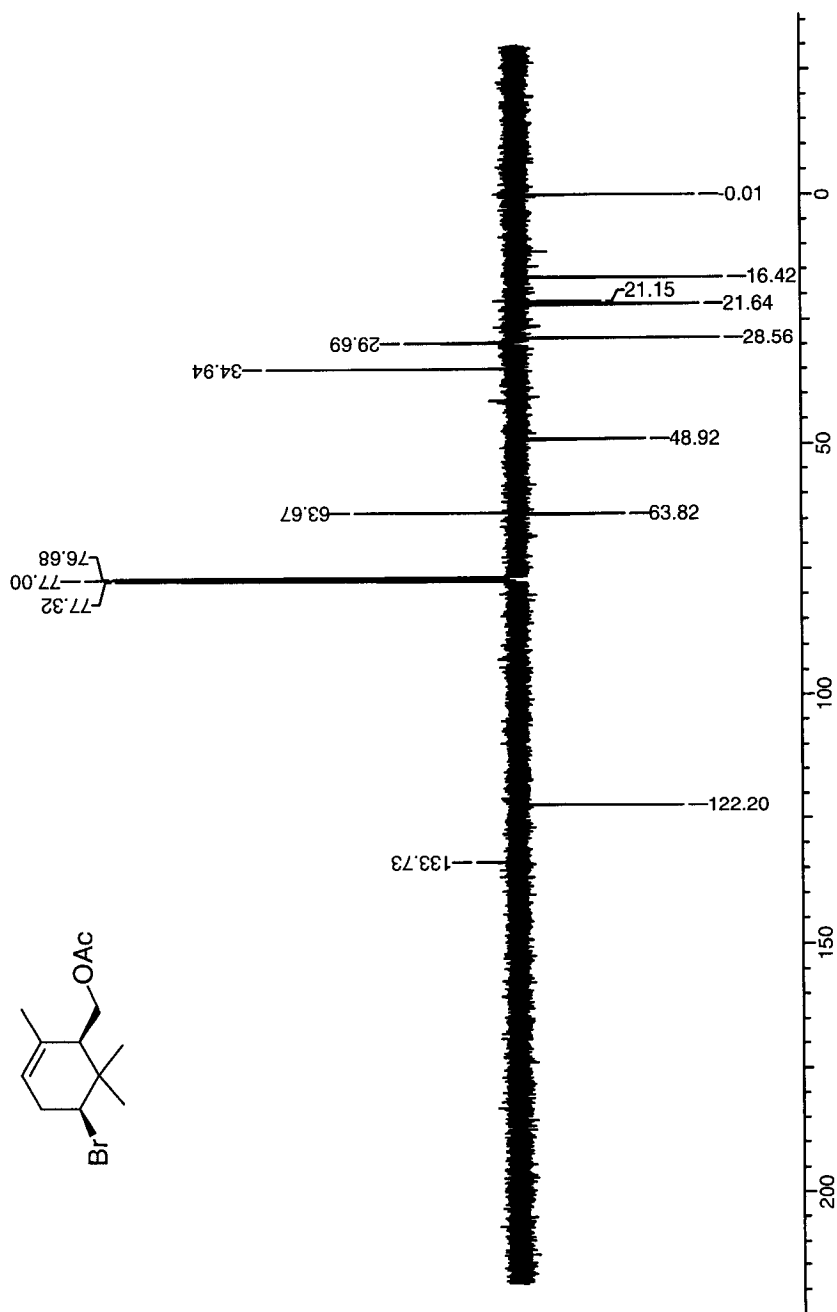
IR spectrum of brominated cyclized geraniol product (8).



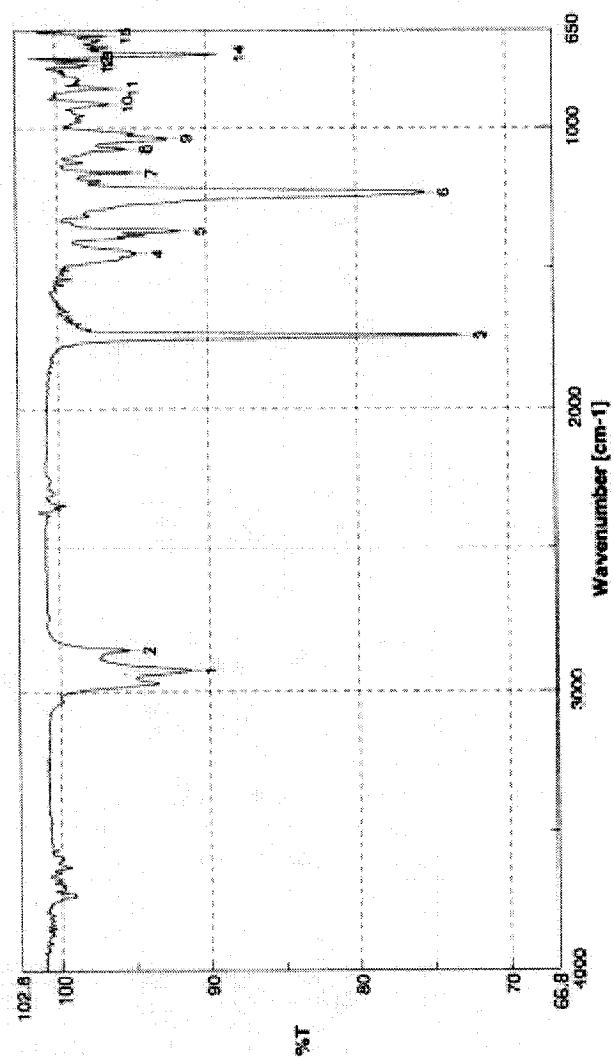
^1H NMR of brominated cyclized geranyl acetate product (**10**).



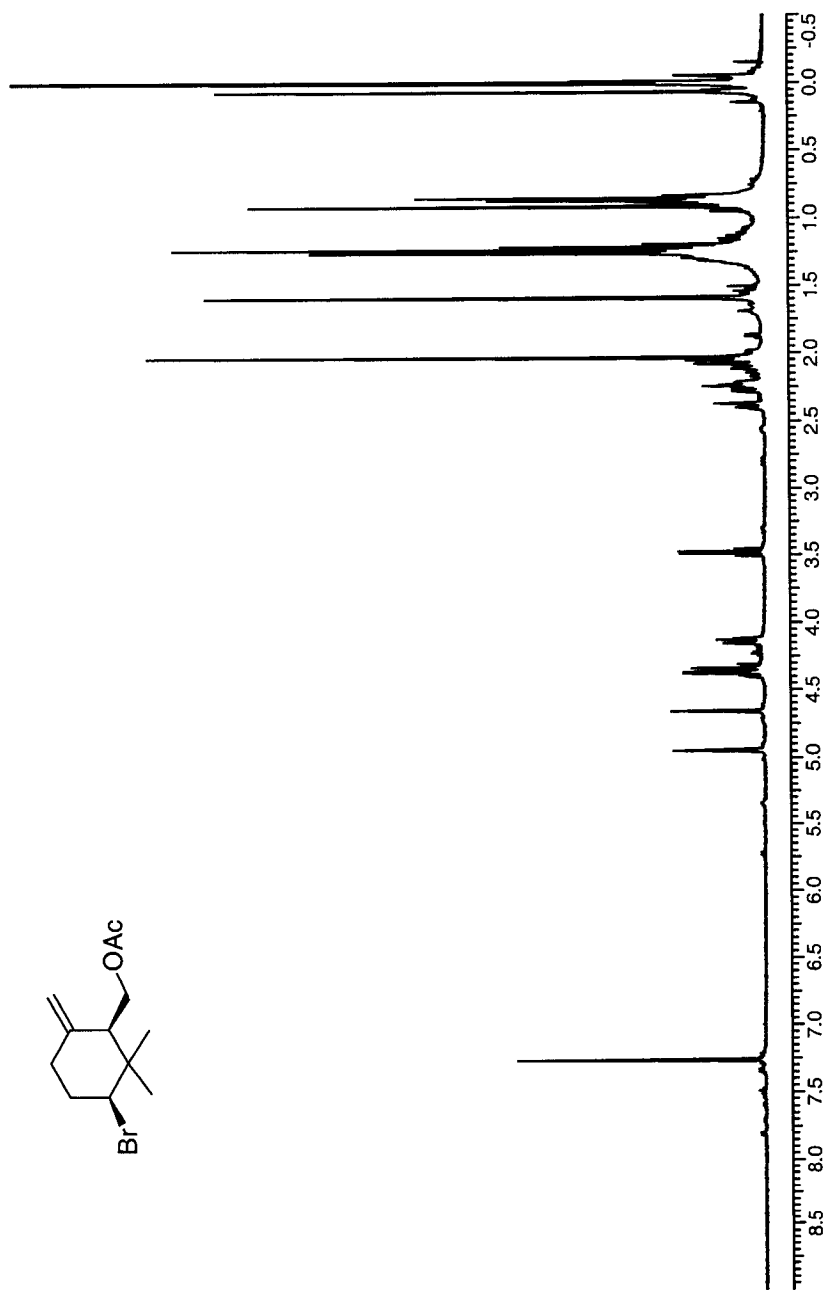
APT spectrum brominated cyclized geranyl acetate product (10).



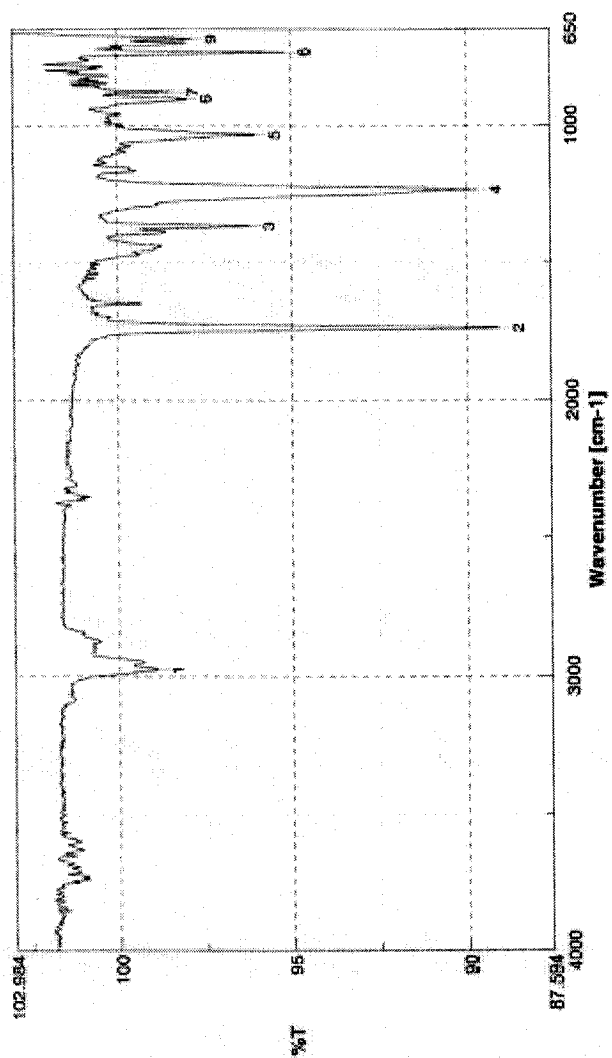
IR spectrum of brominated cyclized geranyl acetate product (10).



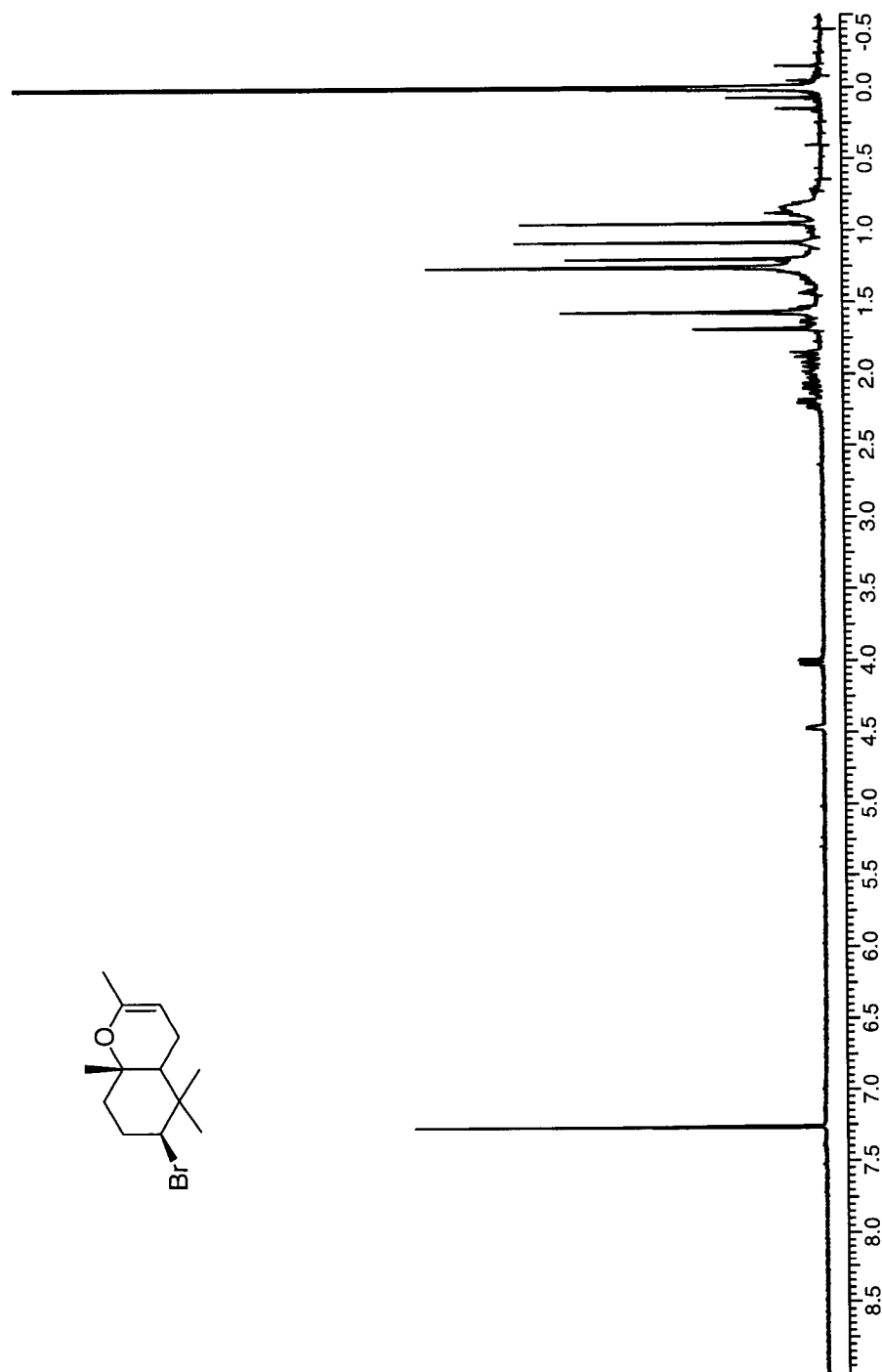
^1H NMR of brominated cyclized geranyl acetate product (**11**).



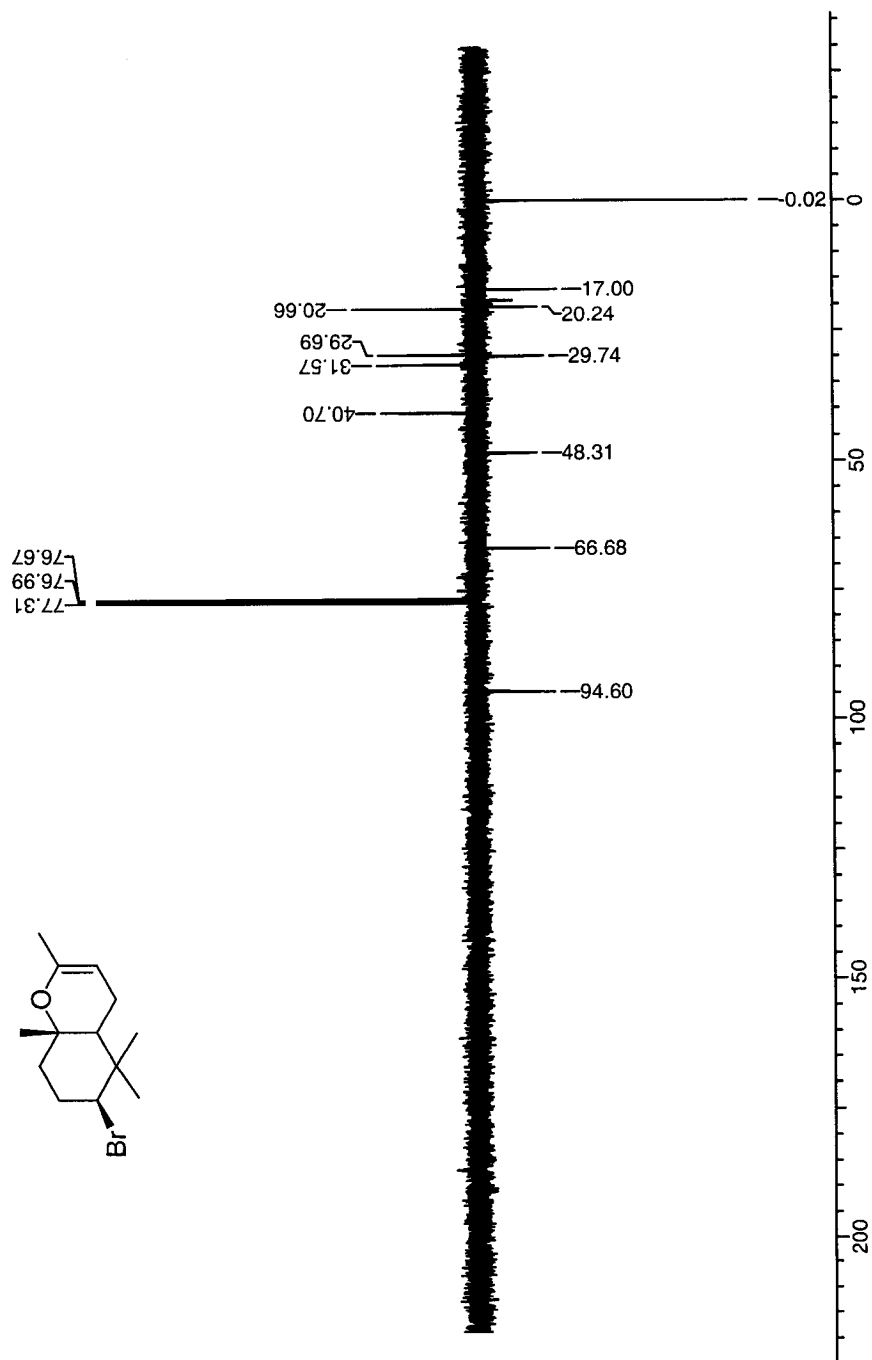
IR spectrum of brominated cyclized geranyl acetate product (11).



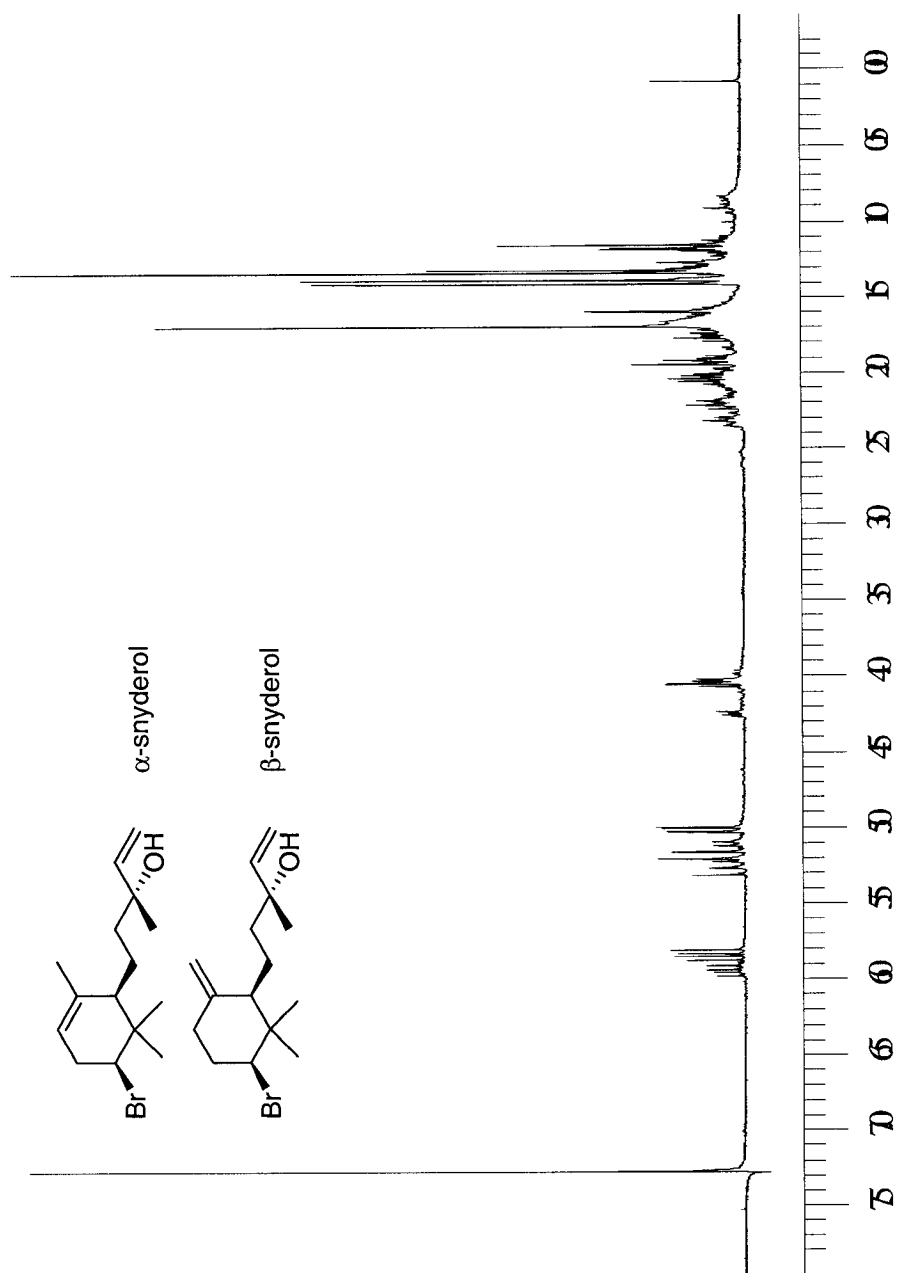
^1H NMR of brominated bicyclic geranyl acetone product (13).



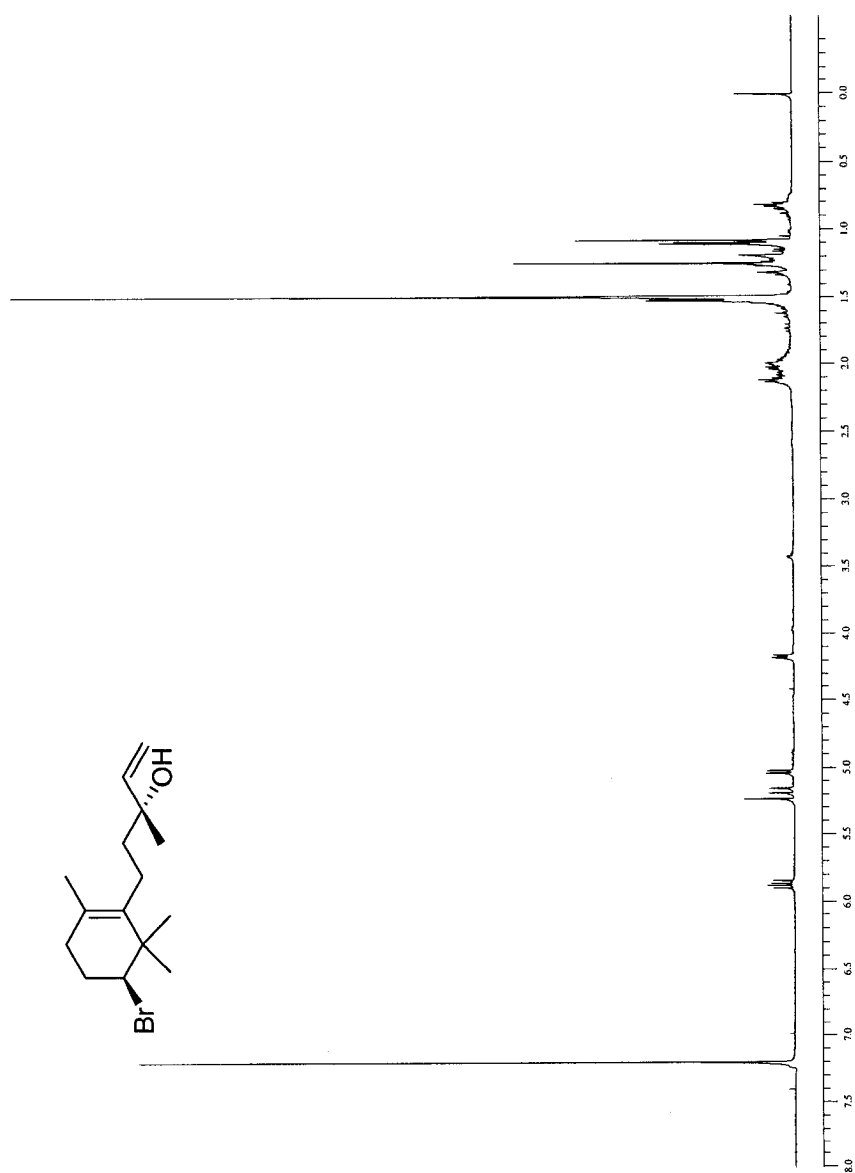
APT spectrum of brominated bicyclic geranyl acetone product (**13**).



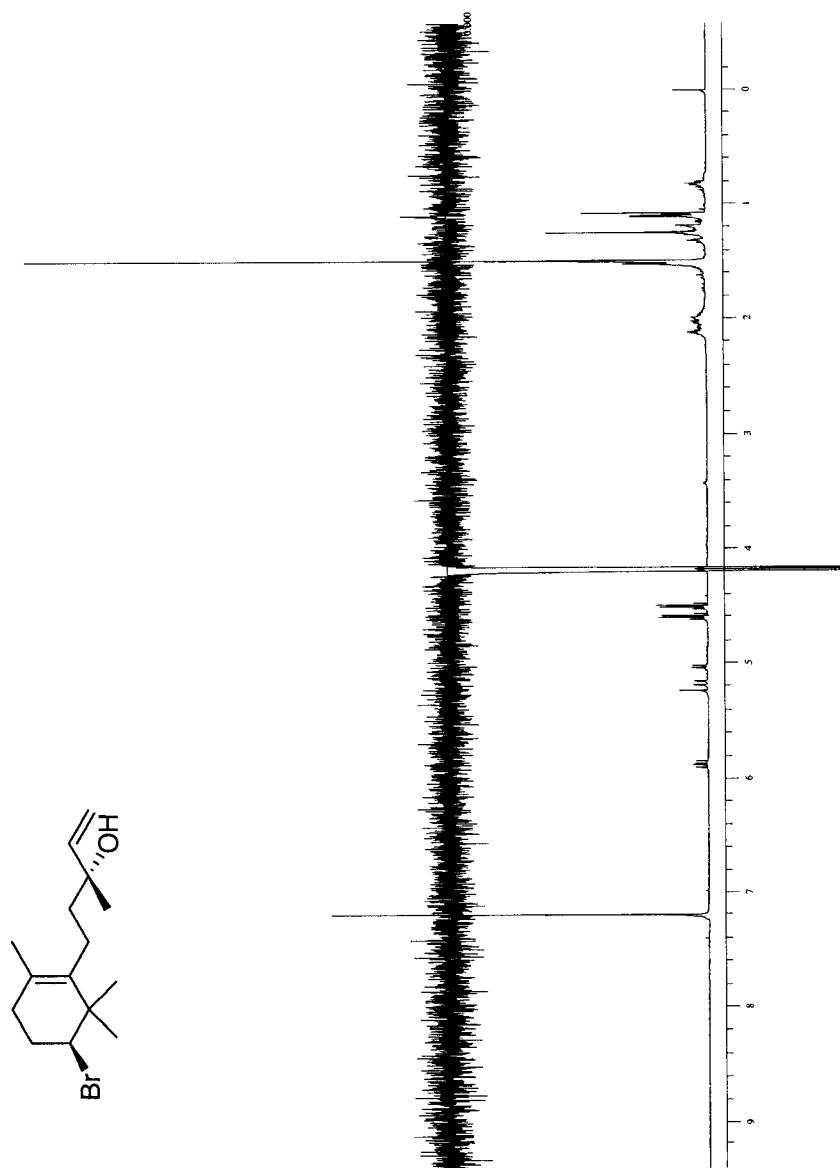
^1H NMR of α -/ β -snyderol (15), (16) mixture.



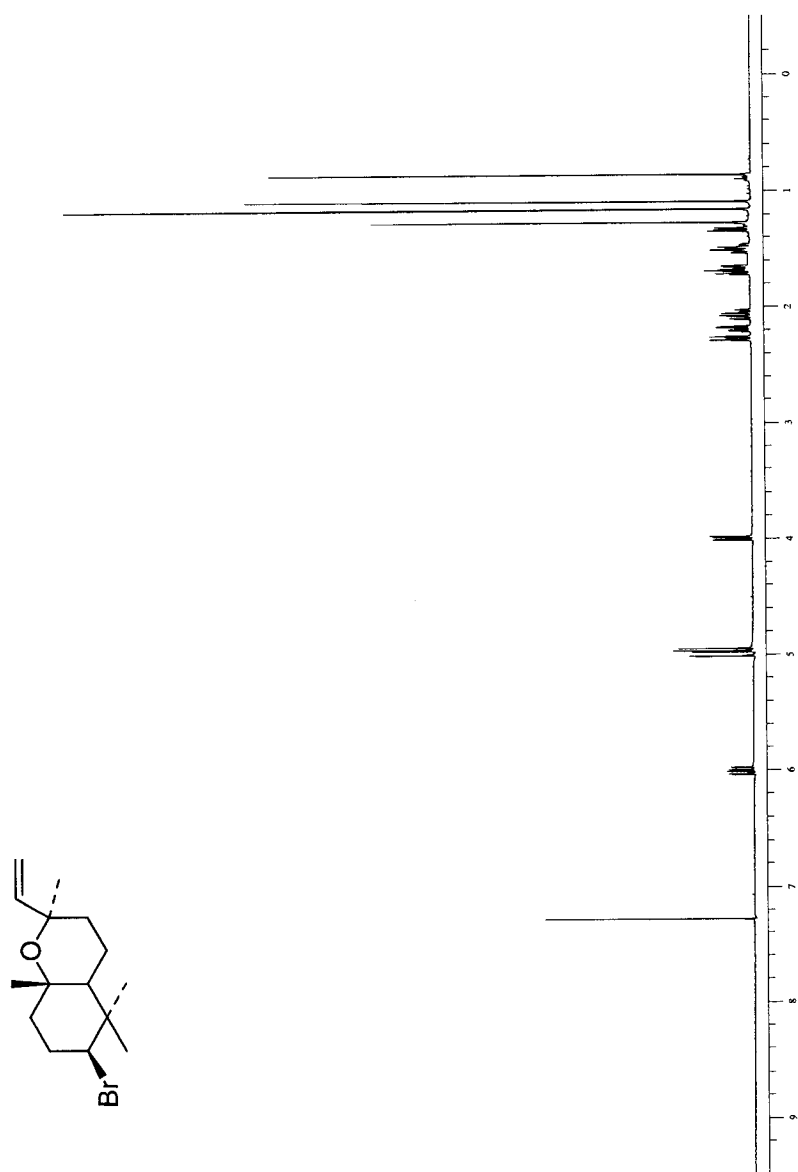
^1H NMR of γ -snyderol, product (17).



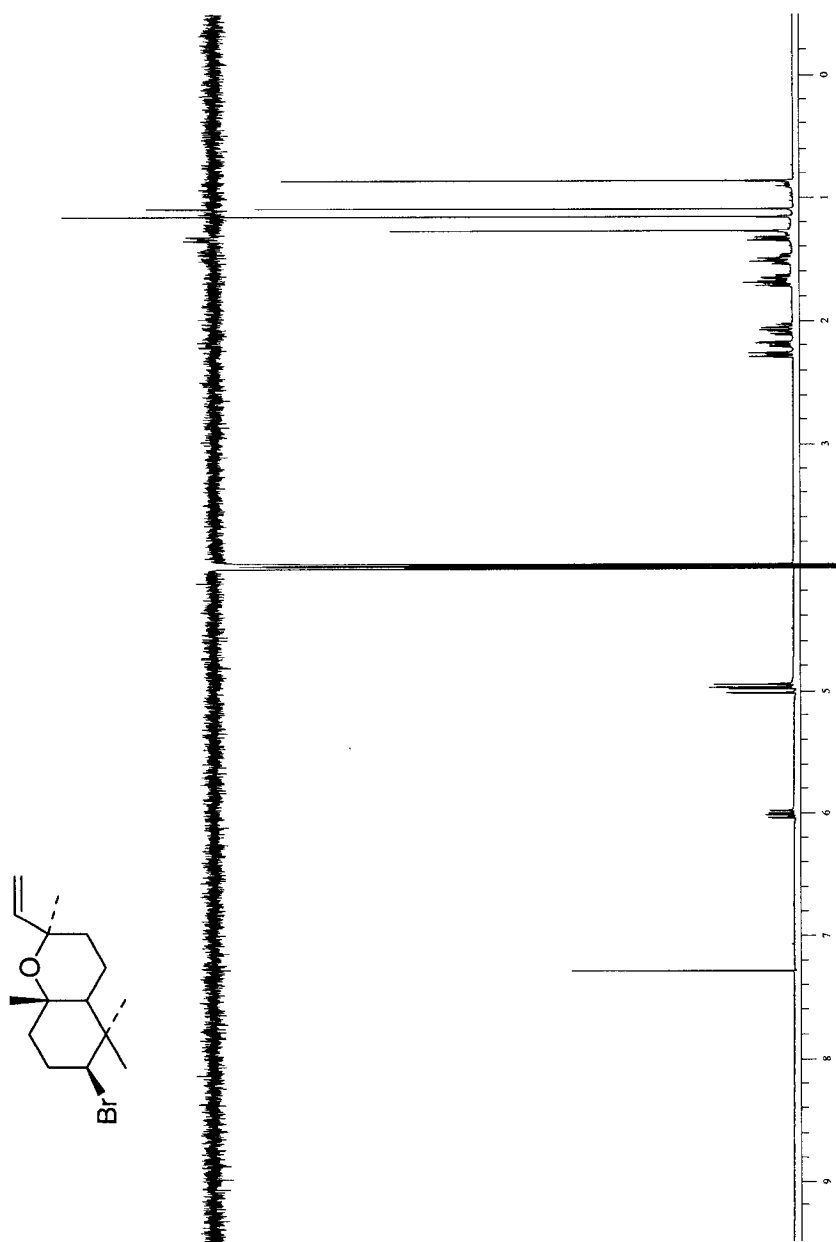
One-dimensional nOe of γ -snyderol (**17**). Irradiation at 4.18 ppm signal



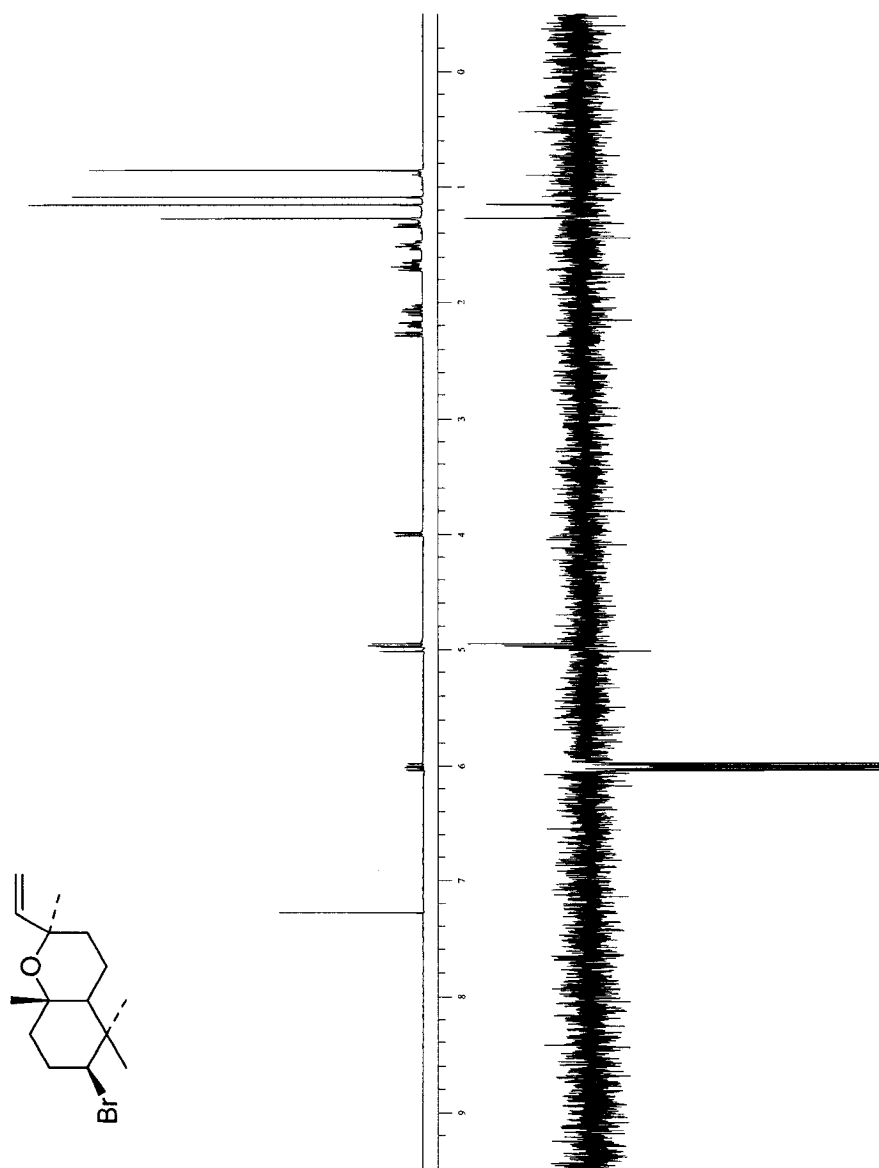
^1H NMR of (+)-3 β -bromo-8-epicaparrapi oxide, product (18).



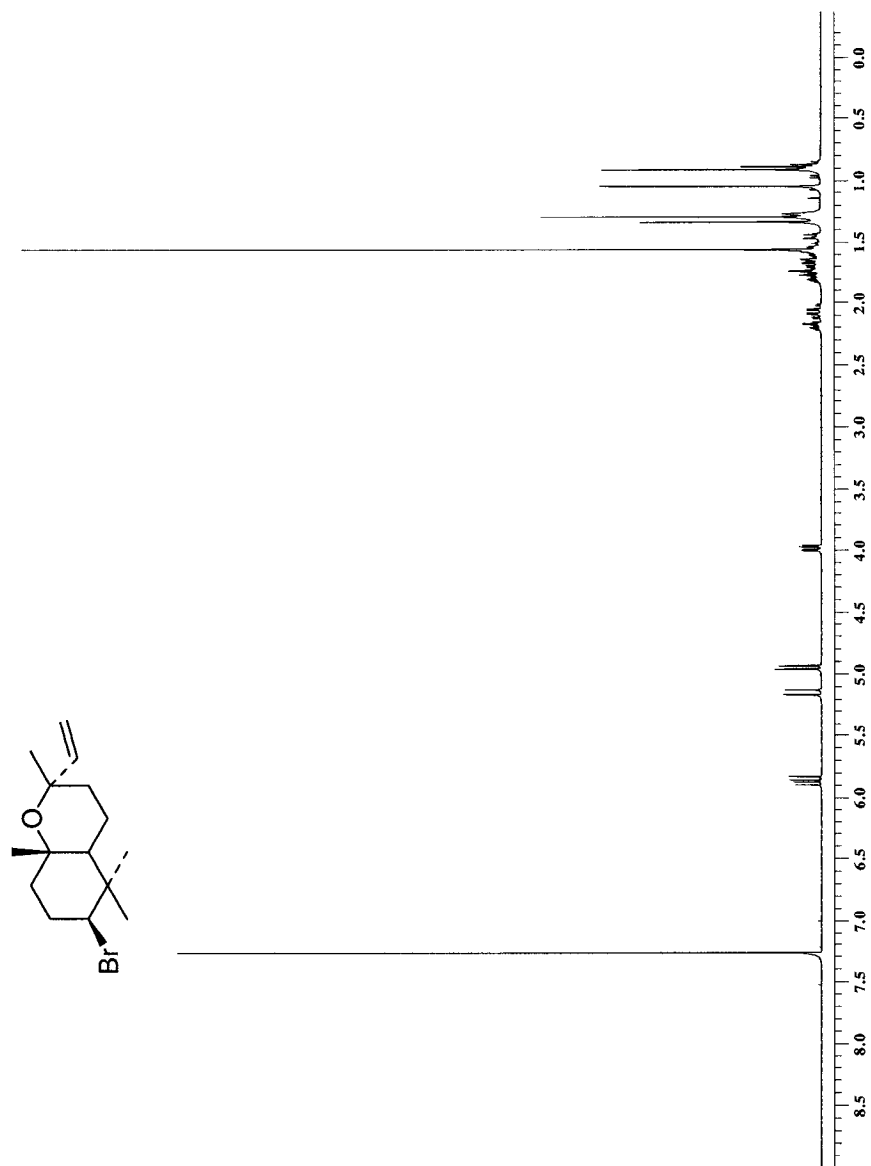
One-dimensional nOe of (+)-3 β -bromo-8-epicaparrapi oxide (**18**).
Irradiation of 4.00 ppm signal.



One-dimensional nOe of (+)-3 β -bromo-8-epicaparrapi oxide (**18**).
Irradiation of 6.00 ppm signal.



^1H NMR of (-)-3 β -bromo-8-epicaparrapi oxide.



APCI mass spectrum of the sodium adduct of α,α -dibrominated-3-oxo-hexanoylhomoserinelactone. Product isolated from reaction with 3-oxo-hexanoylhomoserine lactone with partially purified V-BrPO from the red alga *D. pulchra*.

